Characterization of *Staphylococcus aureus* skin infection using a new *in vivo* proliferation biosensor

Dissertation

zur Erlangung des akademischen Grades

doctor rerum naturalium (Dr. rer. nat.)

genehmigt durch die Fakultät für Naturwissenschaften
der Otto-von-Guericke-Universität Magdeburg

von M. Sc. Elena Anne Seiß (geb. Haas)

geb. am 14.03.1988 in Erkelenz

Gutachter: Prof. Dr. Andreas J. Müller

Prof. Dr. rer. nat. Christiane Wolz

eingereicht am: 08.01.2019

verteidigt am: 26.06.2019

ABSTRACT

M. Sc. Elena A. Seiß (née Haas): “Characterization of *Staphylococcus aureus* skin infection using a new *in vivo* proliferation biosensor”

Distinct bacterial growth rates are decisive for the outcome of infections: First, they impact on the pathogen's susceptibility to both immune effector mechanisms and antibiotic treatment, and can therefore contribute to persistence during chronic or relapsing infections. Second, fast-growing bacteria are a source of more, and different, pathogen-associated molecules than low-proliferating or inactive microbes, thus differentially shaping the immune response. It has however remained difficult to measure bacterial growth rates in the ongoing infection.

Here, I established an *in vivo* biosensor for measuring proliferation of the Gram-positive bacterium *Staphylococcus aureus* (*S. aureus*) on a single cell-level *in vivo*. The method is based on the photoconvertible fluorescence protein mKikume, which can be photoconverted by violet light at any given time point, even during *in vivo* infection in a non-invasive way. This allows determining bacterial proliferation rates as a function of the recovery from photoconversion. Importantly, I could show that indeed bacterial proliferation, and not protein turnover in nonproliferating bacteria, is mainly responsible for the fluorescence recovery after photoconversion readout of the biosensor. Using intravital 2-photon imaging and quantitative fluorescence microscopy, I saw that upon recruitment of $CD45^+$ leukocytes at the site of infection, mainly consisting of neutrophils, and bacterial uptake, a population-wide dampening of *S. aureus* growth occurred. In the context of neutrophil-depleted mice, the reduction in bacterial growth rate was partially rescued, but a new cell population appeared, which was not constituted of monocytes, the other cell population recruited upon *S. aureus* infection, but showed similarities to neutrophils with a downregulated and partially masked GR-1 signal. This residual population might partially compensate the neutrophil depletion phenotype in *S. aureus* containment.

NADPH oxidase constitutes a major antimicrobial effector mechanism of neutrophils. In my experiments, the bacterial growth rate was found to be dampened dependently of NADPH oxidase, suggesting that oxidative burst contributes to the pathogen containment by non-lethal restriction of *S. aureus* proliferation. Furthermore, a cell-extrinsic mode of action of reactive oxygen species produced by NADPH oxidase seems to be involved in the growth dampening.

The possibility to probe, in an ongoing infection, the bacterial growth rate on a single cell-resolved level should provide a powerful tool to investigate the host-pathogen interactions during *S. aureus* infections in the future.

ZUSAMMENFASSUNG

M. Sc. Elena A. Seiß (geb. Haas): „Characterization of *Staphylococcus aureus* skin infection using a new *in vivo* proliferation biosensor"

Die bakterielle Wachstumsrate kann entscheidend für den Verlauf einer Infektion sein: Zum einen beeinflusst sie die Empfänglichkeit für Effektormechanismen des Immunsystems, aber auch die Empfindlichkeit gegenüber Antibiotikabehandlungen. Beides kann persistierende und chronische oder wiederkehrende Infektionen begünstigen. Zum anderen produzieren schnell wachsende Bakterien mehr, und zudem auch unterschiedliche pathogenassoziierte Mustermoleküle als nicht proliferierende Bakterien. Dadurch ist es zu erwarten, dass schnell und langsam wachsende Erreger die Immunantwort unterschiedlich aktivieren. Allerdings war es bislang schwierig und aufwendig, die bakterielle Wachstumsrate während einer Infektion zu bestimmen.

In dieser Arbeit habe ich einen *in vivo* Biosensor etabliert, mit dem das Wachstum des Gram-positiven Bakteriums *Staphylococcus aureus* (*S. aureus*) auf der Einzelzellebene in einer laufenden Infektion gemessen werden kann. Die Methode basiert auf dem Fluoreszenzprotein mKikume, das nicht-invasiv mit violettem Licht zu jedem gewünschten Zeitpunkt während der Infektion von roter zu grüner Fluoreszenz photokonvertiert werden kann. Die bakterielle Wachstumsgeschwindigkeit kann dabei über das Wiedererlangen der ursprünglichen grünen Fluoreszenz bestimmt werden. Hierbei konnte ich zeigen, dass das Wachstum des Bakteriums, und nicht der Proteinumsatz in nichtwachsenden Bakterien, entscheidend für das Wiedererlangen der grünen Fluoreszenz von proliferierenden Bakterien ist.

Mit Hilfe der intravitalen Zweiphotonenmikroskopie, sowie quantitativer Fluoreszenz-mikroskopie, konnte ich im Laufe einer Infektion eine populationsweite Abschwächung im Wachstum von *S. aureus* nachweisen. Dies ging einher mit der Einwanderung von $CD45^+$ Leukozyten, hauptsächlich Neutrophile Granulozyten, an den Ort der Infektion. Durch antikörpervermittelte Dezimierung der Neutrophilen wurde die Dämpfung im Wachstum der Bakterien in einer Hautinfektion vermindert. Jedoch wurde in diesem Fall eine neue Immunzellpopulation rekrutiert, welche nicht als Monozyten identifiziert wurden, dem zweiten bei *S. aureus* Infektion rekrutierten Zelltyp, sondern Merkmale von Neutrophilen Granulozyten aufwiesen. Bei diesen Zellen war das Oberflächenmolekül GR-1 herunterreguliert und teilweise maskiert. Diese Restpopulation könnte den Neutrophilen-Depletionsphänotyp teilweise kompensieren.

Die NADPH-Oxidase gehört zu den wichtigsten antimikrobiellen Effektoren von Neutrophilen und beeinflusst, wie ich in der vorliegenden Arbeit zeigen konnte, das

bakterielle Wachstum signifikant. Darüber hinaus wirken die durch NADPH-Oxidase produzierten Sauerstoffradikale offenbar Zell-extrinsisch und demnach über den Ort ihrer Produktion hinaus. Dadurch können die Radikale auch in benachbarten Neutrophilen eine Einschränkung der Bakterienproliferation auslösen.

Die Möglichkeit, während einer laufenden Infektion Informationen über die bakterielle Wachstumsrate auf Einzelzellebene zu erhalten, könnte sich in Zukunft zu einem wichtigen Werkzeug entwickeln, um die Wechselwirkung zwischen dem Pathogen und dem infizierten Wirt besser zu verstehen.

TABLE OF CONTENTS

ABBREVIATIONS

AF	Alexa Fluor
agr	accessory gene regulator
AhpCF	hydroperoxide reductase
AIP	autoinducing peptide
AMP	antimicrobial peptide
AMT	Aminoethyltrioxsalen
AP	alternative pathway
APC	Allophycocyanin
arl	autolysis-related locus
BHI	Brain Heart Infusion
BMC	bone marrow chimera
bp	base pairs
BV	brilliant violet
CA-MRSA	community associated MRSA
CCCP	Carbonyl cyanide m-chlorophenyl hydrazone
CCR2	C-C-motif chemokine receptor 2
CD	cluster of differentiation
CDP	common dendritic progenitor
CFP	cyan fluorescent protein
CFU	colony forming unit
CHIPS	chemotaxis inhibition protein of *S. aureus*
Clf	clumping factor
CLP	common lymphoid progenitor
CMP	common myeloid progenitors
Cna	Collagen adhesin
CP	capsule polysaccharide
	classical pathway
CR	chemokine receptor
	complement receptor
CXCL	CXC-chemokine ligand
CXCR	CXC-chemokine receptor
Cy	Cyanine dye
DAPI	4′,6-Diamidino-2-phenylindole dihydrochloride
DC	dendritic cell
ddH_2O	double distilled water

$DiOC_2$	3,3′-Diethyloxacarbocyanine iodide
DNA	deoxyribonucleic acid
E. coli	*Escherichia coli*
Eap	extracellular adherence protein
Ecb	extracellular complement-binding protein
ECM	extracellular matrix
EDTA	ethylenediaminetetraacetic acid
Efb	extracellular fibrinogen-binding protein
ELISA	enzyme-linked immunosorbent assay
EpiP	epidermin leader peptide processing serine protease
ESAM	epithelial cell adhesion molecule
ET	exfoliative toxin
FACS	fluorescence-activated cell sorting
FcR	Fc receptor
FCS	fetal calf serum
FITC	fluorescein isothiocyanate conjugate
FMO	fluorescence minus one
Fnbp	fibronectin-binding protein
FSC	Forward Scatter
G-CSF	granulocyte-colony stimulating factor
GFP	green fluorescent protein
GM-CSF	granulocyte-macrophage colony stimulating factor
GMP	granulocyte-macrophage progenitors
H_2O_2	hydrogen peroxide
HA-MRSA	hospital-associated MRSA
hBD	human β- defensins
Hla	α-hemolysin, α-toxin
HPC	hematopoietic progenitor cell
HSC	hematopoietic stem cell
i.p.	intraperitoneally
ICAM	intercellular adhesion molecule
IFN	Interferon
Ig	Immunoglobulin
IL	Interleukin
IT	intermediate-term
IVM	intravital microscopy
JAM	junctional adhesion molecule

k.o.	knock out
KatA	Catalase
kb	kilo bases
KBMA	killed but metabolic active
KC	keratinocyte
L. major	*Leishmania major*
LA-MRSA	livestock-associated MRSA
LB	lysogeny broth
LED	light-emitting diode
LFA	lymphocyte function-associated antigen
LMPP	lymphoid-primed multipotent progenitor
LP	lectin pathway
LSM	laser scanning microscope
LT	long-term
LTA	lipoteichoic acid
Luk	leukotoxin
MAC	membrane attack complex
MACS	Magnetic Activated Cell Sorting
MBL	mannose-binding lectin
MELC	Multi-Epitope Ligand Cartography
MEP	megakaryocyte-erythrocyte progenitor
MFI	mean fluorescence intensity
MHC	histocompatibility complex
MntC	manganese transporter protein C
MPO	myeloperoxidase
MPP	multipotent progenitors
MprF	multiple peptide resistance factor
MRSA	Methicillin-resistant *Staphylococcus aureus*
MSCRAMMs	microbial surface component recognizing adhesive matrix molecules
MSSA	methicillin-susceptible *S. aureus*
NADPH	nicotinamide adenine dinucleotide phosphate hydrogen
NE	neutrophil elastase
NET	neutrophil extracellular trap
NK cell	natural killer cell
NOD	nucleotide-binding oligomerization domain protein
NOX	NADPH oxidase
NSP	neutrophil serine proteases

OatA	O-acetyltransferase A
OD	optical density
OH°	Hydroxyl radical
ORF	open reading frame
p.I.	post infection
PAMP	pathogen-associated molecular pattern
PBS	phosphate-buffered saline
PCR	polymerase chain reaction
PE	phycoerythrin
PECAM	platelet/endothelial cell adhesion molecule
PerCP	peridinin chlorophyll protein
PFA	paraformaldehyde
PGN	primarily peptidoglycan
PITs	pore-induced intracellular traps
PRR	pathogen recognition receptor
PSGL	P-selectin glycoprotein ligand
PSM	phenol-soluble modulin
PTSAg	pyrogenic toxin superantigen
PVL	Panton-Valentine leukocidin
QS	quorum sensing
RNA	ribonucleic acid
ROS	reactive oxygen species
rpm	revolutions per minute
S. aureus	*Staphylococcus aureus*
sae	Staphylococcus aureus exoprotein
SAg	Staphylococcal superantigen
SAK	Staphylokinase
sar	staphylococcal accessory regulator
Sbi	second binding protein of immunoglobulin
SCIN	staphylococcal complement inhibitor
ScpA	Staphopain A
SCVs	small colony variants
SD	standard deviation
SD-IVM	spinning-disc intravital microscopy
SE	staphylococcal enterotoxin
sigB	staphylococcal alternative sigma factor B
SOB	super optimal broth

SOC	super optimal broth with catabolite repression
SOD	superoxide dismutase
SodA	superoxide dismutase A
SOK	surface factor promoting resistance to oxidative killing
SpA	*Staphylococcus* protein A
SSC	Side Scatter
SSCmec	staphylococcal chromosome cassette *mec*
SSL	staphylococcal superantigen-like
Ssp	*staphylococcus* serine protease
SSS	scalded skin syndrome
SSTIs	skin and soft tissue infections
ST	short-term
T_H	helper T cell
TLR	Toll-like receptor
TNF	tumor necrosis factor
TSS	toxic shock syndrome
TSST	including toxic shock syndrome toxin
U	Units
v/v	volume per volume
VCAM	vascular cell adhesion protein
w/v	weight per volume
wt	wild type

1 INTRODUCTION

1.1 *Staphylococcus aureus* – A commensal out of control

1.1.1 Pathogenesis and antibiotic resistance

The coccoid Gram-positive bacterium *Staphylococcus aureus* (*S. aureus*) is about 0.5 to 1.0 µm in diameter and forms grape-like clusters ("*staphylos"* means grape in greek) by multiple symmetrical cell divisions of individual bacteria. The bacterium persistently colonizes around 30% of the human population, whereas an additional 30% of individuals are intermittent carriers (Nouwen *et al.*, 2004). Despite this seemingly harmless occurrence, *S. aureus* can cause a variety of infectious disease pathologies in humans and animals, whereby asymptomatically colonized individuals have a higher risk to be clinically infected (Lowy, 1998).

As a commensal, *S. aureus* colonizes most frequently the nose (Armstrong-Esther, 1976). Other organs that are typically colonized are the skin, throat, perineum, pharynx and, less commonly, the gastrointestinal tract, vagina, and axillae (Williams, 1963; Armstrong-Esther, 1976; Ridley, 1959; Wertheim *et al.*, 2005b; Rimland *et al.*, 1986; Guinan *et al.*, 1982; Dancer *et al.*, 1991). Regular persistent carriers are colonized by a single strain of *S. aureus* over long time periods with a high load, whereas for intermittent carriers the strains can vary over time (VandenBergh *et al.*, 1999; Nouwen *et al.*, 2004). To become a nasal carrier, the nose has first to be reached by *S.* **aureus**, and the bacterium has to adhere there. Afterwards the bacterium needs to overcome the host defenses and has to prevail towards other commensals to be able to propagate in the nose as a persisting pathogen (Wertheim *et al.*, 2005a). The bacteria of the tissue microbial flora compete for adhesion sites or nutrients, and interfere with each other by production of antibiotic compounds or by induction of low-grade host defenses, which some of the microorganisms can withstand better than others and thus obtain a selective advantage (Krismer *et al.*, 2017). However, when the epithelial barrier breaks or the immune system is compromised, a commensal bacterium can turn into a pathogen (Otto, 2009; Lowy, 1998).

A variety of human infections are caused by several Gram-positive bacteria, and besides *S. aureus*, *Staphylococcus epidermidis* is one of the most abundant causative agents of such infections (Otto, 2009; Lowy, 1998). Hence, for definitive diagnosis of a *S. aureus* infection, other coccoid and Gram-positive pathogens, like *Streptococci* and *S. epidermidis* have to be excluded first. For example, *Streptococci* are, in contrast to *S. aureus*, catalase-negative, and *S. epidermidis* is a coagulase-negative *Staphylococcus*, which for a long time has represented the basis for diagnosing *S. aureus* (Facklam *et al.*, 1995; Martinez-

Melendez *et al.*, 2016). For the coagulase test, a colony is mixed with rabbit blood, which than coagulates only in presence of *S. aureus*, but not *S. epidermidis*. Furthermore, *S. aureus* can be identified by other characteristics, as it is positive for urease, ferments mannitol to lactic acid and shows hemolysis on blood agar plates (Reddy *et al.*, 2017; Connolly *et al.*, 2017).
For finding an appropriate therapeutic approach, the virulence factors of the infecting *S. aureus* strain have to be determined. For this, several techniques are available, such as enzyme-linked immunosorbent assay (ELISA), polymerase chain reaction (PCR), real-time PCR, mass spectrometry, and biosensor techniques (Reddy *et al.*, 2014; Zhao *et al.*, 2017; Nagaraj *et al.*, 2014; Chiang *et al.*, 2008; Horsmon *et al.*, 2006; Dupre *et al.*, 2015; Sapsford *et al.*, 2005).

After breaching the physical barriers of the host, *S. aureus* can cause a wide range of clinical infections and syndromes, from minor to superficial skin and soft tissue infections (SSTIs) up to systemic and other life-threatening infections, such as bacteraemia, osteomyelitis, and meningitis. Additionally, the toxins of *S. aureus* can cause toxinoses, such as scalded skin syndrome, food poisoning, and toxic shock syndrome (TSS) (Tong *et al.*, 2015). For persistently colonized individuals and humans with immunosuppression, the risk of *S. aureus* infection is much higher compared to non-carriers (Kluytmans *et al.*, 1997).

S. aureus infections are regularly treated with antibiotics like penicillin, against which the pathogen rapidly develops resistance (Lowy, 2003). Hence, new antibiotics, like methicillin had to be developed. Several common antibiotics and *S. aureus* mechanisms of resistance are listed in **Table 1.1**. Furthermore, relapsing infections are accounted to intracellularly residing *S. aureus*, because these bacteria are assumed to be partially protected against the immune response, and shielded from antibiotics. Related to this, intracellular persistent viable bacteria, so-called small colony variants (SCVs), occur during chronic *S. aureus* infections (Proctor *et al.*, 2006). An important characteristic of these bacteria is the formation of very small, low-pigmented colonies with decreased hemolysis on blood agar plates, and a reversible auxotrophy (Proctor *et al.*, 1994). For such bacteria, it is possible to persist for decades in host cells and withstand antibiotic treatment and the host immune response, a phenotype that seems to be linked to their low proliferation rate (Proctor *et al.*, 1998; Tuchscherr *et al.*, 2011).

Table 1.1: Antibiotics and resistance mechanisms. Combined out of Lacey, 1975, Wilson, 2014, and Howden *et al.*, 2010.

Antibiotic	Group	Target site	*S. aureus* strategy
Clindamycin	Lincosamides	Protein synthesis, 50s ribosomal subunits, peptidyl-transferase center	Drug modification/ degradation, efflux/ membrane permeability, target alteration via modification, target mutation
Erythromycin	Macrolide antibiotics	Protein synthesis, 50s inhibitor, nascent chain elongation	Drug modification/degradation, efflux/membrane permeability, target alteration via modification, target mutation
Methicillin	β-lactam antibiotics	Cell wall synthesis (Binding to DD-transpeptidase)	β-lactam insensitive penicillin-binding protein 2 with transpeptidase domain
Penicillin	β-lactam antibiotics	Cell wall synthesis (Binding to DD-transpeptidase)	Hydrolysis of β-lactam bound (β-lactamase)
Streptomycin	Aminoglycoside antibiotics	Protein synthesis, 30s ribosomal subunits inhibitor, translocation of tRNA	Drug modification/degradation, efflux/membrane permeability, target alteration via modification, target mutation
Tetracycline	Tetracyclines	Protein synthesis, 30s ribosomal subunits inhibitor, translocation of tRNA	Antibiotic efflux, or ribosomal protection
Vancomycin	Glycopeptides	Cell wall synthesis, inhibits late-stage peptidoglycan biosynthesis at the outside the cytoplasmic membrane	Cell wall thickening, reduced cell wall turnover, capsule and restricted vancomycin access

Since the 1960s, methicillin-resistant *S. aureus* (MRSA) are known as an emerging hospital-acquired infection (Barrett *et al.*, 1968). Characteristic of MRSA strains is a mobile genetic element, the staphylococcal chromosome cassette *mec* (SSC*mec*) (Katayama *et al.*, 2000). The SSC*mecA* encodes the resistance against penicillin and confers resistance to a broad spectrum of β-lactam antibiotics. MRSA strains are classified via SSC*mecA*, *B*, *C*, and *D*. Typically, MRSA strains often display multiple resistances to a number of antimicrobial agents, like erythromycin or clindamycin (Speller *et al.*, 1997). The treatment of such multi-drug resistant strains is even more difficult, since they are less susceptible to vancomycin (Bierbaum *et al.*, 1999). Vancomycin is not a β-lactam, but a glycopeptide antibiotic, but also targets the synthesis of the cell membrane of Gram-positive bacteria.

Hospital-associated MRSA (HA-MRSA) is a major reason for nosocomial infections and additionally, patients having a compromised immune system are at higher risk for such infections. Moreover, nasal MRSA carriers have a four times higher risk to develop a nosocomial bacteraemia than carriers of methicillin-susceptible (so-called MSSA) strains

(Pujol *et al.*, 1994). HA-MRSA is very difficult to treat and infections with such strains have a much higher mortality and morbidity than with MSSA (Kock *et al.*, 2010). MRSA infections therefore represent an important socioeconomic problem, with 150,000 patients reported annually in the European Union (Kock *et al.*, 2010). Additionally, in the 1990s, community-associated MRSA (CA-MRSA) infections were reported for the first time (Udo *et al.*, 1993). Such bacterial infections are found in community-based individuals without healthcare system contact. Commonly, CA-MRSA strains were originally reported to mainly cause SSTIs, but are nowadays also found to be responsible for healthcare-associated infection (Otter *et al.*, 2011; Maree *et al.*, 2007). Characteristic for CA-MRSA is a resistance to a lower number of non-β-lactam antibiotics and the presence of a smaller SCC*mec* compared to HA-MRSA strains (Daskalaki *et al.*, 2007; Ito *et al.*, 2003; Ma *et al.*, 2002). Furthermore, the two-component, pore-forming, cytolytic toxin Panton-Valentine leukocidin (PVL), was reported as been strongly associated with CA-MRSA, which makes it more virulent than many HA-MRSA strains, with the toxin causing cell death by necrosis or apoptosis in both mononuclear and polymorphonuclear cells (Boyle-Vavra *et al.*, 2007). However, in recent years, the epidemiological and molecular borders became blurred between CA-MRSA and HA-MRSA (Saiman *et al.*, 2003; Saunders *et al.*, 2007).

While HA- and CA-MRSA are under intensive research due to their importance as human pathogens, *S. aureus* can also infest animals. In particular, livestock-associated MRSA (LA-MRSA) infections are attracting more attention. A first strain was isolated in 1972 from a cow (Devriese *et al.*, 1972) and in 2005, pig farmers in Germany got colonized with the LA-MRSA (Kock *et al.*, 2014). Even though LA-MRSA strains are likely to originate from pig farming, they are reported in several animal species, where they are causing infections like mastitis in dairy cows, sheep or goats (Bradley, 2002; Menzies *et al.*, 2001), osteomyelitis in broiler chickens (McNamee *et al.*, 2000) or mastitis, pododermatitis and subcutaneous abscesses in rabbits (Vancraeynest *et al.*, 2006). Due to their relevance in farm animals, the LA-MRSA have the potential to become an important economic problem.

1.1.2 Staphylococcal virulence factors

The pathogenicity of *S. aureus* is multifactorial and constituted by a series of well-orchestrated factors, including toxins, surface proteins, and enzymes. They are expressed either to be presented at the cell wall or for secretion into the extracellular space. The virulence factors are listed in **Table 1.4** more in detail, and the most important ones are exemplarily described below.

Adhesion

As a first step of colonization, *S. aureus* has to attach to the host tissue. This is mediated by so-called microbial surface component recognizing adhesive matrix molecules (MSCRAMMs), which interact with prominent components of extracellular matrix (ECM) or plasma (Foster *et al.*, 1998). *Staphylococcus* protein A (SpA), fibronectin-binding proteins (Fnbp) A and B, collagen-binding protein, *S. aureus* collagen adhesin (Cna), *staphylococcus* serine protease (Ssp) A, and clumping factor (Clf) A and B belong to such MSCRAMMs (Lowy, 1998; Patti *et al.*, 1994). For example, SpA is considered a member of this group because it can bind, among other functions, to the von Willebrand factor of platelets. This large glycoprotein typically mediates platelet adhesion at sites of endothelial damage (Cheung *et al.*, 2002). With SpA, *S. aureus* can bind to platelets under shear stress, which leads to formation of thrombi and subsequently the possibility for *S. aureus* to bind via Cna to collagen at the subendothelium for infection (Mascari *et al.*, 2003). Such infective thrombi are one possible way for the pathogen to initiate infective endocarditis (Tong *et al.*, 2015).

Exotoxins

By the secretion of enzymes, the bacterium modulates its environment in this way that nutrients become available, or to prevent killing by host cells. Nucleases, proteases, lipases, hyaluronidases and collagenases are representatives of such expressed enzymes (Dinges *et al.*, 2000). For example, the epidermin leader peptide processing serine protease (EpiP) cleaves collagen (Kuhn *et al.*, 2014).

Some *S. aureus* strains produce also exotoxins, including toxic shock syndrome toxin-1 (TSST-1), staphylococcal enterotoxins (SEA, SEB, SEC, SED, SEE, SEG, SEH, and SEI), exfoliative toxins (ETA and ETB), and leucocidin (Dinges *et al.*, 2000). SEs and TSST-1 are grouped as pyrogenic toxin superantigens (PTSAgs) (Lina *et al.*, 2004). Two prominent diseases, which are caused by PTSAgs are TSS and food poisoning (Dinges *et al.*, 2000). TSS is a shock syndrome, based on vascular leakage and respiratory failure, which is mediated by a cytokine storm and pathogen virulence protein-mediated neutrophil activation, based on release of superantigens (SAgs) into the blood stream (Low, 2013).

ETA and ETB, which are not members of the PTSAgs, are responsible for scalded skin syndrome (SSS) (Melish *et al.*, 1970). The SSS is accompanied with skin erythema and separation. The exfoliative toxins hydrolyze an extracellular domain of desmoglein 1, which normally mediates cell-cell adhesion (Amagai *et al.*, 2002). This induces a disruption of keratinocyte adhesion and cleavage within the stratum granulosum and leads subsequently to blister formation (Amagai *et al.*, 2000).

Cytolytic toxins

Cytolytic toxins are used of *S. aureus* to avoid killing by host cells through lysis of target effector cells of the immune system (Menzies *et al.*, 1998). For this, these toxins form two-component hetero-heptameric β-barrel pores in the host membrane. Members of cytolytic toxins are α- (Hla, α-toxin), β- and γ-hemolysin, bicomponent leukotoxins (LukED, LukAB), and PVL (Kaneko *et al.*, 2004). Often, highly virulent *S. aureus* strains secrete cytolytic toxins after phagocytosis or during biofilm formation (Geiger *et al.*, 2012; Dastgheyb *et al.*, 2015). For example, PVL is a pore-forming toxin that induces apoptotic or necrotic cell death of white blood cells (Tong *et al.*, 2015). PVLs are associated with higher infectious *S. aureus* strains in skin infections and bacteraemia (Wang *et al.*, 2007). Additionally, Labandeira-Rey *et al.* showed that PVL alone is sufficient to cause necrotizing pneumonia (Labandeira-Rey *et al.*, 2007).

Another group of cytolytic toxins are phenol-soluble modulins (PSMs), a family of α-helical peptides, which are produced by some *staphylococci*. By PSMα, *S. aureus* can form pores and damage for example keratinocytes during epidermal colonization (Wang *et al.*, 2007; Nakagawa *et al.*, 2017). Thus, the keratinocytes produce the proinflammatory cytokines, like IL-1α, which is followed by IL-17 production and neutrophil recruitment. It is assumed that PSMα is, among other factors, responsible for the inflammation in atopic dermatitis (Nakagawa *et al.*, 2017).

Staphylococcal superantigens

Staphylococcal superantigens (SAgs) are a group of exotoxins to manipulate the immunity of the host. Traditional SAgs are understood as antigens, which bind to major histocompatibility complex (MHC) class II and TCR. This induces undirected T cell activation (Fraser *et al.*, 2008). SAgs can interact through conserved variable-region sites on antigen receptors, mainly Vβ-chain. The main group of SAgs are staphylococcal enterotoxins, but also TSST-1 belongs to SAgs (Tuffs *et al.*, 2018). The crosslinking of TCR of T cell with MHC class II of an antigen presenting cell (APC), in not specific to a processed antigen peptide. Consequently, the activation of T cells by SAgs is not antigen specific, which results in an uncontrolled and polyclonal activation of T cells (Tuffs *et al.*, 2018).

Additional to T cell specific factors, B cell SAgs have been identified. One example is the virulence factor SpA, expressed in soluble form or on the surface of *S. aureus*. It has five Ig-binding domains, which bind the Fcγ domain of IgG and the V_H3 of Fab of IgG and IgM (Roben *et al.*, 1995; Graille *et al.*, 2000). With this protein, the pathogen can cross-link B cell receptors (surface immunoglobulin) at highly conserved regions, and induce polyclonal proliferation of B cells. As a result, *S. aureus* achieves a SAg-induced modulation of the B cell compartment. Another member of B cell SAgs of *S. aureus* is the soluble SED, which binds to V_H4 of Fab of immunoglobulins (Kallee, 1996).

Regulation of virulence factors

The expression of virulence factors is assumed to be mainly regulated by accessory gene regulator (*agr*) and staphylococcal accessory regulator (*sar*), but also *S. aureus* exoprotein (*sae*), staphylococcal alternative sigma factor B (*sigB*) and autolysis-related locus (*arl*) are connected to the global regulatory loci (Bien *et al.*, 2011). The network of the *agr* and *sar* loci is schematically illustrated in **Figure 1.1**. For example, the *agr* locus regulates the production of several secreted toxins, including Hla, proteases and coagulase. The virulence gene regulators can act directly by binding on the promoter of the target gene or indirectly by means of other regulators: *agr* regulates the expression of *spa* (encoding SpA) by regulating the expression of *sarS* (encoding SarS), while SarS activates the expression of *spa* via binding to its promoter (Cheung *et al.*, 2001; Tegmark *et al.*, 2000).

The *agr* operon includes three promoters P1-P3. While P1 regulates the expression of *agrA* (Rajasree *et al.*, 2016), P2 controls the production of the whole Agr-system: AgrB, D, C, and A, grouped as RNAII (Le *et al.*, 2015). The activation of the third promoter, P3, is dependent on AgrA and regulates the production of effector RNAIII (Rajasree *et al.*, 2016). RNAIII regulates several secreted and cell-surface associated virulence factor of *S. aureus*, such as SpA, FnBP-A and -B, PSMs and leukocidins (Arvidson *et al.*, 2001). The activity of the *agr* operon in *S. aureus* is, among other regulators, controlled via quorum sensing (QS). QS enables the regulation of genes as a result of the communication between bacteria and detection of the environment of a bacterium, such as bacteria density (Yarwood *et al.*, 2004). The extracellular quorum signal is given by autoinducing peptide (AIP). The precursor peptide, which maturation takes until it is in the extracellular milieu, is encoded in *agrD* (Ji *et al.*, 1995; Kavanaugh *et al.*, 2007). AgrB transports the AIP precursor through the membrane. The neighboring staphylococcal bacteria then can detect the signal by the histidine kinase sensor AgrC, which phosphorylates its second component AgrA (Lina *et al.*, 1998; Novick *et al.*, 1995). AgrA in turn binds to P2 and P3 of the *agr* locus (Koenig *et al.*, 2004).

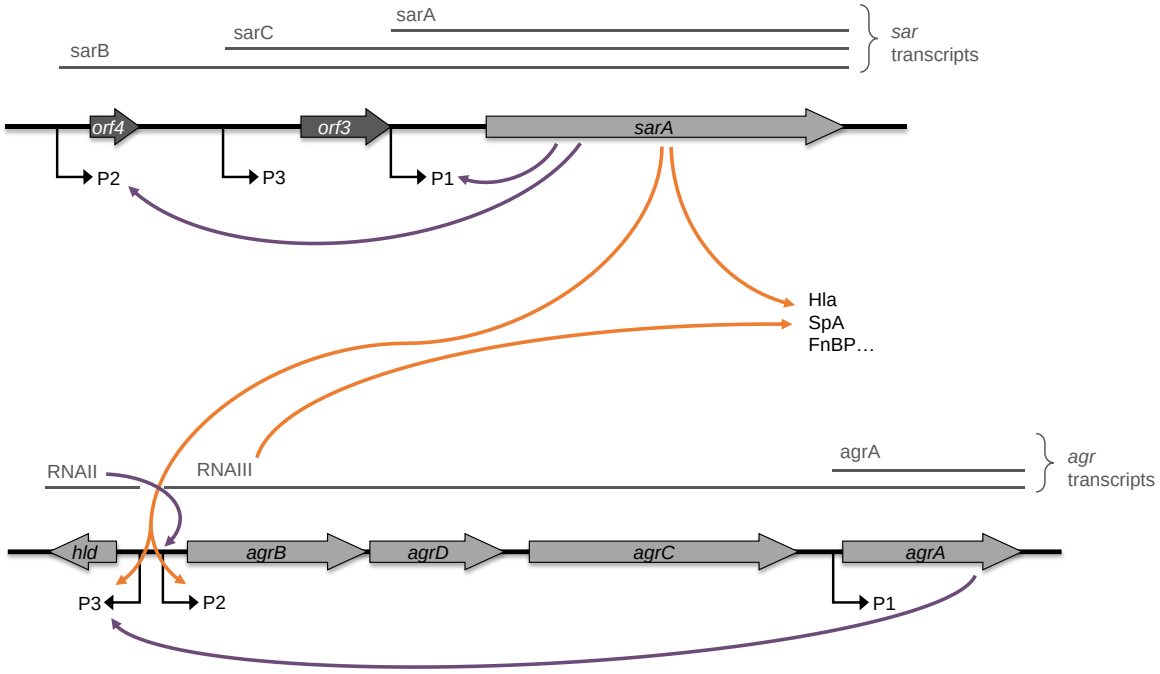

Figure 1.1: The network of the *agr* and *sar* loci. Regulation of virulence factors by staphylococcal accessory regulator A (SarA) and accessory gene regulator (Agr). Purple: internal support of transcription and positive feedback, orange, external regulation of transcription. FnBP= fibronectin-binding protein, Hla= α-hemolysin/ α-toxin, orf= open reading frame, P= promoter, SpA= *S. aureus* protein A. Modified from Bischoff *et al.*, 2001 and Manna *et al.*, 2003.

The *sar* locus contains three overlapping transcripts, *sarA*, *C*, and *B*, with three distinct promoters P1, P3, and P2 (Bayer *et al.*, 1996). It is shown that the P1 promoter is the strongest one and that P1 and P2 are more active in the exponential and early stationary growing phase, as compared to the P3 promoter, which is stronger at the stationary growing phase (Manna *et al.*, 1998). This indicates a QS dependent activity of the promoters. All three transcripts encode SarA. *sarC* encodes additionally the open reading frame (ORF) 3, and *sarB* also ORF3 and 4 (Bayer *et al.*, 1996). SarA is required for an optimal transcription of RNAII and RNAIII in the *agr* locus (Cheung *et al.*, 1997; Cheung *et al.*, 2008).

1.2 The immune response against *S. aureus*

The immune system employs an array of specialized cell types and systems to act against invasive pathogens like *S. aureus*, an overview on which will be given in this chapter. However, the central cell type involved in the host defense against *S. aureus* is the neutrophil. Neutrophils are among the first immune cells in the combat against bacterial infections. Together with other professional phagocytic cells, such as macrophages and monocytes, they contain a set of antimicrobial mechanisms to kill Gram-positive bacteria (Spaan *et al.*, 2013). After phagocytosis of *S. aureus*, neutrophils can kill the bacterium in the phagosomes by antimicrobial peptides (Stapels *et al.*, 2015), which are stored in their granules, together with reactive oxygen species (ROS) (Anderson *et al.*, 2008), which are produced by Nicotinamide adenine dinucleotide phosphate (NADPH) oxidase. Extracellular bacteria can be caught and killed via neutrophil extracellular traps (NETs), which comprise chromatin and antimicrobial proteins (Sollberger *et al.*, 2018b). Individuals with defects in one of these phagocyte-related defenses suffer from severe and life-threatening bacterial infections (Lekstrom-Himes *et al.*, 2000).

1.2.1 The course of the immune response against *S. aureus* infections

The body's primary barrier against pathogens from the surroundings is the skin. On its surface, bacteria are confronted with an environment that is hostile to bacterial growth: commensal organisms that already occupy suitable niches, as well as low temperature and pH. For example, it has been shown that microorganisms naturally occupying the skin inhibit *S. aureus* colonization (Iwase *et al.*, 2010). Furthermore, the corneal layer, which underlies a physical barrier of dead keratinocytes, produces several antimicrobial peptides (AMPs), for example RNase7, with bacteriostatic or bactericidal effects on *S. aureus* (Zhang *et al.*, 2003). A schematic overview on the cutaneous immune system is illustrated in **Figure 1.2**.

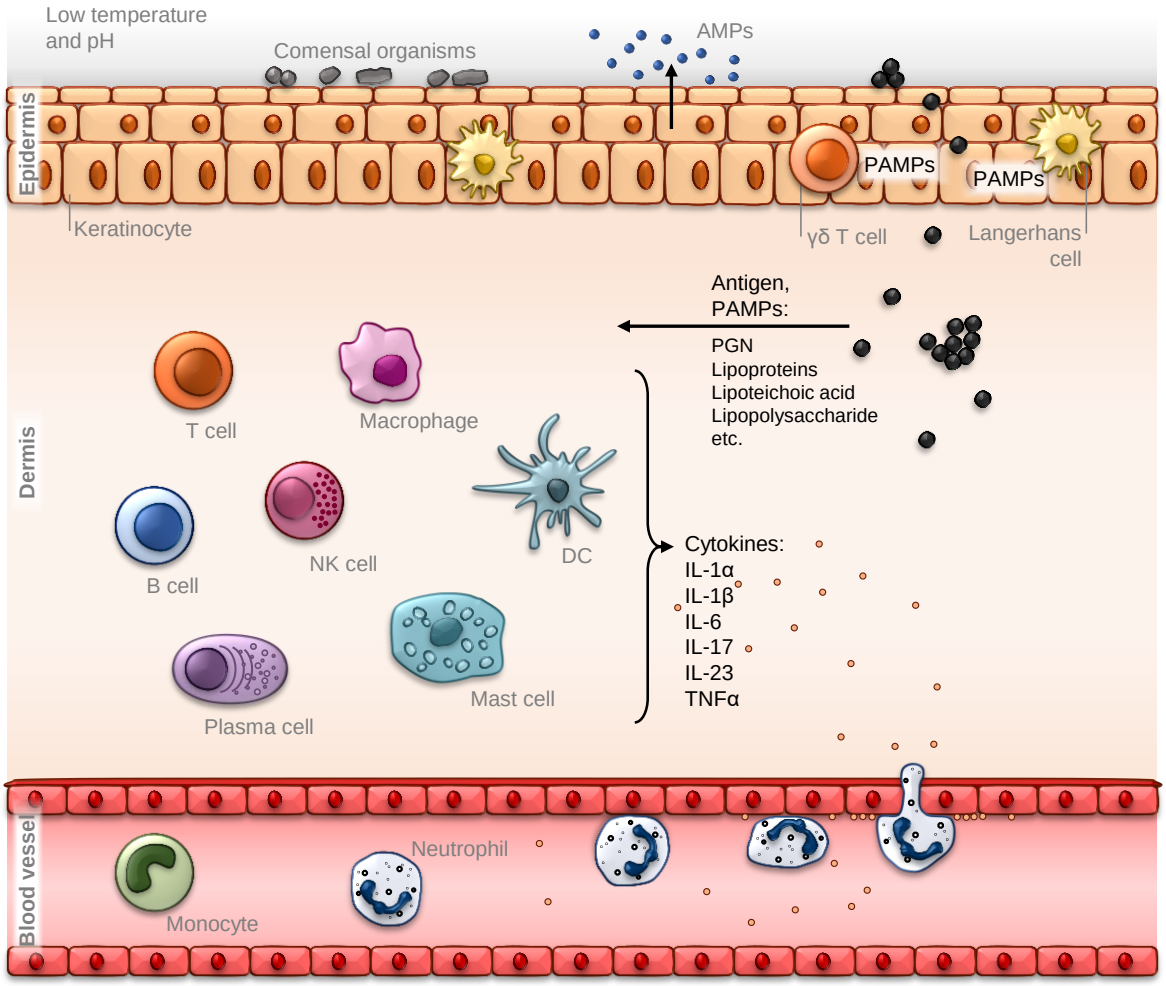

Figure 1.2: Cutaneous immune response. Keratinocytes secrete antimicrobial peptides (AMPs) to prevent infections. Bacteria produce pathogen-associated molecular patterns (PAMPs, PGN= primarily peptidoglycan) during their typical metabolism, which also occur when the bacteria die. Some immune cells recognize these PAMPs and antigens and secrete pro-inflammatory cytokines, like interleukins (IL) and tumor necrosis factor (TNF), to recruit neutrophils and monocytes (DC= dendritic cell, NK cell= natural killer cell). Modified from Miller *et al.*, 2011 and Brandt *et al.*, 2018b.

In case *S. aureus* manages to overcome these initial barriers and invades into the tissue, its presence is detected by pathogen recognition receptors (PRR) of several cells contributing to the cutaneous immune system, like keratinocytes (KCs) or Langerhans cells (Bitschar *et al.*, 2017). Examples for PRRs are Toll-like receptor (TLR) 1, 2, and 6 or, in case of cytosolic presence of PRRs, nucleotide-binding oligomerization domain proteins (NODs), which sense pathogen-associated molecular patterns (PAMPs) of the invading pathogen (Kawai *et al.*, 2011; Miller, 2008). In the lower dermis, macrophages, dendritic cells (DCs), mast cells, B and T cells, natural killer (NK) cells, plasma cells and fibroblasts may detect the pathogen and its PAMPs. The alarmed cells secret pro-inflammatory cytokines, including interleukin (IL) 1α, IL-1β, IL-6, IL-17, IL-23, and tumor necrosis factor (TNF) (Serbina *et al.*, 2003; Wohn *et al.*, 2013; Pasparakis *et al.*, 2014). Specifically, the detection of *S. aureus* by tissue resident DCs or macrophages via their TLR2, activate these cells to produce IL-1α/β, -6 and -23 (Serbina *et al.*, 2003). This in turn is detected by T cells and NK cells in the skin and leads them to produce IL-17A and B (Gray *et al.*, 2011; Cho *et al.*, 2010). Subsequently, neutrophils are recruited as a result of the production of pro-inflammatory cytokines, chemokines and adhesion molecules of stimulated keratinocytes (Miller *et al.*, 2011). T_H17 cells, which are induced as a result of an inflammatory milieu rich in IL-1, IL-6 and IL-23, are producers of IL-17 (A and F). This cytokine in turn strongly enforces the immune response by neutrophils in two ways: first, by inducing the secretion of the chemoattractants for neutrophil recruitment and second, by upregulation of the expression of the granulopoiesis-inducing factors granulocyte-colony stimulating factor (G-CSF) and granulocyte macrophage-colony stimulating factor (GM-CSF), increasing the production of neutrophils (Sandquist *et al.*, 2018). By producing IL-17 and thus powerful effecting on the neutrophil recruitment, T_H17 cells therefore support as adaptive immune cells the innate immune system. Moreover, IL-17 stimulates keratinocytes, in combination with IL-22, to produce more antimicrobial peptides to act against infections (Liang *et al.*, 2006) and furthermore, to produce IL-21 and IL-22, to support wound healing by endothelial cells (Caruso *et al.*, 2009). It is known that patients with gene defects for T_H17 cells suffer from relapsing *S. aureus* infection (Milner *et al.*, 2008).

Recruitment of neutrophils

The cascade of events neutrophil recruitment out of the vasculature into the tissue includes four canonical steps of rolling, adhesion, crawling and transmigration (**Figure 1.3**). Stimulated by recognition of cytokines that are produced by cells at the site of infection, vascular endothelial cells increase surface expression of the adhesion molecules P- and E-selectin (Yao *et al.*, 1996; Bevilacqua *et al.*, 1989). Neutrophil surface ligands like P-selectin glycoprotein ligand (PSGL) -1 bind the selectins, which leads to capturing and subsequently, slowing down of circulating neutrophils and thus rolling along the endothelium (Yago *et al.*, 2010). Additionally, neutrophil chemokine receptors (CR) recognize chemokines expressed by the endothelial cells, which activates their adhesion to the vascular endothelium. In particular, to fully activate neutrophils and induce adhesion to endothelial cells, an additional chemokine signal has to be recognized by CXC-chemokine receptor (CXCR) 2. The CXCR2 is expressed on the surface of circulating neutrophils and senses CXC-chemokine ligand (CXCL) 1, 2, 5 or 8, which mediates chemoattraction, hence recruitment of neutrophils (Massena *et al.*, 2010; Herbold *et al.*, 2010). The activation of the G-protein-coupled CR leads to a change in the conformation of integrins, such as the lymphocyte function-associated antigen (LFA) -1 and macrophage-1 antigen MAC-1 on the cell surface (Blanks *et al.*, 1998; Laudanna *et al.*, 2002). Active integrins exhibit higher affinities for endothelial surface molecules, like the intercellular adhesion molecules ICAM-1 and ICAM-2, whereby the binding of LFA-1 to ICAM-1 is necessary for adhesion of neutrophils (Kuwano *et al.*, 2010; Ledebur *et al.*, 1995). This interaction induces outside-in-signaling in neutrophils, stabilizing their adhesion and initiating crawling cell motility (Gorina *et al.*, 2014; Li *et al.*, 2018). Along the membrane-bound intravascular chemokine gradient, the neutrophils crawl actively by interaction of neutrophil MAC-1 and endothelial ICAM-1 along endothelial cells to appropriate sections for transmigration (Li *et al.*, 2013; Gorina *et al.*, 2014). For paracellular transmigration, cell-cell junctions are preferred, but also regions with low matrix protein expression or a gap between pericytes are chosen by neutrophils. In the transmigration of neutrophils, ICAM-1, ICAM-2, and vascular cell adhesion protein (VCAM) 1 as well as several junctional proteins, like the platelet/endothelial cell adhesion molecule (PECAM) 1, CD99, junctional adhesion molecule (JAM) or epithelial cell adhesion molecule (ESAM) are involved (Griffin *et al.*, 2012; Iademarco *et al.*, 1992; Wang *et al.*, 2006; Kolaczkowska *et al.*, 2013).

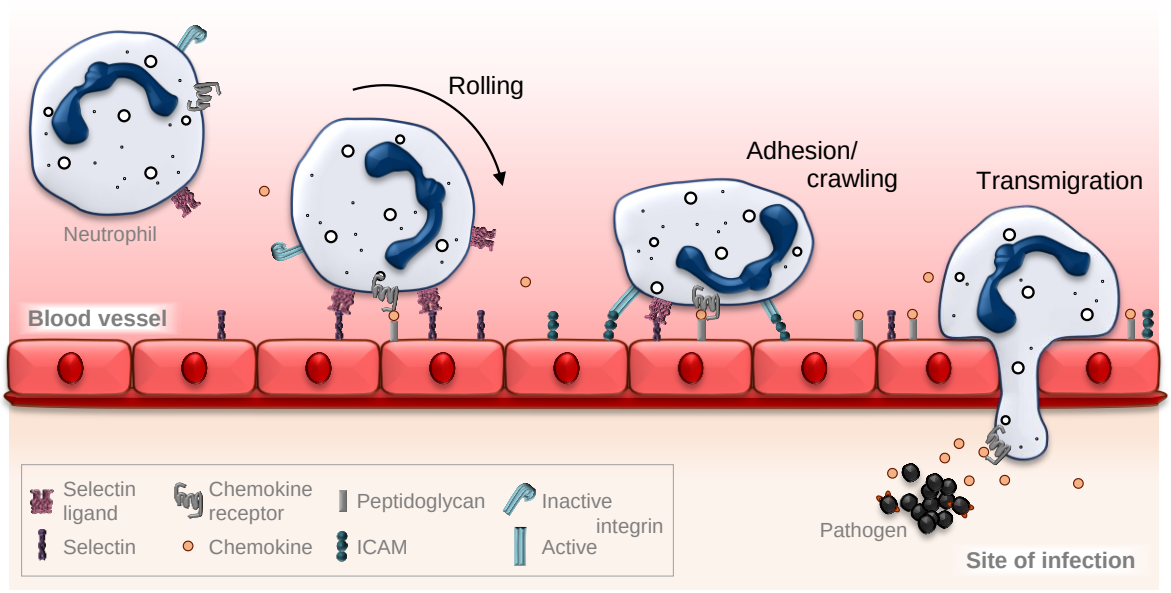

Figure 1.3: Neutrophil recruitment cascade. The canonical steps of neutrophil recruitment out of the vasculature to the site of infection are rolling, adhesion, crawling, and transmigration. On the side of the neutrophils selectin ligands, chemokine receptors, and integrins are involved, which interact with selectins, chemokines, and intercellular adhesion molecules (ICAM) at the surface of the endothelial cells. Modified from Kolaczkowska *et al.*, 2013 and Spaan *et al.*, 2013.

At the site of infection, arriving neutrophils detect PAMPs, small conserved motifs of the pathogen, via surface PRRs, for example TLR2. *S. aureus* produces several surface-bound and secreted PAMPs, such as peptidoglycan (PGN), lipoproteins, lipoteichoic acid (LTA), lipopolysaccharide, CpG-containing DNA and flagellin. Intracellular bacteria are sensed by NOD-like receptors and TLRs. For example, NOD2 detects the *S. aureus* PGN muramyl dipeptide, TLR9 on the other hand is sensitive for CpG-containing DNA (Girardin *et al.*, 2003; Inohara *et al.*, 2003; Chen *et al.*, 2011).

Opsonization of pathogens and chemotaxis

Invading bacteria are sensed and then opsonized by several complement effector molecules, which promotes killing of the pathogen by neutrophils and macrophages, and activation of mast cells. The complement system is an interaction of plasma proteins, in which an enzymatic cascade becomes strengthened and sequentially activated after recognition of a pathogen. Opsonized bacteria are recognized by several complement receptors (CRs) and multiple Fc receptors (FcRs) expressed by professional phagocytes like neutrophils (**Table 1.2**).

Table 1.2: Receptors for opsonization and complement. Combined for complement receptors out of Dustin, 2016 and Ricklin *et al.*, 2010 and for FcγR receptors in mice out of Solomon *et al.*, 2005 and Nimmerjahn *et al.*, 2005.

Receptor	Ligand	Cell types	Function
Complement receptors (CR)			
CR1 (CD35)	C3b, iC3b, C4b	Basophils, eosinophils, macrophages, neutrophils	Induces phagocytosis. Accelerates decay of convertases. C3b/C4b regulation.
CR2 (CD21)	C3d, iC3b	B cells, DCs	Lower threshold for B cell stimulation.
CR3 (CD11b/CD18, Mac-1)	iC3b, C3d, ICAM-1, Fibrinogen	Basophils, DCs, eosinophils, macrophages, neutrophils, T cells	Induces phagocytosis. Modulates IL-12 family in APCs. Enhances migration.
CR4 (CD11c/CD18, p150/95)	iC3b, ICAM-1, -2, VCAM, denatured proteins	DCs, macrophages, neutrophils, T cells	Induces phagocytosis. Enhances migration.
C3aR	C3a	DCs, macrophages	Triggers proinflammatory signalling: chemotaxis, activation.
C5aR (CD88)	C5a	Macrophages, monocytes, neutrophils, T cells	Triggers proinflammatory signalling: chemotaxis, activation.
CRIg	C3b, iC3b	Kupffer cells, macrophages, mast cells	Induces phagocytosis. Regulatory effect on C5 convertases.
Fcγ-Receptors (FcγR)			
FcγRI (CD64)	IgG1, IgG3	DCs, macrophages, monocytes	Stimulatory effect. Induces phagocytosis.
FcγRII (CD32)	IgG1, IgG3	B cells, DCs, macrophages, mast cells, neutrophils, NK cells,	Inhibitory receptor of immunoglobulin-induced B cell activation.
FcγRIII (CD16)	IgG1, IgG3	DCs, macrophages, neutrophils,	Stimulatory effect. Neutrophil recruitment.
FcγRIV (CD16.2)	IgG2, IgE	DCs, macrophages, monocytes, neutrophils	Stimulatory effect.

The presence of bacteria is associated with the occurrence of a variety of different complement components, including the chemoattractants C5a, Ba and C3a, and the opsonin C3b. For example, C3b will be sensed by CR1, which subsequently leads to phagocytosis.

The complement, which is schematically illustrated in **Figure 1.4**, can be divided into the classical (CP), the lectin (LP), and the alternative pathway (AP). In the CP, immunoglobulins bound to the surface of the bacterium, are detected by C1, which contains three subcomponents C1q, C1r and C1s (Schumaker *et al.*, 1987; Colomb *et al.*, 1984). In contrast, the LP is initiated by the recognition of mannose on the surface of the bacterium by mannose-binding lectin (MBL), which activates the MBL-associated serine proteases MASP-1 and MASP-2 (Thiel *et al.*, 1997; Wallis *et al.*, 2010). Both pathways, CP and LP, continue with the formation of the classical C3 convertase, C4b2a, via activation of C4 and C2 (Schumaker *et al.*, 1987; Muller-Eberhard *et al.*, 1967). C4b2a can split C3 into the small fragment C3a, which in turn activates mast cells, and the bigger fragment C3b, which covalently binds to the bacterial surface to opsonize the pathogen (Cooper *et al.*, 1970; Takata *et al.*, 1987). This, supported by various factors (B, D, H, I), activates the AP via the alternative C3 convertase C3bBb, which promotes further splitting of C3 into C3a and C3b and thus further increases opsonization of the bacterium (Pangburn *et al.*, 1981; Pangburn *et al.*, 1978; Fearon *et al.*, 1977). Furthermore, C4bC2a and C3b (coming from the CP and the LP) as well as C3bBb and C3b (coming from the AP) assemble into C5 convertases (Takata *et al.*, 1987; Rawal *et al.*, 2008; Medicus *et al.*, 1976). The C5 convertase cleaves C5 into C5a (a soluble chemoattractant for neutrophils) and C5b. C5b binds to C6, C7 and C8 on the pathogen surface and subsequently polymerizes several molecules of C9 to assemble the membrane attack complex (MAC) (Muller-Eberhard, 1985). MAC assembly can lead to cell death by lysis, as it is inserted into the outer membrane of the bacterium (Podack *et al.*, 1984; Schreiber *et al.*, 1979).

Invading bacteria are opsonized not only by the complement system, but also by soluble antibodies, which are produced by plasma cells in long lasting infections (Bremell *et al.*, 1992; Croze *et al.*, 2009). These antibodies also promote recognition by phagocytes and subsequently uptake and killing. After recognition of the pathogen antigen by a B cell via the B cell receptor (surface immunoglobulin) and its additional activation by T_H cells via MHC class II, the B cell proliferates. The progeny of the cell subsequent differentiates either into antibody-secreting plasma cells or into memory B cells (Shlomchik *et al.*, 2012). In the early stage of antibody production, the immunoglobulin IgM, which in the secreted form is occurring as pentamers, is dominant, but after antigen contact and class switch, IgG is produced (Marshall *et al.*, 2011; MacLennan *et al.*, 2003), which is the most abundant antibody class in the plasma. Both immunoglobulins can function as mediators of opsonization. Professional phagocytes, such as neutrophils and macrophages, recognize the Fc-region of several antibodies on the surface of the bacterium via the FcR (Futosi *et*

al., 2013). The recognition of the antibody by the phagocytes leads to phagocytosis and, subsequently, killing of the pathogen.

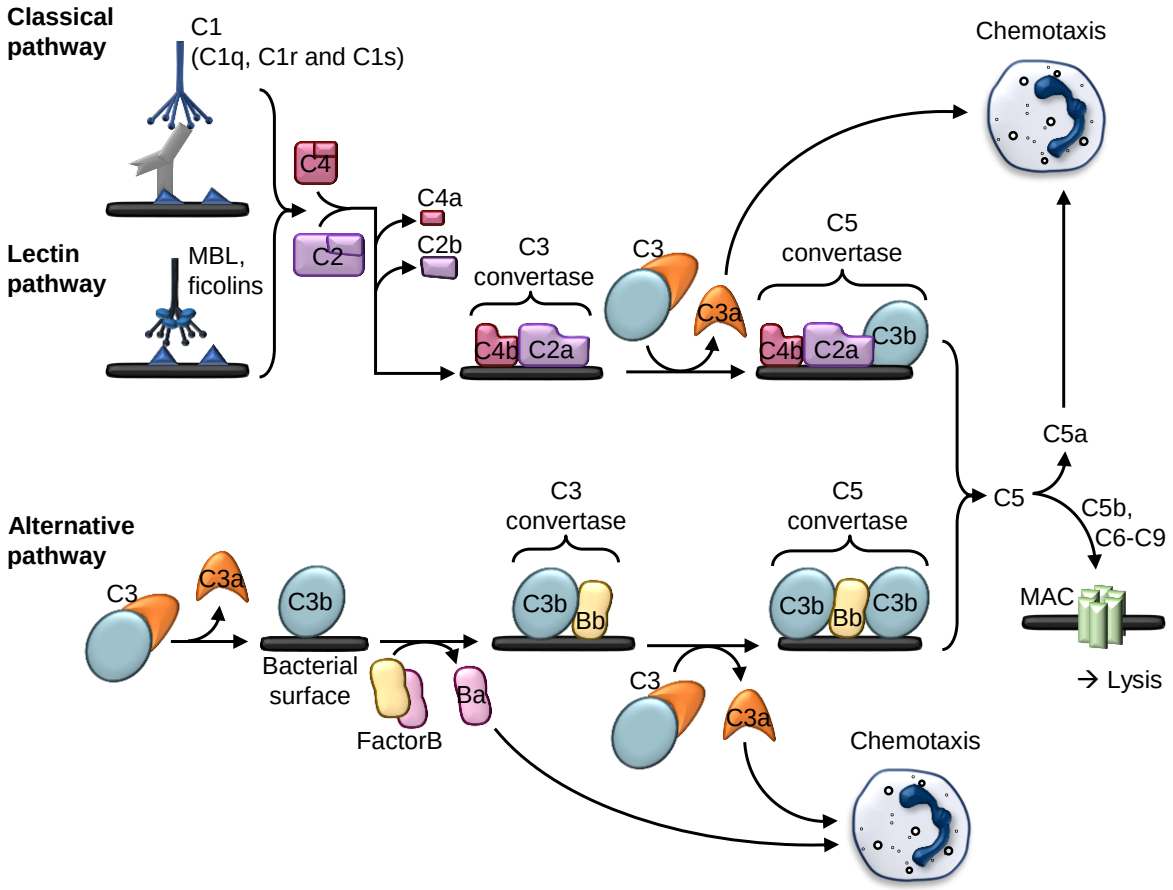

Figure 1.4: The complement system. The complement is acting through three pathways: the classical (CP), lectin (LP), and the alternative (AP) pathway. In the CP and the LP surface molecules of the pathogen are direct (LP) or indirect (CP) detected. Chemotaxis results in the CP and LP out of the anaphylatoxins C3a, C4a, and C5a and in the AP out of the leukotaxins C5a and Ba. The bacterium is opsonized by C3b and lysed via pore formation by the membrane attack complex (MAC). MBL= mannose-binding lectin. Modified from Pietrocola *et al.*, 2017.

1.2.2 Hematopoiesis

Immune cells are formed from precursors of the hematopoetic (greek for blood-making) system. The blood cells are continuously generated in the bone marrow and differentiated out of hematopoietic stem cells (HSCs) in a well-orchestrated hierarchy (**Figure 1.5**). Because of the limited lifetime of many blood cells, a high number of cells have to be generated already in the steady state. For example, neutrophils have a lifetime of hours up to a few days (Tak *et al.*, 2013), resulting in approximately $0.5\text{-}1x10^{11}$ newly generated neutrophils each day (Dancey *et al.*, 1976). During an innate immune response, the hematopoiesis plays an important role to generate sufficient numbers of innate immune cells in the bone marrow required for recruitment to the site of infection or danger (Summers *et al.*, 2010; Glodde *et al.*, 2017). In contrast, the cells of the adaptive immune system or their precursors, already leave the bone marrow before antigen encounter and proliferate in the lymph nodes after stimulation.

Hemostasis, the constant supply of red and white blood cells in sufficient numbers, is based on self-renewal of HSCs, which differentiate into hematopoietic progenitor cells (HPCs) of different proliferative activities, to allow a large-scale cellular amplification.
The HSCs can be classified according to their self-renewal ability in long-term (LT), intermediate-term (IT), and short-term (ST) HSCs. They give rise to HPCs, which can be divided into several subclasses, all of them originating from multipotent progenitors (MPPs). The mature hematopoietic cells have, except for B and T cells as well as tissue-resident macrophages and DCs, no self-renewal ability and just a limited proliferative capacity. Hematopoietic growth factors promote the proliferation and differentiation of HPCs. For example, to get fully mature neutrophils, the G-CSF is necessary, whereas for macrophages, the macrophage colony stimulating factor (M-CSF) is needed, but in both cell types, the GM-CSF plays a role (Gupta *et al.*, 2014). Based on their stimulation, MPPs differentiate into common myeloid progenitors (CMPs), the common dendritic progenitors (CDPs), and lymphoid-primed multipotent progenitors (LMPPs). CMPs develop into megakaryocyte-erythrocyte progenitors (MEPs) or granulocyte-macrophage progenitors (GMPs) while the LMPPs are the precursors of the common lymphoid progenitors (CLPs). The mature blood cells are released from the bone marrow into the peripheral blood and circulate or migrate into tissues or to the lymphatic system.

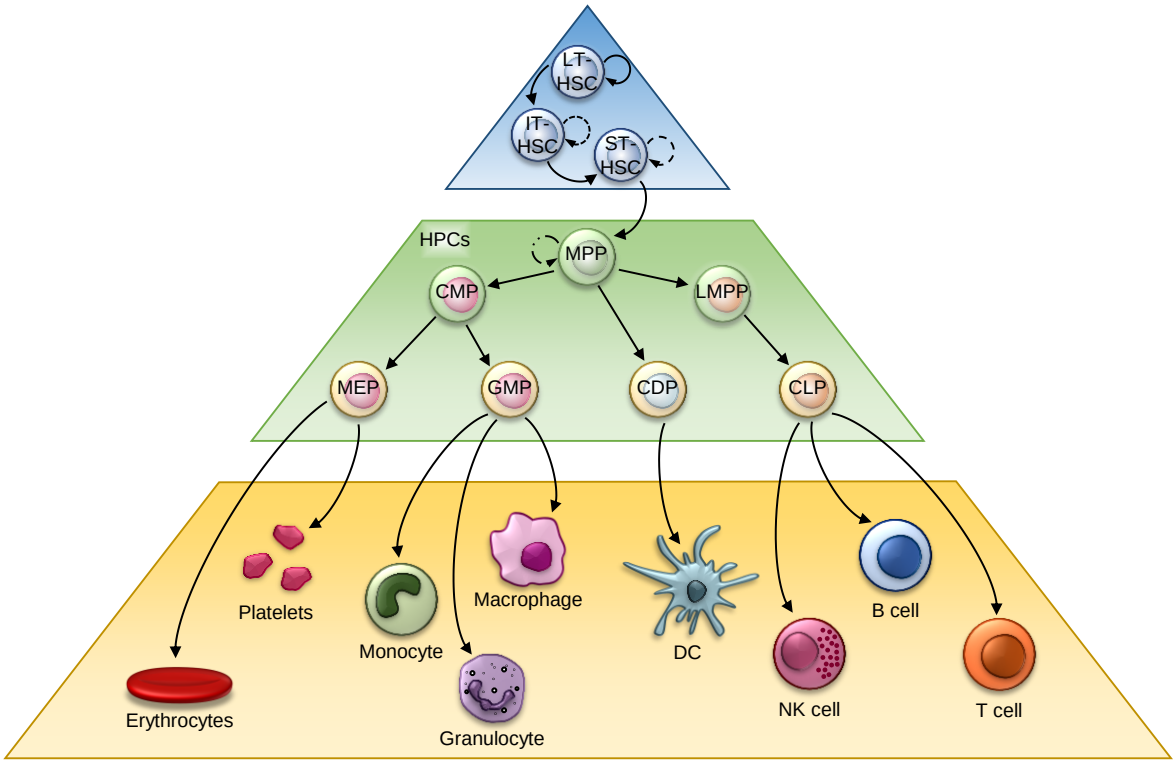

Figure 1.5: Hierarchy of the cell types during hematopoiesis. The blood cells develop out of hematopoietic stem cells (HSCs), hierarchically structured into long-term (LT), intermediate-term (IT), and short-term (ST) HSCs. Solid of dashed/dotted circular arrows are shown according to self-renewal ability. Hematopoietic progenitor cells (HPCs) represent the next level of differentiation: multipotent progenitors (MPPs), common myeloid progenitors (CMPs), lymphoid-primed multipotent progenitors (LMPPs), megakaryocyte-erythrocyte progenitors (MEPs), granulocyte-macrophage progenitors (GMPs), common dendritic progenitors (CDPs), and common lymphoid progenitors (CLPs). The progenitors develop then into mature blood cells. DC= dendritic cell, NK cell= natural killer cell. Modified from Manz *et al.*, 2014.

Granulopoiesis is the generation of granulocytes and a part of the hematopoiesis. The term granulocytes collectively designates the group of neutrophils, eosinophils, and basophils, while neutrophils make around 90% of granulocytes in the peripheral blood. After recruitment of neutrophils to the inflamed tissue, most of them undergo cell death, caused by their antimicrobial mechanisms, such as phagocytosis, ROS production, or NETosis (Kobayashi *et al.*, 2010). Consequently, during an infection, a high number of neutrophils need to be replenished.

During severe systemic infections, or other pathological conditions with extremely high need of neutrophils, emergency granulopoiesis is induced (Manz *et al.*, 2014). In a systemic infection, substantial more neutrophils are required, compared to a local infection. This induces a demand-adapted hematopoiesis. Kwak *et al.* showed that the ROS production of

granulocytes also regulates the proliferation of myeloid progenitors in emergency granulopoiesis (Kwak *et al.*, 2015). Due to the accelerated turnover of neutrophils, not only mature, but also immature neutrophils are released from the bone marrow to the peripheral blood. Because of this large-scale *de novo* generation of neutrophils, the lymphopoieses is reduced in the bone marrow (Manz *et al.*, 2014).

Traditionally, it is claimed that, except from tissue-resident macrophages, the members of the myeloid lineage have a very limited proliferation capacity. However, for immature neutrophils (defined in mice by the surface marker Ly6G being expressed at intermediate levels) an extramedullary proliferation was shown. After a systemic infection of mice with *Streptococcus pneumoniae*, these neutrophils undergo emergency proliferation in the spleen and, by that, increase the pool of mature effector neutrophils (Deniset *et al.*, 2017). This effect is also called extramedullary hematopoiesis. This kind of hematopoiesis has been shown to be caused by a variety of events: A severe bone marrow failure, the therapeutic stimulation to produce blood cells (myelostimulation), systemic disorders through tissue inflammation or injury, and abnormal chemokine production (Johns *et al.*, 2012).

1.2.3 The weapons stockpile of neutrophils

As soon as *S. aureus* is detected by neutrophils in the tissue, these professional phagocytes start their antimicrobial activity, including oxygen-dependent and oxygen-independent strategies (**Figure 1.6**).

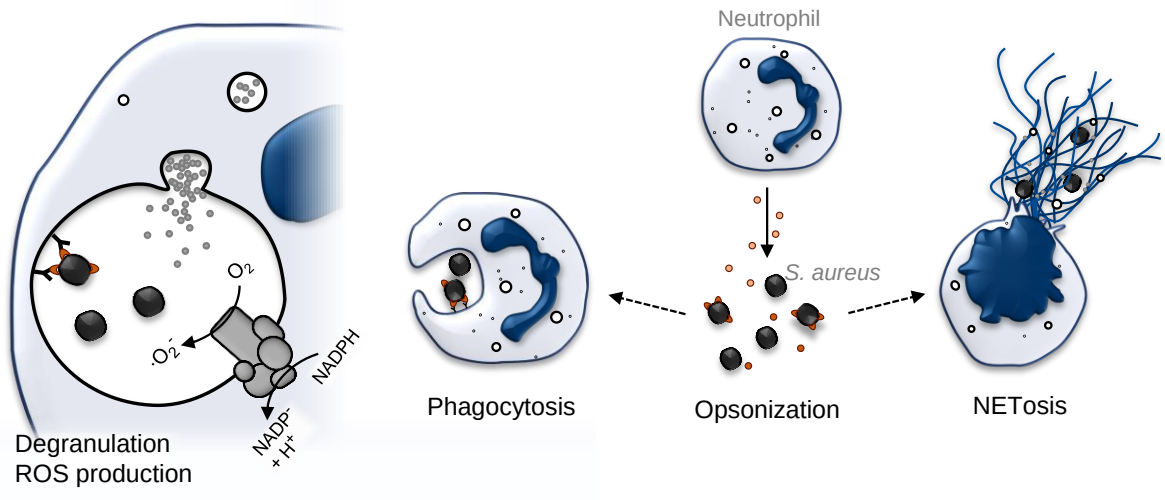

Figure 1.6: Recruitment of and killing by neutrophils. After recruitment of neutrophils via chemokines, they act against the opsonized pathogens via formation of neutrophil extracellular traps (NETs) or phagocytosis. Subsequently neutrophils can kill the bacteria with reactive oxygen species (ROS) or antimicrobial peptides (AMPs) after degranulation**.** Modified from Spaan *et al.*, 2013.

Oxidative burst

The activation of the enzyme complex NADPH oxidase (NOX) in the plasma- and phagosomal-membrane results in an oxidative burst. In case of infection, reactive oxygen species (ROS) can be produced into phagosomes to act against phagocytosed pathogens, but also extracellularly against non-phagocytosed pathogens or microorganisms too big for being engulfed (Boyle *et al.*, 2011). In resting cells, the protein constituents of NOX remain segregated in the cytosol (phox complex p40^{phox}, p47^{phox} and p67^{phox} and the small GTPase protein Rac2) and in the membrane (heterodimer flavocytochrome b_{558}, cytb$_{558,}$ including Nox2/gp91^{phox}, gene named *CYBB*, and p22^{phox}) (El-Benna *et al.*, 2016). For activation of the NOX pathway and maximal degranulation, the priming of neutrophils before activation is necessary (Guthrie *et al.*, 1984).

Neutrophils are primed by microbial products, like LPS, or cytokines, which are secreted during host defense, like TNF, IL-1, IFNγ or GM-CSF (Guthrie *et al.*, 1984; Condliffe *et al.*, 1998; Kegel *et al.*, 1977; Tennenberg *et al.*, 1993; Weisbart *et al.*, 1986). Upon priming of neutrophils, the cytosolic component p47^{phox} is phosphorylated and subsequently changes

its conformation (el Benna *et al.*, 1994), and Rac2 (Rac1 in monocytes) is activated by exchange of GDP to GTP (Diebold *et al.*, 2001; Nguyen *et al.*, 2017). For the activated state of the NOX, the Phox complex compounds ($p40^{phox}$, $p47^{phox}$ and $p67^{phox}$) and the activated Rac2 migrate to the membrane and interact with $cytb_{558}$ (Nguyen *et al.*, 2017). The catalytic core of the NOX is formed by the $cytb_{558}$, containing the electron transferase $gp91^{phox}$. Superoxide anions (O_2^-) are generated by transferring electrons from NADPH (cytosolic) through the membrane to O_2. The resulting superoxide O_2^- is highly reactive and can act in three ways (Nguyen *et al.*, 2017): To kill microorganisms it reacts to other ROS to damage cell membrane, proteins and nucleic acids. To reduce host cell damage, the superoxide dismutase (SOD) converts O_2^- to hydrogen peroxide (H_2O_2). H_2O_2 can oxidize cysteine and methionine residues, which may lead to protein inactivation. Additionally, H_2O_2 either further react by Fe^{3+} to Hydroxyl radical (OH°) or via a granule-localized enzyme myeloperoxidase (MPO) into highly bactericidal hypochlorous acid (HOCl) at neutral or low pH to clear bacteria (Foote *et al.*, 1983; Klebanoff *et al.*, 2013). Furthermore, H_2O_2 can diffuse through neutrophil membranes and, to a limited extent, through pathogens, and thus damage intra- and extracellular pathogens (Morales *et al.*, 2012; Neutze *et al.*, 1996; Ohno *et al.*, 1985). Even if neutrophils have several protective mechanisms against the oxidative stress induced by the oxidative burst, most of them die during their action against pathogens (Kobayashi *et al.*, 2010). However, after apoptosis, other professional phagocytic cells can take them up and the pathogen is still captured (Talley *et al.*, 1995; Peters *et al.*, 2008).

Granules

An oxygen-independent antimicrobial neutrophil activity is the degranulation of cytoplasmic granules via fusion with the plasma membrane (exocytosis) or with phagosomal membranes (degranulation). Granules contain several microbicidal agents, so called antimicrobial peptides (AMPs), or antimicrobial proteins. A selection of such agents which occurs in neutrophils are listed and described in more detail in **Table 1.3**.

AMPs can be either produced by the host cells (e.g. neutrophils, keratinocytes) after a pathogen is recognized, or by commensal microbes at the skin surface to defend their niche (Harder *et al.*, 2013). For example, the cationic AMP human β- defensin (hBD) 2 is produced of keratinocytes after *S. aureus* recognition at the skin surface (Dinulos *et al.*, 2003). Furthermore, all three hBD1-3 are reported to show antibacterial activity against *S. aureus* (Chen *et al.*, 2005). The same is true for cathelicidin LL- 37, but this AMP acts additionally by inhibiting biofilm formation of the pathogen (Dean *et al.*, 2011).

Table 1.3: Antimicrobial proteins and peptides in azurophilic neutrophil granules.

Microbicidal agent	Description	Reference
Azurocidin (Heparin-binding protein)	Serine protease homologue. Increases vascular permeability. Chemotactic for monocytes, fibroblasts and T cells	Campanelli *et al.*, 1990 Gautam *et al.*, 2001 Chertov *et al.*, 1996
Cathelicidins	Bactericidal by membrane permeabilization. Chemotaxis of neutrophils, T cells and monocytes.	Turner *et al.*, 1998 De *et al.*, 2000
Defensins	Cationic AMP, that forms multimeric transmembrane pores and acts subsequently bactericidal by membrane permeabilization.	Ganz *et al.*, 1985 Wimley *et al.*, 1994
Lactoferrin	Iron-binding protein, with bacteriostatic effect by sequestrating of iron. It binds to bacterial cell membrane causing damage.	Oram *et al.*, 1968 Chapple *et al.*, 1998
Lysozyme	Cationic AMP, that degrades the bacterial cell wall (cleveages peptidoglycan polymers) by its muramidase activity.	Selsted *et al.*, 1978
Metalloproteases	Neutrophil collagenase, gelatinase and leukolysin. Degradation of structural components of the extracellular matrix.	Lazarus *et al.*, 1968 Kjeldsen *et al.*, 1992 Pei, 1999
Neutrophil elastase	Degrading of macromolecules, including elastin, collagen, and proteoglycan	Roughley *et al.*, 1977

Neutrophil extracellular traps

Another killing mechanism is constituted by neutrophil extracellular traps (NETs) and is usually accompanied with a specialized form of cell death referred to as NETosis. NETs are combined structures of modified chromatin, granule proteins (e.g. MPO or neutrophil elastase (NE) and cytosolic proteins (e.g. calprotectin) (Brinkmann *et al.*, 2004). Microbes are bound to the chromatin and killed by AMPs and other proteins. Additionally, NETs activate myeloid cells, and promote coagulation (Messina *et al.*, 2002).

There are two types of NETosis, a ROS-dependent and -independent (in addition without need of NE) NET formation. In the more common ROS-dependent type, the hydrogen peroxide produced by NOX is converted in azurophilic granules into halic acids by neutrophil MPO. By this, a protease complex formed by NE, cathepsin G, and azurocidin is selectively released out of the azurosome and translocated into the nucleus (Metzler *et al.*, 2014) where it digests histones and releases the chromatin. The nuclear envelope is disassembled and thereby, the chromatin and cytoplasmic as well as granular proteins get in contact (Fuchs *et al.*, 2007). Finally, the cytoplasmic membrane breaks, and NETs are released (Fuchs *et al.*, 2007). To ultimately release NETs, neutrophil lysis seems to be dependent on the activity of the pore-forming protein gasdermin D (GSDMD) (Sollberger *et al.*, 2018a). GSDMD is typically involved in pyroptosis, the inflammatory type of

programmed cell death activated by caspase-11 in mice (in humans: caspase-4 and caspase-5) (Kayagaki *et al.*, 2015; Shi *et al.*, 2015). However notably, NET release is not mandatory connected to cell death, Yipp *et al.* showed that it is possible for NET forming neutrophils to harbor an intact nucleus and being still able to crawl (Yipp *et al.*, 2012).

1.2.4 Immune evasion strategies of *S. aureus*

S. aureus is equipped with several molecules and strategies to avoid immune response. Distinct mechanisms are described in **Table 1.4** and schematically illustrated in **Figure 1.7**.

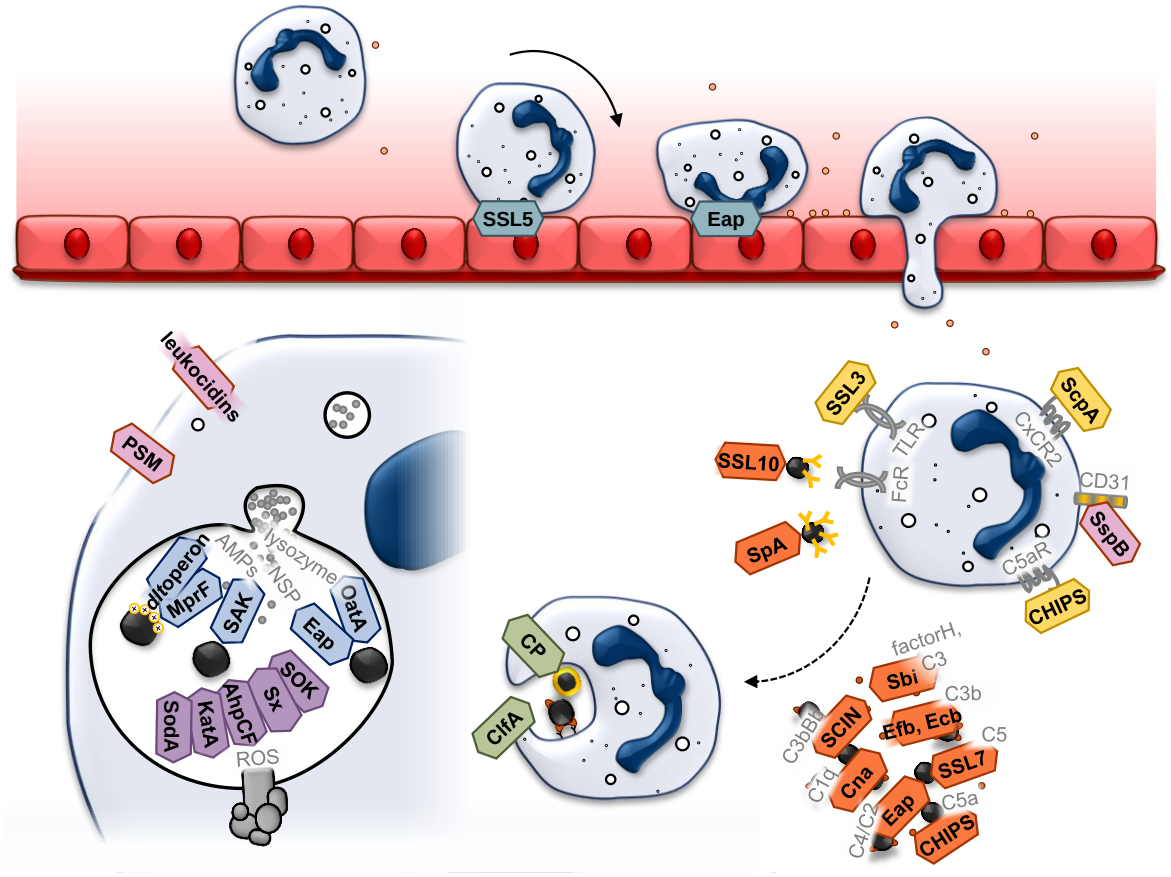

Figure 1.7: Evasion strategies of *S. aureus* against neutrophils. The strategies can be grouped into strategies against neutrophil extravasation (cyan), opsonization (orange), phagocytosis (green), killing by ROS (purple) or antimicrobial agents (blue), and others (yellow) or to kill the neutrophil (pink). The functions are described more in detail in Table 1.4. AhpCF= hydroperoxide reductase, CHIPS= chemotaxis inhibition protein of *S. aureus*, ClfA= clumping factor A, Cna= Collagen adhesin, CP= capsule polysaccharide) Eap= extracellular adherence protein, Ecb= extracellular complement-binding protein, Efb= extracellular fibrinogen-binding protein, NSP= neutrophil serine proteases, OatA= O-acetyltransferase A, PSM= phenol-soluble modulins, KatA= Catalase, MprF= multiple peptide resistance factor, SAK= Staphylokinase, Sbi= second binding protein of immunoglobulin, SCIN= staphylococcal complement inhibitor, ScpA= Staphopain A, SodA= superoxide dismutase A, SOK= surface factor promoting resistance to oxidative killing, SpA= *S. aureus* protein A, SSL= staphylococcal superantigen-like, SspB= *staphylococcus* serine protease B, Sx= Staphyloxanthin. Modified from Spaan *et al.*, 2013 and McGuinness *et al.*, 2016.

To inhibit neutrophil extravasation, staphylococcal superantigen-like 5 prevent neutrophil rolling (Bestebroer *et al.*, 2007) and extracellular adherence protein neutrophil adhesion (Chavakis *et al.*, 2002). For evasion of other steps of immune response, *S. aureus* disrupts bacterial opsonization for example via staphylococcal complement inhibitor, extracellular fibrinogen-binding protein, and capsule polysaccharide (Rooijakkers *et al.*, 2009; Rooijakkers *et al.*, 2005a; Jongerius *et al.*, 2007; Nanra *et al.*, 2013) or inhibition of chemotaxis is possible with chemotaxis inhibition protein of *S. aureus* and Staphopain A (Postma *et al.*, 2004; Laarman *et al.*, 2012). Activation of neutrophils and phagocytosis of *S. aureus* is prevented among other proteins by staphylococcal superantigen-like 10, *S. aureus* protein A and clumping factor A (Bestebroer *et al.*, 2009; Dossett *et al.*, 1969; Higgins *et al.*, 2006).

To avoid killing by ROS, *S. aureus* carries an extensive repertoire of virulence factors: superoxide dismutase A (SodA), catalase (KatA), staphyloxanthin (Sx), etc. (Karavolos *et al.*, 2003; Cosgrove *et al.*, 2007; Liu *et al.*, 2005). The metalloprotein SodA contains Mn as a cofactor and converts as a first step O_2^- into H_2O_2 (Clements *et al.*, 1999). H_2O_2 is than further transformed by the enzyme KatA into H_2O and O_2 (Cosgrove *et al.*, 2007). The carotenoid Sx works as an antioxidant (Liu *et al.*, 2005). To counteract antimicrobial peptides and proteins, the pathogen has also evolved several strategies: For example, via the proteins encoded on the *dlt* operon, host defensins are bound (Jin *et al.*, 2004) and the bacterium could limit the susceptibility for cationic AMPs by staphylokinase or multiple peptide resistance factor (Peschel *et al.*, 1999; Peschel *et al.*, 2001). A third mechanism to avoid killing through neutrophils is to kill in turn the neutrophil. For this purpose, some *S. aureus* strains have virulence factors of the family PSMs, to lyse the neutrophil or they produce leukocidins, to form pores in the membrane of the host cell (Jayasinghe *et al.*, 2005; Geiger *et al.*, 2012).

Table 1.4: *S. aureus* toxins, proteases, and proteins to evade neutrophil response.

Protein	Function	Reference
Extravasation		
SSL5 (staphylococcal superantigen-like 5)	Binding on PSGL-1, by which P-Selectin cannot bind to it and the rolling of neutrophils along the endothelial cells is abrogated.	Bestebroer *et al.*, 2007
Eap (extracellular adherence protein)	Binds to ICAM-1 and thus inhibits the adhesion of neutrophils to the endothelial cells.	Chavakis *et al.*, 2002
Opsonization/ Chemotaxis/ Activation/ Phagocytosis		
ScpA (Staphopain A)	A secreted cysteine protease cleaving the N-terminus of human CXCR2, whereby the proinflammatory signals of the chemokines IL-8 and GROα are blunted	Laarman *et al.*, 2012

Protein	Function	Reference
SspA (*staphylococcus* serine protease A, V8 protease)	The cysteine proteinase moderates adhesion of *S. aureus* to fibronectin by degrading cell surface fibronectin-binding proteins.	Patti *et al.*, 1994 McGavin *et al.*, 1997
SspB (*staphylococcus* serine protease B, Staphopain B)	The cysteine proteinase cleaves CD31 ('do not-eat-me' signal) on the surface of neutrophils, which leads to an engulfment by macrophages.	Smagur *et al.*, 2009
SpA (*S. aureus* protein A)	SpA binds the Fc-region of immunoglobulin and the bacterium becomes coated with IgG in an inappropriate conformation to prevent phagocytosis.	Dossett *et al.*, 1969
ClfA (clumping factor A)	A fibrinogen-binding surface protein that inhibits phagocytosis.	Higgins *et al.*, 2006
CP (capsule polysaccharide)	The phagocytosis is inhibited by preventing opsonization.	Nanra *et al.*, 2013
SAK (Staphylokinase)	Recruits Plasminogen to *S. aureus* surface, which leads subsequently to cleavage of IgG, C3b and iC3b from the bacterial cell wall by plasmin and thereby inhibition of the classical pathway.	Rooijakkers *et al.*, 2005b Bokarewa *et al.*, 2006
CHIPS (chemotaxis inhibition protein of *S. aureus*)	A solubly secreted protein that binds to receptors for C5a and formyl peptide receptors (FPRs) and thus impairs neutrophil chemotaxis.	Postma *et al.*, 2004
SCIN (staphylococcal complement inhibitor)	SCIN and the homologues SCIN-B and -C effect on the lectin, the classical and on the alternative complement pathways. They inhibit the C5 cleavage and it binds to C3bBb, C3 convertase, whereby phagocytosis and bacterial killing is inhibited	Rooijakkers *et al.*, 2009 Rooijakkers *et al.*, 2005a
Eap (extracellular adherence protein)	Eap and its functionally orphan Eap homologs EapH1 and EapH2 inhibit the neutrophil serine proteases (NSPs) NE, proteinase-3 and cathepsin G, which would e.g. cleave the *S. aureus* molecules SCIN and CHIPS. They also inhibit the classical and the lectin pathway by blocking the formation of the C3 proconvertase by binding on C4b.	Stapels *et al.*, 2014 Woehl *et al.*, 2014
Sbi (second binding protein of immunoglobulin)	Can bind the Fc-region of IgG, like SpaA. Furthermore, it binds C3 and human complement regulators factor H to inhibit the alternative pathway and activation	Smith *et al.*, 2011
Cna (Collagen adhesin)	Inhibits the formation of the C1 complex by binding C1q in the classical pathway. Binding to collagen for infection.	Kang *et al.*, 2013
Efb (extracellular fibrinogen-binding) protein and Ecb (extracellular complement-binding)	Act on the alternative pathway convertase via blocking C3b-containing convertase or inhibiting C5 convertase in generating C5a.	Jongerius *et al.*, 2007
SSL3 (staphylococcal superantigen-like)	Binds specifically to the extracellular domain of TLR2 (also in TLR1/2 or TLR2/6 dimers) and inhibits in this way the recognition of bacterial lipoproteins.	Bardoel *et al.*, 2012
SSL5	Binds to glycosylated N-termini of all G protein-coupled receptors (GPCRs) and subsequently inhibition of	Bestebroer *et al.*, 2009

Protein	Function	Reference
	leukocyte activation by chemokines, which require the receptor N-terminus for activation.	
SSL7	Binds the complement component C5, to inhibit generation of C5a and with it opsonization and subsequently phagocytosis and it binds Immunoglobulin A (IgA), to inhibit IgG-FcαRI interaction.	Bestebroer *et al.*, 2010
SSL10	Binds IgG to inhibit recognition by FcRs and complement activation.	Itoh *et al.*, 2010
Killing		
SodA (superoxide dismutase A)	Inactivates harmful superoxide radicals to avoid killing by ROS.	Karavolos *et al.*, 2003
KatA (Catalase)	The catalse converts hydrogen peroxide into oxygen and water to avoid killing by ROS.	Cosgrove *et al.*, 2007
AhpCF (hydroperoxide reductase)	An enzyme with catalase activity to avoid killing by ROS.	Cosgrove *et al.*, 2007
Staphyloxanthin (Sx, golden pigment)	Functions as an antioxidant to avoid killing by ROS.	Liu *et al.*, 2005
SOK (surface factor promoting resistance to oxidative killing)	Reduces sensitivity to singlet oxygen to avoid killing by ROS.	Malachowa *et al.*, 2011
OatA (*O*-acetyltransferase A)	Protects *S. aureus* again degradation of peptidoglycan by the muramidase activity of lysozyme via O-acatylation of peptidoglycan by OatA	Bera *et al.*, 2005
SAK (Staphylokinase)	Inhibits α-defensins by binding them.	Jin *et al.*, 2004
dlt operon	Modification system for D-alanylation of teichoic acids in the cell wall, whereby the negative charge is neutralized, thereby limiting the susceptibility for cationic AMPs, like defensins and protegrins.	Peschel *et al.*, 1999
MprF (multiple peptide resistance factor)	Modifies phosphatidylglycerol with L-lysine, whereby the negative charge and limiting the susceptibility for cationic AMPs is reduced.	Peschel *et al.*, 2001
Bicomponent β-barrel pore-forming leukocidins	Causing osmotic lysis of neutrophils or macrophages by forming heteromultimeric pores in the membrane of host cells. E.g. PVL, Hla	Jayasinghe *et al.*, 2005 Kaneko *et al.*, 2004 Abtin *et al.*, 2014
PSMs (phenol-soluble modulins)	Lysis of neutrophils after phagocytosis.	Wang *et al.*, 2007 Geiger *et al.*, 2012

On top of the molecular evasion strategies, *S. aureus* strongly induces abscess formation by invasion into the tissue, whether by an injury or coming from another site of infection as a trojan horse within neutrophils (Gresham *et al.*, 2000; Krezalek *et al.*, 2018). The presence of the pathogen leads to a massive infiltration of neutrophils. The bacterium is able to influence abscess formation by distinct virulence factors such as ClfA or SpA and inhibit the

antimicrobial mechanisms of the embedded neutrophils within the abscess. Subsequently, an abscess can shield the bacterium from other immune cells and give time for growth and initiating new rounds of infection (Cheng *et al.*, 2011; Cheng *et al.*, 2009). Living bacteria form the core of such an abscess, surrounded of necrotic and healthy neutrophils, tissue debris, and fibrin (Cheng *et al.*, 2011; Kobayashi *et al.*, 2015). A capsule is built up by fibrous material, enclosed by macrophages (Cheng *et al.*, 2011; Brandt *et al.*, 2018a). These macrophages are presumable recruited by chemotaxis of the necrotic neutrophils in the core of the abscess (Fadok *et al.*, 2001).

1.2.5 The challenge to develop an anti-staphylococcal vaccine

The majority of *S. aureus*-isolates from clinical infections show an antibiotic resistance. With the increasing numbers of multidrug-resistant strains, the possibilities to treat patients with antibiotics have become limited. There is just a small group of antibiotics left, such as the glycopeptide antibiotic vancomycin and the oxazolidinone antibiotic linezolid (Reddy *et al.*, 2017). In addition, the numbers of VRSA infections increases, thus it is important to explore suitable treatment and prevention of critical infections alternatively to antibiotic treatment. Furthermore, for people with high risk for *S. aureus* infections, like health care workers, dialysis patients or prison inmates, it would be more beneficial to get a vaccination than an onerous and cumbersome antibiotic therapy.

Until now, just two vaccine approaches reached clinical trial phase III, but both ultimately failed (Reddy *et al.*, 2017). StaphVax from Nabi Biopharmaceuticals was directed against a single virulence factor, the capsule of *S. aureus*. The capsular polysaccharides type 5 (CP5) and 8 (CP8) were conjugated to a non-toxic recombinant *Pseudomonas aeruginosa* exotoxin A (Fattom *et al.*, 2004; Mohamed *et al.*, 2017). The vaccine has reached phase III, but achieved no convincing immune effect, and the patients were only protected for 40 weeks (Fattom *et al.*, 2015). The other approach failing in phase III was SA4Ag from Pfizer (Reddy *et al.*, 2017). In this approach, the two capsular polysaccharides CP5 and CP8 were used, conjugated to the carrier protein CRM197. This vaccine was combined with a mutated recombinant ClfA and a recombinant manganese transporter protein C (MntC, also for iron binding) (Frenck *et al.*, 2017; Begier *et al.*, 2017).

A main problem in developing an efficient and long-time protective vaccine is the skillful evasion and manipulation of the immune system by *S. aureus*. With the pathogen being considered mainly extracellular, vaccination approaches so far have targeted cell wall components or toxins (Zhang *et al.*, 2018). It is not entirely clear why it has been so difficult so elicit effective antibody responses, but part of the explanation might be the fact *S. aureus* is equipped with virulence factors like SCIN to inhibit opsonization, or SpA to prevent targeting by antibodies (Rooijakkers *et al.*, 2005a; Dossett *et al.*, 1969). Furthermore, the bacterium interferes already in an earlier stage with antibody generation, i.e. in misguiding B cells via its SAgs (Kallee, 1996). Additionally to the obstacles, which are imposed by *S. aureus* virulence factors, also the recently described intracellular lifestyle and consequently the protection against the detection of the pathogen by humoral immunity might make the development of a vaccine more difficult.

1.3 *S. aureus* as an intracellular pathogen

Historically, *S. aureus* has been considered an extracellular pathogen, but meanwhile it is often reported that the bacterium can survive within non-professional and also professional phagocytes (Loffler *et al.*, 2014). In a first step, the pathogen has to enter the cell, for this, different invasion mechanisms are possible. After successful invasion, *S. aureus* have to ensure the survival within the host cell.

The MSCRAMMs are essential cell wall adhesins for the adherence to the host tissue and among these, FnBPs are most important for invasion into host cells (Ahmed *et al.*, 2001). Upon binding to the cell surface, a rearrangement of the cytoskeleton of the host cell takes place and the bacterium is actively taken up into the phagosome (Menzies *et al.*, 1998). Additionally, the regulation of the Agr-system seems to have a role in the intracellular lifestyle and therefore in chronic and relapsing infections, as it is reported that around 10% of *S. aureus* isolates exhibit a defect in this regulatory system (Shopsin *et al.*, 2008). Furthermore, in *in vitro* studies with an *agr* mutant a high internalization rate was observed, but a lower cytotoxicity and less inflammation was induced by these intracellular bacteria (Grundmeier *et al.*, 2010).

S. aureus can invade into non-professional phagocytes, persist there and escape again. This course of events is reported for different cell types with different mid-term fates for the host cell. For endothelial cells, the uptake of *S. aureus* can end with host cell disruption after bacterial replication (Lowy *et al.*, 1988; Rollin *et al.*, 2017), apoptosis induced by Hla (Menzies *et al.*, 1998), or intracellular persistence, also including the development of small colony variants (SCVs) (Tuchscherr *et al.*, 2010; Rollin *et al.*, 2017). In epithelial cells, *S. aureus* switches as well into a SCV phenotype (in 28 days) for persistence (Tuchscherr *et al.*, 2011), but is also able to escape into the cytoplasm in an *agr* dependent manner, and to subsequently kill the host cell (Schnaith *et al.*, 2007). Also in osteoblasts, the pathogen can survive and can be found mainly in the cytoplasm of the infected cells (Hudson *et al.*, 1995). For keratinocytes, the uptake can occur in a FnBP-dependent and -independent way *in vitro*, depending on the cell lines involved (Kintarak *et al.*, 2004). Either, keratinocytes die after internalization (Nuzzo *et al.*, 2000) or the bacteria persist and form SCVs (von Eiff *et al.*, 2001). *S. aureus* exhibits a similar behavior in fibroblasts, like in other non-professional phagocytes, where the bacterium escapes from the phagosome, multiplies, and kills the host cell (Murai *et al.*, 1999; Schnaith *et al.*, 2007). Moreover, a protective effect of the intracellular location against antibiotics was demonstrated (Krut *et al.*, 2004).

In contrast to non-professional phagocytes, which have just limited opportunities to defend themselves against invading bacteria, professional phagocytes have many weapons to kill intracellular pathogens, as described in detail for neutrophils in 1.2.3. However, *S. aureus* can also survive and even multiply within professional phagocytes.
Flannagan *et al.* reported that *S. aureus* can multiply *in vitro* in mature phagolysosomes of macrophages and that the bacterium can escape from those compartments, killing the host cell (Flannagan *et al.*, 2016). Furthermore, a following study could identify the acidic environment of the phagolysosomes to be necessary for activation of the resistance against antimicrobial effectors, like AMPs (Flannagan *et al.*, 2018). Moreover, the intracellular location was shown to be a protective environment upon application of the antibiotic gentamycin (Flannagan *et al.*, 2016). In other *in vitro* studies, survival and multiplication of *S. aureus* within DCs was reported, and the escape of the pathogen including host cell death could be observed (Schindler *et al.*, 2012). Additional reservoirs for *S. aureus* were found in systemic mouse infections: Surewaard *et al.* identified phagolysosomes of Kupffer cells (KCs) as host compartment for the pathogen, and described intracellular replication and release of bacteria after cell lysis. Also, it could be shown that liposomal encapsulated vancomycin might be a promising treatment of such intracellular bacteria (Surewaard *et al.*, 2016). Even in neutrophils, survival and growth of *S. aureus* was described after intraperitoneal mouse infections (Gresham *et al.*, 2000). Additionally, Leliefeld *et al.* reported a containment of living bacteria within the phagolysosomes of neutrophils (Leliefeld *et al.*, 2018).

Taken together, *S. aureus* is equipped with many strategies to survive not only in non-professionally phagocytic cells, but also in professional phagocytes. Furthermore, the bacterium is able to escape from the host cells for new infections. Main factors for this behavior are the broad array of virulence factors and their regulation, and the capability of both extra- and intracellular proliferation of the pathogen.

1.4 Approaches to measure bacterial proliferation

To investigate the interaction between the immune system and the pathogen, or the efficacy of a treatment of a disease, information about the pathogen viability and growth behavior is necessary. Especially for *S. aureus*, a pathogen in which adaptation of growth rates during persistence has been observed, such information would be helpful for vaccine development and optimization of treatment strategies. Furthermore, the growth of such a pathogen is of interest regarding antibiotic treatment, which often effects the cell wall formation during cell division.

A variety of approaches are possible to measure proliferation rates, which, including their advantages and disadvantages, are schematically illustrated in **Figure 1.8**. The easiest way to detect proliferation is to count colony forming units (CFUs) in cultures, organs or tissues (Flannagan *et al.*, 2018; Schindler *et al.*, 2012; Surewaard *et al.*, 2016). An increasing cell number over time suggests proliferation, but it is not possible to dissect the influence of killing on the course of pathogen numbers in such kinetics. Also, the analysis is yielding information on the whole bacterial population, and it is not possible to distinguish individual bacteria according to their microenvironment. For microscopy approaches, pulsing of pathogens and cells has been widely used and fluorescent dyes are commercially available. In this approach, the bacterium is labeled with a fluorescent dye, which will be diluted during cell division, whereby proliferating bacteria are less fluorescent than non-growing ones. The dye eFluor-670 was used for *in vitro* infected macrophages (Flannagan *et al.*, 2018) or Syto 60 in spinning-disk intravital microscopy (SD-IVM) imaging of a liver in systemic infected mice (Surewaard *et al.*, 2016). In a similar approach, it is also possible to induce in the pathogen a short term production of the fluorescent dye itself, as demonstrated by Helaine *et al*. for *Salmonella typhimurium*. Here, chemical induction was employed to trigger a short peak of fluorescent protein production, which is diluted during cell division (Helaine *et al.*, 2010). Finally, fluorescence timer approaches, in which a fluorescence protein shifts its fluorescence color time-dependently during maturation, have been established (Claudi *et al.*, 2014; Subach *et al.*, 2009).
In the course of *in vitro* video microscopy of *S. aureus* infected cells, like endothelial cells or DCs, the increase of bacteria number and fluorescence is detectable visually, but hard to quantify (Rollin *et al.*, 2017; Schindler *et al.*, 2012). The same is true for electron microscopy of dividing bacteria, were the separation of the cells by a new cell wall is visible. This is demonstrated for example for bacteria in KCs in a mouse liver (Surewaard *et al.*, 2016), or in DC cultures (Schindler *et al.*, 2012).

For eukaryotic cells, several robust approaches for flow cytometry or microscopy analyses are published and accessible. Agents like carboxyfluorescein diacetate succinimidyl ester (CFSE) are commercially available, which are diluted during cell division (Chang *et al.*, 2007). The same is true for antibodies, which bind to active dividing eukaryotic cells via the nuclear protein Ki-67 in fixed cells (Deniset *et al.*, 2017).

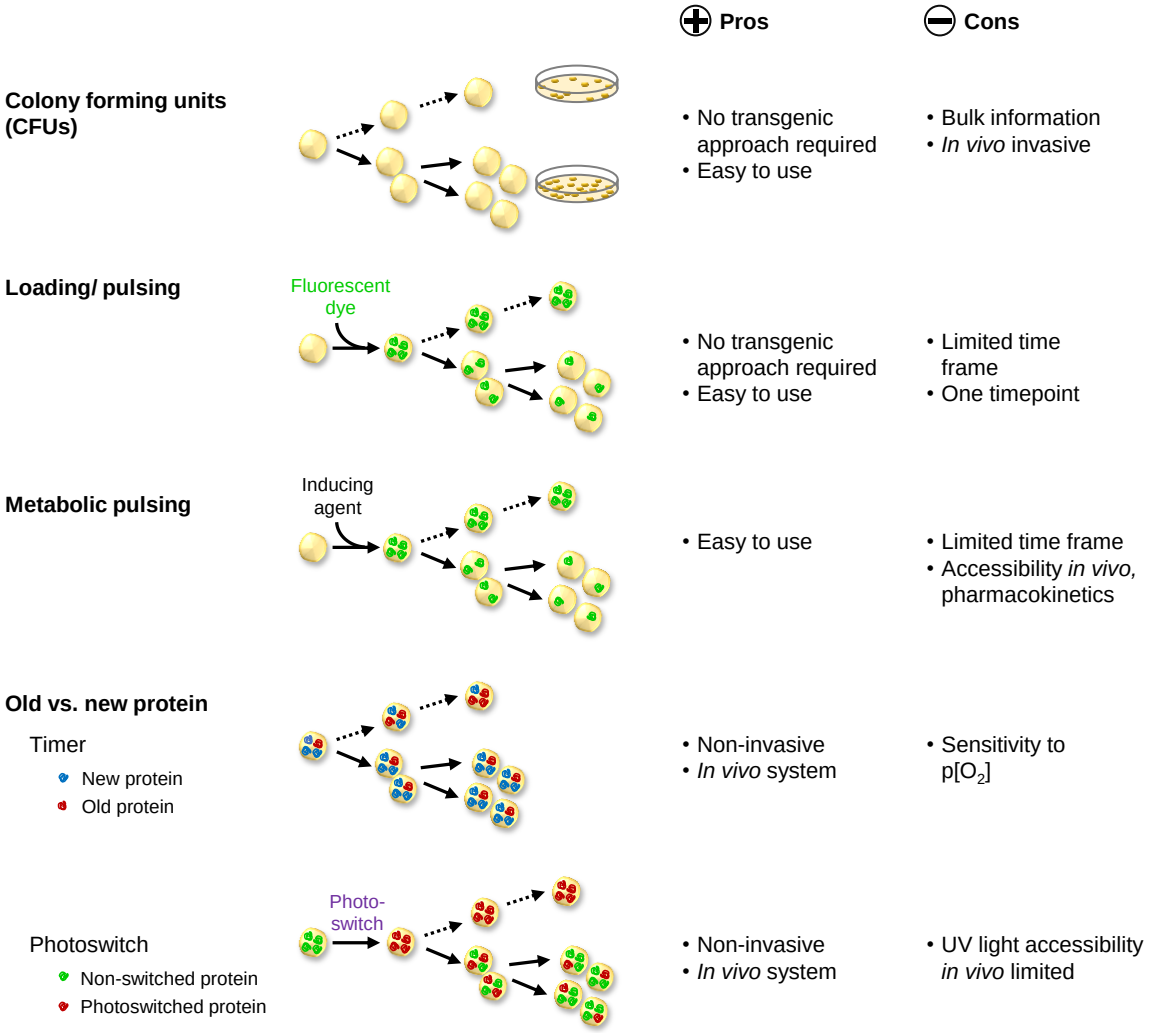

Figure 1.8: Proliferation measurement approaches. Approaches to measure bacterial growth and systems to distinguish between proliferating (solid arrows) bacteria and non-proliferating (dotted arrows) cells.

For the unicellular eukaryotic parasite *Leishmania major* (*L. major*), Müller *et al.* published a *in vivo* proliferation reporter system based on the dilution of the photoconvertible fluorescent protein mKikGR (Habuchi *et al.*, 2008) where the parasite could be tracked for 2-3 days after photoconversion and proliferation could be detected quantitatively (Muller *et al.*, 2013). Heyde *et al.* used this reporter to measure the proliferation rate of *L. major* in mice and *in vitro* in DCs and macrophages (Heyde *et al.*, 2018). The mKikGR from Habuchi

et al. used in this approach is based on a green photoconvertible fluorescent protein KikGR, engineered by Tsutsui *et al*.. The protein originates from the stony coral *Favia favus*, in a homotetrameric form. The new fluorescent protein was dubbed KikGR, because of its original green (G) fluorescence, the photoconverted red (R) fluorescence, and the Japanese name of *Favia* 'Kikume-ishi' (Kik) (Tsutsui *et al.*, 2005). In a further step, the reporter was optimized to get bright fluorescence also in a monomeric (m) version (Habuchi *et al.*, 2008). The green mKikGR is photoconvertible by a 405 nm light pulse into the red mKikGR and can be measured with 475 nm and 555 nm excitation, respectively. The optimized version exhibits a bright and highly photostable fluorescence with applicability for high resolution multicolor microscopy (Habuchi *et al.*, 2008).

1.5 Aims of the study

Staphylococcus aureus (*S. aureus*) is able to break through the skin barrier, reach the blood stream and infect in this way nearly every organ and tissue. Skin and soft tissue infections are the most frequent manifestation of the pathogen, and due to the occurrence of antibiotic resistance, these infections become increasingly more complicated to treat. The growth rate of *S. aureus* has an essential impact on the outcome of an infection. On the one hand, the growth can critically influence the susceptibility against treatment and immune effector mechanisms. On the other hand, depending on the growth rate, different PAMPs are available for the immune system, which influences the way in which immune responses are initiated and maintained. Therefore, to study the growth behavior of *S. aureus*, an *in vivo* proliferation reporter is urgently needed.

The first part of the thesis was to implement a mKikumeGR proliferation reporter system originally described in the eukaryotic parasite *L. major*, to obtain an *in vivo* biosensor for measuring proliferation of the Gram-positive bacterium *S. aureus* on a single cell-level *in vivo*. For this, the fluorescence reporter was adapted for optimal expression in *S. aureus,* and the functionality was shown *in vitro*. Furthermore, the reporter system was tested for application *in vivo* in the ongoing infection, and was shown to be suitable for measuring proliferation with flow cytometry and intravital 2-photon microscopy.

In the second part, I used the *in vivo* biosensor to probe the *S. aureus* growth rate during skin infection in wild type mice over the course of an infection. I consequently was able to show the influence of the immune system-induced changes of the infection microenvironment on the pathogen growth. Furthermore, I characterized the role of neutrophils as the first cellular defense line in the host response against *S. aureus* invasions, and their most important antimicrobial effector function, NADPH oxidase, in subcutaneous *S. aureus* infections. I could show the effect of neutrophils and the reactive oxygen species produced upon their arrival at the site of infection, which I found to critically act on pathogen proliferation rate.

2 MATERIALS AND METHODS

2.1 Material

2.1.1 Vectors and constructs

Table 2.1: Vectors and constructs. pGL485 vector map with cloning sites, and schematic representation of pGL485 derivatives are shown in **Figure 3.1**.

Name	Source
pGL485	Provided by Eva Medina, Helmholtz Centre for Infection Research, Braunschweig
pGL485-GFP	Provided by Eva Medina, Helmholtz Centre for Infection Research, Braunschweig
pLacKikume	This study (see 2.4.1 Plasmid construction and 2.3.1 Bacteria strains)
pKikume	This study (see 2.4.1 Plasmid construction and 2.3.1 Bacteria strains)
pTufAKikume	This study (see 2.4.1 Plasmid construction and 2.3.1 Bacteria strains)

2.1.2 Kits

Table 2.2: Kits.

Kit	Supplier
*Bac*Light™ Bacterial Membrane Potential Kit	Invitrogen
Invisorb Spin Plasmid Mini Two	STRATEC Molecular
Nucleo Spin® Extract II	MACHEREY-NAGEL
NucleoBond® PC 500 EF Kit	MACHEREY-NAGEL
Phagoburst™	Glycotope Biotechnology

2.1.3 Biochemical and chemical reagents

Table 2.3: Antibiotics.

Antibiotic	Stock concentration	Supplier
Ampicillin	100 mg/ml in ddH_2O	Carl Roth
Chloramphenicol	12.5 mg/ml in EtOH	Carl Roth
Erythromycin	10 mg/ml in EtOH	Carl Roth
Gentamycin	10 mg/ml	Gibco
Neomycin sulfate	50 mg/ml in ddH_2O	Sigma-Aldrich
Spectinomycin	100 mg/ml in ddH_2O	Sigma-Aldrich
Penicillin/Streptomycin	10000 U, 10000 µg/ml	Biochrom AG Carl Roth
Tetracycline	5 mg/ml in ddH_2O	Carl Roth

Table 2.4: Biochemical and chemical reagents.

Reagents	Source/Supplier
2-Propanol	Carl Roth
Acetic acid (96% v/v)	Carl Roth
Acetopromacin	Ceva Tiergesundheit
Agar-Agar, Kobe I	Carl Roth
Aminoethyltrioxsalen (AMT, psoralen)	Sigma-Aldrich
Ammonium chloride (NH_4Cl)	Carl Roth
Antarctic phosphatase	New England Biolabs
Anti-Biotin MicroBeads	Miltenyi Biotech
ApaI	New England Biolabs
BD FACS Flow™ Sheath Fluid	BD Bioscience
BD FACS™ Clean Solution	BD Bioscience
BD FACS™ Rinse Solution	BD Bioscience
Brain-Heart-Infusion Broth (BHI Medium)	Carl Roth
Calcium chloride ($CaCl_2$)	Carl Roth
Collagenase	Sigma
CountBright™ Absolute Counting Beads	Invitrogen
CutSmart Buffer (10x)	New England Biolabs
4′,6-Diamidino-2-phenylindole dihydrochloride (DAPI)	Sigma-Aldrich
Defibrinated Sheep Blood	Thermo Scientific
Disodium phosphate (Na_2HPO_4)	Carl Roth
DNA loading dye	Fermentas
EcoRI	Fermentas
Ethanol (99% v/v)	Carl Roth
Ethidium bromide	Carl Roth
Ethylenediaminetetraacetic acid (EDTA)	Carl Roth
Fetal Calf Serum (FCS)	Pan Biothech GmbH
Glycerol	Carl Roth
Ketamine	Medistar
LB Agar	Carl Roth
LB Medium	Carl Roth
L-Glutamin	Gibco
Low melting agarose	Serva
Lysostaphin from *Staphylococcus staphylolyticus*	Sigma-Aldrich
Magnesium chloride ($MgCl_2$)	Carl Roth
Magnesium sulfate ($MgSO_4$)	Carl Roth
Monopotassium phosphate (KH_2PO_4)	Carl Roth
Mouse serum	Recovered from mice

Reagents	Source/Supplier
Paraformaldehyde (PFA)	Carl Roth
PBS Dulbecco (phosphate-buffered saline, without (w/o) Ca^{2+}, Mg^{2+})	Biochrom AG
Poly-L-Lysin	Sigma-Aldrich
Potassium bicarbonate ($KHCO_3$)	Carl Roth
Potassium chloride (KCL)	Carl Roth
Quick-Load® 2-Log DNA Ladder (0.1-10.0 kb)	New England Biolabs
RPMI 1640 medium	Merck
SalI	New England Biolabs
SOC-medium	New England Biolabs
Sodium chloride (NaCl)	Carl Roth
Sodium citrate (Na_3-citrate)	Carl Roth
Sucrose	Carl Roth
T4 ligase	New England Biolabs
T4 ligation buffer	New England Biolabs
Tissue-Tek® O.C.T.™ Compound	Sakura
Tris (hydroxymethyl)-aminomethan (Tris)	Carl Roth
Triton X-100	Sigma-Aldrich
Trypan Blue Solution (0.4%)	Sigma-Aldrich
Trypsin/EDTA	Merck Millipore
Tryptone	Carl Roth
Xylazine (Rompun 2%)	Bayer
Yeast extract	Carl Roth

2.1.4 Antibodies

Table 2.5: Antibodies for negative neutrophil selection via MACS. All antibodies are biotin labeled and diluted in MACS buffer.

Antibody specificity	Clone/ Clonality	Supplier	Dilution from commercial stock
TER119	TER119	BioLegend	1:500
CD5	53-7.3	BD Biosciences	1:200
CD45R	RA3-6B2	BioLegend	1:400
F4/80	BM8	eBioscience (ThermoFisher)	1:100
Ckit/ CD117	2B8	eBioscience (ThermoFisher)	1:500
CD49b	HMa2	eBioscience (ThermoFisher)	1:200

Table 2.6: Antibodies for neutrophil-depletion. Diluted in PBS.

Antibody specificity	Clone	Supplier	Concentration
1A8	1A8	BioXCell	150 µg/100 µl
Rat IgG2a	2A3	BioXCell	150 µg/100 µl

Table 2.7: Antibodies for immunofluorescence labeling.

Antibody specificity	Clone/ Clonality	Supplier	Dilution from commercial stock	Label
CCR2	SA203G11	BioLegend	1:40	BV421
CD11b	M1/70	BioLegend	1:400, 1:200	APC-Cy7
CD11b	M1/70	BioLegend	1:400	PerCP/Cy5.5
CD11b	M1/70	eBioscience	1:120 [MELC]	AF488
CD11c	N418	BioLegend	1:200	BV510
CD11c	N418	BioLegend	1:200	PE
CD11c	N418	BioLegend	1:200	PerCP/Cy5.5
CD16/32	93	BioLegend	1:100	None (Fc-block)
CD4	RM4-5	BioLegend	1:200	BV421
CD4	RM4-5	BioLegend	1:200	AF488
CD45	30-F11	BioLegend	1:200	PerCP/Cy5.5
CD45	30-F11	BioLegend	1:200	APC-Cy7
CD45	30-F11	BD Bioscience	1:80 [MELC]	FITC
CD45.1	A20	BioLegend	1:200	PerCP/Cy5.5
CD45.1	A20	BioLegend	1:240 [MELC]	PE
CD45.2	104	BioLegend	1:100	APC
CD45.2	104	BioLegend	1:200	BV510
CD45.2	104	BioLegend	1:240 [MELC]	FITC
F4/80	BM8	BioLegend	1:200	BV421
Goat anti-rabbit IgG (H+L)	polyclonal	Jackson	1:500	AF647
GR-1	RB6-8C5	BD Bioscience	1:200	PE
I-A/ I-E (MHC II)	M5/114.15.1	BioLegend	1:200	BV510
Ly6C	HK1.4	BioLegend	1:400, 1:200	PE-Cy7
Ly6G	1A8	BioLegend	1:400	BV510
Ly6G	1A8	BioLegend	1:400, 1:200	APC
Ly6G	1A8	BioLegend	1:400	BV421
Ly6G	1A8	BD Bioscience	1:120 [MELC]	FITC
Propidium iodide	-	Sigma	1:5000	None
Rabbit anti-*S. aureus*	polyclonal	Abcam	1:500	None

2.1.5 Buffers and media

Table 2.8: Basic buffers.

Buffer	Reagents	Concentration/Amount
PBS in ddH_2O, pH 7.4	NaCl KCl Na_2HPO_4 KH_2PO_4	140 mM 2.7 mM 8 mM 1.8 mM
Flow cytometry/MACS buffer in PBS	FCS EDTA	0.5% (w/v) 2.5 mM
TAP in 100 ml ddH_2O	Tris Acidic acid EDTA	242 g 57.1 ml 37.3 g
Buffer for lysis of erythrocytes in ddH_2O	NH_4Cl $KHCO_3$ EDTA	155 mM 10 mM 0.1 mM

Table 2.9: Media for molecular biology.

Medium	Reagents	Amount
SOB in 500 ml ddH_2O, pH 7.4, autoclaved	Tryptone Yeast extract NaCl KCl	10 g 2.5 g 292 mg 93 mg
SOC in 98 ml SOB	1 M $MgCl_2$, 1 M $MgSO_4$ 2 M glucose	1 ml 1 ml
Phage buffer	LB medium $CaCl_2$ (1 M stock solution)	 5 mM
Soft Agar (a)	Na_3-citrat (1 M stock solution) Autoclaved agar	20 mM 0.6% (w/v)
Soft Agar (b)	$CaCl_2$ (1 M stock solution) Autoclaved agar	5 mM 0.6% (w/v)
Blood agar	Sheep blood, defibrinated Autoclaved agar	50 ml 500 ml

2.1.6 Technical equipment and software

Table 2.10: Laboratory equipment.

Equipment	Supplier
(Wide) Mini-sub® Cell GT	BioRad
Centrifuge 1-16K	Sigma
Gel documentation station (camera: E.A.S.Y. B-455-F)	Herolab
Gene Pulser II System	BioRad
GeneQuant 1300	Biochrom
HeraSafe HS 12	Heraeus
Incubating orbital shaker	VWR
Incubator	Gesellschaft für Labortechnik
Incubator Hera Cell 150i CO_2 Incubator	Thermo Fisher Scientific
LED diodes 375 nm	Nichia
LED diodes 405 nm	Strato
LSR Fortessa	BD Biosciences
Milli-Q® Integral Water Purification System	Merck Millipore
Multifuge 1 SR/3 SR	Heraeus
NanoDrop 2000 spectrophotometer	Thermo Fisher Scientific
NANOFIL	World Precision Instruments, Inc.
PowerPac 1000	BioRad
Thermomixer comfort	eppendorf
Tube Revolver	Thermo Fisher Scientific

Table 2.11: Software.

Software	Supplier
Ape (A plasmid Editor)	M. Wayne Davis
BD FACS Diva	BD Biosciences
Deconvolution/deblurring algorithm	XCOSM software package
DiscIT	(Moreau *et al.*, 2012)
Fiji software	NIH, http://rsb.info.nih.gov/ij/
FlowJo X software	FlowJo, LLC
Imaris	Bitplane
Las X	Leica
Prism 7 software	GraphPad Inc. Software
ZEN acquisition software	Zeiss

Table 2.12: Microscopes.

Equipment	Supplier
2-photon microscope	
Zeiss LSM 700 Mai Tai DeepSee Ti:Sa laser W Plan-Apochromat 20x/1.0 DIC VIS-IR dipping objective	Zeiss Spectra-Physics Zeiss
Confocal microscope	
TCS SP8 confocal laser scanning microscope 63x/1.40 Oil CS2 objective	Leica Microsystems Leica Microsystems
Confocal microscope [MELC]	
DMI6000 B microscope 40x/NA 1.25 lens Orca Flash 4.0 V2	Leica Leica Hamamatsu
Inverted transmitted light microscope	
Wilovert S	Helmut Hund GmbH
Widefield microscope	
BX61 microscope UPlanApo 40x/0.85 objective F-view camera Illumination system MT20	Olympus Olympus Olympus Olympus

2.2 Mice

Age- and sex-matched wild type C57BL/6J, CD45.1$^+$ (B6.SJL-*Ptprc*^{a}*Pepc*^{b}/BoyJ), *cybb*$^{-/-}$ (B6.129S-*Cybb*^{tm1Din}/J), CFP-expressing (B6.129(ICR)-Tg(CAG-ECFP)CK6Nagy/J) and CX_3CR1-GFP (B6.129P(Cg)-*Ptprc*^{a}*Cx3cr1*^{tm1Litt}/LittJ) mice were bought from Jackson Laboratories (Bar Harbor, MA), B6 albino (B6N-*Tyr*$^{c\text{-}Brd}$/BrdCrCrl) mice were purchased from Charles River (Sulzfeld, Germany), and Catchup^{IVM} mice were obtained by crossing C57BL/6-*Ly6g*$^{tm2621(Cre\text{-}tdTomato)Arte}$ (Hasenberg *et al.*, 2015) mice to B6.Cg-*Gt(ROSA)26Sor*$^{tm14(CAG\text{-}tdTomato)Hze}$ (Madisen *et al.*, 2010) mice (kindly provided by Monika Riek-Burchardt, Otto-von-Guericke-University Magdeburg). All mice were bred under specific pathogen-free conditions at Otto-von-Guericke-University, Magdeburg.

All animal experiments were reviewed and approved by the Ethics Committee of the Office for Veterinary Affairs of the State of Saxony-Anhalt, Germany (permit license number 42502-2-1314 Uni MD) in accordance with legislation of both the European Union (Council Directive 499 2010/63/EU) and the Federal Republic of Germany (according to § 8, Section 1 TierSchG, and TierSchVersV).

2.2.1 Bone marrow isolation

Mice were euthanized by isoflurane treatment and rapid cervical dislocation. Femurs and tibias were isolated and sterilized using ethanol. The bone marrow was collected by centrifugation (10000 rpm, 4°C, 30 sec) of the opened bones in a 0.5 ml tube into a 1.5 ml tube with 100 µl RPMI 1640 medium. By filtering and washing with RPMI 1640 medium through a 100 µm cell strainer the cells of one mouse strain were pooled. After counting and centrifugation (450 xg, 4°C, 10 min), cells were adjusted to required concentration in PBS.

2.2.2 Construction of bone marrow chimeras

As recipient mice, *cybb*$^{-/-}$ mice were lethally irradiated (9.5 Gy) and reconstituted with approx. 40x10^6 bone marrow cells of CD45.1$^+$ and *cybb*$^{-/-}$ (50:50) intravenously. As control, CD45.1$^+$ and C57BL/6J were combined (50:50).

For cell nucleus staining, as recipient mice, C57BL/6J mice were lethally irradiated (9.5 Gy) and reconstituted with approx. 25x10^6 bone marrow cells of CFP-expressing mice intravenously.

The mice were maintained on neomycin sulfate water (2 g/l) for two weeks following transplantation to prevent infection. The mice were earliest infected with *S. aureus* eight weeks after reconstitution.

2.2.3 Depletion of neutrophils

To deplete neutrophils, an anti-mouse Ly6G 1A8 antibody (150 µg in 100 µl PBS) was injected intraperitoneally (i.p.) 6 h before infection. As a control, the rat IgG2a isotype control (anti-Trinitrophenol) was used in the same concentration, for treatment control, alone PBS was injected i.p.. The treatment was repeated 21 h after infection. The depletion of neutrophils was controlled by immunofluorescence staining and measurement via flow cytometry of blood samples at different time points after infection.

2.2.4 Isolation of neutrophils

For *in vitro* studies of neutrophils, these cells were isolated by negative selection via Magnetic Activated Cell Sorting (MACS) from bone marrow. The bone marrow was isolated as described in 2.2.1 (Bone marrow isolation).
After washing the cells with PBS and viable cell counting, 100 µl antibody cocktail (**Table 2.5**) per $1x10^7$ cells was added and incubated in a rotation incubator (4°C, 10 min). After additional washing, the pellet was resuspended in MACS buffer (100 µl per $1x10^7$ cells) and Anti-Biotin MicroBeads (15 µl per $1x10^7$ cells) were supplemented and incubated (4°C, 15 min, rotating). Via LS MACS Columns (Miltenyi Biotech), the neutrophils were isolated, as recommended by the manufacturer.

2.3 Microbiology

2.3.1 Bacteria strains and their cultivation

The gene encoding mKikume (Habuchi *et al.*, 2008) was codon optimized for *S. aureus*, *de novo* synthetized (Eurofins MWG) and inserted using ApaI and EcoRI into the pGL485 plasmid (Cooper *et al.*, 2009) yielding the plasmid pLacKikume. The truncated lacI gene including *pcn* promoter in front of the mKikume were exchanged via ApaI and SalI restriction sited by a construct comprising the *sarA* P1 promotor, *sod* ribosome binding site (RBS) (Malone *et al.*, 2009) and iTag (Catalao *et al.*, 2014) (*de novo* synthetized), resulting in the plasmid pKikume. To generate the pTufAKikume, a construct including the *tufA* promoter and ribosome binding site spanning 300 bp upstream of the *tufA* cds and an iTag (*de novo* synthetized) were cloned into the pKikume plasmid via ApaI and SalI. The recombinant plasmids were introduced into the *S. aureus* strain RN4220 (Kreiswirth *et al.*, 1983) by electroporation. The transfer of the plasmids into the *S. aureus* SH1000 (Horsburgh *et al.*, 2002) was done by phage transduction with bacteriophage 85 (Kwan *et al.*, 2005). GFP-expressing *S. aureus* pGFP have been described previously (Liew *et al.*, 2011).
S. aureus bacteria were cultivated in Brain Heart Infusion (BHI) broth at 37°C with shaking or on 1.5%-agar plates, supplemented with 12.5 µg/mL chloramphenicol. For OD_{600} measurement BHI medium was used as reference and the culture was diluted with BHI medium to obtain OD_{600} values between 0.01 and 1.0. For calculations, OD_{600} 1 was assumed to correspond to 10^8 bacteria/ml. For blood agar, 10% defibrinated sheep blood was added to lysogeny broth (LB) agar.
Escherichia coli (*E. coli*) DH5α was cultivated in LB medium at 37°C with shaking or on LB agar plates, both containing for pGL485-derivates 100 µg/mL spectinomycin or for *de novo* synthetized plasmids form Eurofins MWG 100 µg/ml ampicillin.

2.3.2 *S. aureus* infection

A day culture was inoculated by an overnight culture (16-18 h) to an OD_{600} 0.04-0.06. The bacteria were harvested for infection at OD_{600} 0.4-0.6, which represented the early exponential growth-phase. After washing with cold PBS, the OD_{600} was adjusted to 2.5 in PBS by centrifugation (9000 xg, 5 min, 4°C) and resuspension. The ear skin of mice was intradermally infected at three sites per ear, each with $5x10^4$ bacteria using a 35 gauge syringe.

2.3.3 Determination of bacterial burden in mouse tissue

To analyze colony forming units in the ear, bacteria were isolated from infected ears by homogenization with 15 ml disposable tissue grinders (Fisherbrand) or 15 mL tapered tissue grinders (Wheaton) in 2 ml ice cold PBS. The cells were centrifuged (16500 xg, 3 min, 4°C) after adding of 0.1% triton-X 100 and lysed with 1% triton-X 100 in H_2O. The bacteria in the lymph nodes were isolated by destruction of the lymph node tissue via shear forces with a cannula (18 gauge) and 1% triton-X 100 in H_2O. The bacteria were serially diluted as triplicates in PBS and plated on BHI agar plates. For evaluation, the median of triplicate platings was determined.

2.3.4 Photoconversion

The diode arrays we used are described as a circuit diagram in **Figure 2.1**. For *in vitro* photoconversion, *S. aureus*-pKikume were illuminated in a 96-well plate with violet light at 405 nm wavelength using an assembly of 2x2 LED diodes (Strato, half-viewing angle: 15°; Radiant Power: 10 mW) for 1 min in a distance of 1.7 cm. In **Figure 3.4 b**, the *in vitro* photoconversion of *S. aureus*-pKikume was done by illumination in a petri dish with violet light at 357 nm wavelength by assembling 3x3 LED diodes (Strato, half-viewing angle: 10°; Radiant Power: 10 mW) for 5 min in a distance of 0.8 cm.
Ears of anaesthetized mice were photoconverted with violet light at 405 nm wavelength using an assembly of 3x3 LED diodes (Strato, half-viewing angle: 15°; Radiant Power: 10 mW), for intravital 2-photon microscopy illumination time was set to 1-2 min in a distance of 2 cm, for confocal microscopy, the ears were illuminated from each side for 1 min in a distance of 1.5 cm.

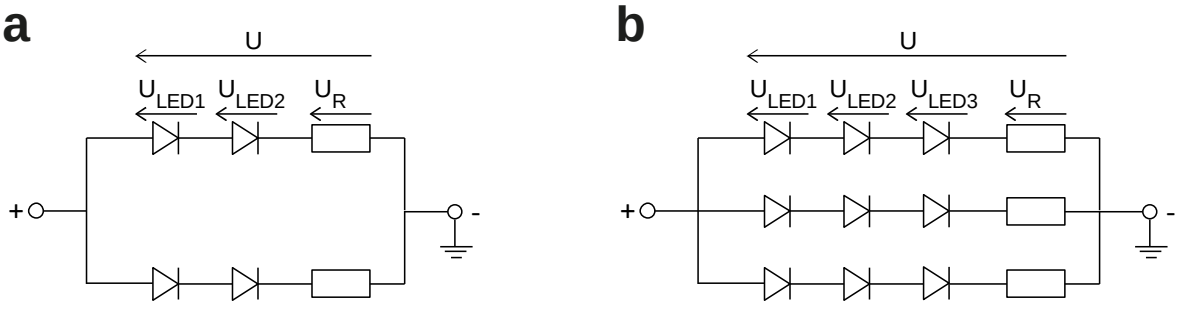

Figure 2.1: Circuit diagrams of diode arrays. a) 2x2 diode array for photoconversion in 96-well plates. 405 nm diodes and 27 Ω resistors with a 9 V power supply. **b)** 3x3 diode array either for photoconversion or DNA crosslinking with 405 nm diodes, 24 Ω resistors, and a 12 V power supply or 375 nm diodes, 47 Ω resistors, and a 12 V power supply, respectively.

2.3.5 Generation of division-incompetent, but metabolically active *S. aureus*

To generate division-incompetent, but metabolically active bacteria, pyrimidine bases of the DNA were crosslinked by psoralen with long-wavelength UVA light (Belanger *et al.*, 2000; Lin *et al.*, 1997). For this, 10 µM of 4'-(aminomethyl)-4,5',8-trimethylpsoralen hydrochloride (Aminoethyltrioxsalen, AMT) were added to 1 ml *S. aureus* culture, directly before use. 0.5 ml of this sample were illuminated in a petri dish on ice with violet light at 357 nm wavelength using an assembly of 3x3 LED diodes (Strato, half-viewing angle: 10°; Radiant Power: 10 mW) for 10 min in a distance of 0.8 cm. The used diode array is described as a circuit diagram in **Figure 2.1 b**.

2.3.6 Measurement of membrane integrity

To measure the viability of the bacteria, the *Bac*Light™ Bacterial Membrane Potential Kit was used according to manufacturer's instructions and measured by flow cytometry. As control for intact membrane potential, a *S. aureus* day culture was used in which the membrane potential was abolished using the proton ionophore carbonyl cyanide 3-chlorophenylhydrazone (CCCP). As indicator, 3,3'-Diethyloxa-carbocyanine iodide ($DiOC_2$) was used, in which green fluorescence (measured at 488 nm excitation and 530/30 nm emission) shifts to red fluorescence (measured at 488 nm excitation and 670/30 nm emission) by self-association in high cytosolic concentrations.

2.4 Molecular biology

2.4.1 Plasmid construction

Specific enzymatic digestion of plasmids was done in two ways. The pLacKikume was prepared with ApaI and EcoRI and the other constructs by the use of ApaI and SalI. The reaction was performed in two steps, as recommended by manufacturer: First with ApaI in CutSmart buffer at 25°C and then after adding of NaCl to reach 50 mM or 100 mM concentration with EcoRI or SalI at 37°C. Digested vectors were dephosphorylated afterwards, by addition of 1 µl antarctic phosphatase and incubating at 37°C.
The enzymatically digested DNA was analyzed by agarose gel electrophoresis. The samples were mixes with 6x DNA loading dye and loaded on an agarose gel (0.6% agarose and 1 µg/ml ethidium bromide in TAP buffer). For size measurement of the fragments Quick-Load® 2-Log DNA Ladder was additionally loaded. The gel was placed in a BIO-RAD Mini DNA system which was filled with TAP buffer. After 30-60 min at 100 V, the DNA fragments were visualized by UV light.
Extraction of fragments from agarose gel was performed with Nucleo Spin® Extract II according manufacturer's instructions. The concentration of processed DNA was measured with the NanoDrop 2000 spectrophotometer.
The plasmids were ligated in an insert to vector molecule ratio of 5:1, mixed with T4 ligase in T4 ligation buffer. Samples were incubated at room temperature overnight and then stored at -20°C.

2.4.2 Transformation of *E. coli*

For transformation of plasmids into chemically competent *E. coli* cells NEB 5-alpha Competent *E. coli* (High Efficiency) from New England Biolabs were used according manufacturer's instructions. 100 µl and 900 µl bacteria solution were plated per LB agar plate (containing selective antibiotic).

2.4.3 Mini- and Maxi-DNA preparation from *E. coli*

To isolate plasmid DNA from *E. coli* cultures, the NucleoBond® PC 500 for large volumes and the Invisorb Spin Plasmid Mini Two for small volumes were used according manufacturer's instructions.

2.4.4 Preparation of *S. aureus* RN4220 electrocompetent cells

A day culture was inoculated by an overnight culture (16-18 h) of *S. aureus* RN4220 (Kreiswirth *et al.*, 1983) to an OD_{600} 0.05. The bacteria were harvested for treatment at OD_{600} 0.4-0.6 by centrifugation of 50 ml volume (2500 xg, 5 min, 4°C) and resuspend in the same volume of 0.5 M sucrose solution. The step was repeated three times in half volume (25, 12.5, 6.25 ml) until the bacteria were resuspend in 350 µl sterile 20% glycerol (v/v in ddH_2O). Aliquods of 60 µl were stored at -80°C.

2.4.5 Electroporation of *S. aureus* RN4220

Electrocompetent cells were thawed on ice, 200 ng plasmid-DNA were added in 1 µl, and incubated for 30 min on ice. The cells were electroporated with a capacity of 25 µFd, 100 Ω and 1, 1.5, or 2 kV (time constant= 2.54-2.60). The bacteria were then diluted with 900 µl cold super optimal broth with catabolite repression (SOC) medium, cultivated for 90 min at 37°C under agitation, and plated on selective antibiotic containing LB agar plates.

2.4.6 Plasmid transduction with bacteriophage 85

The transfer of plasmids from *S. aureus* RN4220 into the *S. aureus* SH1000 (Horsburgh *et al.*, 2002) was done by phage transduction with bacteriophage 85 (Kwan *et al.*, 2005).
In a first step, the phage was loaded with the plasmid. To an overnight culture (16-18 h) of plasmid containing *S. aureus* RN4220, 1 M $CaCl_2$ (End-concentration 5 mM) were added, further cultivated for 5-30 min, and following 300 µl culture were heated up to 52°C for 2 min. 100 µl phage solution (pre-diluted in phage buffer: 10^0, 10^1, 10^2, 10^3, 10^{-4}, and one without phages) were added and incubated (room temperature, 15 min). The phage-bacteria solution were mixed with 4 ml soft agar (a) and cultivated on blood agar plates at 37°C. The plate with confluent lysis was used for phage isolation by washing the soft agar with two times 1 ml phage buffer. The lysate was filtered (0.45 µm) and stored at 4°C.
In the second step, to an overnight culture (16-18 h) were 1 M $CaCl_2$ (End-concentration 5 mM) added, further cultivated for 5-30 min, and 300 µl culture were heated up to 52°C for 2 min. 100 µl phage solution (pre-diluted in phage buffer: 10^0, 10^{-1}, 10^{-2}, and one without phages) were added and incubated (room temperature, 15 min). The phage-bacteria solution were mixed with 3 ml soft agar (b) and cultivated on selective antibiotic containing LB agar plates at 37°C for 24-48 h.

2.5 Flow cytometry

Flow cytometry of bacteria was performed in culture medium or diluted to suitable concentrations with cold PBS. The red mKikume fluorescence signal was measured at 488 nm excitation and 610/20 nm emission, the green mKikume fluorescence signal was measured at 488 nm excitation and 530/30 nm emission.

For analysis of cells recruited to the site of infection, ears were separated into dorsal and ventral sheets using two forceps. The ear sheets were digested with either 1 mg/mL collagenase, 50 ng/mL DNase, 100 µg/mL penicillin/streptomycin and 5 µg/mL tetracycline in RPMI 1640 medium at 37°C and 600 rpm shaking for 60 min, or 2 mg/mL collagenase, 50 ng/mL DNase, and 5 µg/mL tetracycline in RPMI 1640 medium at 37°C and 600 rpm shaking for 30 min. To release the cells, the ear was homogenized through a 70 µm cell strainer (Falcon) and washed with PBS. After centrifugation for 10 min with 1500 rpm at 4°C and washing with flow cytometry buffer, the cells were Fc-blocked using anti-CD16/32 antibody (clone 93), and stained with fluorochrome labelled antibodies (see **Table 2.7**). CountBright™ absolute counting beads were added to the samples before measurement if required. The measurement was performed with an LSRFortessa flow cytometer using the blue 488 nm, the yellow-green 561 nm, and the red 622 nm lasers. The data were analyzed by using the FlowJo X software (FlowJo, LLC).

2.6 Microscopy

2.6.1 Intravital 2-photon microscopy

The mice were anesthetized and prepared for intravital 2-photon imaging. For this, the mouse was placed on a heating stage adjusted to 37°C and one ear was fixed to a metal platform. A coverslip sealed to a surrounding parafilm blanket was placed onto the ear and glued to the platform. 2-photon imaging was performed with a Zeiss LSM 700 equipped with a Mai Tai DeepSee Ti:Sa laser tuned at 920 nm (*S. aureus*-pKikume in B6 albino mice) or 960 nm (*S. aureus*-GFP in Catchup^{IVM} mice) and a W Plan-Apochromat 20x/1.0 DIC VIS-IR dipping objective. For *S. aureus*-pKikume, the emitted signal was split by 490 nm, 520 nm and 555 nm long pass and dichroic mirrors and filtered with 509/22 nm, 500/50 nm (green mKikume) and 589/54 nm (red mKikume) filters before collection with non-descanned detectors. For *S. aureus*-GFP in Catchup^{IVM} mice, the emitted signal was split by 555 nm long pass and 490 nm long pass and dichroic mirrors and filtered with 565/10 nm (red signal, neutrophils), 485 nm short pass (second harmonics) and 500/50 nm (GFP signal) filters before collection with non-descanned detectors.

2.6.2 Confocal microscopy

For *in vitro* imaging of *S. aureus* proliferation, agar pads (2% low melting agarose, 10% FCS, 12.5 µg/mL chloramphenicol in RPMI 1640 medium, without phenol red) on glass bottom dishes (ibidi) were used. For analyzing the bacteria in the tissue, the infected ears were harvested at defined time points, fixed for 8-16 h in 4% paraformaldehyde (PFA) in PBS at 4°C. Afterwards the fluorescence protein was stabilized by incubating the ears for 8-16 h in 20% sucrose at 4°C. The samples were frozen in Tissue-Tek® O.C.T.™ Compound with liquid nitrogen and stored at -80°C. The ears were cut into 20 µm cryosections and placed on Superfrost slides (Thermo Scientific) coated with 0.1% Poly-L-Lysin in ddH_2O and air-dried for 1-2 h before storage at -40°C until use.
Measurement was performed with the TCS SP8 confocal laser scanning microscope using a 63x/1.40 Oil CS2 objective. For proliferation analysis the red mKikume fluorescence signal was measured at 561 nm excitation and 598-638 nm emission, while the green mKikume fluorescence signal was measured at 488 nm excitation and 526-570 nm emission.
To extract data of *S. aureus* uptake by neutrophils, the red tdTomato fluorescence signal (neutrophils in the Catchup^{IVM} mice) was measured at 561 nm excitation and 600-669 nm emission, while the green GFP fluorescence signal (*S. aureus*-pGFP) was measured at 488 nm excitation and 499-565 nm emission.

2.6.3 Staining of tissue sections for confocal microscopy

For immunofluorescence staining of the bacteria, the infected ears (4 h p.I.) were prepared as for confocal microscopy. After storage at -40°C, the tissue was permeabilized with 0.1% triton-X 100 in PBS and stained with polyclonal rabbit anti-*Staphylococcus aureus* and Alexa Fluor 647 conjugated goat anti-rabbit IgG. The fluorescence signal of the antibody staining was measured at 488 nm excitation and 499-525 nm emission, while the green mKikume fluorescence signal was measured at 633 nm excitation and 675-745 nm emission.

To examine the nucleus of the cells, CFP BMCs were used. The infected ears were photoconverted and 16 h p.I. prepared as described for confocal microscopy. The cryosections (5 µm) were again fixed with 4% PFA in PBS, permeabilized with 0.1% triton-X 100 in PBS and stained with DAPI (1 mg/ml, 1:5000). The fluorescence signal of the DAPI staining was measured at 355 nm excitation and 422-452 nm emission and the CFP signal at 458 nm excitation and 461-496 nm emission. The green and red mKikume fluorescence signal was collectively measured at 488 and 633 nm excitation and 514-557 or 565-640 nm emission, respectively.

2.6.4 Widefield microscopy

To test the photoconvertability, a widefield microscope was used. Fluorescence signals were acquired by a BX61 microscope equipped with a UPlanApo 40x/0.85 objective and a F-view camera. Bacteria from a day culture (OD_{600} 0.4-0.6) were pipetted on an agar pad (2% low melting agarose, 10% FCS, 12.5 µg/mL chloramphenicol in RPMI 1640 medium without phenol red) and placed on a coverslip. Photoconversion was performed for 20 s with 436/10 nm by half power of the illumination system MT20.

2.6.5 Multi-Epitope Ligand Cartography (MELC)

For analyzing the immune cells and bacteria in the tissue, the infected ears were harvested at defined time points, fixed for 2 h in 4% PFA in PBS at 4°C. Afterwards the fluorescence was stabilized by incubating the ears for 8-16 h in 20% sucrose at 4°C. The samples were frozen in Tissue-Tek® O.C.T.™ Compound with liquid nitrogen and stored at -80°C. The ears were cut into 10 µm cryosections and placed on Superfrost slides (Thermo Scientific) coated with 0.1% Poly-L-Lysin in H_2O and air-dried for 1-2 h before storage at -40°C until use.

For Multi-Epitope Ligand Cartography (MELC) a MM3.2 Toponome Imaging Cycler (MelTec, Magdeburg) was used at the Institute of Molecular and Clinical Immunology of the

Otto-von-Guericke-University, Magdeburg (Philipsen *et al.*, 2013). Labelled antibodies (**Table 2.7**) were incubated successively and their fluorescence signals were removed by bleaching of the coupled fluorophore, after imaging. A DMI6000B microscope including a 40x/NA1.25 lens and the Orca Flash 4.0 V2 was used for acquiring image stacks of the fluorescence signal for 3D images of 2000x2000 pixels in 15 steps with a voxel size of 6500x6500x400 nm^3. After every staining cycle, an additional phase contrast image was collected. With these images the fluorescence images were automatically aligned voxel-wise (accuracy in XY 1/10 pixel and in Z 1/2 pixel). Illumination faults of the fluorescence images were eliminated with flat-field correction and additionally, the resolution of the fluorescent image stacks was optimized by a deconvolution and deblurring algorithm (XCOSM software package), an interface to Computational Optical Sectioning Microscopy algorithms for removing out-of-focus light in 3D images (Washington University St. Louis, MO).

2.6.6 Image analysis

Bacteria in intravital 2-photon microscopy movies were segmented using the surface detection function of the Imaris software (Bitplane) from combined red and green mKikume fluorescence channels. Fluorescence values and time points of the segmented bacteria for the individual channels were converted into flow cytometry datasets using the DiscIT software (Moreau *et al.*, 2012) and analyzed using the FlowJo X software (FlowJo, LLC).
For analysis of confocal microscopy data, 144x144 µm frames spaced at least 2.5 µm apart were used to detect bacteria in a combined green and red mKikume channel using the threshold and analyze particle functions of the Fiji software (NIH, http://rsb.info.nih.gov/ij/). The macro to analyze images is added in 6.2.1 Macro for automated proliferation measurement. Fluorescence data from the resulting regions of interest were extracted, converted into flow cytometry datasets using the DiscIT software (Moreau *et al.*, 2012) and analyzed using the FlowJo X software (FlowJo, LLC). The combined proliferation indices of all detected bacteria within one frame were used for data representation.
Host cells and bacteria in images of MELC were analyzed in the Fiji software (NIH, http://rsb.info.nih.gov/ij/). By drawing the surroundings of $CD45.1^+$ or $CD45.2^+$ host cells, regions of interest were defined. The cell surface markers were analyzed automatically by 6.2.2 Macro for fluorescence measurement of cell borders in MELC data and the fluorescence of the bacteria was measured with 6.2.3 Macro for bacterial mKikume fluorescence measurement in MELC data. The fluorescence of the bacteria in one cell was normalized to the fluorescence of the bacteria in the $CD45.1^+$ cells or for non-bone marrow chimeras to the bacteria in the wild type cells.

3 RESULTS

3.1 Adaptation of mKikumeGR to *S. aureus* SH1000

S. aureus surface proteins and secreted toxins trigger the production of chemotactic molecules, which results in a massive influx and accumulation of neutrophils at the site of infection (McGuinness *et al.*, 2016). Although *S. aureus* has been shown to be able to withstand and counteract innate cellular immune responses (Abtin *et al.*, 2014; Gresham *et al.*, 2000; Kobayashi *et al.*, 2010), it is unclear how neutrophil effector functions impact on its proliferation. Determination of growth rates during infection is of special interest for *S. aureus* because slow-growing subpopulations of this opportunistic pathogen have been proposed to acquire phenotypic resistance against antibiotic treatment, and give rise to relapsing infections due to lower sensitivity to immune-mediated control mechanisms (Tuchscherr *et al.*, 2011; Krut *et al.*, 2004). However, it has been difficult so far to determine *S. aureus* growth rates *in vivo*, especially beyond the first few rounds of cell division after inoculation (see **Figure 1.8**). Therefore, we generated a proliferation biosensor based on dilution and *de novo* production of the photoconvertible fluorescence protein mKikumeGR (Heyde *et al.*, 2018; Muller *et al.*, 2013; Jarick *et al.*, 2018).

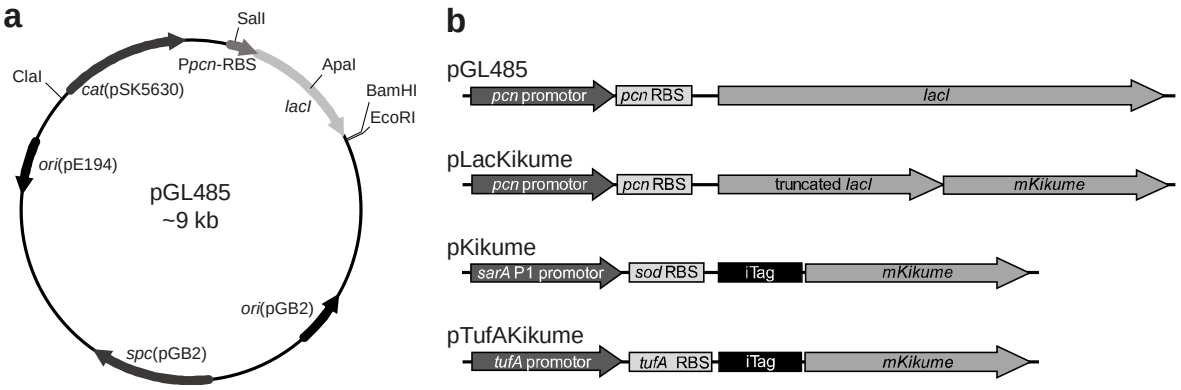

Figure 3.1: Plasmid for mKikume expression in *S. aureus* SH1000. a) pGL485 vector map and cloning sites. **b)** Schematic representation of pGL485 derivatives, which were used for mKikume expression in *S. aureus* SH1000. Sequences of *mKikume* containing constructs are listed in 6.1 Sequences of mKikume constructs. *cat*= chloramphenicol resistance, *ori*= origin for replication, *pcn*= penicillinase promoter, RBS= ribosome binding site, *sod*= superoxide dismutase, *spc*= spectinomycin resistance.

In a first step, different constructs for the use in pGL485 (Cooper *et al.*, 2009) were designed to adapt the mKikumeGR to *S. aureus* SH1000 (**Figure 3.1**). For all approaches, the gene of mKikume was codon optimized by Eurofins MWG for better expression in *S. aureus* (see

for sequence 6.1 Sequences of mKikume constructs) (Catalao *et al.*, 2014). In pLacKikume, the *gfp* gene of pGL485-GFP (Liew *et al.*, 2011) was exchanged to the *mKikume* gene (Habuchi *et al.*, 2008). For optimal fluorescence intensity, a second construct was designed, containing the iTag (Catalao *et al.*, 2014), the *sarA* P1 promoter, and the *sod* RBS (Malone *et al.*, 2009). The iTag is a stretch of 10 amino acids, which has been proposed to increase fluorescence intensity of GFP-like proteins in Gram-positive bacteria (Catalao *et al.*, 2014; Henriques *et al.*, 2013). The *sarA* P1 promoter is described as being highly active during bacterial growth and was already used for expression of GFP in *S. aureus* (Malone *et al.*, 2009; Liese *et al.*, 2013; Manna *et al.*, 1998). As an additional change, the *sod* RBS, which is reported to be a strong and effective RBS for fluorescence protein expression, was introduced (Malone *et al.*, 2009). In the third construct, the promoter and ribosome binding site of *tufA* were used, which were reported for constitutive GFP expression in *S. aureus* (Schlag *et al.*, 2010; Biswas *et al.*, 2006).

In **Figure 3.2**, confocal images of the three constructs and the empty vector pGL485 are compared. Fluorescence for *S. aureus*-pLacKikume was not detectable and for *S. aureus*-pTufAKikume, much less green signal was detected than for *S. aureus*-pKikume. Similar data were measured with flow cytometry analysis of these constructs, also with this analysis, only a small proportion of bacteria were shown to be fluorescent, except for *S. aureus*-pKikume (**Figure 3.2 b**). Additionally, the measurement of green mKikume fluorescence in cultures over time revealed for *S. aureus*-pKikume higher intensities than for the only other fluorescent strain *S. aureus*-pTufAKikume (**Figure 3.2 c**). Because of the high fluorescence intensity, the big amount of fluorescent bacteria (around 80%), and no influence on the bacterial growth while expression of pKikume (**Figure 3.2 c**), all following mKikume experiments were performed with *S. aureus* SH1000-pKikume.

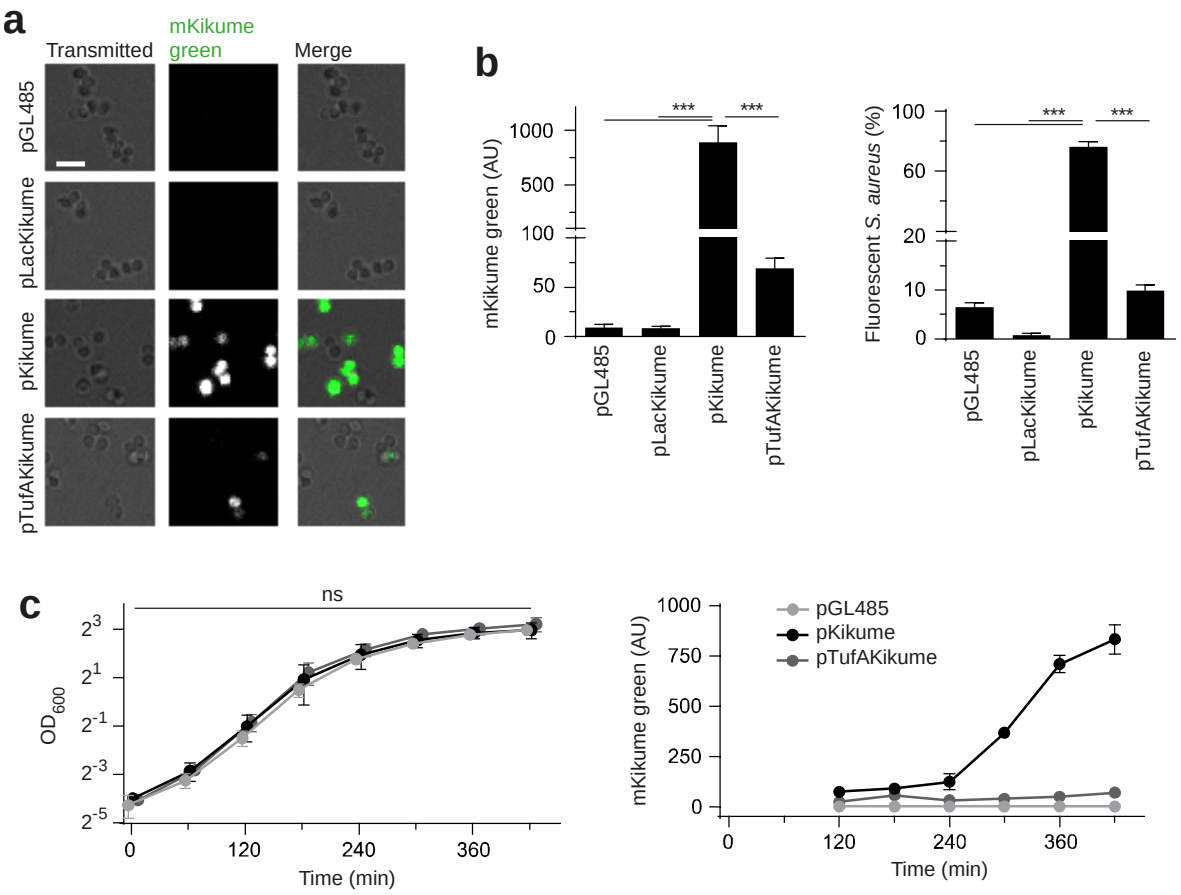

Figure 3.2: Comparison of pGL485 derivates. a) Confocal imaging of *S. aureus*, cultivated for 7 h, with different plasmids in glass bottom dishes. Scale bar, 3 µm. **b)** Flow cytometry analysis of *S. aureus* with different plasmids. Mean (+/- standard deviation) green fluorescence, representing mKikume signal of four individual 7 h cultures (left graph). Mean (+/- standard deviation) percentage of green fluorescent bacteria of four individual 7 h cultures (right graph). ***, p<0.001 as determined by one-way ANOVA. **c)** Growth curves of *S. aureus* cultures containing different plasmids. OD_{600} measurement over time of three individual cultures (left graph). Mean (+/- standard deviation); ns, not significant as determined by two-way ANOVA Measurement of green fluorescence, by flow cytometry, over time of three individual cultures (right graph).

The photoconversion of the mKikume fluorescent protein from green to red was tested via flow cytometry for an exponential growing culture, and via microscopy, for bacteria in the stationary phase (**Figure 3.3**). For estimating the duration of 405 nm illumination suitable for photoconversion, the red to green ratio was calculated, reflecting the decrease of green signal as well as the increase of red fluorescence. A photoconversion for 60 s was found to be suitable, because the biggest decrease in green fluorescent and only slight bleaching of all fluorescence intensities was observed. In the microscope, a sufficient photoconversion from green to red was achieved using UV illumination of 60 s. Thus, the protein can be

photoconverted by violet and UVA light at any given time point, even during infection *in vivo* (**Figure 3.9 a**).

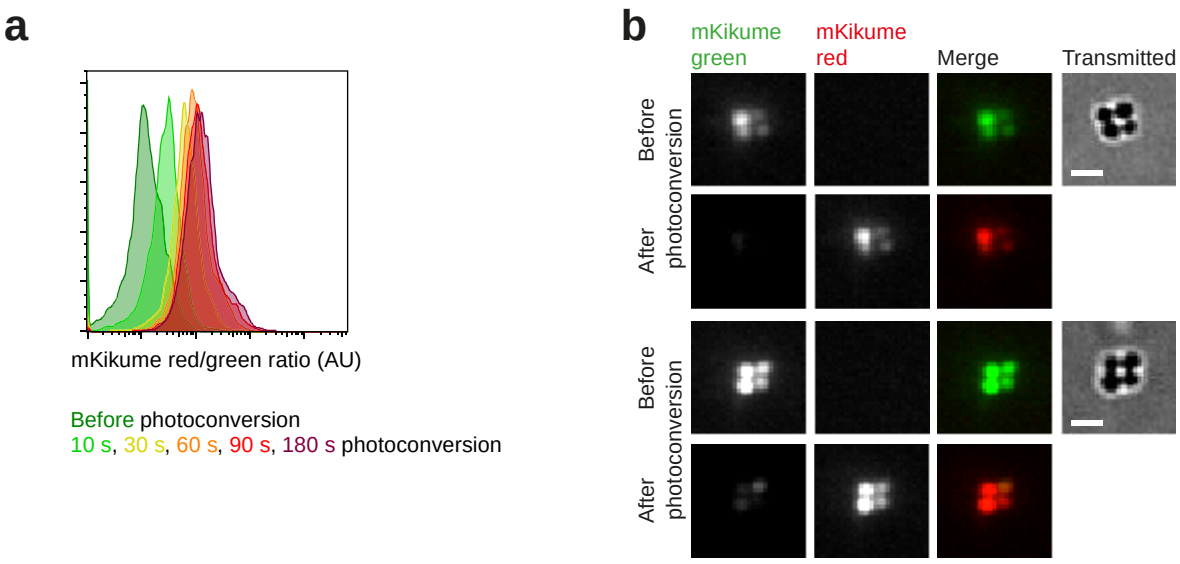

Figure 3.3: Photoconversion of mKikume a) Representative flow cytometry measurement of photoconverted (405 nm) *S. aureus*-pKikume. Cultivated for 3 h. **b)** Widefield microscopy of *S. aureus*-pKikume over night cultures growing on an agar pad before and after photoconversion with violet (405 nm) light. Scale bar, 3 µm.

In a proliferation measurement approach of old versus new protein (see **Figure 1.8**), the proliferation of the bacteria can be measured by the recovery from photoconversion through dilution of "old" red (photoconverted) and *de novo* production of "new" green (non-photoconverted) protein, which is expected to be taking place during growth, but not in proliferation-inactive bacteria (**Figure 3.4 a**). To evaluate the approach, *S. aureus*-pKikume was examined by time lapse microscopy after photoconversion in an *in vitro* system on agar pads. All bacteria were red fluorescent directly after photoconversion, but a recovery of the original, green fluorescence was detectable in dividing bacteria, while the red fluorescence was diluted in a time-dependent manner. In contrast, non-dividing bacteria (next to the dividing cells in **Figure 3.4 b**) retained the red, photoconverted fluorescence (**Figure 3.4 b-c**). Several single bacteria were followed up over time and a quantitative analysis showed an increase in green and decrease in red fluorescence for dividing *S. aureus*, whereas the non-dividing bacteria remained stable in their fluorescence intensities (**Figure 3.4 c**). The calculated mKikume red to green fluorescence ratios showed a very robust change over time for dividing, but not for non-dividing bacteria on a single bacteria level (**Figure 3.4 d**).

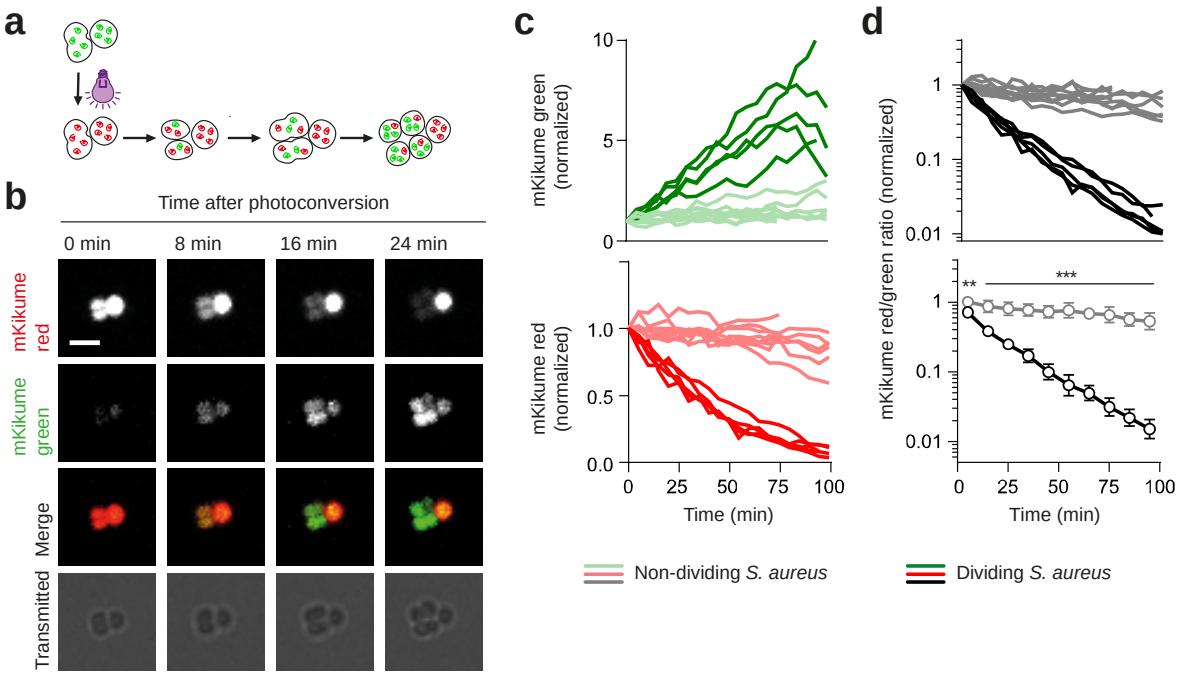

Figure 3.4: Recovery of single bacteria from photoconversion. a) Schematic representation of the fluorescence-based reporter system principle. Proliferating bacteria turn green by dilution of the red fluorescent (photoconverted) protein and *de novo* production of green fluorescent mKikume and non-dividing bacteria stay red. **b)** Confocal time lapse imaging of a photoconverted (375 nm) *S. aureus*-pKikume culture growing on an agar pad. Scale bar, 3 µm. **c)** Normalized red and green fluorescence of dividing (red, green) and non-dividing (pale red and green) bacteria as observed by time lapse imaging on an agar pad. Each curve represents one bacterium followed over up to 100 min. **d)** Ratio of red to green fluorescence of the measurement shown in b). Black curves, dividing bacteria, grey curves, non-dividing bacteria. Upper panel: Each curve represents one bacterium followed over up to 100 min. Lower panel: Mean +/- standard deviation. ***, $p<0.001$; **, $p<0.01$ as determined by two-way ANOVA.

To quantify the recovery from photoconversion not only for single cells, but on the whole population level, flow cytometry analysis was used. Here, the fluorescent bacteria were detected by comparison against the non-fluorescent *S. aureus*-pGL485 (**Figure 3.5 a**). The exponentially growing culture was photoconverted and further cultivated. By taking samples over time, the change of the red to green ratio can be measured. The analysis of exponentially growing *S. aureus* culture showed that the largest change in the red to green ratio occurred in the first 60 min after photoconversion, with a complete recovery from photoconversion after 90 min (**Figure 3.5 b-c**) and a plateau in the development of red to green ratio after this time point. From these data, the optimal readout time point for *S. aureus* growth rate was determined to be 60 min after photoconversion.

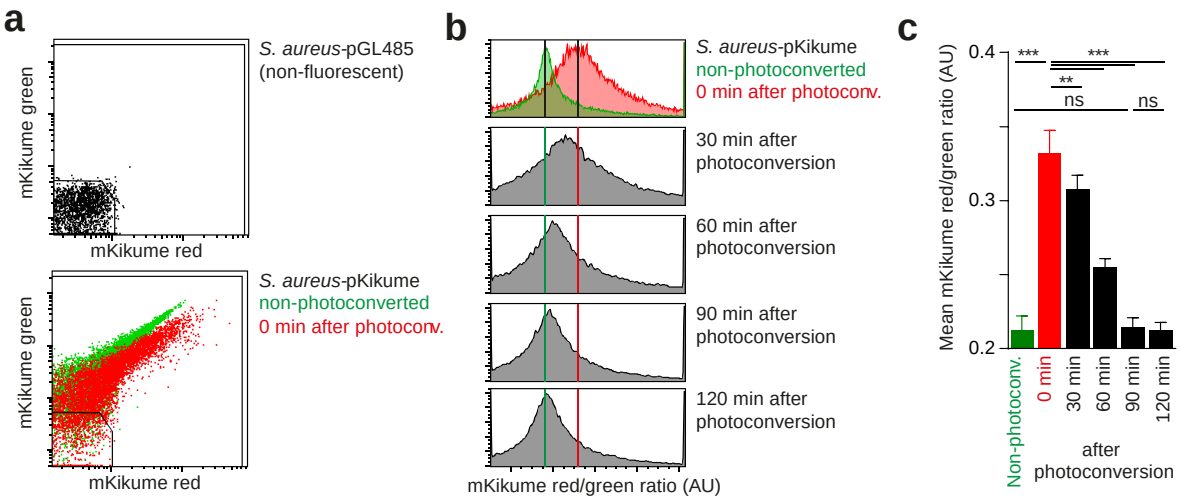

Figure 3.5: Recovery from photoconversion *in vitro*. a) Flow cytometry analysis of non-fluorescent *S. aureus* with the empty-vector pGL485 (upper plot) and *S. aureus*-pKikume (lower plot) non-photovconverted (green) and 0 min after photoconversion (red). A gate for selecting fluorescent bacteria is indicated. **b)** Histogram of the red to green ratio of fluorescent bacteria in a day culture before (green) and after (red and grey) photoconversion gated as indicated in a). Green vertical line: distribution maximum of non-photoconverted bacteria. Red vertical line: distribution maximum of photoconverted bacteria. Data in a) and b) are representative of three individual bacterial cultures. **c)** Mean (+/- standard deviation) mKikume red to green fluorescence ratio development over time of three individual day cultures after photoconversion. ***, $p<0.001$; **, $p<0.01$ as determined by one-way ANOVA.

3.1.1 Division-incompetent, but metabolically active *S. aureus*

In principle, a recovery from photoconversion could also be achieved by protein turnover in live, but non-growing bacteria. Therefore, in order to address the impact of protein turnover in non-dividing bacteria, we employed division-incompetent, but metabolically active *S. aureus.* Brockstedt *et al.* published DNA crosslinking for Gram-positive bacteria by using psoralen and UV light (Brockstedt *et al.*, 2005). The bacterial DNA is crosslinked between the pyrimidine bases by psoralen with long-wavelength UVA light, whereby the distribution of the DNA cannot take place anymore, but the metabolism is still active (Belanger *et al.*, 2000; Lin *et al.*, 1997).

To validate that treatment with UVA and psoralen completely inhibits *S. aureus* SH1000 growth, but the individual treatment conditions have no influence on the bacterial growth, the bacteria were plated as drops in dilutions (**Figure 3.6 a**). Suitable conditions for generating efficient growth inhibition of division-incompetent, but metabolically active bacteria were found to be 10 min UVA light on bacteria mixed with 10 µM psoralen (Aminoethyltrioxsalen, AMT), which were used for further characterization. The viability of the division-incompetent bacteria was investigated via their membrane potential and with it the membrane integrity, which is expected to decline for dying cells. The regular green fluorescent $DiOC_2$ changes to red fluorescence by self-association in high cytosolic concentrations of dying or dead cells, which can be measured via flow cytometry. As shown in **Figure 3.6 b**, no significant (one-way ANOVA) differences in the membrane integrity were found for treated and non-treated cells. Thus, the division-incompetent bacteria were alive like non-treated bacteria. Because of the time frame of 60 min for measurement of the bacterial growth with the biosensor, the cells have to be healthy for 60 min after psoralen/UVA treatment. A comparable membrane integrity was shown for division-incompetent bacteria, compared to untreated *S. aureus* over time to 60 min (**Figure 3.6 c**). Although the division-incompetent bacteria were alive, we observed no significant (two-way ANOVA) reduction in recovery from photoconversion as compared to growth competent controls, which in contrast shows a significant (two-way ANOVA) change in red or green mKikume fluorescence intensity (**Figure 3.6 d**). Therefore, indeed bacterial proliferation and not protein turnover is mainly responsible for fluorescence recovery after photoconversion as a readout of the biosensor.

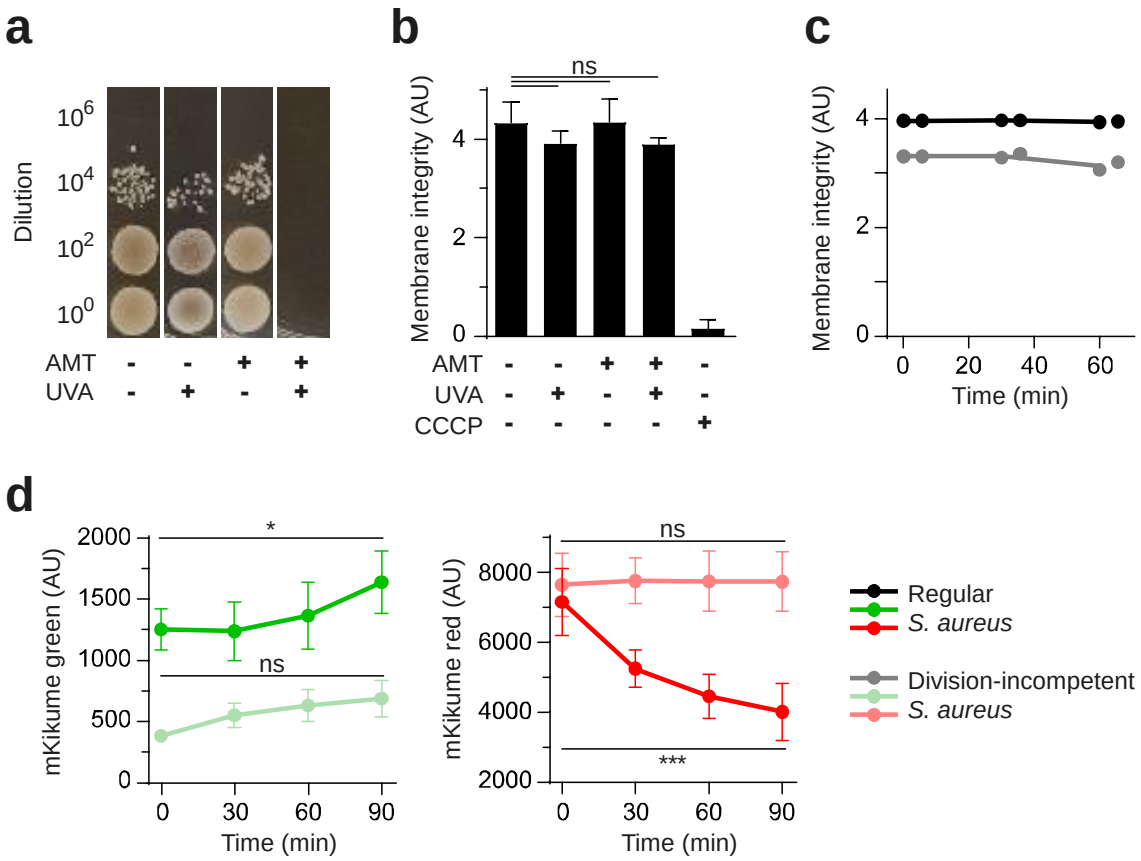

Figure 3.6: Division-incompetent, but metabolically active *S. aureus*. a) Efficiency of growth inhibition after generation of division-incompetent, but metabolically active bacteria. Serial dilutions of control bacteria and bacteria treated with 10 µM psoralen (AMT), or 10 min 375 nm light (UVA), or both. **b)** Flow cytometry measurement of membrane integrity by using $DiOC_2$ of treated bacteria with 10 µM psoralen (AMT) and 10 min 375 nm light (UVA). The protonophore CCCP was used as a low membrane integrity control. Mean of four individual cultures (+/- standard deviation) is shown; ns, not significant as determined by one-way ANOVA. **c)** Membrane integrity of division-incompetent, but metabolically active bacteria (grey) and control *S. aureus*-pKikume (black) over time in culture. **d)** mKikume red and green fluorescence development over time of five to seven individual *S. aureus*-pKikume day cultures. Measurement of fluorescent bacteria by flow cytometry, started after photoconversion of exponential growth (red, green) and division-incompetent (pale red and green) bacteria. Mean +/- standard deviation is shown. ***, $p<0.001$; *, $p<0.05$; ns, not significant as determined by two-way ANOVA.

3.1.2 Intravital imaging of *S. aureus*-pKikume

S. aureus accounts for a large number of skin and soft tissue infections (Tong *et al.*, 2015), which represent a typical clinical manifestation of the pathogen. Therefore, an ear skin infection model was chosen to investigate *S. aureus*-pKikume infections and to examine *S. aureus* proliferation *in vivo*. For this, we analyzed recovery from photoconversion of the biosensor in *S. aureus* during cutaneous infection of the ear using intravital 2-photon microscopy.

A low infection dose of $5x10^4$ *S. aureus* carrying the pKikume reporter plasmid were injected intradermally at three infection site per ear of B6 albino mice, photoconverted by 405 nm illumination at a defined time point post infection (p.I.), and immediately imaged by intravital 2-photon microscopy for subsequent 60 min (**Figure 3.7**).

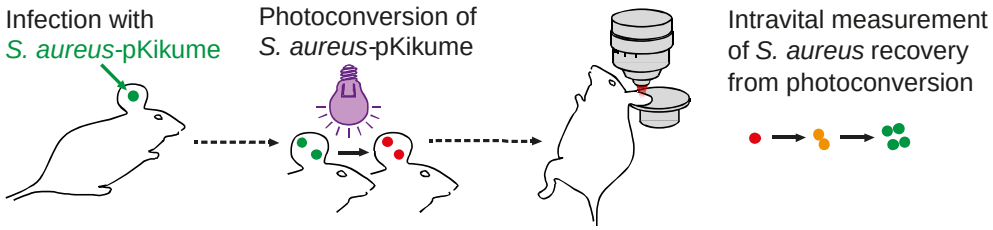

Figure 3.7: Schematic representation of intravital 2-photon microscopy procedure. Mice were infected in the ear at three injection sites with $5x10^4$ *S. aureus*-pKikume each. After a defined period of time, bacteria in the ear were photoconverted and the mKikume red and green fluorescence was measured over time by intravital 2-photon microscopy.

In order to ensure that all bacteria were detectable by their fluorescence during intravital microscopy, we first tested the population-wide mKikume fluorescence by confocal microscopy of fixed tissue sections. For this, we infected ears with *S. aureus*-pKikume, fixed and sectioned them. The cryosections were immunostained against *S. aureus*, and immunofluorescence staining was compared with bacterial mKikume signal at the site of infection. As shown in **Figure 3.8**, the majority of bacteria detectable by immunostaining expressed the mKikume protein at detectable levels and thus, would be visible during intravital 2-photon microscopy.

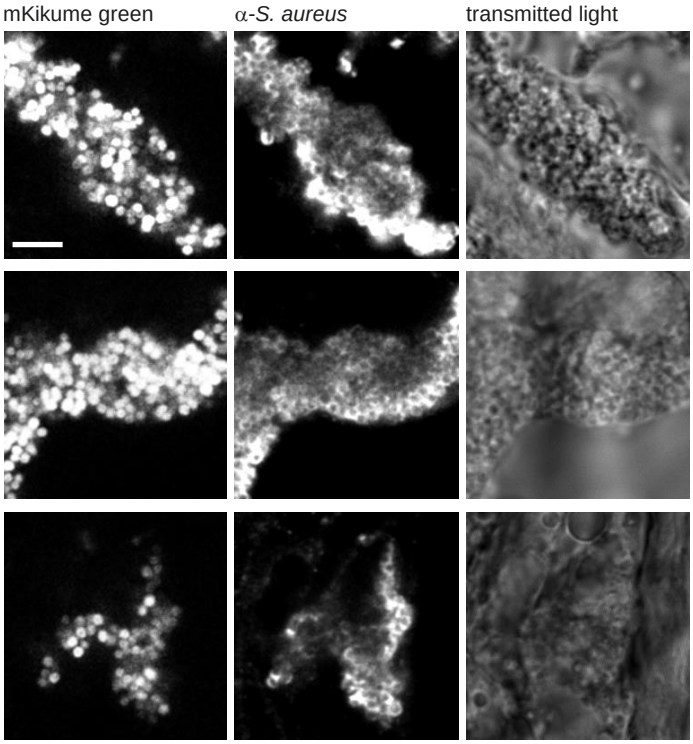

Figure 3.8: ***In vivo*** **control of mKikume fluorescence.** Representative confocal microscopy of *S. aureus*-pKikume (left row) infected mouse ears (4 h p.I.), fixed, cryosectioned, and immunostained against *S. aureus* (middle row). Scale bar, 5 µm.

To analyze the *in vivo* recovery of green mKikume after photoconversion 3 h p.I., three distinct regions of interest were evaluated over time using 2-photon imaging. For the majority of the observed population an increase of green fluorescence (non-photoconverted mKikume) and a decrease of red fluorescence (photoconverted mKikume) was detectable during 2-photon microscopy, while only few bacteria stayed red (**Figure 3.9 a**).

In order to determine *S. aureus* proliferation in a quantitative fashion, we segmented the bacteria using a calculated fluorescence channel with combined red and green fluorescence. Fluorescence data from the segmented objects were extracted and converted into cytometry datasets using the DISCit software (Moreau *et al.*, 2012). In line with the observations in the *in vitro* system, substantial increase in green and decrease in red mKikume fluorescence was detected after photoconversion (**Figure 3.9 a-b**). As a result, the calculated red to green ratio declined over time for *S. aureus*-pKikume in the ear, which indicates bacterial growth. Of note, the quantitative value for proliferation was represented as a constant minus the red to green ratio, and termed “proliferation index”.

Importantly, the mKikume red/green fluorescence ratio (and the calculated proliferation index) reached a plateau within 60 min (**Figure 3.9 c**), which was comparable with the kinetics observed *in vitro* (see **Figure 3.5 b-c**). This suggests that shortly after infection,

S. aureus proliferation in the tissue can reach rates that are comparable to exponential growth *in vitro*.

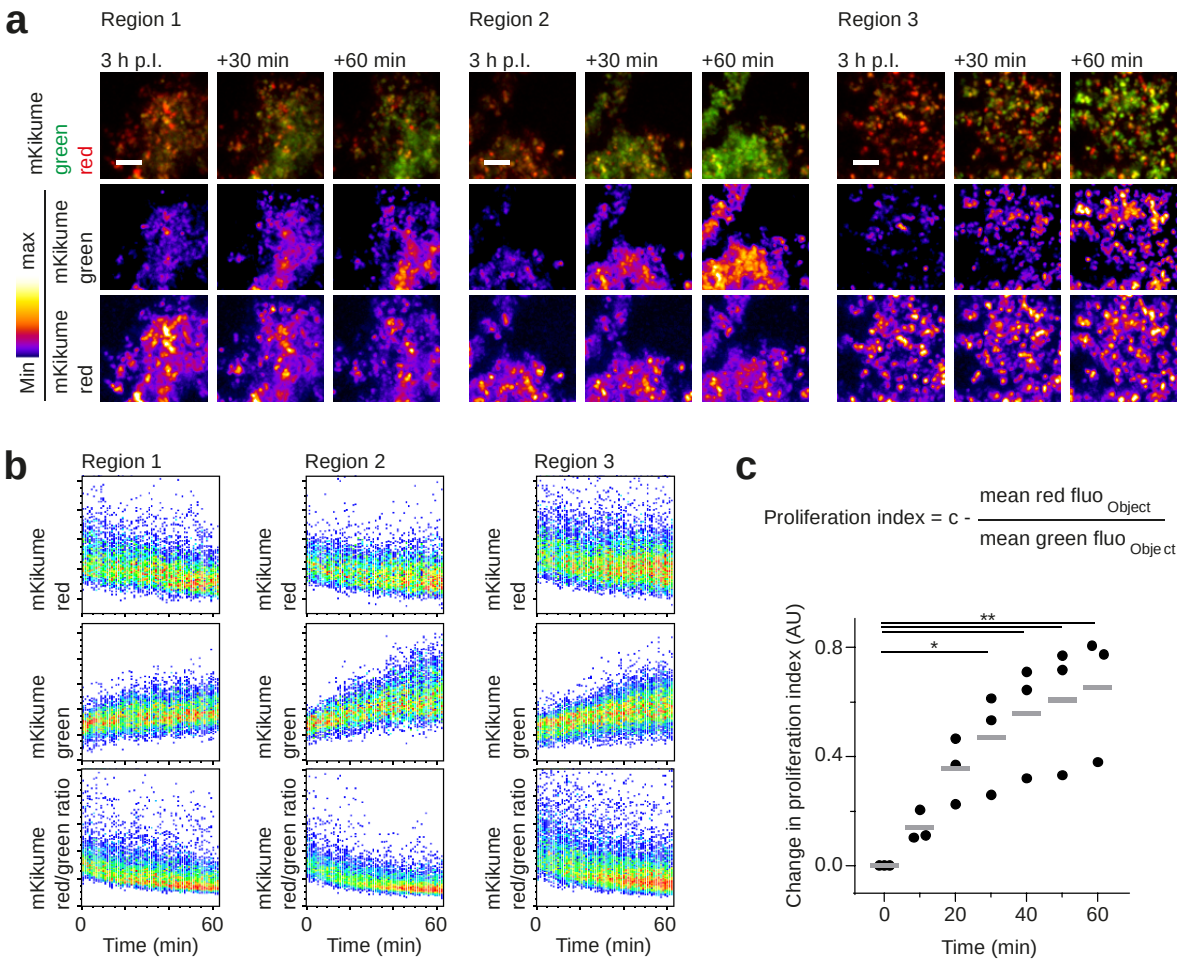

Figure 3.9: ***In vivo* recovery from photoconversion. a)** Examples of three regions of one intravital 2-photon microscopy of an infected mouse ear starting right after photoconversion 3 h p.l.. Projections of three-dimensional images of 20 Z-slices spaced 2 µm are shown. The single red and green fluorescence channels in the middle and bottom rows are shown as heat maps. Scale bar, 10 µm. **b)** Bacteria in the imaged regions shown in b) were automatically 3D-segmented and mean mKikume red and green fluorescence values were extracted for each detected shape and plotted over time. **c)** Red and green fluorescence values were used to calculate a proliferation index for each detected shape. The 80th percentile was calculated, and changes compared to the initial value were plotted in 10 min intervals. Each dot indicates a 10 min interval of one region analyzed in b) and c). Horizontal bar represents the mean. **, $p<0.01$; *, $p<0.05$ as determined by one-way ANOVA (comparison to the initial value).

3.2 The behavior of *S. aureus*-pKikume in wild type mice

The proliferation rates of *S. aureus* over the course of an infection have never been systematically analyzed so far. In order to select the time points suitable for such analysis in the ear infection model, the course of infection in wild type mice was evaluated by the bacterial burden detected by CFUs. Mouse ears were intradermally infected with an exponential growing *S. aureus*-pKikume culture and harvested after 3 h, 16 h, 48 h, and 144 h. The tissue was homogenized with tissue grinders and plated.

3 h p.I., the tissue burden roughly reflected the bacterial number in the inoculum, tendentially less, probably due to the fact that not all bacteria had been efficiently deposited at the infection site. However, the *S. aureus* burden in the tissue increased significantly (one-way ANOVA) by 16 h p.I. (**Figure 3.10**). At later time points, we observed a control of the infection and the reduction of CFU numbers, until the tissue was completely cleared of bacteria six days p.I..

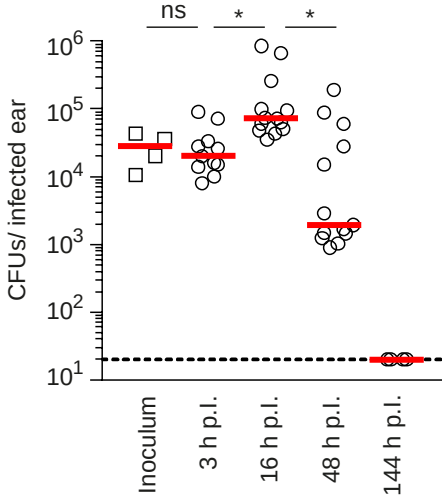

Figure 3.10: Pathogen burden over time in mouse ears infected with *S. aureus*-pKikume. Each symbol represents one individual ear (median of triplicate platings), plating of the inoculum is shown for comparison; horizontal bars represent the median; *, $p<0.05$; ns, not significant as determined by one-way ANOVA.

To investigate the recruited immune cell populations at the different phases of the infection, we digested the infected ear tissue at 3 h and 16 h p.I. and analyzed by flow cytometry and counting beads the number of leukocytes (**Figure 3.11**). The identification of the immune cells by gating according to the used marker is exemplarily shown in **Figure 3.11 a**. In the beginning of infection 3 h p.I., where we had observed that bacterial numbers started to increase, no significant (one-way ANOVA) change in $CD45^+$ leukocyte, neutrophil or

monocyte numbers in the infected ear tissue was measurable (**Figure 3.11 a-b**). In contrast, at the observed peak of the *S. aureus* tissue load at 16 h p.I., we observed a significant (one-way ANOVA) recruitment of CD45$^+$ leukocytes, mainly consisting of neutrophils and some monocytes at the site of infection (**Figure 3.11 a-b**). All other analyzed immune cells, monocyte-derived DCs, macrophages, dermal DCs and CD4$^+$-T cells did not significantly (one-way ANOVA) increase in their observed cell numbers (**Figure 3.11 c**).

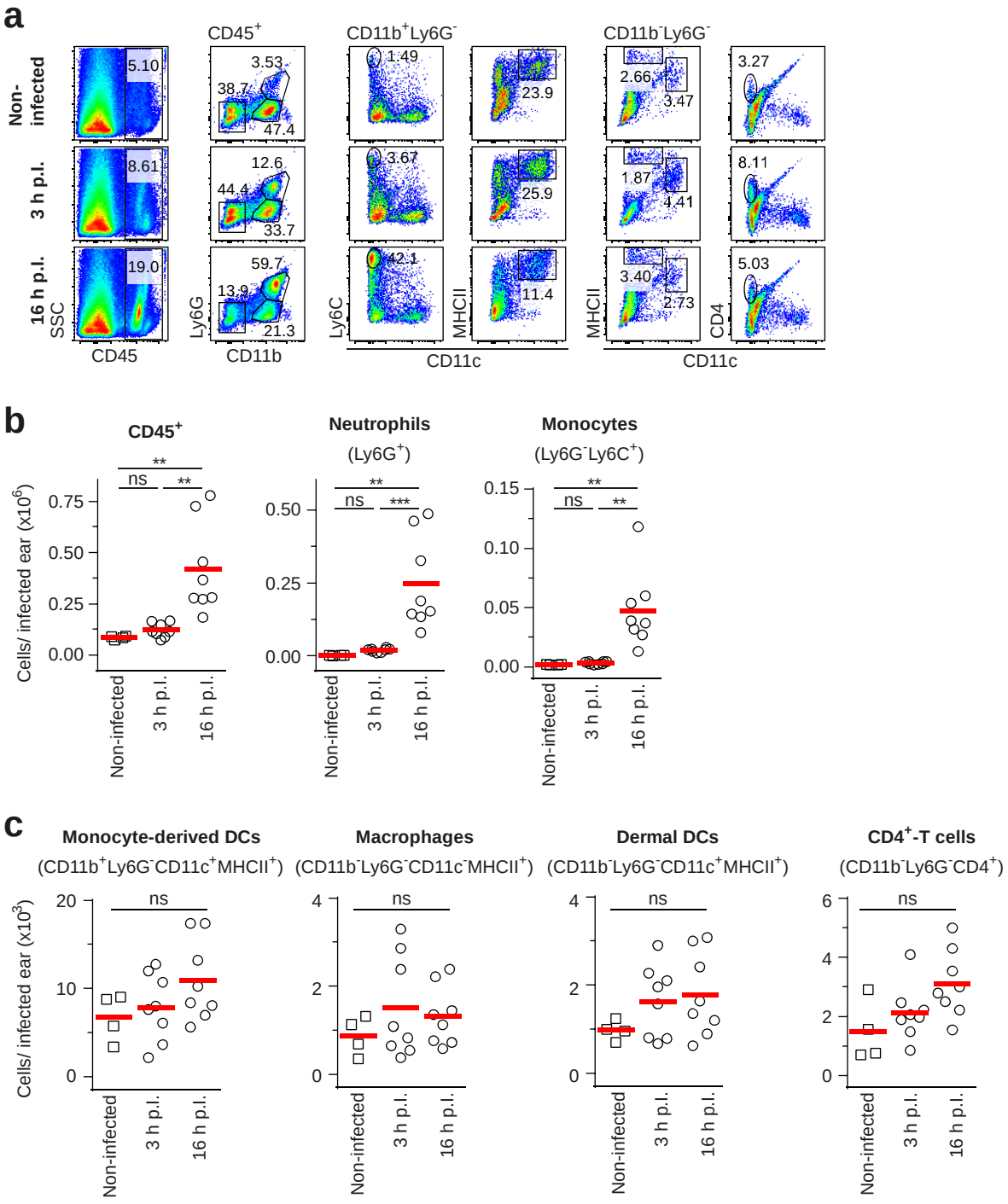

Figure 3.11: Immune cell recruitment in infected mouse ears with *S. aureus*-pKikume. **a)** Example for flow cytometry analysis of leukocytes recruited to the site of *S. aureus*-

pKikume infection at 3 h versus 16 h p.I.. Data from of non-infected mice are shown for comparison. Data are representative of eight infected ears per condition. **b)** Cell counts in infected ears analyzed by flow cytometry and calculated based on counting beads. Gating on $CD45^+$ cells and Neutrophils ($CD11b^+$, $Ly6G^+$) as shown in a) and on Monocytes ($CD11b^+$, $Ly6G^-$, $Ly6C^+$) as shown in **Figure 3.25**. Each dot represents one individual ear; horizontal bars represent the mean; ***, $p<0.001$; **, $p<0.01$, ns, not significant as determined by one-way ANOVA. c) Other immune cell counts in infected ears analyzed by flow cytometry and calculated based on counting beads. Gating as represented in **Figure 3.25**. Each dot represents one individual ear; horizontal bars represent the mean; ns, not significant as determined by one-way ANOVA.

For the purpose of analyzing whether *S. aureus* growth rate was changed in the inflammatory microenvironment at 16 h p.I., we compared bacterial recovery from photoconversion at 3 h versus 16 h p.I. by intravital 2-photon microscopy. We infected the ears with *S. aureus*-pKikume and used the procedure described in **Figure 3.7**, starting time lapse microscopy with 90 s imaging steps, directly after photoconversion at 3 h and 16 h p.I.. The bacteria were, as described in **Figure 3.9**, segmented and measured automatically. The change of the 80^{th} percentile over 10 min imaging was calculated to compare the growth rate of the bacteria in the ear over time. Strikingly, we observed a significant (two-way ANOVA) decline in the rate of recovery from photoconversion at 16 h p.I. compared to 3 h p.I. (**Figure 3.12**). Of note, recovery from photoconversion was not completely abrogated at 16 h p.I.. Thus, we concluded that at 16 h p.I., the observed *S. aureus* were alive, but exhibited a reduced growth as compared to 3 h p.I..

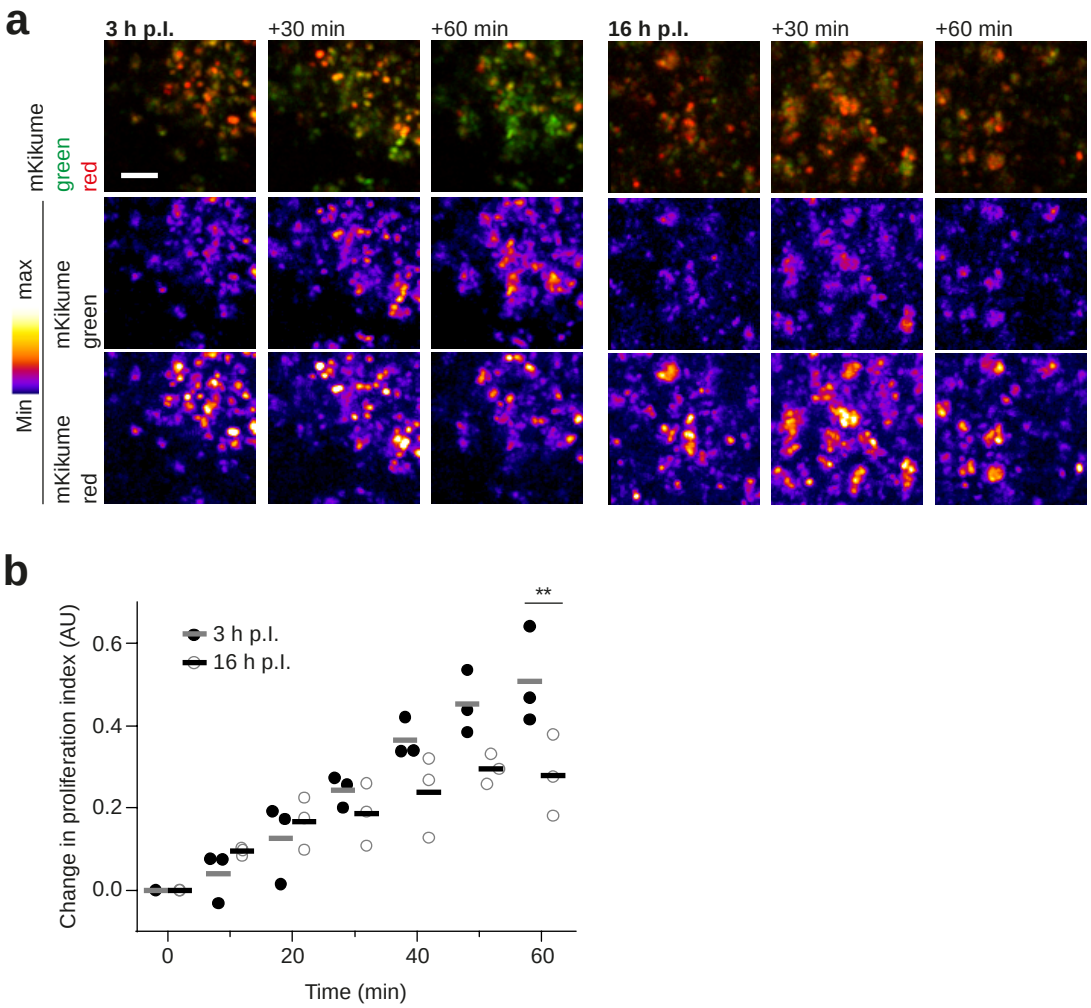

Figure 3.12: Intravital application of *S. aureus*-mKikume for proliferation measurement. **a)** Examples of intravital 2-photon microscopy of infected mouse ears starting after photoconversion 3 h (left panel) versus 16 h (right panel) p.I.. Projections of three-dimensional images of 20 Z-slices spaced 2 µm are shown. The single red and green fluorescence channels in the middle and bottom rows of each panel are shown as heat maps. Scale bar, 10 µm. **b)** Proliferation index measurement by intravital 2-photon microscopy over time at 3 h p.I. (closed symbols) versus 16 h p.I. (open symbols). Representation of the 80th percentile changes in 10 min intervals of three imaged regions. Each dot indicates an analyzed 10 min interval of one region; horizontal bars represent the mean; **, $p<0.01$; as determined by two-way ANOVA.

In order to corroborate the findings obtained with intravital 2-photon microscopy, we devised a quantitative confocal microscopy approach based on cryosections of *S. aureus*-pKikume infected ears fixed 60 min after photoconversion. In line with the observations in the ongoing infection, comparison of confocal images of tissue sections at 3 h and 16 h p.I. in **Figure 3.13 a** showed a much lower recovery from photoconversion at 16 h p.I.. Automated measurement of mKikume red and green fluorescence of such samples was used to

determine the proliferation index in a standardized fashion. This quantitative analysis of proliferation rates determined from the tissue sections revealed a significantly (one-way ANOVA) lower *S. aureus* growth at 16 h versus 3 h p.I. (**Figure 3.13 b**). Additionally, the red to green ratio at 3 h p.I. was comparable with non-photoconverted bacteria. Thus, concomitantly with the onset of the innate immune reaction, the growth rate of the *S. aureus* at the site of infection decreases. Furthermore, the decline of bacteria in the pathogen burden at 48 h p.I. (see **Figure 3.10**) fits to the trend of a lower proliferation rate at this time point, compared to 16 h p.I. (**Figure 3.13 b**).

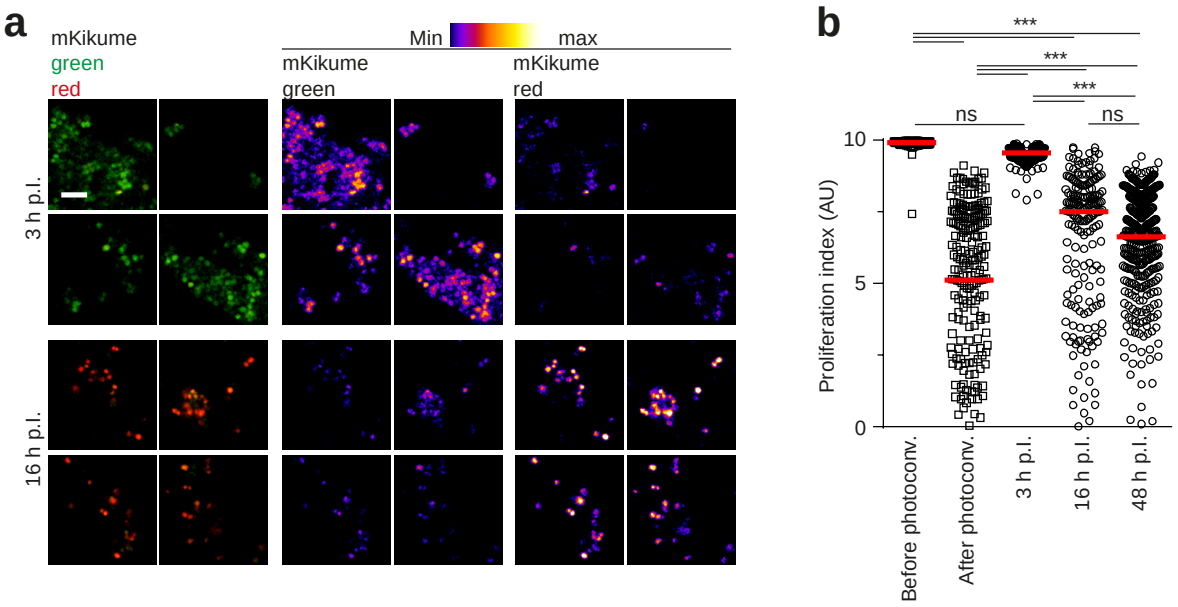

Figure 3.13: Automated proliferation measurement of confocal microscopy. a) Confocal imaging of photoconverted *S. aureus*-pKikume in fixed cryosections of ears infected for 3 h (upper panels) versus 16 h (lower panels), photoconverted 1 h prior to fixation and analysis. Four representative regions are shown per condition, the single red and green fluorescence channels in the middle and right column are shown as heat maps. Scale bar, 5 µm. **b)** Proliferation index of bacteria detected in in fixed cryosections of ears infected for 3 h,16 h and 48 h p.I., photoconverted 1 h prior to fixation and analysis. Confocal images as represented in a) were analyzed automatically. At least 14 confocal images per mouse ear were analyzed in seven to ten ears per time point. For controls six ears per condition were analyzed. Each symbol represents one confocal image; horizontal bars represent the median; ***, p<0.001; ns, not significant as determined by one-way ANOVA.

3.3 Uptake of *S. aureus* by neutrophils

Neutrophils are the first line of cellular defense against microorganisms. These professional phagocytes exert their antimicrobial effector functions by uptake and degradation of *S. aureus* employing a repertoire of antimicrobial peptides and enzymes stored in their granules, the release of neutrophil extracellular traps (NETs), and oxidative burst that is marked by the massive release of reactive oxygen species (ROS) produced by the NADPH oxidase (Stapels *et al.*, 2015; Sollberger *et al.*, 2018b; Anderson *et al.*, 2008).

In order to visualize the interaction of neutrophils with *S. aureus* upon recruitment to the site of infection, we employed Catchup^{IVM} mice, in which neutrophils exhibit red fluorescence dependently of neutrophil-specific Ly6G expression (Hasenberg *et al.*, 2015), infected by GFP-expressing *S. aureus*-pGFP (Liew *et al.*, 2011).
Based on our observations that neutrophils are only beginning to be recruited 3 h p.I. (see **Figure 3.11 b**) we chose this time point for microscopy to be able to monitor single neutrophils and their interactions with *S. aureus*. Using intravital 2-photon microscopy 3 h p.I., we observed in Catchup^{IVM} mice, in which neutrophils express high levels of red fluorescence protein (Hasenberg *et al.*, 2015), the recruitment of the cells, interaction with GFP-expressing *S. aureus* bacteria and the uptake of the bacteria by the neutrophils (**Figure 3.14 a-b**). With confocal microscopy and using three-dimensional representation, we could prove the intracellular localization of green *S. aureus*-pGFP in the red neutrophils at 3 h as well as 16 h p.I. (**Figure 3.14 c-d**). To analyze the localization, we segmented the neutrophils in an automated fashion (using Imaris, Bitplane) into surfaces and defined by these surfaces the intra- and extracellularly localized bacteria. These bacteria were equally segmented and enabled us to calculate how many bacteria were in the neutrophils and how many were localized extracellularly. This quantitative analysis of *S. aureus* cellular localization revealed that while the small number of neutrophils present at 3 h p.I. had taken up about 20% of the bacteria, the majority of *S. aureus* was found within this phagocyte population at 16 h p.I. (**Figure 3.14 e**). Thus, *S. aureus* is phagocytosed by recruited neutrophils right after the onset of the innate immune response.

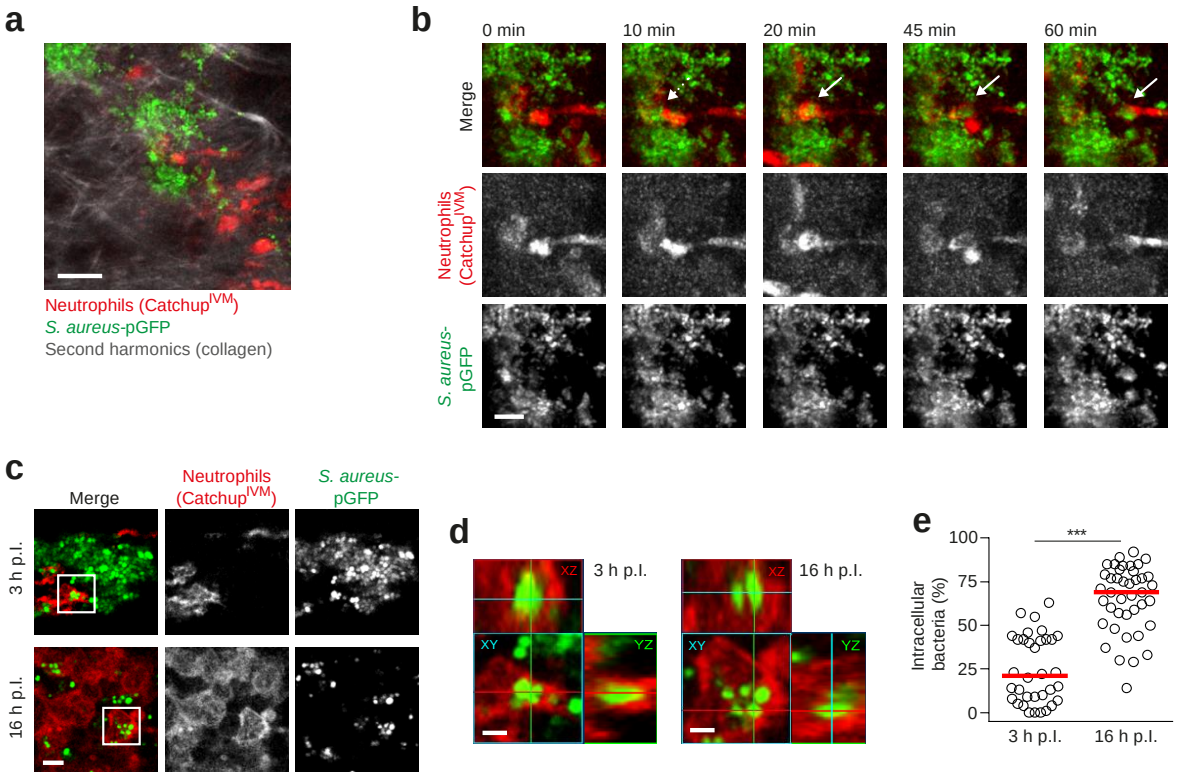

Figure 3.14: Neutrophil uptake of *S. aureus in vivo*. a) Overview of intravital 2-photon microscopy of Catchup^{IVM} neutrophil reporter mice infected with green fluorescent *S. aureus*-pGPF. The projection of a three-dimensional image of 11 Z-slices spaced 3 µm is shown. Scale bar, 20 µm. **b)** Intravital 2-photon microscopy of with *S. aureus*-GFP infected mouse ears (Catchup^{IVM}) starting 4 h p.I.. Projections of three-dimensional images of 11 Z-slices spaced 3 µm are shown. A dotted arrow highlights neutrophil-*S. aureus* interaction, white arrows highlight a neutrophil carrying *S. aureus* bacteria. Scale bar, 10 µm. **c**) Confocal imaging of cryosections from Catchup^{IVM} neutrophil reporter mice infected with *S. aureus*-pGPF in the ear for 3 h and 16 h. Scale bar, 5 µm. **d)** 3D-sections of bacteria (green) within neutrophils (red) shown in c). Scale bar, 2 µm. **e)** Bacteria and neutrophils were automatically 3D-segmented, and bacteria were assigned either inside or outside the detected neutrophil shapes. At least five 3D-segmented volumes (120 x 120 x 20 µm^3) per infected ear in four to five ears per condition were analyzed and the percentage of bacteria localized in neutrophils was calculated for each volume. Each dot represents one analyzed confocal volume; horizontal bars represent the median; ***, p<0.001 as determined by Mann-Whitney test.

3.4 The effect of neutrophil-depletion on *S. aureus* growth

Neutrophils are the main immune cell population recruited after *S. aureus* infection (see **Figure 3.11** and **Figure 3.14**). Additionally, we could detect the control of the skin infection upon occurrence of these professional phagocytes (see **Figure 3.10**). Because of these data, we wanted to investigate the course of infection in mice depleted of neutrophils. Therefore, we abolished the neutrophils with the monoclonal Ly6G-specific 1A8 antibody (Daley *et al.*, 2008). The depleting antibody was used in a dose of 150 µg per mouse. As an isotype control, the rat IgG2a 2A3 antibody, and for mock control PBS, was used. By flow cytometry analysis, the depletion was analyzed in blood samples, staining for neutrophil-markers, including the depleting antibody (**Figure 3.15 a**). We observed that 1A8 antibody administration, but not control antibody, resulted in a complete loss of Ly6G-positive cells from the blood. Importantly, we could also show the ablation of neutrophils using a GR-1 antibody.

Both the 1A8 as well as the GR-1 epitope of Ly6G could be masked by the depleting 1A8 antibody, and therefore prevent staining of neutrophils in 1A8-injected mice. To test for the extent of such an epitope masking, we isolated the cells of infected wild type ears and incubated them with controls or 1A8 antibody. Using flow cytometry, monocytes ($CD11b^{+}$, $Ly6C^{High}$, $Ly6G^{-}$) and neutrophils ($CD11b^{+}$, $Ly6C^{Intermediate}$, $Ly6G^{+}$) were identified in control cells (**Figure 3.15 b**, black and dark grey curves) (Daley *et al.*, 2008). In contrast, complete blocking against the Ly6G (1A8) antibody staining was achieved by pre-incubation with the depleting antibody (**Figure 3.15 b**). Although comparison of the GR-1 signal in 1A8-pre-incubated versus control cells showed a slight reduction of the GR-1 staining for neutrophils the signal was still significantly (one-way ANOVA) higher than for monocytes (**Figure 3.15 b-c**). We therefore concluded that during *in vivo* neutrophil-depletion with the 1A8 antibody, the cells were really depleted from the blood and not undetectable due to masking of the the Ly6G epitope.

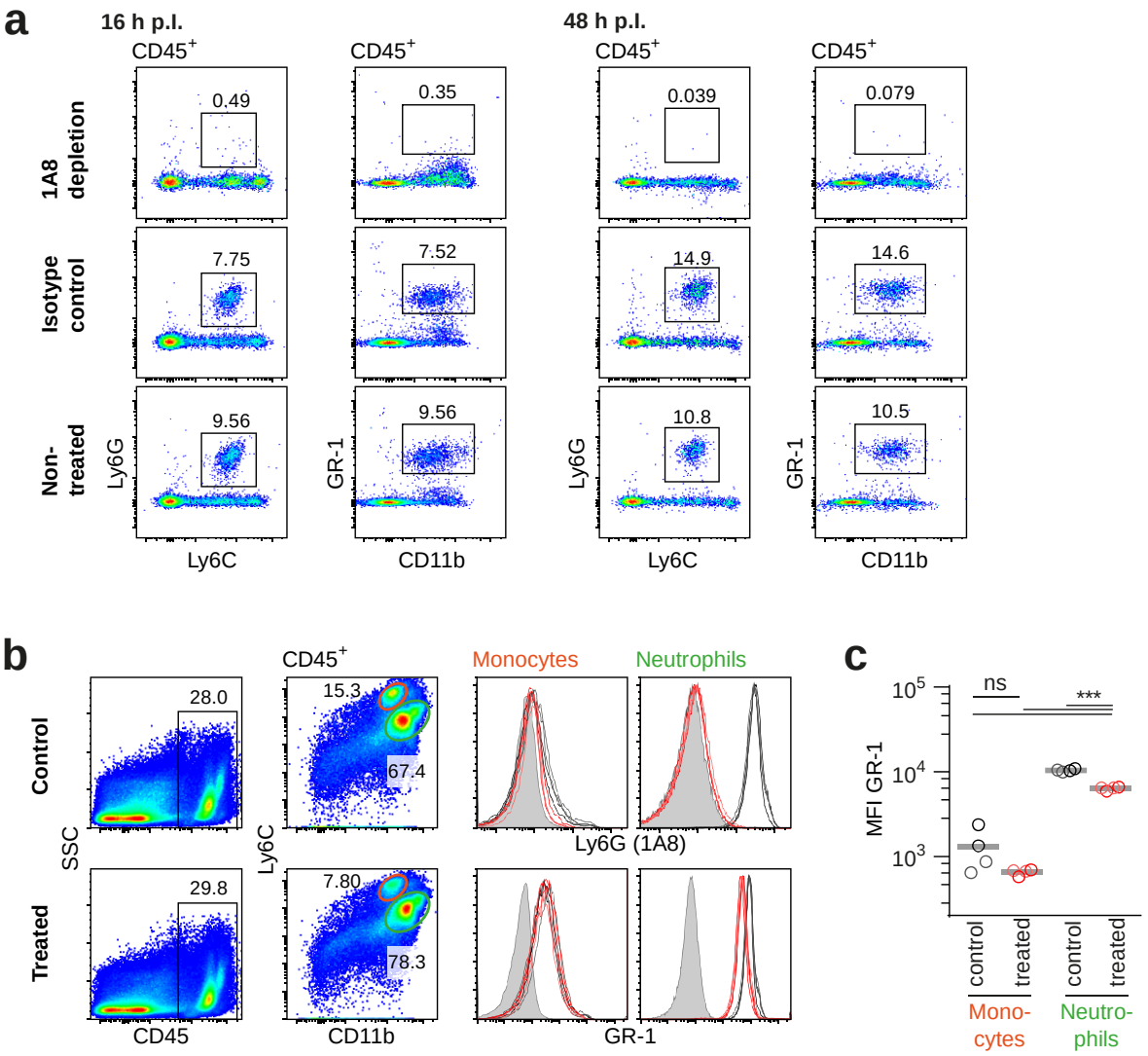

Figure 3.15: Depletion of Ly6G⁺ cells by 1A8 antibody. a) Representative plots of flow cytometry analyses of blood samples to test for neutrophil-depletion with the 1A8 antibody. **b)** Flow cytometry analysis of control and 1A8 antibody treated cells. Immune cells, isolated by digestion form infected mouse ears (16 h p.l.) were incubated with MACS buffer (black), control 2A3 antibody (100 µg/ml, approx. blood concentration, dark gray), or 1A8 antibody (100 µg/ml, pale red or 10 times higher than blood concentration, red) for 30 min. Gating on monocytes ($CD11b^{Intermediate}$, $Ly6C^{High}$, orange) and neutrophils ($CD11b^{High}$, $Ly6C^{Intermediate}$, green) is shown. Isotype control (Rat IgG2a, κ) or FMO (both pale grey, filled histograms) are shown for comparison. **c)** Quantification of mean fluorescence intensity (MFI) of GR-1 signal for detected immune cells as shown in b). ***, p<0.001; ns, not significant as determined by one-way ANOVA.

When we analyzed the *S. aureus*-pKikume infected ear of neutrophil-depleted and control mice, we found the bacterial burden to be equal for both at 3 h p.l. (**Figure 3.16 a**). However, for 16 h and 48 h p.l., the counts of bacteria in the ear were higher than in the control mice, which was significant (one-way ANOVA) at 16 h p.l. and a trend at 48 h p.l. (**Figure 3.16**

a). To compare additionally the number of pathogens in the draining lymph nodes (first cervical lymph node), we homogenized and lysed also these tissues and plated the bacteria. For all three time points 3 h, 16 h, and 48 h p.I. no differences were detectable in the bacterial burden of the lymph nodes (**Figure 3.16 b**). Therefore, the ablation of neutrophils affected bacterial numbers exclusively in tissues and at time points with massive recruitment of these cells.

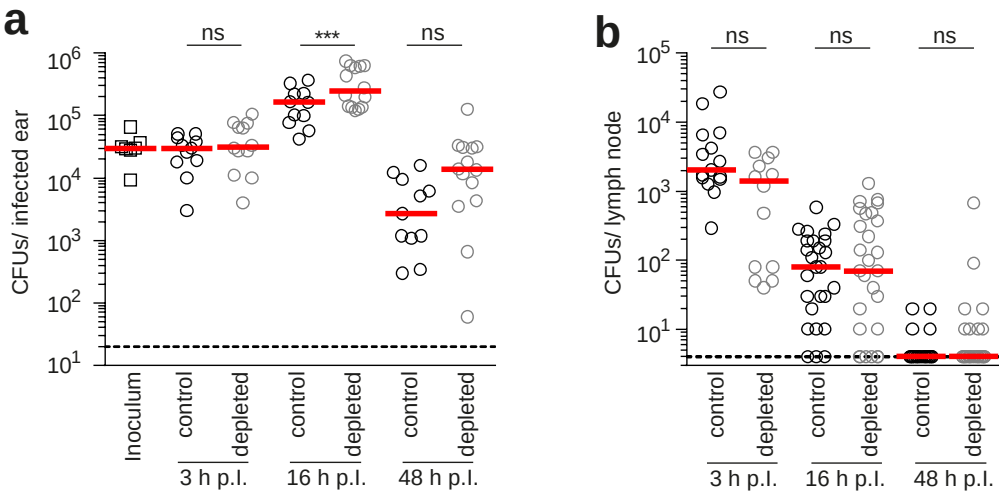

Figure 3.16: Infection of neutrophil-depleted mice with *S. aureus*-pKikume. a) Pathogen burden over time in control (black symbols) versus neutrophil-depleted (grey symbols) mouse ears infected with *S. aureus*-pKikume. Each symbol represents one individual ear (median of triplicates), horizontal bars represent the median, and plating of the inoculum is shown for comparison. ***, p<0.001; ns, not significant as determined by one-way ANOVA. **b)** Pathogen burden over time in lymph nodes of control (black symbols) versus neutrophil-depleted (grey symbols) mice infected with *S. aureus*-pKikume. Each symbol represents the first cervical lymph node (median of triplicates); horizontal bars represent the median; ns, not significant as determined by one-way ANOVA.

By using the *in vivo* biosensor, we then analyzed the bacterial growth in neutrophil-depleted mice. Similar to the analysis of the bacterial burden at 3 h p.I., also for bacterial growth, no differences between control and neutrophil-depleted mice were detectable (**Figure 3.17**). In contrast, for 16 h p.I., an enhanced recovery of green fluorescence by *S. aureus*-pKikume in neutrophil-depleted mice could be observed as compared to non-depleted controls (**Figure 3.17 a**). This was confirmed by the significant (one-way ANOVA) differences in the automatically analyzed bacterial proliferation index for the pathogens in control and neutrophil-depleted mice at 16 h p.I. (**Figure 3.17 b**). In line with the trend of a higher bacterial burden 48 h p.I. in neutrophil-depleted mice, the growth of *S. aureus* was

significantly (one-way ANOVA) elevated at this time point in the mice lacking neutrophils (**Figure 3.17 b**).

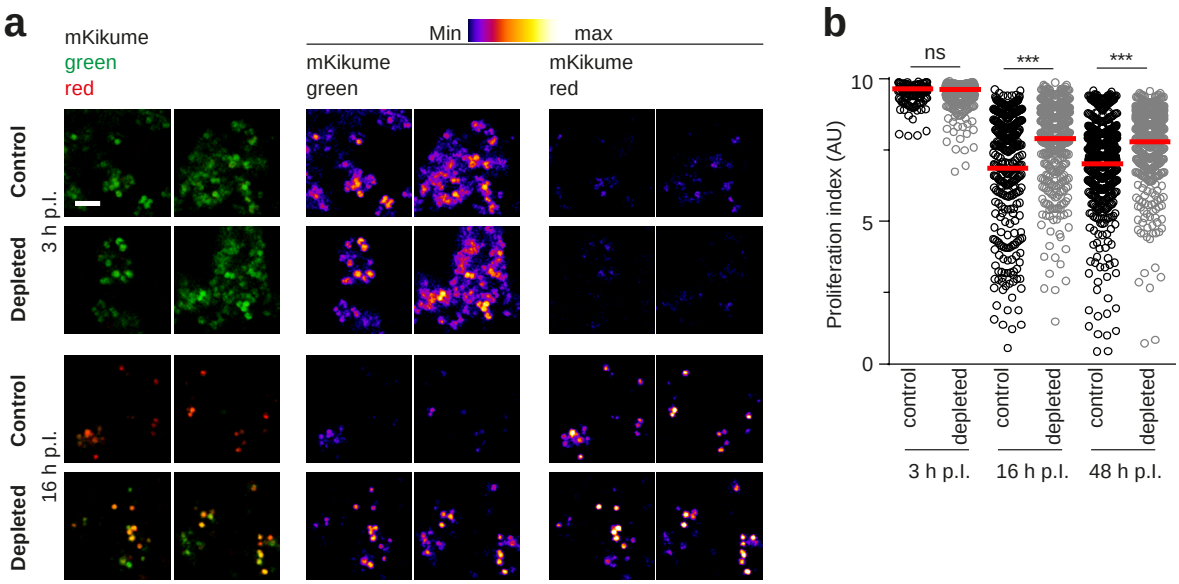

Figure 3.17: Proliferation of *S. aureus*-pKikume in neutrophil-depleted mice. a) Confocal imaging of photoconverted *S. aureus*-pKikume in fixed cryosections of control and neutrophil-depleted mice, infected for 3 h versus 16 h, and photoconverted 1 h prior to fixation and analysis. Two representative regions are shown per condition, the single red and green fluorescence channels in the middle and right column are shown as heat maps. Scale bar, 5 µm. **b)** Proliferation index of bacteria detected in in fixed cryosections of control (black symbols) versus neutrophil-depleted (grey symbols) mouse ears infected with *S. aureus*-pKikume and confocal images as represented in a) were analyzed automatically. At least 17 confocal images per mouse ear were analyzed in eight to twelve ears per condition. Each dot represents one confocal image; horizontal bars represent the median; ***, p<0.001; ns, not significant as determined by one-way ANOVA.

In wild type mice, we had shown that mainly neutrophils were recruited into the ear after *S. aureus* infection (see **Figure 3.11**). After neutrophil-depletion this cell population is not detectable anymore via flow cytometry (**Figure 3.18 a**), but at the same time, a new population of $Ly6C^+$, $CD11b^+$, and $Ly6G^-$ cells appeared, which was higher in CD11b signal than monocytes ($Ly6C^+$, $Ly6G^-$, $CD11b^{Intermediate}$), which were already detectable in infected control mice (**Figure 3.18 a**). Calculation of total cell numbers by counting beads, showed significantly (one-way ANOVA) lower numbers in recruited leukocytes in infected ears of mice depleted of neutrophils compared to control and depletion-control mice (**Figure 3.18 b**). The depletion by the 1A8 antibody reduced the total $CD45^+$ cells by 0.56 or

0.52x10^6 cells (equivalent to 40-70%) at 16 or 48 h p.I., respectively, but the neutrophils in treated mice about 0.57 or 0.9x10^6 cells, which is more than 90% (**Figure 3.18 b**). The remaining cells mainly consisted of monocytes (Ly6C$^+$, Ly6G$^-$, CD11b^{Intermediate}) and the cell type described above not present in non-depleted mice (Ly6C$^+$, Ly6G$^-$, CD11b^{High}). However, both cell types combined were present with 0.14 or 0.55x10^6 cells at 16 or 48 h p.I., respectively (**Figure 3.18 b**). Consequently, a reduction of the total recruited immune cell population, especially neutrophils, was reached by depletion with the 1A8 antibody.

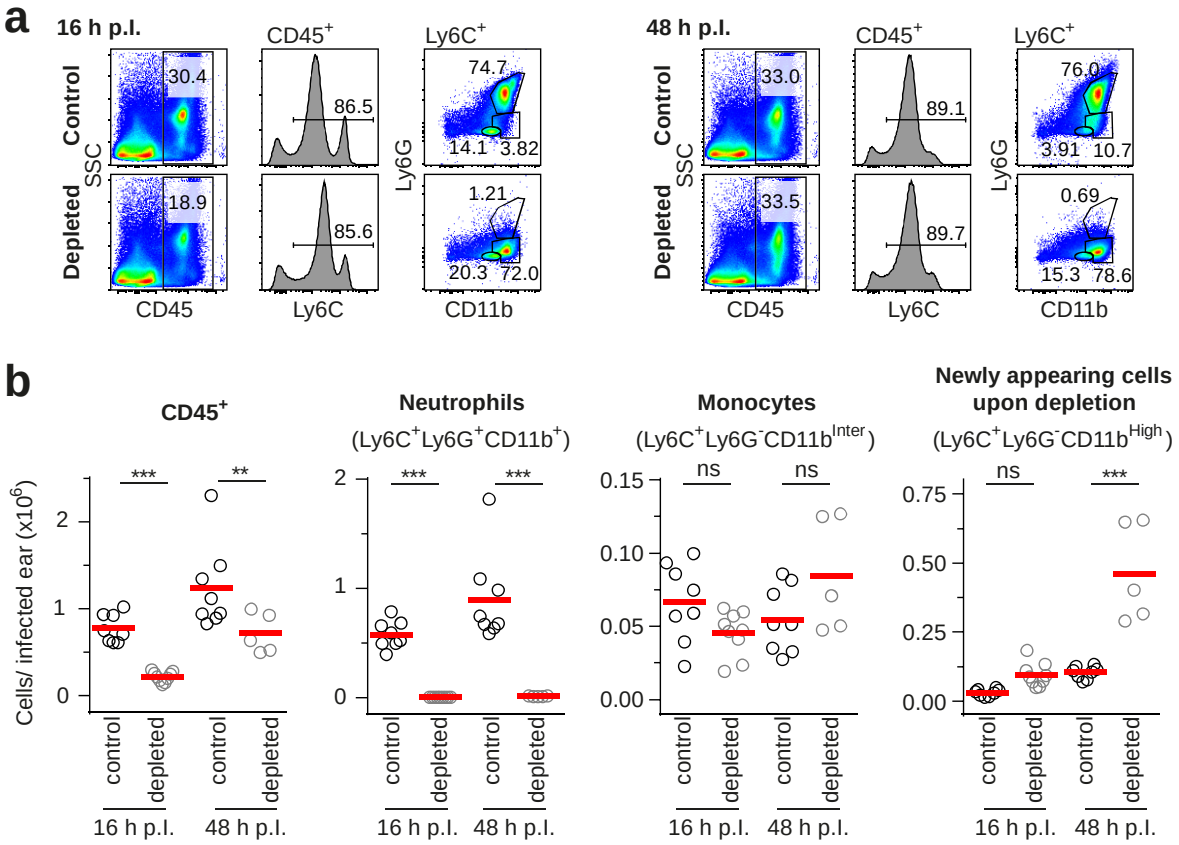

Figure 3.18: Recruitment of immune cells in neutrophil-depleted mice. a) Flow cytometry analysis of leukocytes recruited to the site of *S. aureus*-pKikume infection at 16 h versus 48 h p.I. in control and neutrophil-depleted mice. Data are representative of at least five infected ears per condition. **b)** Cell counts in infected ears analyzed by flow cytometry and calculated based on counting beads. Gating on CD45$^+$ cells, Neutrophils (Ly6C$^+$, CD11b$^+$, Ly6G$^+$) and Monocytes (Ly6C$^+$, CD11b^{intermediate}, Ly6G$^-$), and newly appearing cells upon depletion (Ly6C$^+$, CD11b^{High}, Ly6G$^-$) as shown in a). Each dot represents one individual ear; horizontal bars represent the mean; ***, p<0.001; **, p<0.01; ns, not significant as determined by one-way ANOVA.

In order to test if, in neutrophil-depleted mice, the newly appearing Ly6C$^+$, CD11b^{High}, Ly6G$^-$ cells are, like the neutrophils in control mice (see **Figure 3.14**), the main host cells of

S. aureus, we used flow cytometry. In a first step we had to exclude a cross-infection of immune cells during cell purification. Therefore, in a control experiment, during enzymatic digestion of the infected tissues, a half ear of *S. aureus*-pGL485 infected BL6 mouse ($CD45.2^+$) was processed together with a half ear of *S. aureus*-pGFP infected $CD45.1^+$ mouse. Additionally, 20 µg/ml erythromycin and 2.5 µg/ml lysostaphin were added to kill all extracellular bacteria. By gating on GFP^+ cells, we could detect the host cells of *S. aureus*-pGFP, which should only be present in $CD45.1^+$ neutrophils (**Figure 3.19 a**). We could show that no major exchange of bacteria from the GFP-infected $CD45.1^+$ to the nonfluorescent $CD45.2^+$ cells took place during the purification procedure, thus excluding cross-infection artifacts (**Figure 3.19 a-b**).

To characterize the *S. aureus*-infected host cells, we applied the same gating strategy as used for identification of recruited cells (see **Figure 3.18 a**), except for an additional gating on the GFP^+ cells before identification of $CD45^+$ leukocytes (**Figure 3.19 c**). By this analysis, we could show that the pathogen is, both in control mice as well as in neutrophil-depleted mice, localized within $Ly6C^+$, $CD11b^{High}$ cells, which appeared to be $Ly6G^+$ in the control and $Ly6G^-$ in the depleted mice (**Figure 3.19 d**). Furthermore, more monocytes had phagocytosed *S. aureus* in the neutrophil-depleted mice compared to control mice (**Figure 3.19 d**).

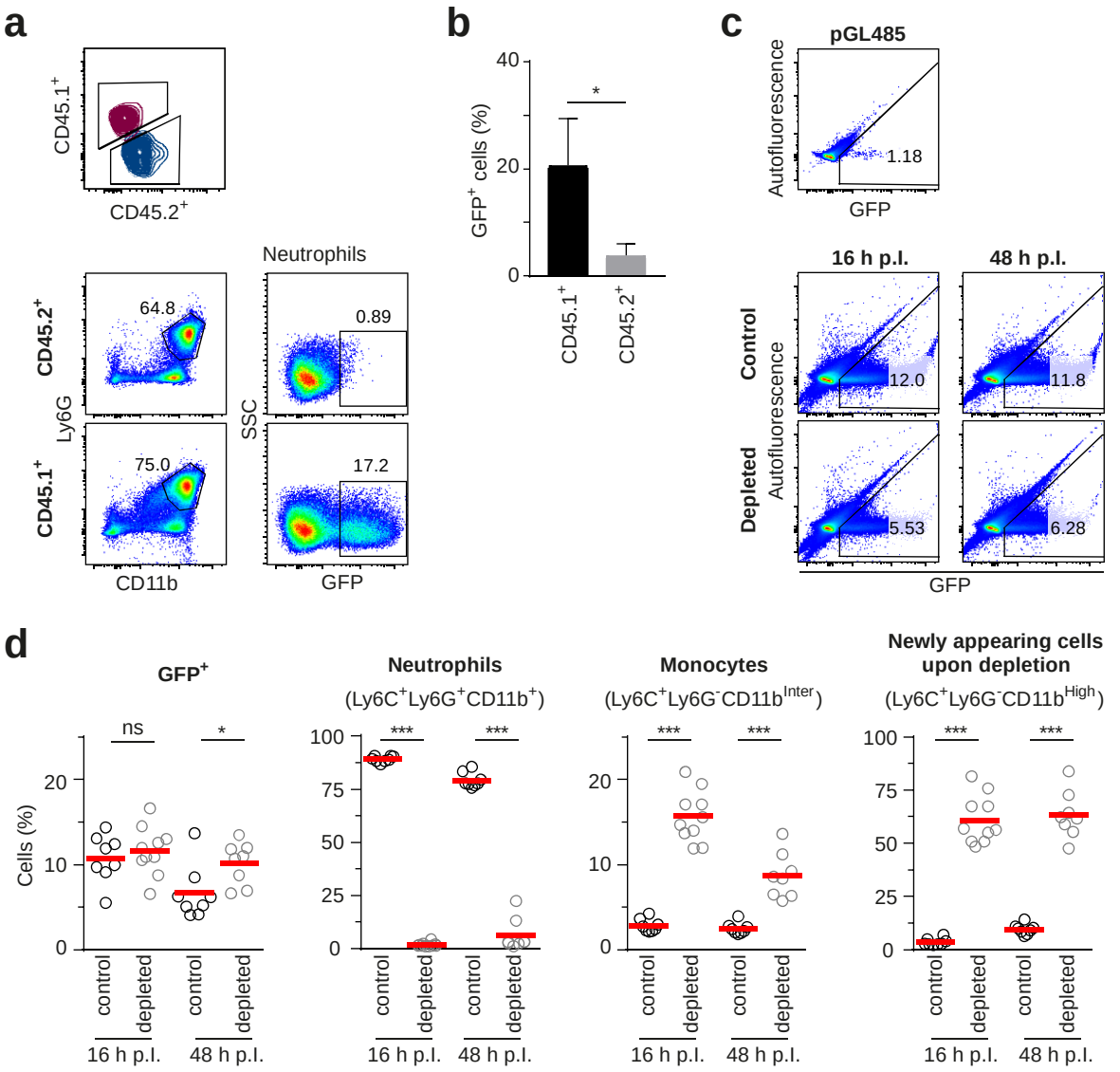

Figure 3.19: Host cells of *S. aureus* in infected neutrophil-depleted mice. a) Flow cytometry analysis excluding cross-infection artifacts during cell isolation. Ears of CD45.1$^+$ mice, infected with *S. aureus*-pGFP and BL6 (CD45.2$^+$) mice infected with *S. aureus*-pGL485. **b)** Percentages of GFP$^+$ neutrophils in combined ears of CD45.1$^+$ mice, infected with *S. aureus*-pGFP and BL6 (CD45.2$^+$) mice infected with *S. aureus*-pGL485 during purification. Bars represent the mean (+/- standard deviation) of three combined ears; *, p<0.05 as determined by paired t-test. **c)** Flow cytometry analysis of recruited host cells at the site of *S. aureus*-pKikume infection at 16 h versus 48 h p.l. in control and neutrophil-depleted mice. After gating for GFP$^+$ cells, further analysis like in **Figure 3.18 a**) shown. Data are representative of at least five infected ears per condition. Leukocytes from *S. aureus*-pGL485 infected mouse ear are shown for comparison. **d)** Cells in infected ears analyzed by flow cytometry. Gating on CD45$^+$ cells, Neutrophils (Ly6C$^+$, CD11b$^+$, Ly6G$^+$), Monocytes (Ly6C$^+$, CD11b^{Intermediate}, Ly6G$^-$), and newly appearing cells upon depletion (Ly6C$^+$, CD11b^{High}, Ly6G$^-$). Each dot represents one individual ear;

horizontal bars represent the mean; ***, p<0.001; *, p<0.05; ns, not significant as determined by one-way ANOVA.

We next wanted to test if the Ly6C^{+}, CD11b^{+}, Ly6G^{-} cells occurring upon 1A8 antibody injection were monocytes with a higher CD11b signal. For this, we used CX_3CR1-GFP mice and CCR2 staining to identify monocytes. The mice were infected with *S. aureus*-pGL485 and the recruited immune cells were gated for a Ly6C^{+}, CD11b^{Intermediate}, Ly6G^{-} *bona fide* monocyted population and the newly occurring Ly6C^{+}, CD11b^{High}, Ly6G^{-} population (**Figure 3.20 a**). The majority of recruited Ly6C^{+}, Ly6G^{-}, CD11b^{Intermediate} population in the control and also depleted mice were also CX_3CR1 and CCR2 positive (**Figure 3.20 b**). Thus, as expected, these cells corresponded to monocytes. In contrast, the population, which appears only upon *S. aureus* infection of neutrophil-depleted mice did not express CX_3CR1 or CCR2 to a substantial amount, and thus were not monocytes (**Figure 3.20**). From these data, we concluded that despite the complete disappearance of neutrophils from the blood, a residual neutrophil-like cell population with Ly6G downregulated or masked is recruited to the site of infection in 1A8 neutrophil-depleted mice.

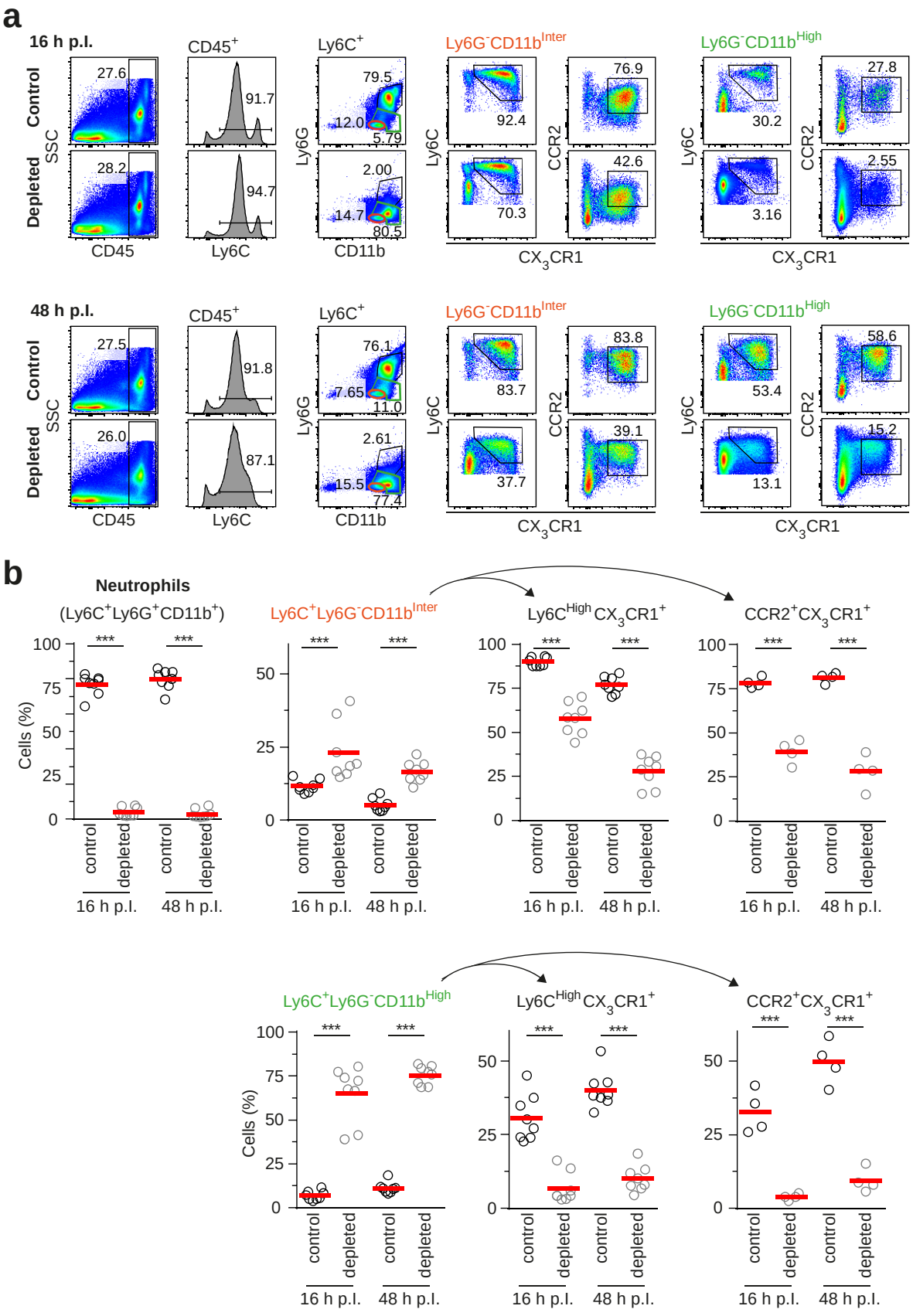

Figure 3.20: Analysis of recruited monocytes in infected ears of neutrophil-depleted mice. **a)** Flow cytometry analysis of leukocytes recruited to the site of *S. aureus*-pKikume infection at 16 h versus 48 h p.l. in control and neutrophil-depleted CX_3CR1-GFP mice.

Data are representative for eight (in case of CCR2 for four) infected ears per condition. **b)** Cells in infected ear, are analyzed by flow cytometry as represented in a). Gating on Neutrophils ($Ly6C^+$, $CD11b^+$, $Ly6G^+$), Monocytes ($Ly6C^{High}$, $CD11b^+$, $Ly6G^-$, CX_3CR1^+) divided in $Ly6C^+$, $CD11b^{High}$, $Ly6G^-$ (orange) and $Ly6C^+$, $CD11b^{intermediate}$, $Ly6G^-$ (green) cells. Each dot represents one individual ear; horizontal bars represent the mean; ***, $p<0.001$; as determined by one-way ANOVA.

To test if the $Ly6C^{Intermediate}$, $CD11b^{High}$, $Ly6G^-$ population appearing in neutrophil-depleted mice was already detectable at an early time point before recruitment, we analyzed the bone marrow of neutrophil-depleted versus control mice. We found in neutrophil-depleted mice a significant (one-way ANOVA) increased population of $Ly6G^-$, $CD11b^+$ cells as compared to control mice (**Figure 3.21**), however monocyte numbers as determined by CX_3CR1 expression were unchanged. Additionally, we could show that the neutrophil-depletion by the 1A8 antibody is already effective in the bone marrow (**Figure 3.21**), but we saw for 16 h and 48 h p.I. no differences in the pattern of the SSC versus CD45 signal for the leukocytes (see **Figure 3.21 a**). However, the Ly6G negative cells were at the same time CX_3CR1 negative, underlining that these cells were most likely no monocytes (**Figure 3.21 b**), but neutrophil-like cells with Ly6G decreased or masked.

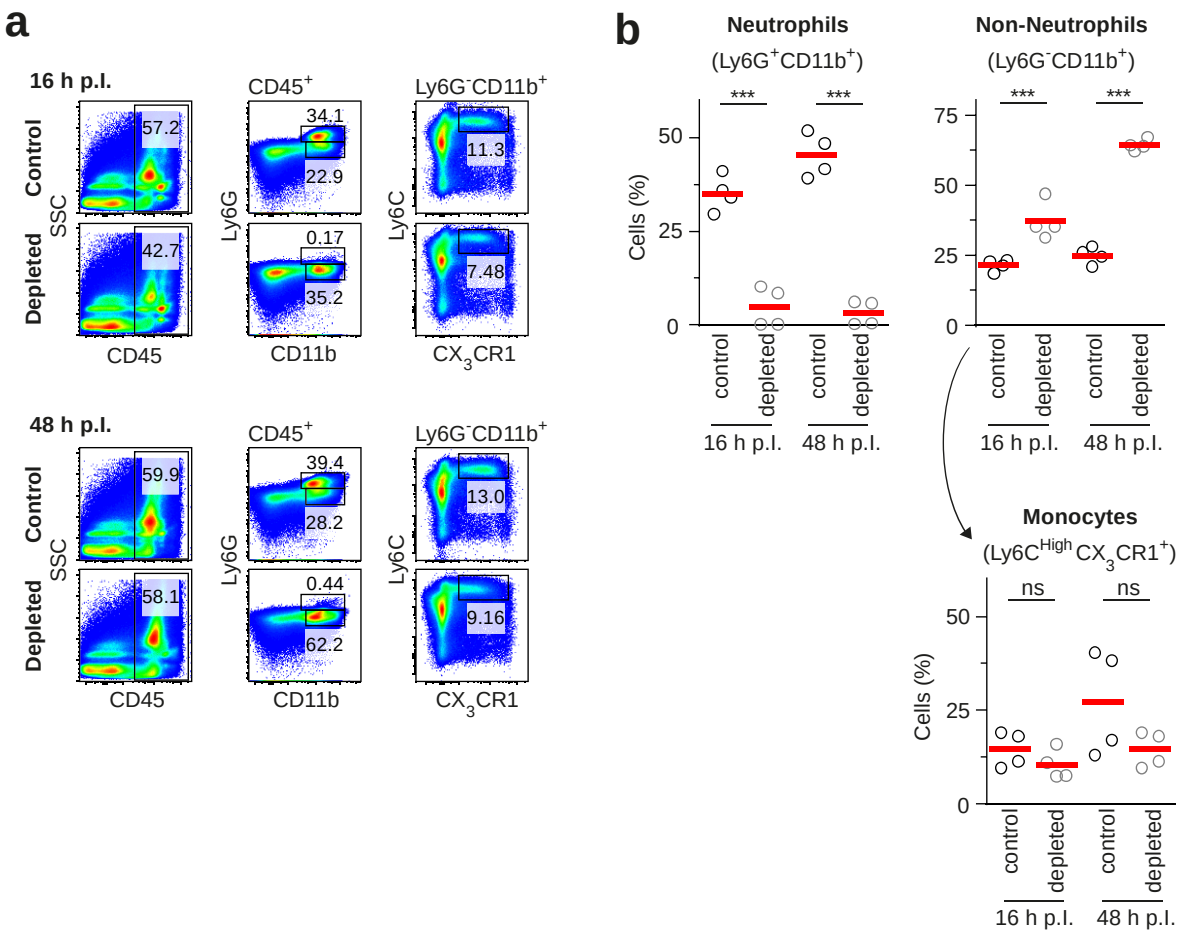

Figure 3.21: Analysis of bone marrow leukocytes in infected neutrophil-depleted mice. a) Flow cytometry analysis of leukocytes in bone marrow of *S. aureus*-pKikume infected control and neutrophil-depleted mice at 16 h versus 48 h p.l.. Data are representative of four infected mice per condition. **b)** Cell in bone marrow of infected mice analyzed by flow cytometry like represented in a). Gating on Neutrophils ($Ly6C^+$, $CD11b^+$, $Ly6G^+$), non-Neutrophils ($Ly6C^+$, $CD11b^+$, $Ly6G^-$) and Monocytes ($CD11b^+$, $Ly6G^-$, $Ly6C^{High}$, CX_3CR1^+). Each dot represents one mouse; horizontal bars represent the mean; ***, $p<0.001$; ns, not significant as determined by one-way ANOVA.

After showing by flow cytometry that the $Ly6C^{Intermediate}$, $CD11b^{High}$, $Ly6G^-$ cells in *S. aureus* infected neutrophil-depleted mice were not monocytes (**Figure 3.20** and **Figure 3.21**) we wanted to further characterize these cells according to their nucleus morphology. Therefore, we reconstituted lethally irradiated wild type mice with CFP-expressing cells, depleted their neutrophils by 1A8 antibody, and infected them with *S. aureus*-pKikume. We stained the DNA of the cells in the cryosectioned ear tissue with DAPI.

Interestingly, we found both in the infected ear of control as well as neutrophil-depleted mice a similar nuclear morphology of the recruited immune cells (**Figure 3.22**). In particular, the

shape of the nuclei in both, control and neutrophil-depleted mice, was lobulated as described for granulocyte nuclei of neutrophils (Hoffmann *et al.*, 2007).

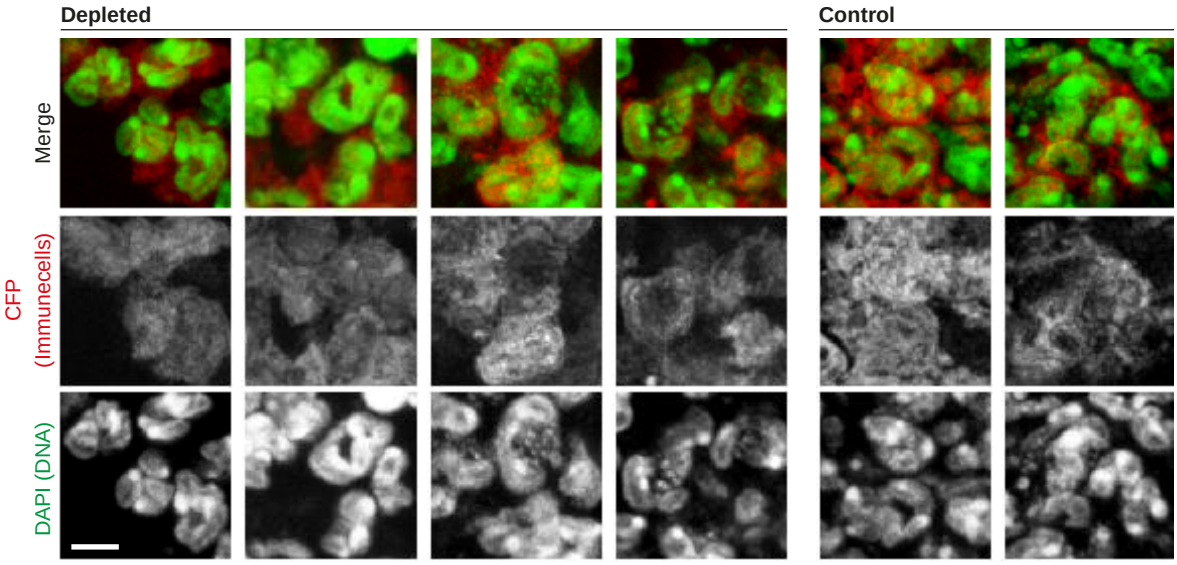

Figure 3.22: Nuclei characterization of newly appearing cells upon neutrophil-depletion. Confocal imaging of fixed and DAPI stained cryosections of control and neutrophil-depleted CFP-BMCs, infected with *S. aureus*-pKikume for 16 h. The projection of a three-dimensional image of 3 Z-slices spaced 1 µm is shown. Each row represents an individual ear. Scale bar, 5 µm.

We could show the depletion of neutrophils from the blood after treatment of the mice with the 1A8 antibody (see **Figure 3.15**). By flow cytometry analysis, we identified a newly occurring cell population ($Ly6C^{+}$, $Ly6G^{-}$, $CD11b^{High}$) in *S. aureus* infected neutrophil-depleted mouse ears (see **Figure 3.18**), which is not characterized as monocytes (see **Figure 3.20**) and exhibited nuclei like similar to the recruited neutrophils in infected control mice (see **Figure 3.22**). Because of these results, we decided to analyze in the recruited cells, additionally to Ly6G itself, the GR-1 epitope, which is less specific for Ly6G, but also less likely to be masked by the depleting 1A8 antibody. As observed before, no Ly6G signal was detectable for in neutrophil-depleted mice (**Figure 3.23**). However, with the GR-1 antibody a reduced GR-1 expression on the surface of the newly appearing cell type ($Ly6C^{Intermediate}$, $CD11b^{High}$, $Ly6G^{-}$) was measured. Compared to the GR-1 signal on the cells of control mice, the signal was significantly (one-way ANOVA) reduced, but still much higher (fivefold) than the FMO control (**Figure 3.23**). Since we could not detect any GR-1 signal in blood samples of neutrophil-depleted mice, we concluded that the Ly6G is partially masked by the depletion 1A8 antibody and additionally downregulated or not yet expressed on these cells, suggesting these cells could be immature neutrophils.

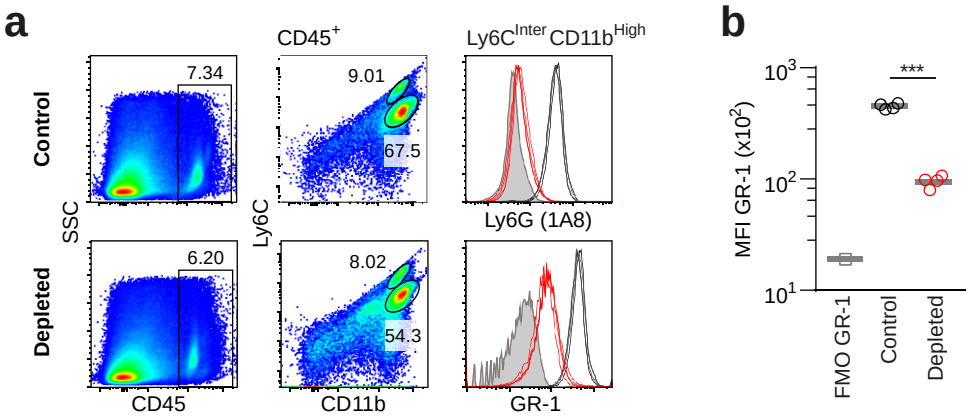

Figure 3.23: Masking versus lower expression of Ly6G in neutrophil-depleted mice. a) Flow cytometry analysis of recruited immune cells in infected control and neutrophil-depleted mouse ears. Immune cells, isolated by digestion (30 min) from infected ears (16 h p.I.) of control (PBS, black; 2A3, dark grey) or neutrophil-depleted (1A8, red) mice. Gating on neutrophil-like cells ($Ly6C^{Intermediate}$, $CD11b^{High}$) is shown. Isotype control (Rat IgG2a, κ) or FMO (both pale grey) are shown for comparison. **b)** Quantification of mean fluorescence intensity (MFI) of GR-1 signal for detected immune cells ($Ly6C^{Intermediate}$, $CD11b^{High}$) as shown in a). FMO for GR-1 is shown for comparison. Each dot represents one ear; horizontal bars represent the mean. ***, $p<0.001$ as determined by one-way ANOVA.

3.5 The effect of NADPH oxidase on *S. aureus* growth

We had, in our previous experiments, observed that in neutrophil-depleted mice, neutrophil-like cells still are recruited to the site of infection and are a host cell of the bacteria (see **Figure 3.19** and **Figure 3.20**). NADPH oxidase constitutes a major antimicrobial effector mechanism of neutrophils (see 1.2.3 The weapons stockpile of neutrophils). In addition to its importance for oxidative burst acting directly against phagocytosed microorganisms, superoxides produced by this enzyme can trigger the release of neutrophil extracellular traps (Sollberger *et al.*, 2018b; Anderson *et al.*, 2008). We therefore decided to investigate the specific impact of this antimicrobial "weapon" on *S. aureus*. Whether NADPH oxidase activity can impair pathogen proliferation rates or mediates direct killing of *S. aureus* without overt impact on its proliferation has remained completely unknown. We therefore set out to analyze *S. aureus* proliferation rates in NADPH oxidase-deficient *cybb*$^{-/-}$ mice, where the gene of Nox2/gp91^{phox}, a membrane domain of the NADPH oxidase, is knocked out.

Plating of the homogenized infected ear tissue exhibited a significant (one-way ANOVA) increase in the *S. aureus* burden of *cybb*$^{-/-}$ compared to wild type mice at the peak of the infection at 16 h p.I. (**Figure 3.24 a**). In contrast, there were no differences in pathogen numbers at 3 h and 48 h p.I. (**Figure 3.24 a**). Additionally, we plated the draining lymph nodes (first cervical lymph nodes) to measure also here the bacterial burden. In **Figure 3.24 b** the decrease in bacterial burden over time for both, *cybb*$^{-/-}$ and wild type mice is plotted. But, although not significant (one-way ANOVA) difference was detectable, a trend to elevated pathogen numbers in the lymph nodes of *cybb*$^{-/-}$ mice was observed.

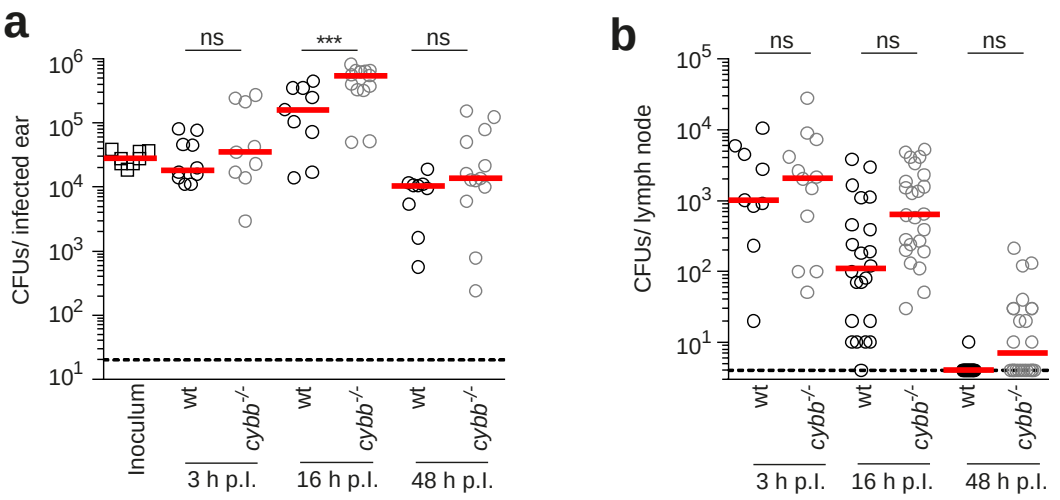

Figure 3.24: Bacterial tissue burden in ROS deficient mice. a) Pathogen burden at 3 h, 16 h, and 48 h p.l. in wild type (black symbols) and *cybb*$^{-/-}$ (grey symbols) mice infected with *S. aureus*-pKikume. Each symbol represents one individual ear (median of triplicates), plating of the inoculum is shown for comparison; horizontal bars represent the median; ***, p<0.001; ns, not significant as determined by one-way ANOVA. **c)** Pathogen burden over time in draining lymph nodes of wild type (black symbols) versus *cybb*$^{-/-}$ (grey symbols) mice infected with *S. aureus*-pKikume. Each symbol represents the first cervical lymph node corresponding to one infected ear. Horizontal bars represent the median; ns, not significant as determined by one-way ANOVA.

Based on the observation of higher CFU numbers at the peak of the infection in *cybb*$^{-/-}$ mice, we wanted to investigate the role of recruited leukocytes in these animals with an impaired antimicrobial response. For this, the leukocyte recruitment to the site of infection was analyzed by flow cytometry. At 3 h p.l., were no differences between uninfected, wild type and ROS-deficient mice visible (**Figure 3.25**). At 16 h p.l., although we had observed a higher bacterial burden in *cybb*$^{-/-}$ mice, we observed at the same time, an increased recruitment of leukocytes, mainly monocytes and neutrophils to the site of infection (**Figure 3.25**). The same increase in neutrophil numbers was detectable at 48 h p.l. in *cybb*$^{-/-}$ mice, whereas monocytes were just elevated to the level of wild type controls. No other cell types were increased in numbers upon infection up to 48 h p.l. neither in wild type nor in ROS-deficient mice (**Figure 3.25**).

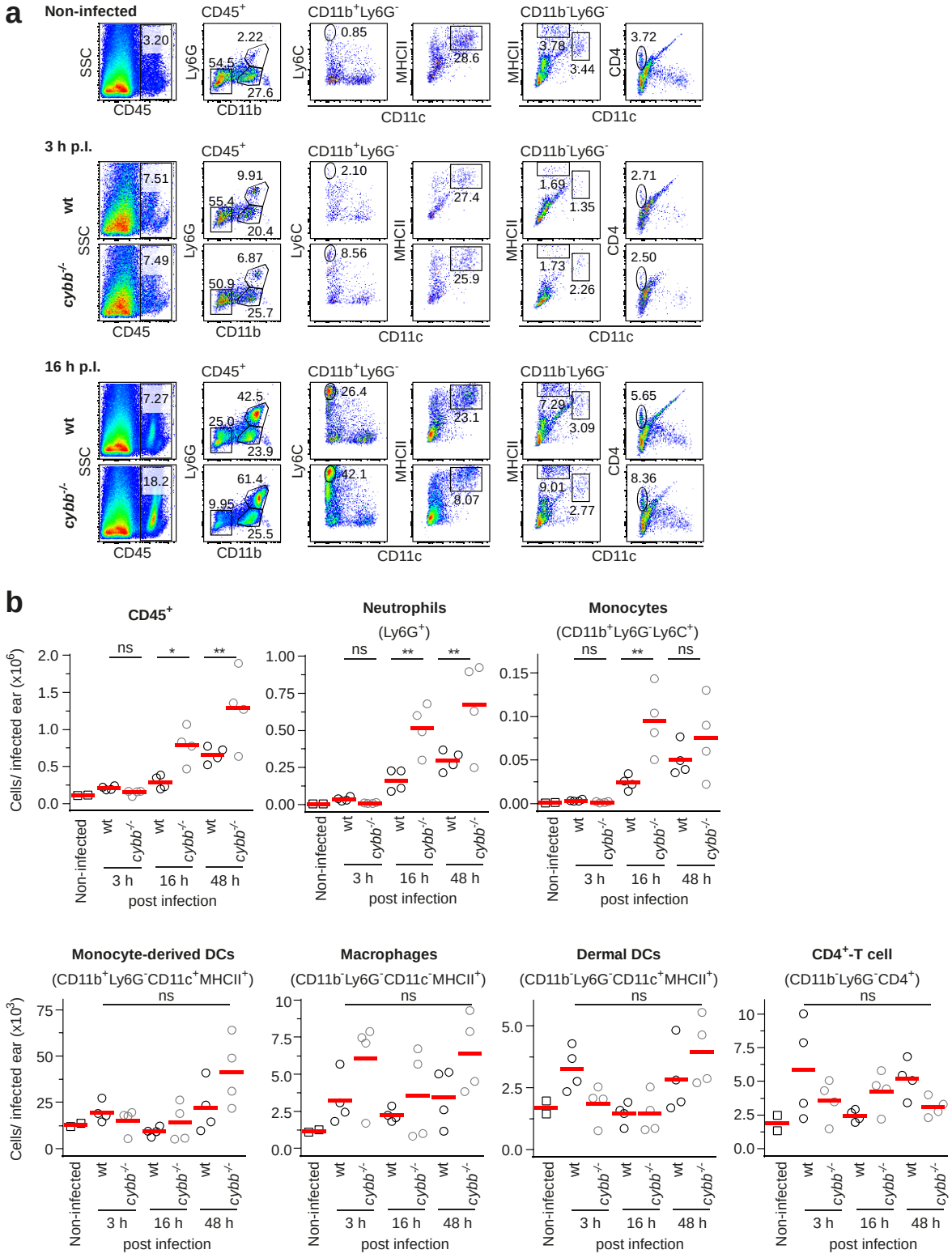

Figure 3.25: Recruitment of immune cells at site of infection in NADPH oxidase-deficient mice.

a) Flow cytometry analysis of leukocytes recruited to the site of *S. aureus*-pKikume infection at 3 h versus 16 h p.i. in wild type and *cybb*$^{-/-}$ mice. Data from of non-infected mice are shown for comparison. Data are representative of at least 8 infected ears per condition. **b)** Cell counts in infected ears analyzed by flow cytometry and calculated based on counting beads. Gating on CD45^{+} cells, Neutrophils (CD11b^{+}, Ly6G^{+}) and Monocytes (CD11b^{+}, Ly6G^{-}, Ly6C^{+}), CD4^{+}-T cells (CD11b^{-}, Ly6G^{-}, CD4^{+}), Macrophages

(CD11b$^-$, Ly6G$^-$, CD11c$^-$, MHC II$^+$), Dermal DCs (CD11b$^-$, Ly6G$^-$, CD11c$^+$, MHC II$^+$) and Monocyte-derived DCs (CD11b$^+$, Ly6G$^-$, CD11c$^+$, MHC II$^+$). Data are shown from two independent experiments. Each dot represents one individual ear; horizontal bars represent the mean; ns, not significant as determined by one-way ANOVA.

After we had shown that the bacterial burden was significantly elevated in *cybb*$^{-/-}$ mice (see **Figure 3.24**) and more leukocytes were recruited compared to infected wild type mice (see **Figure 3.25**), we were now interested in the impact of NADPH oxidase in this microenvironment on the growth behavior of the pathogen. Already in the confocal images, a higher recovery from photoconversion at 16 h p.I. could be observed for *S. aureus*-pKikume in *cybb*$^{-/-}$ mice (**Figure 3.26 a**). Quantitative analysis of the mKikume biosensor revealed significant higher *S. aureus* proliferation rates in *cybb*$^{-/-}$ mice compared to wild type at 16 h and 48 h, but not at 3 h p.I. (**Figure 3.26 b**). Therefore, NADPH oxidase activity can contribute to the reduction of bacterial numbers by dampening *S. aureus* growth.

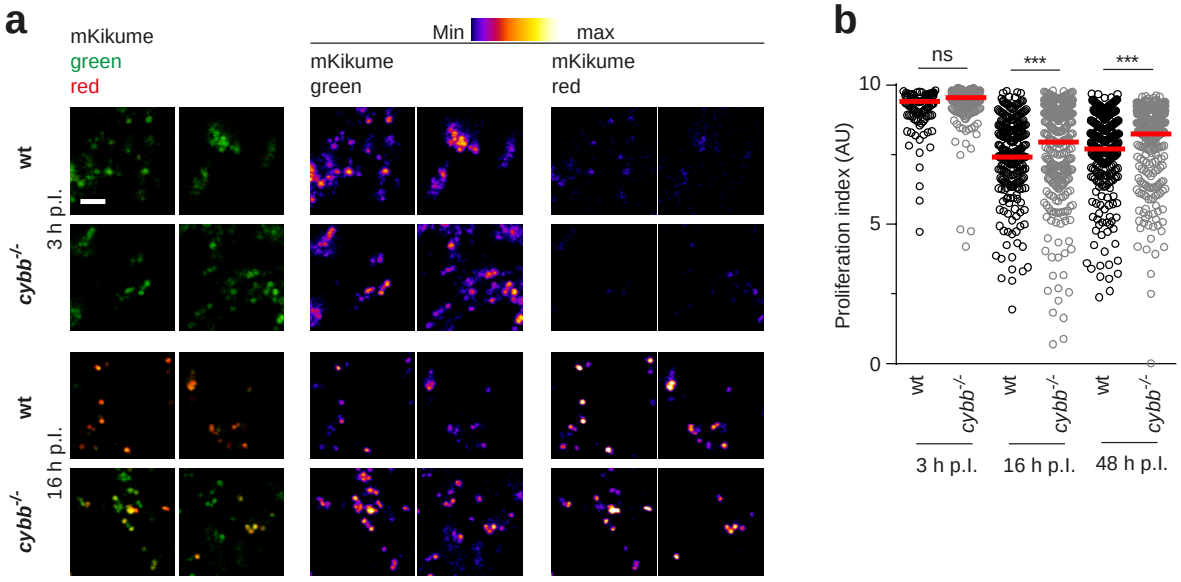

Figure 3.26: Proliferation of *S. aureus*-pKikume in oxidative burst-incompetent mice **a)** Confocal imaging of photoconverted *S. aureus*-pKikume in fixed cryosections of wild type and *cybb*$^{-/-}$ mice infected for 3 h versus 16 h, photoconverted 1 h prior to fixation and analysis. Two representative regions are shown per condition, the single red and green fluorescence channels in the middle and right column are shown as heat maps. Scale bar, 5 µm. **b)** Proliferation index of bacteria detected in in fixed cryosections of wild type (black symbols) versus *cybb*$^{-/-}$ (grey symbols) mouse ears infected with *S. aureus*-pKikume and confocal images as represented in a) were analyzed automatically. At least 21 confocal images per mouse ear were analyzed in four to ten ears per condition. Each dot represents one confocal image; horizontal bars represent the median; ***, p<0.001; ns, not significant as determined by one-way ANOVA.

3.6 Perspectives for further analysis – Cell-extrinsic effect of ROS

It was already shown that ROS can also take their effect extracellularly (Boyle *et al.*, 2011) and diffuse through cell membranes (Morales *et al.*, 2012; Neutze *et al.*, 1996; Ohno *et al.*, 1985). With respect to the higher growth rate of *S. aureus* in NAPDH oxidase deficient mice (see **Figure 3.26**), the question arises if the cells at the infection site could influence each other in acting against *S. aureus* via ROS. To examine if the dampening effect of the oxidative burst on *S. aureus* proliferation is cell-intrinsic, or has a cell-extrinsic component, we prepared bone marrow chimeras reconstituted with 1:1 mixtures of *cybb*$^{-/-}$ (CD45.2^{+}) and wild type CD45.1^{+} bone marrow as described schematically in **Figure 3.27**. A mixture of C57BL/6J (CD45.2^{+}) and wild type CD45.1^{+} cells were used as wild type control, additionally, we tested infected C57BL/6J wild type and *cybb*$^{-/-}$ complete knock out mice were the different cellular genotypes could not influence each other.

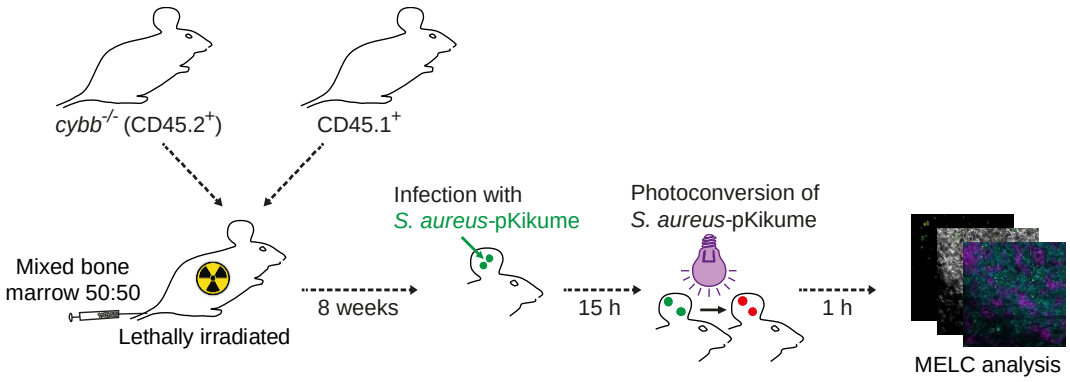

Figure 3.27: Schematic representation of bone marrow chimera preparation. As CD45.2^{+} donor mice were either *cybb*$^{-/-}$ or C57BL/6J (wild type control) mice used to reconstitute lethally irradiated *cybb*$^{-/-}$ mice. After 8 weeks the mice were infected in the ear at three injection sites with 5x10^{4} bacteria each with *S. aureus*-pKikume. MELC analysis was performed with fixed cryosections.

For Multi-Epitope Ligand Cartography (MELC), the ear tissue was stained for several markers, including CD45, CD45.1, CD11b and Ly6G (**Figure 3.28 a**). By subtraction of the CD45.1 signal from the CD45 signal, we calculated a channel for CD45.2 since the staining for CD45.2 turned out to be not sensitive enough in MELC (data not shown) (**Figure 3.28 a-b** and see 6.2.2 Macro for fluorescence measurement of cell borders in MELC data). The tissue sections were analyzed by drawing band regions of interest along the cell surfaces followed by automated measurement of the cell surface signal (see 6.2.2 Macro for fluorescence measurement of cell borders in MELC data) and the green and red mKikume signal of the intracellular *S. aureus*-pKikume (see 6.2.3 Macro for bacterial mKikume

fluorescence measurement in MELC data). By using the CD45.1$^+$ to CD45.2$^+$ signal, we distinguished between the two cell types in the BMCs. Out of the red and green signal in the cells, we calculated a proliferation index normalized to the red to green ratio in all wild type (CD45.1 cells or C57BL/6J mice) cells per experiment (**Figure 3.28 c**). Interestingly, we observed no difference in the bacterial growth between wild type and *cybb*$^{-/-}$ cells in the BMCs, but as expected, between wild type and *cybb*$^{-/-}$ complete knock out mice. Therefore, we conclude that the effect of ROS production on the proliferation of *S. aureus* has to be cell-extrinsic (**Figure 3.28 c**).

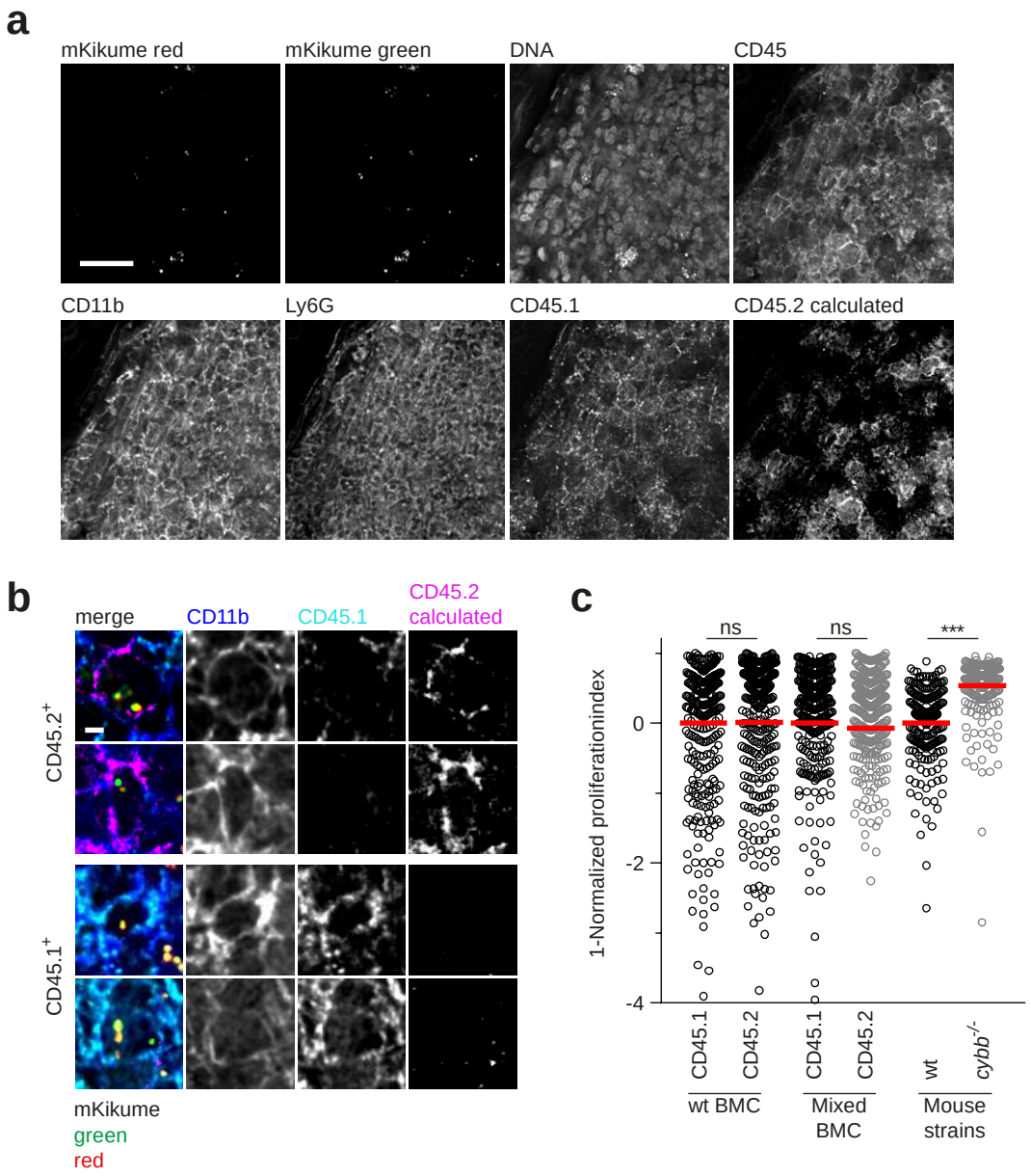

Figure 3.28: MELC analysis of infected ear tissue. a) Corrected MELC images of immune cells and *S. aureus*-pKikume in fixed cryosections of bone marrow chimera infected for 16 h, photoconverted 1 h prior to fixation. Scale bar, 20 µm. **b)** Representative images of CD45.1$^+$ and CD45.2$^+$ cells in mixed bone marrow chimeras (BMC). Scale bar, 2 µm.

c) Each dot represents one cell analyzed. Data are pooled from two independent experiments. The data of each cell (both, CD45.1$^+$ and CD45.2$^+$) in one experiment was normalized to the mean over all CD45.1$^+$ cells (and on wt cells for comparison of independent wild type versus *cybb*$^{-/-}$ mice, column 5 and 6) in each respective experiment. Bacteria in wild type (black symbols) versus *cybb*$^{-/-}$ (grey symbols) cells for six ears per BMC-condition and at least three ears of wild type or *cybb*$^{-/-}$ complete knock out were analyzed, with at least three images per ear and 15 cells per cell type in BMC or 20 cells in mice strains. Each dot represents one analyzed cell; horizontal bars represent the mean; ***, p<0.001; ns, not significant as determined by one-way ANOVA.

When analyzing the localization of CD45.1$^+$ and CD45.2$^+$ cells, we found patches of either genotype clustering together. This was not only the case in infected ears of BMC containing CD45.1$^+$ and *cybb*$^{-/-}$ cells, but also in controls which only harbor CD45.1$^+$ and CD45.2$^+$ wild type cells (**Figure 3.29**). This finding was unexpected since for neutrophils recruited from the bloodstream (independently of their CD45.1 or CD45.2 surface expression), a completely random distribution would be the most likely localization pattern expected. Therefore, the neutrophil occurrence at the site of infection might be more complex than previously assumed.

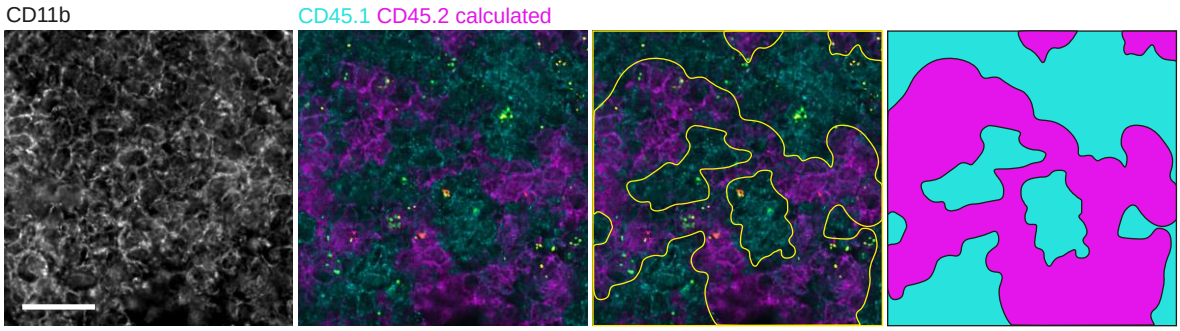

Figure 3.29: Patches in infected CD45.1$^+$/CD45.2$^+$ BMCs. Representative image of a *S. aureus*-pKikume infected BMC mouse ears. Corrected MELC images in fixed cryosections of bone marrow chimera infected for 16 h and photoconverted 1 h prior to fixation. In this example the BMC contains CD45.1$^+$ (cyan) and *cybb*$^{-/-}$ (CD45.2$^+$, magenta) cells. For exemplification, the borders of the patches were drawn in yellow and filled. Scale bar, 20 µm.

4 DISCUSSION

To understand the lifestyle, physiological state and, especially, the persistence behavior of *S. aureus*, is of high interest because all these factors influence the infection course via activation of the immune system and susceptibility to treatment. Many antibiotics are targeting the formation of the cell wall or the protein biosynthesis (see **Table 1.1**), which emphasizes the connection between pathogen growth and susceptibility to antibiotics. However, the emergence and spread of antibiotic-resistant *S. aureus* increases constantly. Besides the acquisition of genetic traits which confer resistance to antimicrobial treatment, the application of antibiotics which inhibit cell wall biosynthesis might additionally be complicated by the occurrence of phenotypical resistance. Bacteria that withstand such antibiotic treatments often exhibit small colony forming units transiently. This temporary downregulation of the replication rate is believed to reduce the points of attack for cell wall synthesis inhibition. Furthermore, it is possible that the immune response, or immune evasion mechanisms, impact on *S. aureus* growth rate, and consequently impose an indirect influence on phenotypic antibiotic resistance as well. Therefore, a measurement of the bacterial growth rate during infection is a fundamentally important parameter for understanding bacterial behavior during infection and treatment, but has remained difficult to measure so far. A major aim of this study was to develop and characterize such a bacterial growth measurement system for *S. aureus*.

4.1 Measurement of bacterial growth

To date, there are different possibilities of determining pathogen proliferation rates of bacteria, which were already listed in **Figure 1.8**.

The most common way to show bacterial growth is to count colony forming units at several time points, and to display their increase over the time (Lowy *et al.*, 1988; Cooper *et al.*, 2009; Abtin *et al.*, 2014). But to determine the bacterial burden via CFUs is insufficient for determining the mode of action of pathogen containment, as it cannot distinguish whether pathogen numbers are controlled via killing of the bacteria, or reduction of the proliferation rate, which in principle can be non-lethal for the microbes. Thus, to use bacterial burden and bacterial growth as interchangeable terms is misleading. Also, to measure a change in the bacterial burden using CFUs, the infected animal has to be killed to extract the infected tissue, whereby this method is always an end point approach. Moreover, data obtained by CFU measurement only gives information about the whole population and not about single cell growth rates, which would be important to get better insights into the role of bacterial growth in the context of pathogen interactions with cells of the immune system.

To investigate such immune cell and pathogen interactions, or to get more detailed insights into the efficiency of the treatment of an infection, microscopy of the dilution of fluorescent proteins or dyes has been applied recently to detect pathogen growth (Surewaard *et al.*, 2016; Flannagan *et al.*, 2016; Deniset *et al.*, 2017). One way to do so is to load the bacteria of interest with a fluorescent dye and inject them afterwards. In this way, Surewaard *et al.* detected replication of MRSA within Kupffer cells by dilution of the dye Syto 60 using spinning-disc intravital microscopy (SD-IVM) imaging eight hours after infection (Surewaard *et al.*, 2016). Likewise, the replication of *S. aureus* USA300 was shown after phagocytosis in macrophages 12 h p.I. by eFluor-670 labeled bacteria. Furthermore, for the eukaryotic parasite *L. major*, Chang *et al.* used CFSE staining to detect serial cell divisions by flow cytometry within five days (Chang *et al.*, 2007). Nevertheless, for all these approaches, the limiting factor is the short window of measurement after dye loading. The fluorophores are diluted at the first round of replication after loading the cells, and measurement accuracy decreases from this time point on. Consequently, the growth can only be tracked for a short time after the initial infection, however afterwards, for example in persistent pathogens or biofilm formation, a measurement of growth rates is not possible anymore.

Another approach in dilution of fluorescent dyes is to pulse fluorescent protein expression using metabolite-induced promotor constructs. Therefore, Helaine *et al.* equipped *Salmonella enterica* with reporter plasmids including IPTG- or arabinose-dependent promoters controlling genes encoding for GFP and DsRed (Helaine *et al.*, 2010). By selectively inducing the respective fluorescence genes by metabolite administration, they

could follow up the bacterial proliferation up to ten generations in *in vitro* experiments, as well as *in vivo*. The advantage of this method is that the proliferation measurement is not limited to one single time point, but can be repeated by providing the inducing agent during the experiment and then following proliferation-related fluorescence protein dilution. However, the homogenous accessibility of the tissue of interest for the inducer is critical *in vivo*, thus it is conceivable that the pharmacokinetics in the tissue limits the application of such approaches in several organs. Related to this, pharmacokinetic effects might make it hard to control the exact time point of pulsing, whereby this approach is not unrestrictedly suitable for *in vivo* experiments.

As a pulse-free alternative, Claudi *et al*. introduced the application of fluorescent timer proteins. These proteins change their fluorescence spectrum over the time in a slow maturation kinetics. Thus, the measurement of old versus new fluorescent protein exhibiting differential spectral properties allows the identification of high proliferating pathogens *in vivo* by their *de novo* protein production (Claudi *et al.*, 2014). There are several established protein timers, and the time dependent conformational change of such proteins was already reported for fluorescence timers with a broad spectrum of maturation times (Subach *et al.*, 2009). The advantage of this approach is that no access to the tissue, neither surgically, optically, or pharmacologically is needed before analysis, and that the measurement is possible over a long time period. However, the measurement is limited to a very well-defined micromilieu, as the maturation kinetics of the timers depends heavily on oxygen tension (Claudi *et al.*, 2014). As this maturation kinetics, not the actual fluorescence protein content is the main determinant for the proliferation measurement readout, its use for the investigation of innate effector mechanisms is complicated, especially in heavily inflamed microenvironments. In these settings, the oxidative conditions can change rapidly and dramatically, e.g. by oxidative burst (Wiese *et al.*, 2012).

The use of the photoconvertible fluorescence protein mKikumeGR, which already worked in the unicellular eukaryotic parasite *L. major* (Heyde *et al.*, 2018), circumvents many of the different disadvantages described for other proliferation measurement approaches. One aim of this study was to adapt the *in vivo* proliferation biosensor mKikumeGR to *S. aureus* SH1000. One problem of photoconvertible fluorescence protein expression in bacteria had already been solved in the original construct by Habuchi *et al.*, i.e. the monomeric expression of this photoconvertible protein, since multimeric forms of fluorescence proteins often exhibit difficulties during translation in prokaryotes (Habuchi *et al.*, 2008). After testing different expression constructs for *S. aureus*, the pKikume plasmid turned out to be the most successful one (see **Figure 3.2**). Of note, the simple insertion of the *mKikume* gene into the pGL485, did not result in a measurable expression of the fluorescence protein (see **Figure 3.2 a-b**), although for GFP in pGL485 showed bright green fluorescence. This might

be due to several reasons, since the intensity of fluorescent protein signals can depend on factors like stability, brightness, and maturation time, which already widely vary for GFP-like proteins (Nienhaus *et al.*, 2009).

Comparing the bacterial growth *in vitro* via OD_{600} measurement, we could not detect any significant difference between the empty vector pGL485 and the two tested expression vectors pKikume and pTufAKikume (see **Figure 3.2 c**). Liew *et al.* could already show that the expression of a fluorescent protein in *S. aureus* SH1000 by pGL485 shows no relevant impact on the bacterial growth behavior (Liew *et al.*, 2011).

In their original publication, describing the photoconvertible protein, Habuchi *et al.* tested the photoconversion from green to red fluorescence of mKikumeGR by illumination of violet light at 405 nm and demonstrated an irreversible conversion (Habuchi *et al.*, 2008). The used wavelength of 405 nm was also suitable for the by *S. aureus* expressed mKikume (see **Figure 3.3**) and additionally, the illumination with violet light at 375 nm resulted in a complete photoconversion (see **Figure 3.4 b**). Similar to Heyde *et al.*, we observed a one minute long illumination at 405 nm as expedient (Heyde *et al.*, 2018). As a result of the fast replication of *S. aureus* in exponentially growing of *in vitro* cultures, the total recovery time (and therefore, readout time) of the pathogen from photoconversion is much faster compared to the already used reporter in *L. major*, which needs 48 h from photoconversion until readout (see **Figure 3.4 c-d** and **Figure 3.5 b-c**).

To be sure that the change from red to green fluorescence is dependent on bacterial growth and not mainly a consequence of protein turnover in the non-dividing bacterium, a control using non-growing bacteria was performed. For this, we generated division-incompetent, but metabolically active *S. aureus* based on protocols established for other pathogens (Brockstedt *et al.*, 2005). We found that 10 µM psoralen together with an illumination of 10 min UVA-light (375 nm) inhibits *S. aureus* growth, but the bacteria were still alive, while the individual treatments with UVA or psoralen showed no effect. Meynet *et al.* established comparable treatment conditions for *Pseudomonas aeruginosa* (Meynet *et al.*, 2018). With the division-incompetent, but metabolically active *S. aureus*, we demonstrated that the bacterial division, and not the protein turnover in non-dividing bacteria, is responsible for changes in the fluorescence observed within 60 minutes (see **Figure 3.6**).

A second step to adapt the mKikume proliferation biosensor for *S. aureus* was to show its applicability during *in vivo* infection. We could show, by identification of the bacteria via an anti-*S. aureus* antibody, that nearly all bacteria at site of infection were detectable by their mKikume fluorescence (see **Figure 3.8**). Furthermore, the photoconversion about 60 seconds was, as seen *in vitro* and for *L. major*, also suitable for the bacteria in the mouse ear (see **Figure 3.9 a**; Heyde *et al.*, 2018). Based on our *in vivo* data, where we saw still non-dividing red bacteria after 60 minutes, we used, as well as *in vitro*, 60 minutes for

recovery from photoconversion to distinguish between proliferating and non-proliferating bacteria (see **Figure 3.9**).

Taken together, we established a functional fluorescence reporter system with many advantages over existing methods of measuring bacterial proliferation. This makes it possible to measure *in vivo* in a non-invasive approach the proliferation of *S. aureus* at any time point after infection in real-time by intravital 2-photon microscopy of the ongoing infection.

4.2 Bacterial growth in wild type mice

The mouse infection is a widespread model to investigate S*. aureus* infections via several routes. In particular, intravenous, intraperitoneal, subcutaneous and intranasal infection protocols have been previously established (Kim *et al.*, 2014). Because skin and soft tissue pathologies are a frequent manifestation of *S. aureus* infection (Tong *et al.*, 2015), we used a skin injection model to investigate *S. aureus*-pKikume infections and to examine *S. aureus* proliferation *in vivo*.

To define suitable time points for analyzing *S. aureus* skin infection, we determined the course of infection in wild type mice by the bacterial burden detected via CFUs. In the very beginning, we saw no increase in the bacterial burden compared to the inoculum, but even a decrease (see **Figure 3.10**). This can be explained either by dying bacteria due to the procedure or by the very likely possibility that not all bacteria adhere at infection site and are lost from the infection site when a part of the inoculum flows back through the injection channel. This was also the case in other skin infection models and higher infection doses (Molne *et al.*, 2000). Additionally, the used *S. aureus* strain SH1000 contains low amounts of SspA (Horsburgh *et al.*, 2002), which belongs to the group of MSCRAMMs, and is crucial in the adherence of microorganisms in the host as the first step of colonization (Patti *et al.*, 1994; Foster *et al.*, 1998). Nevertheless, we could define a peak of bacteria burden in the tissue for 16 h p.I., followed by a significant decline at 48 h p.I. and complete disappearance of the bacteria at 144 h p.I. (see **Figure 3.10**).The fast kinetic is most likely due to the low infection dose, which we had chosen because of the applicability for intravital imaging on a single cell level. However, also for higher infection doses, a similar course of infection, albeit with slower kinetics, but ultimately resulting in a sterile infection, was already reported (Molne *et al.*, 2000; Abtin *et al.*, 2014). In accordance with the course of the pathogen burden in the wild type mouse, immune cells start to appear after 3 h p.I. (see **Figure 3.11**). The number of neutrophils and monocytes were significantly increased at 16 h p.I. (see **Figure 3.11**), which was followed by the strong reduction in bacterial burden between 16 h and 48 h p.I.. This underlines the importance and fast effect of neutrophils in the clearance of the *S. aureus* infection. Except for monocytes and neutrophils, none of the other detected $CD45^+$ cells had significant changes in their number during *S. aureus* infection. The recruitment of neutrophils as a main constituent of cellular immune responses shortly after *S. aureus* skin injection is well known and in line with our data (Molne *et al.*, 2000; Abtin *et al.*, 2014). Monocytes, the other immune cell type which we observed to be increased, have been shown to be important for the rapid control of bacterial pathogens as well, for example after *S. aureus* and *Salmonella* infection (Bost *et al.*, 2001).

Whether the decrease of the bacterial burden in the second part of infection is mainly due to killing by the recruited neutrophils, or an additional reduction of bacterial proliferation was contributing substantially to control of the infection was not clear until now. In the first 16 h after the infection, the proliferation is evident from the increase in the tissue burden (see **Figure 3.10**). We were also able to observe this proliferative activity during intravital 2-photon microscopy of infected mouse ears at 3 h p.I. (see **Figure 3.12**). Of note, not all bacteria turned green, but the overall population exhibited a major green fluorescence recovery within one hour of imaging (see **Figure 3.12 a**, left panel). In contrast, the bacteria in the infected ear were less proliferating during intravital imaging at 16 h p.I.. This suggests that the recruited neutrophils, in addition to their well-known killing activity, exert a dampening effect on the bacterial growth (Spaan *et al.*, 2013).

Widefield or confocal fluorescence microscopy can give insights into *in vivo* skin infections, but the possibilities in tissue depth or resolution are limited. The histological examination or electron microscopy, where a view along the whole infection depth is possible, also in other tissues than the skin, only offers a single time point of interactions or behavior of immune cells and pathogen (Abtin *et al.*, 2014; Surewaard *et al.*, 2016). Therefore, 2-photon microscopy provides the possibility to measure cell-cell interactions and cell behavior in real time and in several organs or tissues *in vivo* (Liese *et al.*, 2013; Muller *et al.*, 2013; Abtin *et al.*, 2014). The applicability of the biosensor for intravital 2-photon microscopy and the possibility to follow the proliferation rate at certain time points in the same infection, opens several new opportunities to investigate the host pathogen interaction during infection with *S. aureus*. For example, the interaction of immune cells or the effect of pharmacological treatment at the site of infection can be investigated in correlation with the bacterial growth rate on a single cell level. Vice versa, with the information of the bacterial growth rate, the phenotypic resistance regarding treatments or antimicrobial effectors could be predicted.

At 48 h p.I. intravital imaging would in principle still be suitable for detecting single bacteria and measuring their proliferation rate. Nevertheless, since the infection had started to be cleared and the bacteria were not densely populating the site of infection anymore, most probably due to neutrophil infiltration, the overall proliferation rate of the population would be hard to determine for this time point via 2-photon microscopy. To measure pathogen proliferation at additional later time points, we devised a quantitative confocal microscopy approach, which based on cryosections of *S. aureus*-pKikume infected ears. With this standardized method, we got comparable data on bacterial growth rate as compared to intravital imaging for 3 h and 16 h p.I. (see **Figure 3.12** and **Figure 3.13 a**). Furthermore, by the automated analysis of the confocal images, the significant reduction of the bacterial proliferation at 16 h as compared to 3 h p.I., could be verified also at 48 h p.I. (see **Figure**

3.13 b). Thus, a quantitative application of the biosensor for confocal imaging is possible in a standardized fashion.

During intravital imaging of Catchup^{IVM} mice infected with *S. aureus*-pGFP, we observed a rapid phagocytosis of the bacteria upon neutrophil recruitment (see **Figure 3.14 a-b**), as expected from reports in the literature (Campbell, 1990; Molne *et al.*, 2000; Abtin *et al.*, 2014). Complementary to this, we showed in confocal microscopy that the majority of *S. aureus* is rapidly taken up by recruited neutrophils upon their appearance at the site of infection (see **Figure 3.11** and **Figure 3.14**). Of note, the arrival of neutrophils coincided with a reduction but not complete termination of bacterial growth. Interestingly, other *in vitro* studies also suggest that *S. aureus* growth is not completely abolished within professional phagocytes. For example, bacterial proliferation has been shown in the lysosomal compartment of macrophages (Flannagan *et al.*, 2018) and in dendritic cells (Schindler *et al.*, 2012). Similarly, it was shown that the bacteria could grow within Kupffer cells in the liver after a systemic infection (Surewaard *et al.*, 2016). Also for neutrophils, intracellular survival, but also replication has been demonstrated (Gresham *et al.*, 2000). In line with this, we show a residual proliferation of *S. aureus* also at 16 h p.I., when the vast majority of the bacteria is located within recruited neutrophils (see **Figure 3.13** and **Figure 3.14**). Nevertheless, compared to the mainly extracellular bacteria at 3 h p.I., pathogen growth is substantially reduced.

In addition to the bacterial growth, the killing of bacteria by the immune system, or through antimicrobial treatment is the main factor impacting the course of an infection. However, it is hard to measure this factor quantitatively. Although a reduction in bacterial burden over the time indicates bacterial killing, quantitative analysis by imaging fluorescence protein labeled pathogens at the site of infection is difficult, since fluorescence increase due to proliferation and decrease due to killing are difficult to disentangle. Of note, the use of photoconvertible fluorescence proteins could even provide a basis for measuring bacterial killing: Because we could show that the change in the photoconverted fluorescence is not depending on protein turnover, the population-wide red fluorescence should stay stable over time after photoconversion. Thus in principle, a net reduction in red fluorescence determined over the whole bacterial population could be only achieved as a consequence of killing. Such a modified use of photoconvertible fluorescence protein could be an interesting perspective for future applications.

4.3 The effect of neutrophil-depletion on *S. aureus* growth

Neutrophils are the major cell type at the front line of host defense against invading microorganisms. Therefore, they are essential for limiting *S. aureus* skin infections and hold a well-established role in protecting against intradermally injected *S. aureus* bacteria (Molne *et al.*, 2000).

Ly6G is exclusively expressed on murine neutrophils and the 1A8 antibody binds specifically to this surface molecule (Fleming *et al.*, 1993; Daley *et al.*, 2008). Thus, we decided to deplete murine neutrophils with this antibody (Daley *et al.*, 2008; Hurrell *et al.*, 2015). After treatment of mice with the 1A8 antibody and infection of the ears, we could not detect any neutrophils in their blood, neither by Ly6G staining, nor by staining with the less specific GR-1 antibody (see **Figure 3.15 a**). We tested additionally for a possible masking of the epitope using the GR-1 antibody by pre-incubation of the 1A8 depletion antibody *in vitro*, but we could not find a relevant hindrance for GR-1 binding (see **Figure 3.15 b**).

In the course of infection, the depletion of neutrophils had no effect on the bacterial burden at 3 h after *S. aureus* infection. This data are in line with the findings in wild type mice that at this early time point, the neutrophils had no relevant effect, because they were only starting to arrive at the site of infection, and already by numbers had not yet been able to take up a substantial part of the bacterial population. Additionally, Mölne *et al.* showed in their *S. aureus* skin infection study no difference between neutrophil-depleted (GR-1 mAb) and control mice in the first hours p.I., even with a higher infection dose (Molne *et al.*, 2000). Nevertheless, a higher bacterial burden in the infected ears was detected for neutrophil-depleted mice compared to wild type mice at 16 h and 48 h p.I. (see **Figure 3.16 a**). Of note, the elevated bacterial burden was not reflected in higher bacterial numbers in the draining lymph nodes (see **Figure 3.16 b**).

The measured bacterial growth, as determined by confocal microscopy, reflected well the data obtained by CFU measurement. At 3 h p.I. no differences were detectable between *S. aureus* in neutrophil-depleted and control mice, which was expected since the neutrophils hat only started to appear at the site of infection. At the later time points, where we had observed in the wild type mice a growth-dampening of the bacteria, the bacteria in neutrophil-depleted mice exhibited a significantly higher proliferation rate than those in control mice (see **Figure 3.17**). However, the growth was not rescued to the level of growth in bacteria at early infection time points. Thus, there were still effects in place which prevented the bacteria from reaching maximal growth rates.

In flow cytometry analysis, we defined monocytes ($CD11b^{+}$, $Ly6C^{High}$, $Ly6G^{-}$) and neutrophils ($CD11b^{+}$, $Ly6C^{Intermediate}$, $Ly6G^{+}$) as described in literature (Daley *et al.*, 2008) and could show a depletion of neutrophils in the blood (additionally with GR-1) and in the

ear. Of note, a decrease in the whole $CD45^+$ cell population in infected ears took place upon neutrophil-depletion, indicating a reduction of the whole immune cell number. Similar monocyte numbers were recruited to the site of *S. aureus* infection in neutrophil-depleted and control mice. However, one reason for the bacterial growth rate being still partially reduced upon neutrophil-depletion could be a newly appearing cell type, which is $Ly6C^+$, $Ly6G^-$, and $CD11b^{High}$, and highly increased at 48 h p.I. (see **Figure 3.18**). Thus, we wanted to characterize this cell type in the neutrophil-depleted mice.

In a first step, we investigated if the newly appearing cells are phagocytosing *S. aureus* at the same efficiency as neutrophils do in the control mice by flow cytometry analysis (see **Figure 3.19 c**). We found out that, even if they were not recruited more efficiently, monocytes seem to partially take over the task of the depleted neutrophils and phagocytosed more (up to five times more) bacteria than in the control mice, a phenomenon that declined at 48 h p.I., when more $Ly6C^+$, $Ly6G^-$, and $CD11b^{High}$ cells were recruited. Of note, these newly recruited cells were the major cell population phagocytosing *S. aureus* upon neutrophil-depletion (see **Figure 3.19 d**).

For *Leishmania mexicana* skin infection, it has been reported that upon neutrophil-depletion the number of inflammatory monocytes and monocyte-derived DCs in the dermis was increased (Hurrell *et al.*, 2015). Thus, we tested whether the newly appearing cell type could be another monocyte subtype than the already detected inflammatory monocytes ($Ly6C^+$, $Ly6G^-$, $CD11b^{Intermediate}$). Hence, we stained the newly appearing cells in the ear and bone marrow for Ly6C, CX_3CR1 and CCR2, all markers for monocytes. From the data, we concluded that the newly appearing population already occurred in the bone marrow, but these cells were no monocytes.

In the following, we used BMC with CFP-expressing bone marrow cells to mark the recruited immune cells during confocal microscopy. Furthermore, with DAPI staining in fixed cryosections of infected mouse ears of neutrophil-depleted and control mice, we investigated the nuclear morphology of recruited immune cells around the site of infection (see **Figure 3.22**). Interestingly, in both groups of mice, immune cells with a nuclear morphology typical for for mouse-neutrophils were recruited (Hoffmann *et al.*, 2007). Complementary, some of the detected cells had already phagocytosed *S. aureus* bacteria, which were detected in the DAPI channel too (see **Figure 3.22**, row three and four).

Finally, we tested infected ears of neutrophil-depleted mice for GR-1 expression, although in blood samples, no GR-1 signal was detectable for neutrophil-depleted mice. While gating for $Ly6C^{High}$ and $Ly6C^{Intermediate}$ against the CD11b signal, we differentiated between monocytes and neutrophils (control mice) or newly appearing cells (neutrophil-depleted mice). The newly appearing cells exhibited still GR-1 on their surface, even if the signal was significantly lower than for the neutrophils in control mice (see **Figure 3.23**). In contrast to

this finding, Daley *et al.* measured the recruited immune cells to skin wounds and they detected for these cells in neutrophil-depleted mice no GR-1 signal (Daley *et al.*, 2008). Also, Hurrel *et al.* could not detect any GR-1 positive neutrophils in the skin after depletion during *Leishmania mexicana* infections (Hurrell *et al.*, 2015). A possible reason for the more efficient depletion in the *Leishmania* model could be a different recruitment kinetics resulting in lower neutrophils in the blood vessels and thus, a lower consumption of antibody and cells. Nevertheless, a partial depletion was in any case reached, detectable by a significant reduction of $CD45^+$ cells in infected ears of 1A8 treated mice (see **Figure 3.18**).

Taken together, upon *S. aureus* skin infection of neutrophil-depleted mice, a new population of cells appeared, which were not monocytes, but showed similarities to neutrophils, like the CD11b and Ly6C expression and the nuclear morphology. Thus, we concluded that these cells had to be neutrophils with downregulated and partially masked GR-1 signal. A lower Ly6G signal was reported for immature neutrophils, which were recruited after systemic *Streptococcus pneumoniae* infections of mice (Deniset *et al.*, 2017). These $Ly6G^{Intermediate}$ immature neutrophils had their origin in emergency proliferation in the spleen and were therefore positive for the proliferation marker Ki-67 (Deniset *et al.*, 2017). Of note, after *S. aureus* infection absolutely no GR-1 was detectable in blood samples of depleted mice, while the blood vessels are the main route of neutrophils during recruitment.

Nevertheless, the dampening of *S. aureus* growth at later time points, at which we observed the newly appearing cell type, suggests that already the uptake by immature neutrophils or neutrophil-like phagocytes might be sufficient to substantially inhibit pathogen growth.

4.4 The effect of NADPH oxidase on *S. aureus* growth

Reactive oxygen generated by the NADPH oxidase of professional phagocytic cells is the mechanism of killing invading microorganisms (Kuhns *et al.*, 2010; Ward *et al.*, 1983). Therefore, already a residual production of NADPH oxidase leads to an improvement of immune defense against pathogens (Kuhns *et al.*, 2010). Vice versa, deficiencies in ROS production, like in chronic granulomatous disease patients, results in severe bacterial and fungal infections and chronic autoimmune manifestations, which demands treatment regimens such as antibiotic prophylaxis and regular interferon-γ injections (Malmvall *et al.*, 1993; Rawat *et al.*, 2016).

To model the absence of NADPH oxidase in mice, we used *cybb*$^{-/-}$ mice, in which the same gene is affected as in the most widespread X-linked recessive form of the disease, the gp91phox (Rawat *et al.*, 2016). As expected, we could not detect any differences in the tissue burden between wild type and *cybb*$^{-/-}$ mice in the beginning of infection, at 3 h p.I. which fits well with the neutrophils only beginning to arrive at this time point (see **Figure 3.24**). Additionally, leukocyte recruitment as well as the bacterial growth rate was not different between *cybb*$^{-/-}$ and wild type mice for this time point (see **Figure 3.26**). In contrast, we saw significant differences at later time points: Since the neutrophils were not able to produce ROS, the growth of *S. aureus* was not that much dampened anymore, resulting in a higher proliferation rate and consequently in an increased bacterial burden at 16 h and 48 h p.I. for *cybb*$^{-/-}$ mice compared to wild type mice (see **Figure 3.24** and **Figure 3.26**). Nevertheless, a significantly increased recruitment of neutrophils and monocytes was observed in the *cybb*$^{-/-}$ mice (see **Figure 3.25**). However, this enhanced recruitment of leukocytes was not effectively compensating for the absence of oxidative burst in dampening the bacterial proliferation or killing of the pathogen.

Besides the effect on the bacteria by ROS themselves, induction of an additional killing mechanism for extracellular pathogens, neutrophil extracellular traps, are dependent on the production of ROS (Sollberger *et al.*, 2018b). Therefore, in *cybb*$^{-/-}$ mice, the induction of NETs is expected to be strongly reduced and in consequence, the killing of extracellular pathogen should be inhibited. But at the same time, we had observed in the Catchup^{IVM} experiments that most of the bacteria are taken up at 16 h p.I., where the biggest differences between *cybb*$^{-/-}$ and wildtype mice are detectable. Thus, the reduction of NET formation should not dramatically influence the growth of these intracellular bacteria. Therefore, we conclude that the recruited phagocytic cells rely on NADPH oxidase not only to kill directly *S. aureus*, but also to restrict bacterial growth non-lethally.

In lung infections with *E. coli*, Gao *et al.* could demonstrate a much severe infection course in NADPH oxidase-deficient mice, resulting in a higher bacterial burden, and more

recruitment of polymorphonuclear leukocytes (Gao *et al.*, 2002). Likewise, in systemic infections of *cybb*$^{-/-}$ mice with the highly virulent *S. aureus* strain USA300 Surewaard *et al.* detected a tenfold higher bacterial burden in the spleen as compared to wild type mice (Surewaard *et al.*, 2016). There are some possible reasons for the increase of the number of neutrophils at the site of infection which we observe for *S. aureus*-infected *cybb*$^{-/-}$ mice (see **Figure 3.25**): Due to a higher bacterial burden, more PAMPs are detectable and subsequently, more chemokines are secreted at the site of infection, which leads to a stronger recruitment of neutrophils (Molne *et al.*, 2000). Under normal conditions, the production of reactive oxygen species leads also to damage of recruited neutrophils at the site of infection (Harbort *et al.*, 2015; Kobayashi *et al.*, 2010). However, since a large proportion of reactive oxygen species are missing in *cybb*$^{-/-}$ mice, also the oxidative stress for the neutrophils is lower, whereby the neutrophils might undergo less cell death. Additionally, NETosis, by NET formation should not take place as extensively in *cybb*$^{-/-}$ mice, because the main inducing factor, high ROS concentrations, is lacking. Thus, less neutrophils are expected to die during infections of *cybb*$^{-/-}$ mice and might therefore accumulate in higher numbers.

Nevertheless, the *S. aureus* infection was controlled in the *cybb*$^{-/-}$ mice, despite the inability of ROS production. Leliefeld *et al.* reported that the containment of *S. aureus* in human neutrophils is not depending on NADPH oxidase functionality, but on acidification of the phagosome (Leliefeld *et al.*, 2018). Additionally, in our study, the *S. aureus* strain SH1000 was used, which was reported to contain less amounts of the exoprotein α-toxin (Hla) (Horsburgh *et al.*, 2002). Consequently, this strain is impaired in inducing neutrophil apoptosis via Hla (Menzies *et al.*, 1998) and might thus inefficiently evade the containment by neutrophils, even if these are not fully functional. Along the same line, for skin infection with a ΔHla *S. aureus* strains, a significantly higher recruitment of neutrophils and stronger clearance of the bacteria infection is reported (Abtin *et al.*, 2014).

Consequently, NADPH oxidase-deficient neutrophils, which are not able to produce ROS anymore, or which might be immature in case of excessive granulopoiesis, seem to be sufficient to substantially restrict *S. aureus* SH1000 in bacterial growth.

4.5 Perspectives for further analysis – Cell-extrinsic effect of ROS

Pre-activation of neutrophils during their recruitment is essential for maximal degranulation and the full activation of the NADPH oxidase pathway (Guthrie *et al.*, 1984). Furthermore, H_2O_2 can diffuse through neutrophil membranes and, to a limited extent, through pathogens, and damage both, phagocytosed and non-phagocytosed pathogens (Morales *et al.*, 2012; Neutze *et al.*, 1996; Ohno *et al.*, 1985). Thus, the question has been raised whether the activity of the NADPH oxidase acts only cell-intrinsic or if diffusing ROS could rescue the incapacity of a neighboring cell to produce ROS. Such a cell-extrinsic effect was already shown for nitric oxide (NO), which is produced by inducible NO synthase of *L. major* containing phagocytes and diffuses into bystander cells to promote pathogen killing there (Olekhnovitch *et al.*, 2014). Moreover, NADPH oxidase shows in an indirect way a cell-extrinsic effect, by ROS-dependent NET formation (Sollberger *et al.*, 2018b). Also, a concept similar to NETs but taking effect intracellularly are pore-induced intracellular traps (PITs), which were reported for macrophages infected with *Salmonella* during a lytic cell death, called pyroptosis (Jorgensen *et al.*, 2016). Such PITs seemed to be dependent of Gasdermin and consequently also of NADPH oxidase. Thus, is would also be reasonable to assume that NADPH oxidase would have cell-intrinsic effects, which are inhibited for *cybb*$^{-/-}$ cells. At any rate, the knock out of functional NADPH oxidase seems to have more effects than just inhibiting oxidative burst and is much more complicated in the subsequent consequences than expected.

Using CD45.1^{+}/*cybb*$^{-/-}$ mixed bone marrow chimeras, we could not detect any significant difference in pathogen growth dampening between wild type and knock out cells when present at the same site of infection, which was in contrast to the comparison between wild type and complete knock out mice (see **Figure 3.28**). Thus, we assume a cell-extrinsic effect of ROS, which affects also the bacteria in neighboring host cells. It would be very interesting to investigate if the collective production of ROS, and thus the net proportion of NADPH oxidase-competent cells determines the extent of pathogen containment or whether there are residual cell-intrinsic modes of action of NADPH oxidase.

While analyzing MELC images of the BMCs described above, we observed patches of up to twenty cells expressing the same congenic cell marker (CD45.1 or CD45.2) at the site of infection (see **Figure 3.29**). A possible explanation for these patches is a clonal recruitment to the site of infection. While irradiating the mice, we destroyed the hematopoetic cells of the bone marrow and during reconstitution, the immigrated donor cells are likely to expand in their bone marrow niches and form clonal clusters in the bones. Starting from such clusters, it might be possible that during infection, the bone marrow stem cells do not synchronously start to proliferate, and thus, release of newly generated neutrophils occurs

in a limited number of clonal bone marrow niches. This would lead subsequently to a partially clonal invasion of leukocytes into the infected tissue. Another possibility which has to be considered is extramedullary hematopoiesis: During strong infections, such as systemic *Streptococcus pneumoniae* infection, extramedullary emergency proliferation was shown for immature neutrophils in the spleen (Deniset *et al.*, 2017). However, as exemplarily shown in **Figure 3.29**, patches are formed out of ten to twenty neutrophils. For a clonal expansion at the site of infection, the original cell had to undergo minimal four cell divisions, which is very unlikely during a time frame of maximal 16 h. Nevertheless, the neutrophil occurrence at the site of infection might be more complex than previously assumed.

5 REFERENCES

Abtin A, Jain R, Mitchell AJ, Roediger B, Brzoska AJ, Tikoo S, Cheng Q, Ng LG, Cavanagh LL, von Andrian UH, Hickey MJ, Firth N, Weninger W (2014). Perivascular macrophages mediate neutrophil recruitment during bacterial skin infection. Nat Immunol *15***,** 45-53.

Ahmed S, Meghji S, Williams RJ, Henderson B, Brock JH, Nair SP (2001). Staphylococcus aureus fibronectin binding proteins are essential for internalization by osteoblasts but do not account for differences in intracellular levels of bacteria. Infect Immun *69***,** 2872-2877.

Amagai M, Matsuyoshi N, Wang ZH, Andl C, Stanley JR (2000). Toxin in bullous impetigo and staphylococcal scalded-skin syndrome targets desmoglein 1. Nat Med *6***,** 1275-1277.

Amagai M, Yamaguchi T, Hanakawa Y, Nishifuji K, Sugai M, Stanley JR (2002). Staphylococcal exfoliative toxin B specifically cleaves desmoglein 1. J Invest Dermatol *118***,** 845-850.

Anderson KE, Boyle KB, Davidson K, Chessa TA, Kulkarni S, Jarvis GE, Sindrilaru A, Scharffetter-Kochanek K, Rausch O, Stephens LR, Hawkins PT (2008). CD18-dependent activation of the neutrophil NADPH oxidase during phagocytosis of Escherichia coli or Staphylococcus aureus is regulated by class III but not class I or II PI3Ks. Blood *112***,** 5202-5211.

Armstrong-Esther CA (1976). Carriage patterns of Staphylococcus aureus in a healthy non-hospital population of adults and children. Ann Hum Biol *3***,** 221-227.

Arvidson S, Tegmark K (2001). Regulation of virulence determinants in Staphylococcus aureus. Int J Med Microbiol *291***,** 159-170.

Bardoel BW, Vos R, Bouman T, Aerts PC, Bestebroer J, Huizinga EG, Brondijk TH, van Strijp JA, de Haas CJ (2012). Evasion of Toll-like receptor 2 activation by staphylococcal superantigen-like protein 3. J Mol Med (Berl) *90***,** 1109-1120.

Barrett FF, McGehee RF, Jr., Finland M (1968). Methicillin-resistant Staphylococcus aureus at Boston City Hospital. Bacteriologic and epidemiologic observations. N Engl J Med *279***,** 441-448.

Bayer MG, Heinrichs JH, Cheung AL (1996). The molecular architecture of the sar locus in Staphylococcus aureus. J Bacteriol *178***,** 4563-4570.

Begier E, Seiden DJ, Patton M, Zito E, Severs J, Cooper D, Eiden J, Gruber WC, Jansen KU, Anderson AS, Gurtman A (2017). SA4Ag, a 4-antigen Staphylococcus aureus vaccine, rapidly induces high levels of bacteria-killing antibodies. Vaccine *35***,** 1132-1139.

Belanger KJ, Kelly DJ, Mettille FC, Hanson CV, Lippert LE (2000). Psoralen photochemical inactivation of Orientia tsutsugamushi in platelet concentrates. Transfusion *40***,** 1503-1507.

Bera A, Herbert S, Jakob A, Vollmer W, Gotz F (2005). Why are pathogenic staphylococci so lysozyme resistant? The peptidoglycan O-acetyltransferase OatA is the major determinant for lysozyme resistance of Staphylococcus aureus. Mol Microbiol *55*, 778-787.

Bestebroer J, Aerts PC, Rooijakkers SH, Pandey MK, Kohl J, van Strijp JA, de Haas CJ (2010). Functional basis for complement evasion by staphylococcal superantigen-like 7. Cell Microbiol *12*, 1506-1516.

Bestebroer J, Poppelier MJ, Ulfman LH, Lenting PJ, Denis CV, van Kessel KP, van Strijp JA, de Haas CJ (2007). Staphylococcal superantigen-like 5 binds PSGL-1 and inhibits P-selectin-mediated neutrophil rolling. Blood *109*, 2936-2943.

Bestebroer J, van Kessel KP, Azouagh H, Walenkamp AM, Boer IG, Romijn RA, van Strijp JA, de Haas CJ (2009). Staphylococcal SSL5 inhibits leukocyte activation by chemokines and anaphylatoxins. Blood *113*, 328-337.

Bevilacqua MP, Stengelin S, Gimbrone MA, Jr., Seed B (1989). Endothelial leukocyte adhesion molecule 1: an inducible receptor for neutrophils related to complement regulatory proteins and lectins. Science *243*, 1160-1165.

Bien J, Sokolova O, Bozko P (2011). Characterization of Virulence Factors of Staphylococcus aureus: Novel Function of Known Virulence Factors That Are Implicated in Activation of Airway Epithelial Proinflammatory Response. J Pathog *2011*, 601905.

Bierbaum G, Fuchs K, Lenz W, Szekat C, Sahl HG (1999). Presence of Staphylococcus aureus with reduced susceptibility to vancomycin in Germany. Eur J Clin Microbiol Infect Dis *18*, 691-696.

Bischoff M, Entenza JM, Giachino P (2001). Influence of a functional sigB operon on the global regulators sar and agr in Staphylococcus aureus. J Bacteriol *183*, 5171-5179.

Biswas R, Voggu L, Simon UK, Hentschel P, Thumm G, Gotz F (2006). Activity of the major staphylococcal autolysin Atl. FEMS Microbiol Lett *259*, 260-268.

Bitschar K, Wolz C, Krismer B, Peschel A, Schittek B (2017). Keratinocytes as sensors and central players in the immune defense against Staphylococcus aureus in the skin. J Dermatol Sci *87*, 215-220.

Blanks JE, Moll T, Eytner R, Vestweber D (1998). Stimulation of P-selectin glycoprotein ligand-1 on mouse neutrophils activates beta 2-integrin mediated cell attachment to ICAM-1. Eur J Immunol *28*, 433-443.

Bokarewa MI, Jin T, Tarkowski A (2006). Staphylococcus aureus: Staphylokinase. Int J Biochem Cell Biol *38*, 504-509.

Bost KL, Bento JL, Petty CC, Schrum LW, Hudson MC, Marriott I (2001). Monocyte chemoattractant protein-1 expression by osteoblasts following infection with Staphylococcus aureus or Salmonella. J Interferon Cytokine Res *21*, 297-304.

Boyle-Vavra S, Daum RS (2007). Community-acquired methicillin-resistant Staphylococcus aureus: the role of Panton-Valentine leukocidin. Lab Invest *87*, 3-9.

Boyle KB, Gyori D, Sindrilaru A, Scharffetter-Kochanek K, Taylor PR, Mocsai A, Stephens LR, Hawkins PT (2011). Class IA phosphoinositide 3-kinase beta and delta regulate neutrophil oxidase activation in response to Aspergillus fumigatus hyphae. J Immunol *186***,** 2978-2989.

Bradley A (2002). Bovine mastitis: an evolving disease. Vet J *164***,** 116-128.

Brandt SL, Klopfenstein N, Wang S, Winfree S, McCarthy BP, Territo PR, Miller L, Serezani CH (2018a). Macrophage-derived LTB4 promotes abscess formation and clearance of Staphylococcus aureus skin infection in mice. PLoS Pathog *14***,** e1007244.

Brandt SL, Putnam NE, Cassat JE, Serezani CH (2018b). Innate Immunity to Staphylococcus aureus: Evolving Paradigms in Soft Tissue and Invasive Infections. J Immunol *200***,** 3871-3880.

Bremell T, Abdelnour A, Tarkowski A (1992). Histopathological and serological progression of experimental Staphylococcus aureus arthritis. Infect Immun *60***,** 2976-2985.

Brinkmann V, Reichard U, Goosmann C, Fauler B, Uhlemann Y, Weiss DS, Weinrauch Y, Zychlinsky A (2004). Neutrophil extracellular traps kill bacteria. Science *303***,** 1532-1535.

Brockstedt DG, Bahjat KS, Giedlin MA, Liu W, Leong M, Luckett W, Gao Y, Schnupf P, Kapadia D, Castro G, Lim JY, Sampson-Johannes A, Herskovits AA, Stassinopoulos A, Bouwer HG, Hearst JE, Portnoy DA, Cook DN, Dubensky TW, Jr. (2005). Killed but metabolically active microbes: a new vaccine paradigm for eliciting effector T-cell responses and protective immunity. Nat Med *11***,** 853-860.

Campanelli D, Detmers PA, Nathan CF, Gabay JE (1990). Azurocidin and a homologous serine protease from neutrophils. Differential antimicrobial and proteolytic properties. J Clin Invest *85***,** 904-915.

Campbell PA (1990). The neutrophil, a professional killer of bacteria, may be controlled by T cells. Clin Exp Immunol *79***,** 141-143.

Caruso R, Botti E, Sarra M, Esposito M, Stolfi C, Diluvio L, Giustizieri ML, Pacciani V, Mazzotta A, Campione E, Macdonald TT, Chimenti S, Pallone F, Costanzo A, Monteleone G (2009). Involvement of interleukin-21 in the epidermal hyperplasia of psoriasis. Nat Med *15***,** 1013-1015.

Catalao MJ, Figueiredo J, Henriques MX, Gomes JP, Filipe SR (2014). Optimization of fluorescent tools for cell biology studies in Gram-positive bacteria. PLoS One *9***,** e113796.

Chang HK, Thalhofer C, Duerkop BA, Mehling JS, Verma S, Gollob KJ, Almeida R, Wilson ME (2007). Oxidant generation by single infected monocytes after short-term fluorescence labeling of a protozoan parasite. Infect Immun *75***,** 1017-1024.

Chapple DS, Mason DJ, Joannou CL, Odell EW, Gant V, Evans RW (1998). Structure-function relationship of antibacterial synthetic peptides homologous to a helical surface region on human lactoferrin against Escherichia coli serotype O111. Infect Immun *66***,** 2434-2440.

Chavakis T, Hussain M, Kanse SM, Peters G, Bretzel RG, Flock JI, Herrmann M, Preissner KT (2002). Staphylococcus aureus extracellular adherence protein serves as anti-inflammatory factor by inhibiting the recruitment of host leukocytes. Nat Med *8*, 687-693.

Chen J, Nag S, Vidi PA, Irudayaraj J (2011). Single molecule in vivo analysis of toll-like receptor 9 and CpG DNA interaction. PLoS One *6*, e17991.

Chen X, Niyonsaba F, Ushio H, Okuda D, Nagaoka I, Ikeda S, Okumura K, Ogawa H (2005). Synergistic effect of antibacterial agents human beta-defensins, cathelicidin LL-37 and lysozyme against Staphylococcus aureus and Escherichia coli. J Dermatol Sci *40*, 123-132.

Cheng AG, DeDent AC, Schneewind O, Missiakas D (2011). A play in four acts: Staphylococcus aureus abscess formation. Trends Microbiol *19*, 225-232.

Cheng AG, Kim HK, Burts ML, Krausz T, Schneewind O, Missiakas DM (2009). Genetic requirements for Staphylococcus aureus abscess formation and persistence in host tissues. FASEB J *23*, 3393-3404.

Chertov O, Michiel DF, Xu L, Wang JM, Tani K, Murphy WJ, Longo DL, Taub DD, Oppenheim JJ (1996). Identification of defensin-1, defensin-2, and CAP37/azurocidin as T-cell chemoattractant proteins released from interleukin-8-stimulated neutrophils. J Biol Chem *271*, 2935-2940.

Cheung AL, Bayer MG, Heinrichs JH (1997). sar Genetic determinants necessary for transcription of RNAII and RNAIII in the agr locus of Staphylococcus aureus. J Bacteriol *179*, 3963-3971.

Cheung AL, Nishina K, Manna AC (2008). SarA of Staphylococcus aureus binds to the sarA promoter to regulate gene expression. J Bacteriol *190*, 2239-2243.

Cheung AL, Projan SJ, Gresham H (2002). The Genomic Aspect of Virulence, Sepsis, and Resistance to Killing Mechanisms in Staphylococcus aureus. Curr Infect Dis Rep *4*, 400-410.

Cheung AL, Schmidt K, Bateman B, Manna AC (2001). SarS, a SarA homolog repressible by agr, is an activator of protein A synthesis in Staphylococcus aureus. Infect Immun *69*, 2448-2455.

Chiang YC, Liao WW, Fan CM, Pai WY, Chiou CS, Tsen HY (2008). PCR detection of Staphylococcal enterotoxins (SEs) N, O, P, Q, R, U, and survey of SE types in Staphylococcus aureus isolates from food-poisoning cases in Taiwan. Int J Food Microbiol *121*, 66-73.

Cho JS, Pietras EM, Garcia NC, Ramos RI, Farzam DM, Monroe HR, Magorien JE, Blauvelt A, Kolls JK, Cheung AL, Cheng G, Modlin RL, Miller LS (2010). IL-17 is essential for host defense against cutaneous Staphylococcus aureus infection in mice. J Clin Invest *120*, 1762-1773.

Claudi B, Sprote P, Chirkova A, Personnic N, Zankl J, Schurmann N, Schmidt A, Bumann D (2014). Phenotypic variation of Salmonella in host tissues delays eradication by antimicrobial chemotherapy. Cell *158*, 722-733.

Clements MO, Watson SP, Foster SJ (1999). Characterization of the major superoxide dismutase of Staphylococcus aureus and its role in starvation survival, stress resistance, and pathogenicity. J Bacteriol *181*, 3898-3903.

Colomb MG, Arlaud GJ, Villiers CL (1984). Structure and activation of C1: current concepts. Complement *1*, 69-80.

Condliffe AM, Kitchen E, Chilvers ER (1998). Neutrophil priming: pathophysiological consequences and underlying mechanisms. Clin Sci (Lond) *94*, 461-471.

Connolly J, Boldock E, Prince LR, Renshaw SA, Whyte MK, Foster SJ (2017). Identification of Staphylococcus aureus Factors Required for Pathogenicity and Growth in Human Blood. Infect Immun *85*.

Cooper EL, Garcia-Lara J, Foster SJ (2009). YsxC, an essential protein in Staphylococcus aureus crucial for ribosome assembly/stability. BMC Microbiol *9*, 266.

Cooper NR, Muller-Eberhard HJ (1970). The reaction mechanism of human C5 in immune hemolysis. J Exp Med *132*, 775-793.

Cosgrove K, Coutts G, Jonsson IM, Tarkowski A, Kokai-Kun JF, Mond JJ, Foster SJ (2007). Catalase (KatA) and alkyl hydroperoxide reductase (AhpC) have compensatory roles in peroxide stress resistance and are required for survival, persistence, and nasal colonization in Staphylococcus aureus. J Bacteriol *189*, 1025-1035.

Croze M, Dauwalder O, Dumitrescu O, Badiou C, Gillet Y, Genestier AL, Vandenesch F, Etienne J, Lina G (2009). Serum antibodies against Panton-Valentine leukocidin in a normal population and during Staphylococcus aureus infection. Clin Microbiol Infect *15*, 144-148.

Daley JM, Thomay AA, Connolly MD, Reichner JS, Albina JE (2008). Use of Ly6G-specific monoclonal antibody to deplete neutrophils in mice. J Leukoc Biol *83*, 64-70.

Dancer SJ, Noble WC (1991). Nasal, axillary, and perineal carriage of Staphylococcus aureus among women: identification of strains producing epidermolytic toxin. J Clin Pathol *44*, 681-684.

Dancey JT, Deubelbeiss KA, Harker LA, Finch CA (1976). Neutrophil kinetics in man. J Clin Invest *58*, 705-715.

Daskalaki M, Otero JR, Sanz F, Chaves F (2007). Bacteremia due to clonally derived methicillin-resistant, gentamicin-susceptible isolates and methicillin-susceptible, gentamicin-resistant isolates of Staphylococcus aureus. J Clin Microbiol *45*, 3446-3448.

Dastgheyb SS, Villaruz AE, Le KY, Tan VY, Duong AC, Chatterjee SS, Cheung GY, Joo HS, Hickok NJ, Otto M (2015). Role of Phenol-Soluble Modulins in Formation of Staphylococcus aureus Biofilms in Synovial Fluid. Infect Immun *83*, 2966-2975.

De Y, Chen Q, Schmidt AP, Anderson GM, Wang JM, Wooters J, Oppenheim JJ, Chertov O (2000). LL-37, the neutrophil granule- and epithelial cell-derived cathelicidin, utilizes formyl peptide receptor-like 1 (FPRL1) as a receptor to chemoattract human peripheral blood neutrophils, monocytes, and T cells. J Exp Med *192*, 1069-1074.

Dean SN, Bishop BM, van Hoek ML (2011). Natural and synthetic cathelicidin peptides with anti-microbial and anti-biofilm activity against Staphylococcus aureus. BMC Microbiol *11*, 114.

Deniset JF, Surewaard BG, Lee WY, Kubes P (2017). Splenic Ly6G(high) mature and Ly6G(int) immature neutrophils contribute to eradication of S. pneumoniae. J Exp Med *214*, 1333-1350.

Devriese LA, Van Damme LR, Fameree L (1972). Methicillin (cloxacillin)-resistant Staphylococcus aureus strains isolated from bovine mastitis cases. Zentralbl Veterinarmed B *19*, 598-605.

Diebold BA, Bokoch GM (2001). Molecular basis for Rac2 regulation of phagocyte NADPH oxidase. Nat Immunol *2*, 211-215.

Dinges MM, Orwin PM, Schlievert PM (2000). Exotoxins of Staphylococcus aureus. Clin Microbiol Rev *13*, 16-34, table of contents.

Dinulos JG, Mentele L, Fredericks LP, Dale BA, Darmstadt GL (2003). Keratinocyte expression of human beta defensin 2 following bacterial infection: role in cutaneous host defense. Clin Diagn Lab Immunol *10*, 161-166.

Dossett JH, Kronvall G, Williams RC, Jr., Quie PG (1969). Antiphagocytic effects of staphylococcal protein A. J Immunol *103*, 1405-1410.

Dupre M, Gilquin B, Fenaille F, Feraudet-Tarisse C, Dano J, Ferro M, Simon S, Junot C, Brun V, Becher F (2015). Multiplex quantification of protein toxins in human biofluids and food matrices using immunoextraction and high-resolution targeted mass spectrometry. Anal Chem *87*, 8473-8480.

Dustin ML (2016). Complement Receptors in Myeloid Cell Adhesion and Phagocytosis. Microbiol Spectr *4*.

El-Benna J, Hurtado-Nedelec M, Marzaioli V, Marie JC, Gougerot-Pocidalo MA, Dang PM (2016). Priming of the neutrophil respiratory burst: role in host defense and inflammation. Immunol Rev *273*, 180-193.

el Benna J, Faust LP, Babior BM (1994). The phosphorylation of the respiratory burst oxidase component p47phox during neutrophil activation. Phosphorylation of sites recognized by protein kinase C and by proline-directed kinases. J Biol Chem *269*, 23431-23436.

Facklam R, Elliott JA (1995). Identification, classification, and clinical relevance of catalase-negative, gram-positive cocci, excluding the streptococci and enterococci. Clin Microbiol Rev *8*, 479-495.

Fadok VA, Bratton DL, Henson PM (2001). Phagocyte receptors for apoptotic cells: recognition, uptake, and consequences. J Clin Invest *108*, 957-962.

Fattom A, Fuller S, Propst M, Winston S, Muenz L, He D, Naso R, Horwith G (2004). Safety and immunogenicity of a booster dose of Staphylococcus aureus types 5 and 8 capsular polysaccharide conjugate vaccine (StaphVAX) in hemodialysis patients. Vaccine *23*, 656-663.

Fattom A, Matalon A, Buerkert J, Taylor K, Damaso S, Boutriau D (2015). Efficacy profile of a bivalent Staphylococcus aureus glycoconjugated vaccine in adults on hemodialysis: Phase III randomized study. Hum Vaccin Immunother *11*, 632-641.

Fearon DT, Austen KF (1977). Activation of the alternative complement pathway due to resistance of zymosan-bound amplification convertase to endogenous regulatory mechanisms. Proc Natl Acad Sci U S A *74*, 1683-1687.

Flannagan RS, Heit B, Heinrichs DE (2016). Intracellular replication of Staphylococcus aureus in mature phagolysosomes in macrophages precedes host cell death, and bacterial escape and dissemination. Cell Microbiol *18*, 514-535.

Flannagan RS, Kuiack RC, McGavin MJ, Heinrichs DE (2018). Staphylococcus aureus Uses the GraXRS Regulatory System To Sense and Adapt to the Acidified Phagolysosome in Macrophages. MBio *9*.

Fleming TJ, Fleming ML, Malek TR (1993). Selective expression of Ly-6G on myeloid lineage cells in mouse bone marrow. RB6-8C5 mAb to granulocyte-differentiation antigen (Gr-1) detects members of the Ly-6 family. J Immunol *151*, 2399-2408.

Foote CS, Goyne TE, Lehrer RI (1983). Assessment of chlorination by human neutrophils. Nature *301*, 715-716.

Foster TJ, Hook M (1998). Surface protein adhesins of Staphylococcus aureus. Trends Microbiol *6*, 484-488.

Fraser JD, Proft T (2008). The bacterial superantigen and superantigen-like proteins. Immunol Rev *225*, 226-243.

Frenck RW, Jr., Creech CB, Sheldon EA, Seiden DJ, Kankam MK, Baber J, Zito E, Hubler R, Eiden J, Severs JM, Sebastian S, Nanra J, Jansen KU, Gruber WC, Anderson AS, Girgenti D (2017). Safety, tolerability, and immunogenicity of a 4-antigen Staphylococcus aureus vaccine (SA4Ag): Results from a first-in-human randomised, placebo-controlled phase 1/2 study. Vaccine *35*, 375-384.

Fuchs TA, Abed U, Goosmann C, Hurwitz R, Schulze I, Wahn V, Weinrauch Y, Brinkmann V, Zychlinsky A (2007). Novel cell death program leads to neutrophil extracellular traps. J Cell Biol *176*, 231-241.

Futosi K, Fodor S, Mocsai A (2013). Neutrophil cell surface receptors and their intracellular signal transduction pathways. Int Immunopharmacol *17*, 638-650.

Ganz T, Selsted ME, Szklarek D, Harwig SS, Daher K, Bainton DF, Lehrer RI (1985). Defensins. Natural peptide antibiotics of human neutrophils. J Clin Invest *76*, 1427-1435.

Gao XP, Standiford TJ, Rahman A, Newstead M, Holland SM, Dinauer MC, Liu QH, Malik AB (2002). Role of NADPH oxidase in the mechanism of lung neutrophil sequestration and microvessel injury induced by Gram-negative sepsis: studies in p47phox-/- and gp91phox-/- mice. J Immunol *168*, 3974-3982.

Gautam N, Olofsson AM, Herwald H, Iversen LF, Lundgren-Akerlund E, Hedqvist P, Arfors KE, Flodgaard H, Lindbom L (2001). Heparin-binding protein (HBP/CAP37): a missing link in neutrophil-evoked alteration of vascular permeability. Nat Med *7*, 1123-1127.

Geiger T, Francois P, Liebeke M, Fraunholz M, Goerke C, Krismer B, Schrenzel J, Lalk M, Wolz C (2012). The stringent response of Staphylococcus aureus and its impact on survival after phagocytosis through the induction of intracellular PSMs expression. PLoS Pathog *8*, e1003016.

Girardin SE, Boneca IG, Viala J, Chamaillard M, Labigne A, Thomas G, Philpott DJ, Sansonetti PJ (2003). Nod2 is a general sensor of peptidoglycan through muramyl dipeptide (MDP) detection. J Biol Chem *278*, 8869-8872.

Glodde N, Bald T, van den Boorn-Konijnenberg D, Nakamura K, O'Donnell JS, Szczepanski S, Brandes M, Eickhoff S, Das I, Shridhar N, Hinze D, Rogava M, van der Sluis TC, Ruotsalainen JJ, Gaffal E, Landsberg J, Ludwig KU, Wilhelm C, Riek-Burchardt M, Muller AJ, Gebhardt C, Scolyer RA, Long GV, Janzen V, Teng MWL, Kastenmuller W, Mazzone M, Smyth MJ, Tuting T, Holzel M (2017). Reactive Neutrophil Responses Dependent on the Receptor Tyrosine Kinase c-MET Limit Cancer Immunotherapy. Immunity *47*, 789-802 e789.

Gorina R, Lyck R, Vestweber D, Engelhardt B (2014). beta2 integrin-mediated crawling on endothelial ICAM-1 and ICAM-2 is a prerequisite for transcellular neutrophil diapedesis across the inflamed blood-brain barrier. J Immunol *192*, 324-337.

Graille M, Stura EA, Corper AL, Sutton BJ, Taussig MJ, Charbonnier JB, Silverman GJ (2000). Crystal structure of a Staphylococcus aureus protein A domain complexed with the Fab fragment of a human IgM antibody: structural basis for recognition of B-cell receptors and superantigen activity. Proc Natl Acad Sci U S A *97*, 5399-5404.

Gray EE, Suzuki K, Cyster JG (2011). Cutting edge: Identification of a motile IL-17-producing gammadelta T cell population in the dermis. J Immunol *186*, 6091-6095.

Gresham HD, Lowrance JH, Caver TE, Wilson BS, Cheung AL, Lindberg FP (2000). Survival of Staphylococcus aureus inside neutrophils contributes to infection. J Immunol *164*, 3713-3722.

Griffin GK, Newton G, Tarrio ML, Bu DX, Maganto-Garcia E, Azcutia V, Alcaide P, Grabie N, Luscinskas FW, Croce KJ, Lichtman AH (2012). IL-17 and TNF-alpha sustain neutrophil recruitment during inflammation through synergistic effects on endothelial activation. J Immunol *188*, 6287-6299.

Grundmeier M, Tuchscherr L, Bruck M, Viemann D, Roth J, Willscher E, Becker K, Peters G, Loffler B (2010). Staphylococcal strains vary greatly in their ability to induce an inflammatory response in endothelial cells. J Infect Dis *201*, 871-880.

Guinan ME, Dan BB, Guidotti RJ, Reingold AL, Schmid GP, Bettoli EJ, Lossick JG, Shands KN, Kramer MA, Hargrett NT, Anderson RL, Broome CV (1982). Vaginal colonization with Staphylococcus aureus in healthy women: a review of four studies. Ann Intern Med *96*, 944-947.

Gupta D, Shah HP, Malu K, Berliner N, Gaines P (2014). Differentiation and characterization of myeloid cells. Curr Protoc Immunol *104*, Unit 22F 25.

Guthrie LA, McPhail LC, Henson PM, Johnston RB, Jr. (1984). Priming of neutrophils for enhanced release of oxygen metabolites by bacterial lipopolysaccharide. Evidence for increased activity of the superoxide-producing enzyme. J Exp Med *160*, 1656-1671.

Habuchi S, Tsutsui H, Kochaniak AB, Miyawaki A, van Oijen AM (2008). mKikGR, a monomeric photoswitchable fluorescent protein. PLoS One *3*, e3944.

Harbort CJ, Soeiro-Pereira PV, von Bernuth H, Kaindl AM, Costa-Carvalho BT, Condino-Neto A, Reichenbach J, Roesler J, Zychlinsky A, Amulic B (2015). Neutrophil oxidative burst activates ATM to regulate cytokine production and apoptosis. Blood *126*, 2842-2851.

Harder J, Schroder JM, Glaser R (2013). The skin surface as antimicrobial barrier: present concepts and future outlooks. Exp Dermatol *22*, 1-5.

Hasenberg A, Hasenberg M, Mann L, Neumann F, Borkenstein L, Stecher M, Kraus A, Engel DR, Klingberg A, Seddigh P, Abdullah Z, Klebow S, Engelmann S, Reinhold A, Brandau S, Seeling M, Waisman A, Schraven B, Gothert JR, Nimmerjahn F, Gunzer M (2015). Catchup: a mouse model for imaging-based tracking and modulation of neutrophil granulocytes. Nat Methods *12*, 445-452.

Helaine S, Thompson JA, Watson KG, Liu M, Boyle C, Holden DW (2010). Dynamics of intracellular bacterial replication at the single cell level. Proc Natl Acad Sci U S A *107*, 3746-3751.

Henriques MX, Catalao MJ, Figueiredo J, Gomes JP, Filipe SR (2013). Construction of improved tools for protein localization studies in Streptococcus pneumoniae. PLoS One *8*, e55049.

Herbold W, Maus R, Hahn I, Ding N, Srivastava M, Christman JW, Mack M, Reutershan J, Briles DE, Paton JC, Winter C, Welte T, Maus UA (2010). Importance of CXC chemokine receptor 2 in alveolar neutrophil and exudate macrophage recruitment in response to pneumococcal lung infection. Infect Immun *78*, 2620-2630.

Heyde S, Philipsen L, Formaglio P, Fu Y, Baars I, Hobbel G, Kleinholz CL, Seiss EA, Stettin J, Gintschel P, Dudeck A, Bousso P, Schraven B, Muller AJ (2018). CD11c-expressing Ly6C+CCR2+ monocytes constitute a reservoir for efficient Leishmania proliferation and cell-to-cell transmission. PLoS Pathog *14*, e1007374.

Higgins J, Loughman A, van Kessel KP, van Strijp JA, Foster TJ (2006). Clumping factor A of Staphylococcus aureus inhibits phagocytosis by human polymorphonuclear leucocytes. FEMS Microbiol Lett *258*, 290-296.

Hoffmann K, Sperling K, Olins AL, Olins DE (2007). The granulocyte nucleus and lamin B receptor: avoiding the ovoid. Chromosoma *116*, 227-235.

Horsburgh MJ, Aish JL, White IJ, Shaw L, Lithgow JK, Foster SJ (2002). sigmaB modulates virulence determinant expression and stress resistance: characterization of a functional rsbU strain derived from Staphylococcus aureus 8325-4. J Bacteriol *184*, 5457-5467.

Horsmon JR, Cao CJ, Khan AS, Gostomski MV, Valdes JJ, O'Connell KP (2006). Real-time fluorogenic PCR assays for the detection of entA, the gene encoding staphylococcal enterotoxin A. Biotechnol Lett *28*, 823-829.

Howden BP, Davies JK, Johnson PD, Stinear TP, Grayson ML (2010). Reduced vancomycin susceptibility in Staphylococcus aureus, including vancomycin-intermediate and heterogeneous vancomycin-intermediate strains: resistance mechanisms, laboratory detection, and clinical implications. Clin Microbiol Rev *23*, 99-139.

Hudson MC, Ramp WK, Nicholson NC, Williams AS, Nousiainen MT (1995). Internalization of Staphylococcus aureus by cultured osteoblasts. Microb Pathog *19*, 409-419.

Hurrell BP, Schuster S, Grun E, Coutaz M, Williams RA, Held W, Malissen B, Malissen M, Yousefi S, Simon HU, Muller AJ, Tacchini-Cottier F (2015). Rapid Sequestration of Leishmania mexicana by Neutrophils Contributes to the Development of Chronic Lesion. PLoS Pathog *11*, e1004929.

Iademarco MF, McQuillan JJ, Rosen GD, Dean DC (1992). Characterization of the promoter for vascular cell adhesion molecule-1 (VCAM-1). J Biol Chem *267*, 16323-16329.

Inohara N, Ogura Y, Fontalba A, Gutierrez O, Pons F, Crespo J, Fukase K, Inamura S, Kusumoto S, Hashimoto M, Foster SJ, Moran AP, Fernandez-Luna JL, Nunez G (2003). Host recognition of bacterial muramyl dipeptide mediated through NOD2. Implications for Crohn's disease. J Biol Chem *278*, 5509-5512.

Ito T, Okuma K, Ma XX, Yuzawa H, Hiramatsu K (2003). Insights on antibiotic resistance of Staphylococcus aureus from its whole genome: genomic island SCC. Drug Resist Updat *6*, 41-52.

Itoh S, Hamada E, Kamoshida G, Yokoyama R, Takii T, Onozaki K, Tsuji T (2010). Staphylococcal superantigen-like protein 10 (SSL10) binds to human immunoglobulin G (IgG) and inhibits complement activation via the classical pathway. Mol Immunol *47*, 932-938.

Iwase T, Uehara Y, Shinji H, Tajima A, Seo H, Takada K, Agata T, Mizunoe Y (2010). Staphylococcus epidermidis Esp inhibits Staphylococcus aureus biofilm formation and nasal colonization. Nature *465*, 346-349.

Jarick KJ, Mokhtari Z, Scheller L, Hartweg J, Thusek S, Le DD, Ranecky M, Shaikh H, Qureischi M, Heinze KG, Beilhack A (2018). Photoconversion of Alloreactive T Cells in Murine Peyer's Patches During Acute Graft-Versus-Host Disease: Tracking the Homing Route of Highly Proliferative Cells In Vivo. Front Immunol *9*, 1468.

Jayasinghe L, Bayley H (2005). The leukocidin pore: evidence for an octamer with four LukF subunits and four LukS subunits alternating around a central axis. Protein Sci *14*, 2550-2561.

Ji G, Beavis RC, Novick RP (1995). Cell density control of staphylococcal virulence mediated by an octapeptide pheromone. Proc Natl Acad Sci U S A *92*, 12055-12059.

Jin T, Bokarewa M, Foster T, Mitchell J, Higgins J, Tarkowski A (2004). Staphylococcus aureus resists human defensins by production of staphylokinase, a novel bacterial evasion mechanism. J Immunol *172*, 1169-1176.

Johns JL, Christopher MM (2012). Extramedullary hematopoiesis: a new look at the underlying stem cell niche, theories of development, and occurrence in animals. Vet Pathol *49*, 508-523.

Jongerius I, Kohl J, Pandey MK, Ruyken M, van Kessel KP, van Strijp JA, Rooijakkers SH (2007). Staphylococcal complement evasion by various convertase-blocking molecules. J Exp Med *204*, 2461-2471.

Jorgensen I, Zhang Y, Krantz BA, Miao EA (2016). Pyroptosis triggers pore-induced intracellular traps (PITs) that capture bacteria and lead to their clearance by efferocytosis. J Exp Med *213*, 2113-2128.

Kallee E (1996). Bennhold's analbuminemia: a follow-up study of the first two cases (1953-1992). J Lab Clin Med *127*, 470-480.

Kaneko J, Kamio Y (2004). Bacterial two-component and hetero-heptameric pore-forming cytolytic toxins: structures, pore-forming mechanism, and organization of the genes. Biosci Biotechnol Biochem *68*, 981-1003.

Kang M, Ko YP, Liang X, Ross CL, Liu Q, Murray BE, Hook M (2013). Collagen-binding microbial surface components recognizing adhesive matrix molecule (MSCRAMM) of Gram-positive bacteria inhibit complement activation via the classical pathway. J Biol Chem *288*, 20520-20531.

Karavolos MH, Horsburgh MJ, Ingham E, Foster SJ (2003). Role and regulation of the superoxide dismutases of Staphylococcus aureus. Microbiology *149*, 2749-2758.

Katayama Y, Ito T, Hiramatsu K (2000). A new class of genetic element, staphylococcus cassette chromosome mec, encodes methicillin resistance in Staphylococcus aureus. Antimicrob Agents Chemother *44*, 1549-1555.

Kavanaugh JS, Thoendel M, Horswill AR (2007). A role for type I signal peptidase in Staphylococcus aureus quorum sensing. Mol Microbiol *65*, 780-798.

Kawai T, Akira S (2011). Toll-like receptors and their crosstalk with other innate receptors in infection and immunity. Immunity *34*, 637-650.

Kayagaki N, Stowe IB, Lee BL, O'Rourke K, Anderson K, Warming S, Cuellar T, Haley B, Roose-Girma M, Phung QT, Liu PS, Lill JR, Li H, Wu J, Kummerfeld S, Zhang J, Lee WP, Snipas SJ, Salvesen GS, Morris LX, Fitzgerald L, Zhang Y, Bertram EM, Goodnow CC, Dixit VM (2015). Caspase-11 cleaves gasdermin D for non-canonical inflammasome signalling. Nature *526*, 666-671.

Kegel SM, Dorsey TJ, Rowen M, Taylor WF (1977). Cardiac death in mucocutaneous lymph node syndrome. Am J Cardiol *40*, 282-286.

Kim HK, Missiakas D, Schneewind O (2014). Mouse models for infectious diseases caused by Staphylococcus aureus. J Immunol Methods *410*, 88-99.

Kintarak S, Whawell SA, Speight PM, Packer S, Nair SP (2004). Internalization of Staphylococcus aureus by human keratinocytes. Infect Immun *72*, 5668-5675.

Kjeldsen L, Bjerrum OW, Askaa J, Borregaard N (1992). Subcellular localization and release of human neutrophil gelatinase, confirming the existence of separate gelatinase-containing granules. Biochem J *287 (Pt 2)*, 603-610.

Klebanoff SJ, Kettle AJ, Rosen H, Winterbourn CC, Nauseef WM (2013). Myeloperoxidase: a front-line defender against phagocytosed microorganisms. J Leukoc Biol *93*, 185-198.

Kluytmans J, van Belkum A, Verbrugh H (1997). Nasal carriage of Staphylococcus aureus: epidemiology, underlying mechanisms, and associated risks. Clin Microbiol Rev *10*, 505-520.

Kobayashi SD, Braughton KR, Palazzolo-Ballance AM, Kennedy AD, Sampaio E, Kristosturyan E, Whitney AR, Sturdevant DE, Dorward DW, Holland SM, Kreiswirth BN, Musser JM, DeLeo FR (2010). Rapid neutrophil destruction following phagocytosis of Staphylococcus aureus. J Innate Immun *2*, 560-575.

Kobayashi SD, Malachowa N, DeLeo FR (2015). Pathogenesis of Staphylococcus aureus abscesses. Am J Pathol *185*, 1518-1527.

Kock R, Ballhausen B, Bischoff M, Cuny C, Eckmanns T, Fetsch A, Harmsen D, Goerge T, Oberheitmann B, Schwarz S, Selhorst T, Tenhagen BA, Walther B, Witte W, Ziebuhr W, Becker K (2014). The impact of zoonotic MRSA colonization and infection in Germany. Berl Munch Tierarztl Wochenschr *127*, 384-398.

Kock R, Becker K, Cookson B, van Gemert-Pijnen JE, Harbarth S, Kluytmans J, Mielke M, Peters G, Skov RL, Struelens MJ, Tacconelli E, Navarro Torne A, Witte W, Friedrich AW (2010). Methicillin-resistant Staphylococcus aureus (MRSA): burden of disease and control challenges in Europe. Euro Surveill *15*, 19688.

Koenig RL, Ray JL, Maleki SJ, Smeltzer MS, Hurlburt BK (2004). Staphylococcus aureus AgrA binding to the RNAIII-agr regulatory region. J Bacteriol *186*, 7549-7555.

Kolaczkowska E, Kubes P (2013). Neutrophil recruitment and function in health and inflammation. Nat Rev Immunol *13*, 159-175.

Kreiswirth BN, Lofdahl S, Betley MJ, O'Reilly M, Schlievert PM, Bergdoll MS, Novick RP (1983). The toxic shock syndrome exotoxin structural gene is not detectably transmitted by a prophage. Nature *305*, 709-712.

Krezalek MA, Hyoju S, Zaborin A, Okafor E, Chandrasekar L, Bindokas V, Guyton K, Montgomery CP, Daum RS, Zaborina O, Boyle-Vavra S, Alverdy JC (2018). Can Methicillin-resistant Staphylococcus aureus Silently Travel From the Gut to the Wound and Cause Postoperative Infection? Modeling the "Trojan Horse Hypothesis". Ann Surg *267*, 749-758.

Krismer B, Weidenmaier C, Zipperer A, Peschel A (2017). The commensal lifestyle of Staphylococcus aureus and its interactions with the nasal microbiota. Nat Rev Microbiol *15*, 675-687.

Krut O, Sommer H, Kronke M (2004). Antibiotic-induced persistence of cytotoxic Staphylococcus aureus in non-phagocytic cells. J Antimicrob Chemother *53*, 167-173.

Kuhn ML, Prachi P, Minasov G, Shuvalova L, Ruan J, Dubrovska I, Winsor J, Giraldi M, Biagini M, Liberatori S, Savino S, Bagnoli F, Anderson WF, Grandi G (2014). Structure and protective efficacy of the Staphylococcus aureus autocleaving protease EpiP. FASEB J *28*, 1780-1793.

Kuhns DB, Alvord WG, Heller T, Feld JJ, Pike KM, Marciano BE, Uzel G, DeRavin SS, Priel DA, Soule BP, Zarember KA, Malech HL, Holland SM, Gallin JI (2010). Residual NADPH oxidase and survival in chronic granulomatous disease. N Engl J Med *363*, 2600-2610.

Kuwano Y, Spelten O, Zhang H, Ley K, Zarbock A (2010). Rolling on E- or P-selectin induces the extended but not high-affinity conformation of LFA-1 in neutrophils. Blood *116*, 617-624.

Kwak HJ, Liu P, Bajrami B, Xu Y, Park SY, Nombela-Arrieta C, Mondal S, Sun Y, Zhu H, Chai L, Silberstein LE, Cheng T, Luo HR (2015). Myeloid cell-derived reactive oxygen species externally regulate the proliferation of myeloid progenitors in emergency granulopoiesis. Immunity *42*, 159-171.

Kwan T, Liu J, DuBow M, Gros P, Pelletier J (2005). The complete genomes and proteomes of 27 Staphylococcus aureus bacteriophages. Proc Natl Acad Sci U S A *102***,** 5174-5179.

Laarman AJ, Mijnheer G, Mootz JM, van Rooijen WJ, Ruyken M, Malone CL, Heezius EC, Ward R, Milligan G, van Strijp JA, de Haas CJ, Horswill AR, van Kessel KP, Rooijakkers SH (2012). Staphylococcus aureus Staphopain A inhibits CXCR2-dependent neutrophil activation and chemotaxis. EMBO J *31***,** 3607-3619.

Labandeira-Rey M, Couzon F, Boisset S, Brown EL, Bes M, Benito Y, Barbu EM, Vazquez V, Hook M, Etienne J, Vandenesch F, Bowden MG (2007). Staphylococcus aureus Panton-Valentine leukocidin causes necrotizing pneumonia. Science *315***,** 1130-1133.

Lacey RW (1975). Antibiotic resistance plasmids of Staphylococcus aureus and their clinical importance. Bacteriol Rev *39***,** 1-32.

Laudanna C, Kim JY, Constantin G, Butcher E (2002). Rapid leukocyte integrin activation by chemokines. Immunol Rev *186***,** 37-46.

Lazarus GS, Brown RS, Daniels JR, Fullmer HM (1968). Human granulocyte collagenase. Science *159***,** 1483-1485.

Le KY, Otto M (2015). Quorum-sensing regulation in staphylococci-an overview. Front Microbiol *6***,** 1174.

Ledebur HC, Parks TP (1995). Transcriptional regulation of the intercellular adhesion molecule-1 gene by inflammatory cytokines in human endothelial cells. Essential roles of a variant NF-kappa B site and p65 homodimers. J Biol Chem *270***,** 933-943.

Lekstrom-Himes JA, Gallin JI (2000). Immunodeficiency diseases caused by defects in phagocytes. N Engl J Med *343***,** 1703-1714.

Leliefeld PHC, Pillay J, Vrisekoop N, Heeres M, Tak T, Kox M, Rooijakkers SHM, Kuijpers TW, Pickkers P, Leenen LPH, Koenderman L (2018). Differential antibacterial control by neutrophil subsets. Blood Adv *2***,** 1344-1355.

Li N, Mao D, Lu S, Tong C, Zhang Y, Long M (2013). Distinct binding affinities of Mac-1 and LFA-1 in neutrophil activation. J Immunol *190***,** 4371-4381.

Li N, Yang H, Wang M, Lu S, Zhang Y, Long M (2018). Ligand-specific binding forces of LFA-1 and Mac-1 in neutrophil adhesion and crawling. Mol Biol Cell *29***,** 408-418.

Liang SC, Tan XY, Luxenberg DP, Karim R, Dunussi-Joannopoulos K, Collins M, Fouser LA (2006). Interleukin (IL)-22 and IL-17 are coexpressed by Th17 cells and cooperatively enhance expression of antimicrobial peptides. J Exp Med *203***,** 2271-2279.

Liese J, Rooijakkers SH, van Strijp JA, Novick RP, Dustin ML (2013). Intravital two-photon microscopy of host-pathogen interactions in a mouse model of Staphylococcus aureus skin abscess formation. Cell Microbiol *15***,** 891-909.

Liew AT, Theis T, Jensen SO, Garcia-Lara J, Foster SJ, Firth N, Lewis PJ, Harry EJ (2011). A simple plasmid-based system that allows rapid generation of tightly controlled gene expression in Staphylococcus aureus. Microbiology *157***,** 666-676.

Lin L, Cook DN, Wiesehahn GP, Alfonso R, Behrman B, Cimino GD, Corten L, Damonte PB, Dikeman R, Dupuis K, Fang YM, Hanson CV, Hearst JE, Lin CY, Londe HF, Metchette K, Nerio AT, Pu JT, Reames AA, Rheinschmidt M, Tessman J, Isaacs ST, Wollowitz S, Corash L (1997). Photochemical inactivation of viruses and bacteria in platelet concentrates by use of a novel psoralen and long-wavelength ultraviolet light. Transfusion *37***,** 423-435.

Lina G, Bohach GA, Nair SP, Hiramatsu K, Jouvin-Marche E, Mariuzza R, International Nomenclature Committee for Staphylococcal S (2004). Standard nomenclature for the superantigens expressed by Staphylococcus. J Infect Dis *189***,** 2334-2336.

Lina G, Jarraud S, Ji G, Greenland T, Pedraza A, Etienne J, Novick RP, Vandenesch F (1998). Transmembrane topology and histidine protein kinase activity of AgrC, the agr signal receptor in Staphylococcus aureus. Mol Microbiol *28***,** 655-662.

Liu GY, Essex A, Buchanan JT, Datta V, Hoffman HM, Bastian JF, Fierer J, Nizet V (2005). Staphylococcus aureus golden pigment impairs neutrophil killing and promotes virulence through its antioxidant activity. J Exp Med *202***,** 209-215.

Loffler B, Tuchscherr L, Niemann S, Peters G (2014). Staphylococcus aureus persistence in non-professional phagocytes. Int J Med Microbiol *304***,** 170-176.

Low DE (2013). Toxic shock syndrome: major advances in pathogenesis, but not treatment. Crit Care Clin *29***,** 651-675.

Lowy FD (1998). Staphylococcus aureus infections. N Engl J Med *339***,** 520-532.

Lowy FD (2003). Antimicrobial resistance: the example of Staphylococcus aureus. J Clin Invest *111***,** 1265-1273.

Lowy FD, Fant J, Higgins LL, Ogawa SK, Hatcher VB (1988). Staphylococcus aureus--human endothelial cell interactions. J Ultrastruct Mol Struct Res *98***,** 137-146.

Ma XX, Ito T, Tiensasitorn C, Jamklang M, Chongtrakool P, Boyle-Vavra S, Daum RS, Hiramatsu K (2002). Novel type of staphylococcal cassette chromosome mec identified in community-acquired methicillin-resistant Staphylococcus aureus strains. Antimicrob Agents Chemother *46***,** 1147-1152.

MacLennan IC, Toellner KM, Cunningham AF, Serre K, Sze DM, Zuniga E, Cook MC, Vinuesa CG (2003). Extrafollicular antibody responses. Immunol Rev *194***,** 8-18.

Madisen L, Zwingman TA, Sunkin SM, Oh SW, Zariwala HA, Gu H, Ng LL, Palmiter RD, Hawrylycz MJ, Jones AR, Lein ES, Zeng H (2010). A robust and high-throughput Cre reporting and characterization system for the whole mouse brain. Nat Neurosci *13***,** 133-140.

Malachowa N, Kohler PL, Schlievert PM, Chuang ON, Dunny GM, Kobayashi SD, Miedzobrodzki J, Bohach GA, Seo KS (2011). Characterization of a Staphylococcus aureus surface virulence factor that promotes resistance to oxidative killing and infectious endocarditis. Infect Immun *79***,** 342-352.

Malmvall BE, Follin P (1993). Successful interferon-gamma therapy in a chronic granulomatous disease (CGD) patient suffering from Staphylococcus aureus hepatic abscess and invasive Candida albicans infection. Scand J Infect Dis *25***,** 61-66.

Malone CL, Boles BR, Lauderdale KJ, Thoendel M, Kavanaugh JS, Horswill AR (2009). Fluorescent reporters for Staphylococcus aureus. J Microbiol Methods *77*, 251-260.

Manna AC, Bayer MG, Cheung AL (1998). Transcriptional analysis of different promoters in the sar locus in Staphylococcus aureus. J Bacteriol *180*, 3828-3836.

Manna AC, Cheung AL (2003). sarU, a sarA homolog, is repressed by SarT and regulates virulence genes in Staphylococcus aureus. Infect Immun *71*, 343-353.

Manz MG, Boettcher S (2014). Emergency granulopoiesis. Nat Rev Immunol *14*, 302-314.

Maree CL, Daum RS, Boyle-Vavra S, Matayoshi K, Miller LG (2007). Community-associated methicillin-resistant Staphylococcus aureus isolates causing healthcare-associated infections. Emerg Infect Dis *13*, 236-242.

Marshall JL, Zhang Y, Pallan L, Hsu MC, Khan M, Cunningham AF, MacLennan IC, Toellner KM (2011). Early B blasts acquire a capacity for Ig class switch recombination that is lost as they become plasmablasts. Eur J Immunol *41*, 3506-3512.

Martinez-Melendez A, Morfin-Otero R, Villarreal-Trevino L, Camacho-Ortiz A, Gonzalez-Gonzalez G, Llaca-Diaz J, Rodriguez-Noriega E, Garza-Gonzalez E (2016). Molecular epidemiology of coagulase-negative bloodstream isolates: detection of Staphylococcus epidermidis ST2, ST7 and linezolid-resistant ST23. Braz J Infect Dis *20*, 419-428.

Mascari LM, Ross JM (2003). Quantification of staphylococcal-collagen binding interactions in whole blood by use of a confocal microscopy shear-adhesion assay. J Infect Dis *188*, 98-107.

Massena S, Christoffersson G, Hjertstrom E, Zcharia E, Vlodavsky I, Ausmees N, Rolny C, Li JP, Phillipson M (2010). A chemotactic gradient sequestered on endothelial heparan sulfate induces directional intraluminal crawling of neutrophils. Blood *116*, 1924-1931.

McGavin MJ, Zahradka C, Rice K, Scott JE (1997). Modification of the Staphylococcus aureus fibronectin binding phenotype by V8 protease. Infect Immun *65*, 2621-2628.

McGuinness WA, Kobayashi SD, DeLeo FR (2016). Evasion of Neutrophil Killing by Staphylococcus aureus. Pathogens *5*.

McNamee PT, Smyth JA (2000). Bacterial chondronecrosis with osteomyelitis ('femoral head necrosis') of broiler chickens: a review. Avian Pathol *29*, 477-495.

Medicus RG, Gotze O, Muller-Eberhard HJ (1976). Alternative pathway of complement: recruitment of precursor properdin by the labile C3/C5 convertase and the potentiation of the pathway. J Exp Med *144*, 1076-1093.

Melish ME, Glasgow LA (1970). The staphylococcal scalded-skin syndrome. N Engl J Med *282*, 1114-1119.

Menzies BE, Kourteva I (1998). Internalization of Staphylococcus aureus by endothelial cells induces apoptosis. Infect Immun *66*, 5994-5998.

Menzies PI, Ramanoon SZ (2001). Mastitis of sheep and goats. Vet Clin North Am Food Anim Pract *17*, 333-358, vii.

Messina CG, Reeves EP, Roes J, Segal AW (2002). Catalase negative Staphylococcus aureus retain virulence in mouse model of chronic granulomatous disease. FEBS Lett *518*, 107-110.

Metzler KD, Goosmann C, Lubojemska A, Zychlinsky A, Papayannopoulos V (2014). A myeloperoxidase-containing complex regulates neutrophil elastase release and actin dynamics during NETosis. Cell Rep *8*, 883-896.

Meynet E, Laurin D, Lenormand JL, Camara B, Toussaint B, Le Gouellec A (2018). Killed but metabolically active Pseudomonas aeruginosa-based vaccine induces protective humoral- and cell-mediated immunity against Pseudomonas aeruginosa pulmonary infections. Vaccine *36*, 1893-1900.

Miller LS (2008). Toll-like receptors in skin. Adv Dermatol *24*, 71-87.

Miller LS, Cho JS (2011). Immunity against Staphylococcus aureus cutaneous infections. Nat Rev Immunol *11*, 505-518.

Milner JD, Brenchley JM, Laurence A, Freeman AF, Hill BJ, Elias KM, Kanno Y, Spalding C, Elloumi HZ, Paulson ML, Davis J, Hsu A, Asher AI, O'Shea J, Holland SM, Paul WE, Douek DC (2008). Impaired T(H)17 cell differentiation in subjects with autosomal dominant hyper-IgE syndrome. Nature *452*, 773-776.

Mohamed N, Wang MY, Le Huec JC, Liljenqvist U, Scully IL, Baber J, Begier E, Jansen KU, Gurtman A, Anderson AS (2017). Vaccine development to prevent Staphylococcus aureus surgical-site infections. Br J Surg *104*, e41-e54.

Molne L, Verdrengh M, Tarkowski A (2000). Role of neutrophil leukocytes in cutaneous infection caused by Staphylococcus aureus. Infect Immun *68*, 6162-6167.

Morales EH, Calderon IL, Collao B, Gil F, Porwollik S, McClelland M, Saavedra CP (2012). Hypochlorous acid and hydrogen peroxide-induced negative regulation of Salmonella enterica serovar Typhimurium ompW by the response regulator ArcA. BMC Microbiol *12*, 63.

Moreau HD, Lemaitre F, Terriac E, Azar G, Piel M, Lennon-Dumenil AM, Bousso P (2012). Dynamic in situ cytometry uncovers T cell receptor signaling during immunological synapses and kinapses in vivo. Immunity *37*, 351-363.

Muller-Eberhard HJ (1985). Transmembrane channel-formation by five complement proteins. Biochem Soc Symp *50*, 235-246.

Muller-Eberhard HJ, Polley MJ, Calcott MA (1967). Formation and functional significance of a molecular complex derived from the second and the fourth component of human complement. J Exp Med *125*, 359-380.

Muller AJ, Aeschlimann S, Olekhnovitch R, Dacher M, Spath GF, Bousso P (2013). Photoconvertible pathogen labeling reveals nitric oxide control of Leishmania major infection in vivo via dampening of parasite metabolism. Cell Host Microbe *14*, 460-467.

Murai M, Sakurada J, Seki K, Shinji H, Hirota Y, Masuda S (1999). Apoptosis observed in BALB/3T3 cells having ingested Staphylococcus aureus. Microbiol Immunol *43*, 653-661.

Nagaraj S, Ramlal S, Sripathy MH, Batra HV (2014). Development and evaluation of a novel combinatorial selective enrichment and multiplex PCR technique for molecular detection of major virulence-associated genes of enterotoxigenic Staphylococcus aureus in food samples. J Appl Microbiol *116*, 435-446.

Nakagawa S, Matsumoto M, Katayama Y, Oguma R, Wakabayashi S, Nygaard T, Saijo S, Inohara N, Otto M, Matsue H, Nunez G, Nakamura Y (2017). Staphylococcus aureus Virulent PSMalpha Peptides Induce Keratinocyte Alarmin Release to Orchestrate IL-17-Dependent Skin Inflammation. Cell Host Microbe *22*, 667-677 e665.

Nanra JS, Buitrago SM, Crawford S, Ng J, Fink PS, Hawkins J, Scully IL, McNeil LK, Aste-Amezaga JM, Cooper D, Jansen KU, Anderson AS (2013). Capsular polysaccharides are an important immune evasion mechanism for Staphylococcus aureus. Hum Vaccin Immunother *9*, 480-487.

Neutze JM, White HD (1996). Comparing health expenditure. N Z Med J *109*, 388.

Nguyen GT, Green ER, Mecsas J (2017). Neutrophils to the ROScue: Mechanisms of NADPH Oxidase Activation and Bacterial Resistance. Front Cell Infect Microbiol *7*, 373.

Nienhaus GU, Wiedenmann J (2009). Structure, dynamics and optical properties of fluorescent proteins: perspectives for marker development. Chemphyschem *10*, 1369-1379.

Nimmerjahn F, Bruhns P, Horiuchi K, Ravetch JV (2005). FcgammaRIV: a novel FcR with distinct IgG subclass specificity. Immunity *23*, 41-51.

Nouwen JL, Ott A, Kluytmans-Vandenbergh MF, Boelens HA, Hofman A, van Belkum A, Verbrugh HA (2004). Predicting the Staphylococcus aureus nasal carrier state: derivation and validation of a "culture rule". Clin Infect Dis *39*, 806-811.

Novick RP, Projan SJ, Kornblum J, Ross HF, Ji G, Kreiswirth B, Vandenesch F, Moghazeh S (1995). The agr P2 operon: an autocatalytic sensory transduction system in Staphylococcus aureus. Mol Gen Genet *248*, 446-458.

Nuzzo I, Sanges MR, Folgore A, Carratelli CR (2000). Apoptosis of human keratinocytes after bacterial invasion. FEMS Immunol Med Microbiol *27*, 235-240.

Ohno Y, Gallin JI (1985). Diffusion of extracellular hydrogen peroxide into intracellular compartments of human neutrophils. Studies utilizing the inactivation of myeloperoxidase by hydrogen peroxide and azide. J Biol Chem *260*, 8438-8446.

Olekhnovitch R, Ryffel B, Muller AJ, Bousso P (2014). Collective nitric oxide production provides tissue-wide immunity during Leishmania infection. J Clin Invest *124*, 1711-1722.

Oram JD, Reiter B (1968). Inhibition of bacteria by lactoferrin and other iron-chelating agents. Biochim Biophys Acta *170*, 351-365.

Otter JA, French GL (2011). Community-associated meticillin-resistant Staphylococcus aureus strains as a cause of healthcare-associated infection. J Hosp Infect *79*, 189-193.

Otto M (2009). Staphylococcus epidermidis--the 'accidental' pathogen. Nat Rev Microbiol *7*, 555-567.

Pangburn MK, Muller-Eberhard HJ (1978). Complement C3 convertase: cell surface restriction of beta1H control and generation of restriction on neuraminidase-treated cells. Proc Natl Acad Sci U S A *75***,** 2416-2420.

Pangburn MK, Schreiber RD, Muller-Eberhard HJ (1981). Formation of the initial C3 convertase of the alternative complement pathway. Acquisition of C3b-like activities by spontaneous hydrolysis of the putative thioester in native C3. J Exp Med *154***,** 856-867.

Pasparakis M, Haase I, Nestle FO (2014). Mechanisms regulating skin immunity and inflammation. Nat Rev Immunol *14***,** 289-301.

Patti JM, Allen BL, McGavin MJ, Hook M (1994). MSCRAMM-mediated adherence of microorganisms to host tissues. Annu Rev Microbiol *48***,** 585-617.

Pei D (1999). Leukolysin/MMP25/MT6-MMP: a novel matrix metalloproteinase specifically expressed in the leukocyte lineage. Cell Res *9***,** 291-303.

Peschel A, Jack RW, Otto M, Collins LV, Staubitz P, Nicholson G, Kalbacher H, Nieuwenhuizen WF, Jung G, Tarkowski A, van Kessel KP, van Strijp JA (2001). Staphylococcus aureus resistance to human defensins and evasion of neutrophil killing via the novel virulence factor MprF is based on modification of membrane lipids with l-lysine. J Exp Med *193***,** 1067-1076.

Peschel A, Otto M, Jack RW, Kalbacher H, Jung G, Gotz F (1999). Inactivation of the dlt operon in Staphylococcus aureus confers sensitivity to defensins, protegrins, and other antimicrobial peptides. J Biol Chem *274***,** 8405-8410.

Peters NC, Egen JG, Secundino N, Debrabant A, Kimblin N, Kamhawi S, Lawyer P, Fay MP, Germain RN, Sacks D (2008). In vivo imaging reveals an essential role for neutrophils in leishmaniasis transmitted by sand flies. Science *321***,** 970-974.

Philipsen L, Engels T, Schilling K, Gurbiel S, Fischer KD, Tedford K, Schraven B, Gunzer M, Reichardt P (2013). Multimolecular analysis of stable immunological synapses reveals sustained recruitment and sequential assembly of signaling clusters. Mol Cell Proteomics *12***,** 2551-2567.

Pietrocola G, Nobile G, Rindi S, Speziale P (2017). Staphylococcus aureus Manipulates Innate Immunity through Own and Host-Expressed Proteases. Front Cell Infect Microbiol *7***,** 166.

Podack ER, Tschopp J (1984). Membrane attack by complement. Mol Immunol *21***,** 589-603.

Postma B, Poppelier MJ, van Galen JC, Prossnitz ER, van Strijp JA, de Haas CJ, van Kessel KP (2004). Chemotaxis inhibitory protein of Staphylococcus aureus binds specifically to the C5a and formylated peptide receptor. J Immunol *172***,** 6994-7001.

Proctor RA, Balwit JM, Vesga O (1994). Variant subpopulations of Staphylococcus aureus as cause of persistent and recurrent infections. Infect Agents Dis *3***,** 302-312.

Proctor RA, Kahl B, von Eiff C, Vaudaux PE, Lew DP, Peters G (1998). Staphylococcal small colony variants have novel mechanisms for antibiotic resistance. Clin Infect Dis *27 Suppl 1***,** S68-74.

Proctor RA, von Eiff C, Kahl BC, Becker K, McNamara P, Herrmann M, Peters G (2006). Small colony variants: a pathogenic form of bacteria that facilitates persistent and recurrent infections. Nat Rev Microbiol *4*, 295-305.

Pujol M, Pena C, Pallares R, Ayats J, Ariza J, Gudiol F (1994). Risk factors for nosocomial bacteremia due to methicillin-resistant Staphylococcus aureus. Eur J Clin Microbiol Infect Dis *13*, 96-102.

Rajasree K, Fasim A, Gopal B (2016). Conformational features of the Staphylococcus aureus AgrA-promoter interactions rationalize quorum-sensing triggered gene expression. Biochem Biophys Rep *6*, 124-134.

Rawal N, Rajagopalan R, Salvi VP (2008). Activation of complement component C5: comparison of C5 convertases of the lectin pathway and the classical pathway of complement. J Biol Chem *283*, 7853-7863.

Rawat A, Bhattad S, Singh S (2016). Chronic Granulomatous Disease. Indian J Pediatr *83*, 345-353.

Reddy P, Ramlal S, Sripathy MH, Batra HV (2014). Development and evaluation of IgY ImmunoCapture PCR ELISA for detection of Staphylococcus aureus enterotoxin A devoid of protein A interference. J Immunol Methods *408*, 114-122.

Reddy PN, Srirama K, Dirisala VR (2017). An Update on Clinical Burden, Diagnostic Tools, and Therapeutic Options of Staphylococcus aureus. Infect Dis (Auckl) *10*, 1179916117703999.

Ricklin D, Hajishengallis G, Yang K, Lambris JD (2010). Complement: a key system for immune surveillance and homeostasis. Nat Immunol *11*, 785-797.

Ridley M (1959). Perineal carriage of Staph. aureus. Br Med J *1*, 270-273.

Rimland D, Roberson B (1986). Gastrointestinal carriage of methicillin-resistant Staphylococcus aureus. J Clin Microbiol *24*, 137-138.

Roben PW, Salem AN, Silverman GJ (1995). VH3 family antibodies bind domain D of staphylococcal protein A. J Immunol *154*, 6437-6445.

Rollin G, Tan X, Tros F, Dupuis M, Nassif X, Charbit A, Coureuil M (2017). Intracellular Survival of Staphylococcus aureus in Endothelial Cells: A Matter of Growth or Persistence. Front Microbiol *8*, 1354.

Rooijakkers SH, Ruyken M, Roos A, Daha MR, Presanis JS, Sim RB, van Wamel WJ, van Kessel KP, van Strijp JA (2005a). Immune evasion by a staphylococcal complement inhibitor that acts on C3 convertases. Nat Immunol *6*, 920-927.

Rooijakkers SH, van Wamel WJ, Ruyken M, van Kessel KP, van Strijp JA (2005b). Anti-opsonic properties of staphylokinase. Microbes Infect *7*, 476-484.

Rooijakkers SH, Wu J, Ruyken M, van Domselaar R, Planken KL, Tzekou A, Ricklin D, Lambris JD, Janssen BJ, van Strijp JA, Gros P (2009). Structural and functional implications of the alternative complement pathway C3 convertase stabilized by a staphylococcal inhibitor. Nat Immunol *10*, 721-727.

Roughley PJ, Barrett AJ (1977). The degradation of cartilage proteoglycans by tissue proteinases. Proteoglycan structure and its susceptibility to proteolysis. Biochem J *167***,** 629-637.

Saiman L, O'Keefe M, Graham PL, 3rd, Wu F, Said-Salim B, Kreiswirth B, LaSala A, Schlievert PM, Della-Latta P (2003). Hospital transmission of community-acquired methicillin-resistant Staphylococcus aureus among postpartum women. Clin Infect Dis *37***,** 1313-1319.

Sandquist I, Kolls J (2018). Update on regulation and effector functions of Th17 cells. F1000Res *7***,** 205.

Sapsford KE, Taitt CR, Loo N, Ligler FS (2005). Biosensor detection of botulinum toxoid A and staphylococcal enterotoxin B in food. Appl Environ Microbiol *71***,** 5590-5592.

Saunders A, Panaro L, McGeer A, Rosenthal A, White D, Willey BM, Gravel D, Bontovics E, Yaffe B, Katz K (2007). A nosocomial outbreak of community-associated methicillin-resistant Staphylococcus aureus among healthy newborns and postpartum mothers. Can J Infect Dis Med Microbiol *18***,** 128-132.

Schindler D, Gutierrez MG, Beineke A, Rauter Y, Rohde M, Foster S, Goldmann O, Medina E (2012). Dendritic cells are central coordinators of the host immune response to Staphylococcus aureus bloodstream infection. Am J Pathol *181***,** 1327-1337.

Schlag M, Biswas R, Krismer B, Kohler T, Zoll S, Yu W, Schwarz H, Peschel A, Gotz F (2010). Role of staphylococcal wall teichoic acid in targeting the major autolysin Atl. Mol Microbiol *75***,** 864-873.

Schnaith A, Kashkar H, Leggio SA, Addicks K, Kronke M, Krut O (2007). Staphylococcus aureus subvert autophagy for induction of caspase-independent host cell death. J Biol Chem *282***,** 2695-2706.

Schreiber RD, Morrison DC, Podack ER, Muller-Eberhard HJ (1979). Bactericidal activity of the alternative complement pathway generated from 11 isolated plasma proteins. J Exp Med *149***,** 870-882.

Schumaker VN, Zavodszky P, Poon PH (1987). Activation of the first component of complement. Annu Rev Immunol *5***,** 21-42.

Selsted ME, Martinez RJ (1978). Lysozyme: primary bactericidin in human plasma serum active against Bacillus subtilis. Infect Immun *20***,** 782-791.

Serbina NV, Salazar-Mather TP, Biron CA, Kuziel WA, Pamer EG (2003). TNF/iNOS-producing dendritic cells mediate innate immune defense against bacterial infection. Immunity *19***,** 59-70.

Shi J, Zhao Y, Wang K, Shi X, Wang Y, Huang H, Zhuang Y, Cai T, Wang F, Shao F (2015). Cleavage of GSDMD by inflammatory caspases determines pyroptotic cell death. Nature *526***,** 660-665.

Shlomchik MJ, Weisel F (2012). Germinal center selection and the development of memory B and plasma cells. Immunol Rev *247***,** 52-63.

Shopsin B, Drlica-Wagner A, Mathema B, Adhikari RP, Kreiswirth BN, Novick RP (2008). Prevalence of agr dysfunction among colonizing Staphylococcus aureus strains. J Infect Dis *198***,** 1171-1174.

Smagur J, Guzik K, Bzowska M, Kuzak M, Zarebski M, Kantyka T, Walski M, Gajkowska B, Potempa J (2009). Staphylococcal cysteine protease staphopain B (SspB) induces rapid engulfment of human neutrophils and monocytes by macrophages. Biol Chem *390***,** 361-371.

Smith EJ, Visai L, Kerrigan SW, Speziale P, Foster TJ (2011). The Sbi protein is a multifunctional immune evasion factor of Staphylococcus aureus. Infect Immun *79***,** 3801-3809.

Sollberger G, Choidas A, Burn GL, Habenberger P, Di Lucrezia R, Kordes S, Menninger S, Eickhoff J, Nussbaumer P, Klebl B, Kruger R, Herzig A, Zychlinsky A (2018a). Gasdermin D plays a vital role in the generation of neutrophil extracellular traps. Sci Immunol *3*.

Sollberger G, Tilley DO, Zychlinsky A (2018b). Neutrophil Extracellular Traps: The Biology of Chromatin Externalization. Dev Cell *44***,** 542-553.

Solomon S, Kassahn D, Illges H (2005). The role of the complement and the Fc gamma R system in the pathogenesis of arthritis. Arthritis Res Ther *7***,** 129-135.

Spaan AN, Surewaard BG, Nijland R, van Strijp JA (2013). Neutrophils versus Staphylococcus aureus: a biological tug of war. Annu Rev Microbiol *67***,** 629-650.

Speller DC, Johnson AP, James D, Marples RR, Charlett A, George RC (1997). Resistance to methicillin and other antibiotics in isolates of Staphylococcus aureus from blood and cerebrospinal fluid, England and Wales, 1989-95. Lancet *350***,** 323-325.

Stapels DA, Geisbrecht BV, Rooijakkers SH (2015). Neutrophil serine proteases in antibacterial defense. Curr Opin Microbiol *23***,** 42-48.

Stapels DA, Ramyar KX, Bischoff M, von Kockritz-Blickwede M, Milder FJ, Ruyken M, Eisenbeis J, McWhorter WJ, Herrmann M, van Kessel KP, Geisbrecht BV, Rooijakkers SH (2014). Staphylococcus aureus secretes a unique class of neutrophil serine protease inhibitors. Proc Natl Acad Sci U S A *111***,** 13187-13192.

Subach FV, Subach OM, Gundorov IS, Morozova KS, Piatkevich KD, Cuervo AM, Verkhusha VV (2009). Monomeric fluorescent timers that change color from blue to red report on cellular trafficking. Nat Chem Biol *5***,** 118-126.

Summers C, Rankin SM, Condliffe AM, Singh N, Peters AM, Chilvers ER (2010). Neutrophil kinetics in health and disease. Trends Immunol *31***,** 318-324.

Surewaard BG, Deniset JF, Zemp FJ, Amrein M, Otto M, Conly J, Omri A, Yates RM, Kubes P (2016). Identification and treatment of the Staphylococcus aureus reservoir in vivo. J Exp Med *213***,** 1141-1151.

Tak T, Tesselaar K, Pillay J, Borghans JA, Koenderman L (2013). What's your age again? Determination of human neutrophil half-lives revisited. J Leukoc Biol *94***,** 595-601.

Takata Y, Kinoshita T, Kozono H, Takeda J, Tanaka E, Hong K, Inoue K (1987). Covalent association of C3b with C4b within C5 convertase of the classical complement pathway. J Exp Med *165***,** 1494-1507.

Talley AK, Dewhurst S, Perry SW, Dollard SC, Gummuluru S, Fine SM, New D, Epstein LG, Gendelman HE, Gelbard HA (1995). Tumor necrosis factor alpha-induced apoptosis in human neuronal cells: protection by the antioxidant N-acetylcysteine and the genes bcl-2 and crmA. Mol Cell Biol *15***,** 2359-2366.

Tegmark K, Karlsson A, Arvidson S (2000). Identification and characterization of SarH1, a new global regulator of virulence gene expression in Staphylococcus aureus. Mol Microbiol *37***,** 398-409.

Tennenberg SD, Fey DE, Lieser MJ (1993). Oxidative priming of neutrophils by interferon-gamma. J Leukoc Biol *53***,** 301-308.

Thiel S, Vorup-Jensen T, Stover CM, Schwaeble W, Laursen SB, Poulsen K, Willis AC, Eggleton P, Hansen S, Holmskov U, Reid KB, Jensenius JC (1997). A second serine protease associated with mannan-binding lectin that activates complement. Nature *386***,** 506-510.

Tong SY, Davis JS, Eichenberger E, Holland TL, Fowler VG, Jr. (2015). Staphylococcus aureus infections: epidemiology, pathophysiology, clinical manifestations, and management. Clin Microbiol Rev *28***,** 603-661.

Tsutsui H, Karasawa S, Shimizu H, Nukina N, Miyawaki A (2005). Semi-rational engineering of a coral fluorescent protein into an efficient highlighter. EMBO Rep *6***,** 233-238.

Tuchscherr L, Heitmann V, Hussain M, Viemann D, Roth J, von Eiff C, Peters G, Becker K, Loffler B (2010). Staphylococcus aureus small-colony variants are adapted phenotypes for intracellular persistence. J Infect Dis *202***,** 1031-1040.

Tuchscherr L, Medina E, Hussain M, Volker W, Heitmann V, Niemann S, Holzinger D, Roth J, Proctor RA, Becker K, Peters G, Loffler B (2011). Staphylococcus aureus phenotype switching: an effective bacterial strategy to escape host immune response and establish a chronic infection. EMBO Mol Med *3***,** 129-141.

Tuffs SW, Haeryfar SMM, McCormick JK (2018). Manipulation of Innate and Adaptive Immunity by Staphylococcal Superantigens. Pathogens *7*.

Turner J, Cho Y, Dinh NN, Waring AJ, Lehrer RI (1998). Activities of LL-37, a cathelin-associated antimicrobial peptide of human neutrophils. Antimicrob Agents Chemother *42***,** 2206-2214.

Udo EE, Pearman JW, Grubb WB (1993). Genetic analysis of community isolates of methicillin-resistant Staphylococcus aureus in Western Australia. J Hosp Infect *25***,** 97-108.

Vancraeynest D, Haesebrouck F, Deplano A, Denis O, Godard C, Wildemauwe C, Hermans K (2006). International dissemination of a high virulence rabbit Staphylococcus aureus clone. J Vet Med B Infect Dis Vet Public Health *53***,** 418-422.

VandenBergh MF, Yzerman EP, van Belkum A, Boelens HA, Sijmons M, Verbrugh HA (1999). Follow-up of Staphylococcus aureus nasal carriage after 8 years: redefining the persistent carrier state. J Clin Microbiol *37***,** 3133-3140.

von Eiff C, Becker K, Metze D, Lubritz G, Hockmann J, Schwarz T, Peters G (2001). Intracellular persistence of Staphylococcus aureus small-colony variants within keratinocytes: a cause for antibiotic treatment failure in a patient with darier's disease. Clin Infect Dis *32***,** 1643-1647.

Wallis R, Mitchell DA, Schmid R, Schwaeble WJ, Keeble AH (2010). Paths reunited: Initiation of the classical and lectin pathways of complement activation. Immunobiology *215***,** 1-11.

Wang R, Braughton KR, Kretschmer D, Bach TH, Queck SY, Li M, Kennedy AD, Dorward DW, Klebanoff SJ, Peschel A, DeLeo FR, Otto M (2007). Identification of novel cytolytic peptides as key virulence determinants for community-associated MRSA. Nat Med *13***,** 1510-1514.

Wang S, Voisin MB, Larbi KY, Dangerfield J, Scheiermann C, Tran M, Maxwell PH, Sorokin L, Nourshargh S (2006). Venular basement membranes contain specific matrix protein low expression regions that act as exit points for emigrating neutrophils. J Exp Med *203***,** 1519-1532.

Ward PA, Till GO, Kunkel R, Beauchamp C (1983). Evidence for role of hydroxyl radical in complement and neutrophil-dependent tissue injury. J Clin Invest *72***,** 789-801.

Weisbart RH, Golde DW, Gasson JC (1986). Biosynthetic human GM-CSF modulates the number and affinity of neutrophil f-Met-Leu-Phe receptors. J Immunol *137***,** 3584-3587.

Wertheim HF, Melles DC, Vos MC, van Leeuwen W, van Belkum A, Verbrugh HA, Nouwen JL (2005a). The role of nasal carriage in Staphylococcus aureus infections. Lancet Infect Dis *5***,** 751-762.

Wertheim HF, Verveer J, Boelens HA, van Belkum A, Verbrugh HA, Vos MC (2005b). Effect of mupirocin treatment on nasal, pharyngeal, and perineal carriage of Staphylococcus aureus in healthy adults. Antimicrob Agents Chemother *49***,** 1465-1467.

Wiese M, Gerlach RG, Popp I, Matuszak J, Mahapatro M, Castiglione K, Chakravortty D, Willam C, Hensel M, Bogdan C, Jantsch J (2012). Hypoxia-mediated impairment of the mitochondrial respiratory chain inhibits the bactericidal activity of macrophages. Infect Immun *80***,** 1455-1466.

Williams RE (1963). Healthy carriage of Staphylococcus aureus: its prevalence and importance. Bacteriol Rev *27***,** 56-71.

Wilson DN (2014). Ribosome-targeting antibiotics and mechanisms of bacterial resistance. Nat Rev Microbiol *12***,** 35-48.

Wimley WC, Selsted ME, White SH (1994). Interactions between human defensins and lipid bilayers: evidence for formation of multimeric pores. Protein Sci *3***,** 1362-1373.

Woehl JL, Stapels DAC, Garcia BL, Ramyar KX, Keightley A, Ruyken M, Syriga M, Sfyroera G, Weber AB, Zolkiewski M, Ricklin D, Lambris JD, Rooijakkers SHM, Geisbrecht BV (2014). The extracellular adherence protein from Staphylococcus aureus inhibits the classical and lectin pathways of complement by blocking formation of the C3 proconvertase. J Immunol *193***,** 6161-6171.

Wohn C, Ober-Blobaum JL, Haak S, Pantelyushin S, Cheong C, Zahner SP, Onderwater S, Kant M, Weighardt H, Holzmann B, Reizis B, Becher B, Prens EP, Clausen BE (2013). Langerin(neg) conventional dendritic cells produce IL-23 to drive psoriatic plaque formation in mice. Proc Natl Acad Sci U S A *110***,** 10723-10728.

Yago T, Shao B, Miner JJ, Yao L, Klopocki AG, Maeda K, Coggeshall KM, McEver RP (2010). E-selectin engages PSGL-1 and CD44 through a common signaling pathway to induce integrin alphaLbeta2-mediated slow leukocyte rolling. Blood *116***,** 485-494.

Yao L, Pan J, Setiadi H, Patel KD, McEver RP (1996). Interleukin 4 or oncostatin M induces a prolonged increase in P-selectin mRNA and protein in human endothelial cells. J Exp Med *184***,** 81-92.

Yarwood JM, Bartels DJ, Volper EM, Greenberg EP (2004). Quorum sensing in Staphylococcus aureus biofilms. J Bacteriol *186***,** 1838-1850.

Yipp BG, Petri B, Salina D, Jenne CN, Scott BN, Zbytnuik LD, Pittman K, Asaduzzaman M, Wu K, Meijndert HC, Malawista SE, de Boisfleury Chevance A, Zhang K, Conly J, Kubes P (2012). Infection-induced NETosis is a dynamic process involving neutrophil multitasking in vivo. Nat Med *18***,** 1386-1393.

Zhang J, Dyer KD, Rosenberg HF (2003). Human RNase 7: a new cationic ribonuclease of the RNase A superfamily. Nucleic Acids Res *31***,** 602-607.

Zhang X, Marichannegowda MH, Rakesh KP, Qin HL (2018). Master mechanisms of Staphylococcus aureus: consider its excellent protective mechanisms hindering vaccine development! Microbiol Res *212-213***,** 59-66.

Zhao Y, Zhu A, Tang J, Tang C, Chen J (2017). Identification and measurement of staphylococcal enterotoxin M from Staphylococcus aureus isolate associated with staphylococcal food poisoning. Lett Appl Microbiol *65***,** 27-34.

6 APPENDIX

6.1 Sequences of mKikume constructs

6.1.1 pLacKikume

CTGGTATTTGGACTCCTGTAAAGAATGACTTCAAAGAGTTTTATGATTTATACCTTTCTGATGTAG
AGAAATATAATGGTTCGGGGAAATTGTTTCCCAAAACACCTATACCTGAAAATGCTTTTTCTCTTT
CTATTATTCCATGGACTTCATTTACTGGGTTTAACTTAAATATCAATAATAATAGTAATTACCTTC
TACCCATTATTACAGCAGGAAAATTCATTAATAAAGGTAATTCAATATATTTACCGCTATCTTTAC
AGGTACATCATTCTGTTTGTGATGGTTATCATGCAGGATTGTTTATGAACTCTATTCAGGAATTGT
CAGATAGGCCTAATGACTGGCTTTTATAATATGAGATAATGCCGACTGTCGACCTGCAGGCATGCA
AGCTAATTCGGTGGAAACGAGGTCATCATTTCCTTCCGAAAAAACGGTTGCATTTAAATCTTACAT
ATGTAATACTTTCAAAGACTACATTTGTAAGATTTGATGTTTGAGTCGGCTGAAAGATCGTACGTA
CCAATTATTGTTTCGTGATTGTTCAAGCCATAACACTGTAGGGATAGTGGAAAGAGTGCTTCATCT
GGTTACGATCAATCAAATATTCAAACGGAGGGAGACGATTTTGATGAAACCAGTAACGTTATACGA
TGTCGCAGAGTATGCCGGTGTCTCTTATCAGACCGTTTCCCGCGTGGTGAACCAGGCCAGCCACGT
TTCTGCGAAAACGCGGGAAAAAGTGGAAGCGGCGATGGCGGAGCTGAATTACATTCCCAACCGCGT
GGCACAACAACTGGCGGGCAAACAGTCGTTGCTGATTGGCGTTGCCACCTCCAGTCTGGCCCTGCA
CGCGCCGTCGCAAATTGTCGCGGCGATTAAATCTCGCGCCGATCAACTGGGTGCCAGCGTGGTGGT
GTCGATGGTAGAACGAAGCGGCGTCGAAGCCTGTAAAGCGGCGGTGCACAATCTTCTCGCGCAACG
CGTCAGTGGGCTGATCATTAACTATCCGCTGGATGACCAGGATGCCATTGCTGTGGAAGCTGCCTG
CACTAATGTTCCGGCGTTATTTCTTGATGTCTCTGACCAGACACCCATCAACAGTATTATTTTCTC
CCATGAAGACGGTACGCGACTGGGCGTGGAGCATCTGGTCGCATTGGGTCACCAGCAAATCGCGCT
GTTAGCGGGCCCATTAAGTATGGTTTCAGTGATAACATCAGAGATGAAAATCGAATTACGTATGGA
AGGATCTGTAAATGGCCATAAGTTTGTCATTACAGGTAAAGGTTCAGGTAGACCTTATGAAGGTAC
ACAAACAGTTGATTTAACGGTTATAGAAGGAGGTCCATTACCATTTGCATTTGACATTCTAACAAC
AGCTTTTCATTATGGCAATAGAGTATTCGTTGAATATCCAGAAGAGATTGTAGATTACTTCAAACA
GTCTTTTCCTGAAGGTTATTCATGGGAAAGAAGTATGAGCTATGAAGATGGTGGTATTTGTTTAGC
AACTAATAACATCACTATGAAGAAAGATGGCTCAAATACATTCGTGAATGAAATTCGATTTGATGG
TACAAATTTTCCAGCAAATGGTCCTGTTATGCAACGTAAAACGGTAAAATGGGAACCAAGTACTGA
GAAAATGTATGTACGTGATGGAGTTTTGAAAGGTGATGTTGAAATGGCTCTTTTGTTAGAAGGTGG
AGGCCATTATCGCTGTGATTTTCGTACTACGTATAAAGCGAAGAAAGTCGTACAATTACCGGATTA
CCACTATGTGGATCATCAAATGGAAATTACTAGTCATGACAAAGACTATAACAAAGTTAAAGCGTA
TGAACATGCTAAAGCATACTCTGGTACATATCGAGGAGCAAAATACGAATTTGAAGCATAAGAATT
CCCGACAGTAAGACGGGTAAGCCTGTTGATGATACCGCTGCCTTACTGGGTGCATTAGCCAGTCTG
AATGACCTGTCACGGGATAATCCGAAGTGGTCAGACTGGAAAATC

*pcn*Promoter + RBS

truncated *LacI*

mKikumeGR – Staphylococcus aureus optimized

SalI/ApaI/EcoRI enzyme restriction site

6.1.2 pKikume

CTGGTATTTGGACTCCTGTAAAGAATGACTTCAAAGAGTTTTATGATTTATACCTTTCTGATGTAG
AGAAATATAATGGTTCGGGGAAATTGTTTCCCAAAACACCTATACCTGAAAATGCTTTTTCTCTTT
CTATTATTCCATGGACTTCATTTACTGGGTTTAACTTAAATATCAATAATAATAGTAATTACCTTC
TACCCATTATTACAGCAGGAAAATTCATTAATAAAGGTAATTCAATATATTTACCGCTATCTTTAC
AGGTACATCATTCTGTTTGTGATGGTTATCATGCAGGATTGTTTATGAACTCTATTCAGGAATTGT
CAGATAGGCCTAATGACTGGCTTTTATAATATGAGATAATGCCGACTGTCGACCATATGTGATATT
TTTGACTAAACCAAATGCTAACCCAGAAATACAATCACTGTGTCTAATGAATAATTTGTTTTATAA
ACACTTTTTTGTTTACTTCTCATTTTTAATTAGTTATAATTAACTAAATAATAGAGCATTAAATAT
ATTTAATAAAACTTATTTAATGCAAAATTATGACTAACATATCTATAATAAATAAAGATTAGATAT
CAATATATTATCGGGCAAATGTATCGAGCAAGGTACCTCAAATTAGGAGGATGATTATTTATGCCG
ACATTAGAAATAGCACAGGGCCCATTAAGTATGGTTTCAGTGATAACATCAGAGATGAAAATCGAA
TTACGTATGGAAGGATCTGTAAATGGCCATAAGTTTGTCATTACAGGTAAAGGTTCAGGTAGACCT
TATGAAGGTACACAAACAGTTGATTTAACGGTTATAGAAGGAGGTCCATTACCATTTGCATTTGAC
ATTCTAACAACAGCTTTTCATTATGGCAATAGAGTATTCGTTGAATATCCAGAAGAGATTGTAGAT
TACTTCAAACAGTCTTTTCCTGAAGGTTATTCATGGGAAAGAAGTATGAGCTATGAAGATGGTGGT
ATTTGTTTAGCAACTAATAACATCACTATGAAGAAAGATGGCTCAAATACATTCGTGAATGAAATT
CGATTTGATGGTACAAATTTTCCAGCAAATGGTCCTGTTATGCAACGTAAAACGGTAAAATGGGAA
CCAAGTACTGAGAAAATGTATGTACGTGATGGAGTTTTGAAAGGTGATGTTGAAATGGCTCTTTTG
TTAGAAGGTGGAGGCCATTATCGCTGTGATTTTCGTACTACGTATAAAGCGAAGAAAGTCGTACAA
TTACCGGATTACCACTATGTGGATCATCAAATGGAAATTACTAGTCATGACAAAGACTATAACAAA
GTTAAAGCGTATGAACATGCTAAAGCATACTCTGGTACATATCGAGGAGCAAAATACGAATTTGAA
GCATAAGAATTCCCGACAGTAAGACGGGTAAGCCTGTTGATGATACCGCTGCCTTACTGGGTGCAT
TAGCCAGTCTGAATGACCTGTCACGGGATAATCCGAAGTGGTCAGACTGGAAAATC

*SarA*Promoter

*Sod*RBS

iTag

mKikumeGR – Staphylococcus aureus optimized

SalI/ApaI/EcoRI enzyme restriction site

6.1.3 pTufAKikume

CTGGTATTTGGACTCCTGTAAAGAATGACTTCAAAGAGTTTTATGATTTATACCTTTCTGATGTAG
AGAAATATAATGGTTCGGGGAAATTGTTTCCCAAAACACCTATACCTGAAAATGCTTTTTCTCTTT
CTATTATTCCATGGACTTCATTTACTGGGTTTAACTTAAATATCAATAATAATAGTAATTACCTTC
TACCCATTATTACAGCAGGAAAATTCATTAATAAAGGTAATTCAATATATTTACCGCTATCTTTAC
AGGTACATCATTCTGTTTGTGATGGTTATCATGCAGGATTGTTTATGAACTCTATTCAGGAATTGT
CAGATAGGCCTAATGACTGGCTTTTATAATATGAGATAATGCCGACTGTCGACCATATGTTCGGTT
ATGCAACATCATTACGTTCAAACACTCAAGGTCGCGGTACTTACACTATGTACTTCGATCACTATG
CTGAAGTTCCAAAATCAATCGCTGAAGATATTATCAAGAAAAATAAAGGTGAATAATATAACTTGT
TTTGACTAGCTAGCCTAGGTTAAAATACAAGGTGAGCTTAAATGTAAGCTATCATCTTTATAGTTT
GATTTTTGGGGTGAATGCATTATAAAAGAATTGTAAAATTCTTTTTGCATCGCTATAAATAATTTC
TCATGATGGTGAGAAACTATCATGAGAGAGTTCGAGGAGGTTTAATTAATGCCGACATTAGAAATA
GCACAGGGCCCATTAAGTATGGTTTCAGTGATAACATCAGAGATGAAAATCGAATTACGTATGGAA
GGATCTGTAAATGGCCATAAGTTTGTCATTACAGGTAAAGGTTCAGGTAGACCTTATGAAGGTACA
CAAACAGTTGATTTAACGGTTATAGAAGGAGGTCCATTACCATTTGCATTTGACATTCTAACAACA
GCTTTTCATTATGGCAATAGAGTATTCGTTGAATATCCAGAAGAGATTGTAGATTACTTCAAACAG
TCTTTTCCTGAAGGTTATTCATGGGAAAGAAGTATGAGCTATGAAGATGGTGGTATTTGTTTAGCA
ACTAATAACATCACTATGAAGAAAGATGGCTCAAATACATTCGTGAATGAAATTCGATTTGATGGT
ACAAATTTTCCAGCAAATGGTCCTGTTATGCAACGTAAAACGGTAAAATGGGAACCAAGTACTGAG
AAAATGTATGTACGTGATGGAGTTTTGAAAGGTGATGTTGAAATGGCTCTTTTGTTAGAAGGTGGA
GGCCATTATCGCTGTGATTTTCGTACTACGTATAAAGCGAAGAAAGTCGTACAATTACCGGATTAC
CACTATGTGGATCATCAAATGGAAATTACTAGTCATGACAAAGACTATAACAAAGTTAAAGCGTAT
GAACATGCTAAAGCATACTCTGGTACATATCGAGGAGCAAAATACGAATTTGAAGCATAAGAATTC
CCGACAGTAAGACGGGTAAGCCTGTTGATGATACCGCTGCCTTACTGGGTGCATTAGCCAGTCTGA
ATGACCTGTCACGGGATAATCCGAAGTGGTCAGACTGGAAAATC

*Tuf*APromoter + RBS

iTag

mKikumeGR – Staphylococcus aureus optimized

SalI/ApaI/EcoRI enzyme restriction site

6.2 Macros for image analysis using Fiji software

6.2.1 Macro for automated proliferation measurement

```
run("Bio-Formats Macro Extensions");
folder = getNumber("Number of folders to analyze :", 0);
dir = newArray(folder);
// Selects the folders containing the lif files to be analyzed
for (i = 0; i<folder; i++) {
	dir[i] = getDirectory("Choose a Directory");
	print(dir[i]);
}
waitForUser("Check whether adequate folders have been selected then click OK or kill thread");

// Recovers the paths of the .lif files to be analyzed
for (j = 0; j<folder; j++) {
	list = getFileList(dir[j]);
	for (k=0; k<list.length; k++) {
		if (endsWith(list[k], "lif") == 1) {
			lifpath = dir[j]+list[k];
			print(lifpath);
			Ext.setId(lifpath);
			Ext.getSeriesCount(seriesCount);
			//print(seriesCount);
			for (l=0; l<seriesCount; l++) {
				h=l+1;
				run("Bio-Formats Importer", "open=["+lifpath+"] autoscale color_mode=Default open_files view=Hyperstack stack_order=XYCZT series_"+h);
				title = getTitle();
				num = 8 + lastIndexOf(title, "Position");
				position = substring(title, num);

roiManager("reset");
run("Clear Results");
rename("Bild");
```

```
run("Split Channels");
selectWindow("C3-Bild");
close();
imageCalculator("Average create stack", "C1-Bild","C4-Bild");

// Measurement of the 1st Z plane
        selectWindow("Result of C1-Bild");
        run("Duplicate...", "duplicate range=1-1");
        bug=isOpen("Result of C1-Bild-1");
        print("series "+h+" creation 1st bug is "+bug);
        selectWindow("Result of C1-Bild-1");
        run("Smooth");
        run("Subtract Background...", "rolling=5 sliding");
        setThreshold(40, 255);
        //setThreshold(40, 255);
        setOption("BlackBackground", false);
        run("Convert to Mask");
        run("Analyze Particles...", "size=0.1-5 exclude add");

count=roiManager("count");
if (count>0) {
        //measures area and C1 mean values (mKikume short green)
        selectWindow("C1-Bild");
        run("Duplicate...", "duplicate range=1-1");
        selectWindow("C1-Bild-1");
        run("Set Measurements...", "area mean redirect=None decimal=3");
        count=roiManager("count");
        for (i=0; i<count; i++) {
                roiManager("Select", i);
                run("Measure");
        }
        selectWindow("C1-Bild-1");
        close();

        //measures C2 mean values (mKikume long green)
        selectWindow("C2-Bild");
        run("Duplicate...", "duplicate range=1-1");
```

```
	selectWindow("C2-Bild-1");
	count=roiManager("count");
	for (i=0; i<count; i++) {
		roiManager("Select", i);
		run("Measure");
	}
	for (m=count; m<nResults; m++) {
		newparameter=getResult("Mean", m);
		setResult("KikLGreen", m-count, newparameter);
	}
	IJ.deleteRows(count, nResults-1);
	selectWindow("C2-Bild-1");
	close();

	//measures C4 mean values (mKikume Red)
	selectWindow("C4-Bild");
	run("Duplicate...", "duplicate range=1-1");
	selectWindow("C4-Bild-1");
	count=roiManager("count");
	for (i=0; i<count; i++) {
		roiManager("Select", i);
		run("Measure");
	}
	for (m=count; m<nResults; m++) {
		newparameter=getResult("Mean", m);
		setResult("KikRed", m-count, newparameter);
	}
	IJ.deleteRows(count, nResults-1);
	selectWindow("C4-Bild-1");
	close();
}
bug=isOpen("Result of C1-Bild-1");
print("bug is "+bug);
selectWindow("Result of C1-Bild-1");
close();
roiManager("reset");
```

```
// Measurement of the 4th Z plane
	selectWindow("Result of C1-Bild");
	run("Duplicate...", "duplicate range=4-4");
	bug=isOpen("Result of C1-Bild-1");
	print("series "+h+" creation 4th bug is "+bug);
	selectWindow("Result of C1-Bild-1");
	run("Smooth");
	run("Subtract Background...", "rolling=5 sliding");
	setThreshold(40, 255);
	//setThreshold(40, 255);
	setOption("BlackBackground", false);
	run("Convert to Mask");
	run("Analyze Particles...", "size=0.1-5 exclude add");

count=roiManager("count");
if (count>0) {
//measures area and C1 mean values (mKikume short green)
	selectWindow("C1-Bild");
	run("Duplicate...", "duplicate range=4-4");
	selectWindow("C1-Bild-1");
	run("Set Measurements...", "area mean redirect=None decimal=3");
	count=roiManager("count");
	for (i=0; i<count; i++) {
		roiManager("Select", i);
		run("Measure");
	}
	selectWindow("C1-Bild-1");
	close();
//measures C2 mean values (mKikume long green)
	selectWindow("C2-Bild");
	run("Duplicate...", "duplicate range=4-4");
	selectWindow("C2-Bild-1");
	count=roiManager("count");
	for (i=0; i<count; i++) {
		roiManager("Select", i);
		run("Measure");
	}
```

```
	for (m=nResults-count; m<nResults; m++) {
		newparameter=getResult("Mean", m);
		setResult("KikLGreen", m-count, newparameter);
	}
	IJ.deleteRows(nResults-count, nResults-1);
	selectWindow("C2-Bild-1");
	close();
//measures C4 mean values (mKikume Red)
	selectWindow("C4-Bild");
	run("Duplicate...", "duplicate range=4-4");
	selectWindow("C4-Bild-1");
	count=roiManager("count");
	for (i=0; i<count; i++) {
		roiManager("Select", i);
		run("Measure");
	}
	for (m=nResults-count; m<nResults; m++) {
		newparameter=getResult("Mean", m);
		setResult("KikRed", m-count, newparameter);
	}
	IJ.deleteRows(nResults-count, nResults-1);
	selectWindow("C4-Bild-1");
	close();
}
bug=isOpen("Result of C1-Bild-1");
print("bug is "+bug);
selectWindow("Result of C1-Bild-1");
close();
roiManager("reset");

// Measurement of the 8th Z plane
	selectWindow("Result of C1-Bild");
	run("Duplicate...", "duplicate range=8-8");
	bug=isOpen("Result of C1-Bild-1");
	print("series "+h+" creation 8th bug is "+bug);
	selectWindow("Result of C1-Bild-1");
	run("Smooth");
```

```
	run("Subtract Background...", "rolling=5 sliding");
	setThreshold(40, 255);
	//setThreshold(40, 255);
	setOption("BlackBackground", false);
	run("Convert to Mask");
	run("Analyze Particles...", "size=0.1-5 exclude add");

count=roiManager("count");
if (count>0) {
//measures area and C1 mean values (mKikume short green)
	selectWindow("C1-Bild");
	run("Duplicate...", "duplicate range=8-8");
	selectWindow("C1-Bild-1");
	run("Set Measurements...", "area mean redirect=None decimal=3");
	count=roiManager("count");
	for (i=0; i<count; i++) {
		roiManager("Select", i);
		run("Measure");
	}
	selectWindow("C1-Bild-1");
	close();
//measures C2 mean values (mKikume long green)
	selectWindow("C2-Bild");
	run("Duplicate...", "duplicate range=8-8");
	selectWindow("C2-Bild-1");
	count=roiManager("count");
	for (i=0; i<count; i++) {
		roiManager("Select", i);
		run("Measure");
	}
	for (m=nResults-count; m<nResults; m++) {
		newparameter=getResult("Mean", m);
		setResult("KikLGreen", m-count, newparameter);
	}
	IJ.deleteRows(nResults-count, nResults-1);
	selectWindow("C2-Bild-1");
	close();
```

```
//measures C4 mean values (mKikume Red)
	selectWindow("C4-Bild");
	run("Duplicate...", "duplicate range=8-8");
	selectWindow("C4-Bild-1");
	count=roiManager("count");
	for (i=0; i<count; i++) {
		roiManager("Select", i);
		run("Measure");
	}
	for (m=nResults-count; m<nResults; m++) {
		newparameter=getResult("Mean", m);
		setResult("KikRed", m-count, newparameter);
	}
	IJ.deleteRows(nResults-count, nResults-1);
	selectWindow("C4-Bild-1");
	close();
}
bug=isOpen("Result of C1-Bild-1");
print("bug is "+bug);
selectWindow("Result of C1-Bild-1");
close();
roiManager("reset");

// Measurement of the 11th Z plane
	selectWindow("Result of C1-Bild");
	run("Duplicate...", "duplicate range=11-11");
	bug=isOpen("Result of C1-Bild-1");
	print("series "+h+" creation 11th bug is "+bug);
	selectWindow("Result of C1-Bild-1");
	run("Smooth");
	run("Subtract Background...", "rolling=5 sliding");
	setThreshold(40, 255);
	//setThreshold(40, 255);
	setOption("BlackBackground", false);
	run("Convert to Mask");
	run("Analyze Particles...", "size=0.1-5 exclude add");
```

```
count=roiManager("count");
if (count>0) {
//measures area and C1 mean values (mKikume short green)
	selectWindow("C1-Bild");
	run("Duplicate...", "duplicate range=11-11");
	selectWindow("C1-Bild-1");
	run("Set Measurements...", "area mean redirect=None decimal=3");
	count=roiManager("count");
	for (i=0; i<count; i++) {
		roiManager("Select", i);
		run("Measure");
	}
	selectWindow("C1-Bild-1");
	close();
//measures C2 mean values (mKikume long green)
	selectWindow("C2-Bild");
	run("Duplicate...", "duplicate range=11-11");
	selectWindow("C2-Bild-1");
	count=roiManager("count");
	for (i=0; i<count; i++) {
		roiManager("Select", i);
		run("Measure");
	}

	for (m=nResults-count; m<nResults; m++) {
		newparameter=getResult("Mean", m);
		setResult("KikLGreen", m-count, newparameter);
	}
	IJ.deleteRows(nResults-count, nResults-1);
	selectWindow("C2-Bild-1");
	close();
//measures C4 mean values (mKikume red)
	selectWindow("C4-Bild");
	run("Duplicate...", "duplicate range=11-11");
	selectWindow("C4-Bild-1");
	count=roiManager("count");
	for (i=0; i<count; i++) {
```

```
                roiManager("Select", i);
                run("Measure");
        }
        for (m=nResults-count; m<nResults; m++) {
                newparameter=getResult("Mean", m);
                setResult("KikRed", m-count, newparameter);
        }
        IJ.deleteRows(nResults-count, nResults-1);
        selectWindow("C4-Bild-1");
        close();
}
bug=isOpen("Result of C1-Bild-1");
print("bug is "+bug);
selectWindow("Result of C1-Bild-1");
close();
roiManager("reset");

// Measurement of the 15th Z plane
        selectWindow("Result of C1-Bild");
        run("Duplicate...", "duplicate range=15-15");
        bug=isOpen("Result of C1-Bild-1");
        print("series "+h+" creation 15th bug is "+bug);
        selectWindow("Result of C1-Bild-1");
        run("Smooth");
        run("Subtract Background...", "rolling=5 sliding");
        setThreshold(40, 255);
        //setThreshold(40, 255);
        setOption("BlackBackground", false);
        run("Convert to Mask");
        run("Analyze Particles...", "size=0.1-5 exclude add");

count=roiManager("count");
if (count>0) {
//measures area and C1 mean values (mKikume short green)
        selectWindow("C1-Bild");
        run("Duplicate...", "duplicate range=15-15");
        selectWindow("C1-Bild-1");
```

```
	run("Set Measurements...", "area mean redirect=None decimal=3");
	count=roiManager("count");
	for (i=0; i<count; i++) {
		roiManager("Select", i);
		run("Measure");
	}
	selectWindow("C1-Bild-1");
	close();
//measures C2 mean values (mKikume long green)
	selectWindow("C2-Bild");
	run("Duplicate...", "duplicate range=15-15");
	selectWindow("C2-Bild-1");
	count=roiManager("count");
	for (i=0; i<count; i++) {
		roiManager("Select", i);
		run("Measure");
	}
	for (m=nResults-count; m<nResults; m++) {
		newparameter=getResult("Mean", m);
		setResult("KikLGreen", m-count, newparameter);
	}
	IJ.deleteRows(nResults-count, nResults-1);
	selectWindow("C2-Bild-1");
	close();
//measures C4 mean values (mKikume red)
	selectWindow("C4-Bild");
	run("Duplicate...", "duplicate range=15-15");
	selectWindow("C4-Bild-1");
	count=roiManager("count");
	for (i=0; i<count; i++) {
		roiManager("Select", i);
		run("Measure");
	}
	for (m=nResults-count; m<nResults; m++) {
		newparameter=getResult("Mean", m);
		setResult("KikRed", m-count, newparameter);
	}
```

```
        IJ.deleteRows(nResults-count, nResults-1);
        selectWindow("C4-Bild-1");
        close();
}
bug=isOpen("Result of C1-Bild-1");
print("bug is "+bug);
selectWindow("Result of C1-Bild-1");
close();
roiManager("reset");
selectWindow("C1-Bild");
close();
selectWindow("C2-Bild");
close();
selectWindow("C4-Bild");
close();
selectWindow("Result of C1-Bild");
close();
```

// Adds position number to the the result table

```
                if (nResults>0) {
                        for (w=0; w<nResults; w++) {
                        setResult("Position", w, position);
                        }
                }
```

// Updates and saves results as xls file

```
                if (l==0) {
                        selectWindow("Results");
                        excel0 = replace(lifpath, "lif", "xls");
                        print(excel0);
                        saveAs("Results", excel0);
                }

                else {
                        if (nResults>0) {
                        area=newArray(nResults);
                        mean=newArray(nResults);
```

```
                    kikgreen=newArray(nResults);
                    kikred=newArray(nResults);
                    pos=newArray(nResults);
                        for (z=0; z<nResults; z++) {
                        area[z] = getResult("Area", z);
                        mean[z] = getResult("Mean", z);
                        kikgreen[z] = getResult("KikLGreen", z);
                        kikred[z] = getResult("KikRed", z);
                        pos[z] = getResult("Position", z);
                    }

                    selectWindow("Results");
                    run("Close");
                    open(excel0);
                    size = lengthOf(area);
                    start = nResults;
                    end = nResults+size;
                    ind=0;

                    for (g=start; g<end; g++) {
                        setResult("Area", g, area[ind]);
                        setResult("Mean", g, mean[ind]);
                        setResult("KikLGreen", g, kikgreen[ind]);
                        setResult("KikRed", g, kikred[ind]);
                        setResult("Position", g, pos[ind]);
                        ind=ind+1;
                    }

                    selectWindow("Results");
                    saveAs("Results", excel0);
                    run("Close");
                    }
                }
            }
```

// Filtering of excel data

```
open(excel0);
```

```
nResults();
                }
        }
}

waitForUser("Analysis completed. Click OK to exit the macro.");
```

6.2.2 Macro for fluorescence measurement of cell borders in MELC data

```
image=getString("enter image number", "Folder name")
subfolder=getString("deblurred?", "Folder name")

run("Image Sequence...", "open=File path"); "+image+"\\Folder name\\"+subfolder+"\\
file=PBS_400_37_001 sort");
	rename("KikumeRed");
run("Image Sequence...", "open=File path"+image+"\\Folder name\\"+subfolder+"\\
file=PBS_400_116_001 sort");
	rename("KikumeGreen");
run("Image Sequence...", "open=File path"+image+"\\Folder name\\"+subfolder+"\\
file=CD11b sort");
	rename("CD11b");
run("Image Sequence...", "open=File path"+image+"\\Folder name\\"+subfolder+"\\
file=CD45_1_400 sort");
	rename("CD45_1");
run("Image Sequence...", "open=File path"+image+"\\Folder name\\"+subfolder+"\\
file=CD45_400_116 sort");
	rename("CD45");
imageCalculator("Subtract stack", "CD45","CD45_1");
selectWindow("CD45");
	rename("CD45_2_calc");
run("Merge Channels...", "c1=KikumeRed c2=KikumeGreen c3=CD11b c5=CD45_1
c6=CD45_2_calc create");
run("Channels Tool...");
Stack.setChannel(2)
	run("Yellow");
Stack.setChannel(1)
	run("Yellow");
Stack.setActiveChannels("11011");
	run("Brightness/Contrast...");

// define and safe regions of interest
roiManager("Save", "File path"+experiment+"\\Cells_RoiSet_"+image+".zip");

// Measurement of cell borders
```

```
image=getString("enter image number", "Folder name")
subfolder=getString("deblurred?", "Folder name")
experiment=getString("enter experiment number", "Experiment number")

count=roiManager("count");
for (i=0; i<count; i++) {
        roiManager("Select", i);
        run("Area to Line");
        run("Line to Area");
        run("Enlarge...", "enlarge=1");
        roiManager("Update");
}

roiManager("Save", "File path"+experiment+"\\Outlines_RoiSet_"+image+".zip");
roiManager("reset");
run("Clear Results");
```

//loads cell masks and measures Staph mKikume expression in mean of the whole cell

```
roiManager("Open", "File path"+experiment+"\\Cells_RoiSet_"+image+".zip");

Stack.setChannel(1)
run("Set Measurements...", "area mean redirect=None decimal=3");
count=roiManager("count");
for (i=0; i<count; i++) {
        roiManager("select", i);
        run("Measure");
}

Stack.setChannel(2)
run("Set Measurements...", "area mean redirect=None decimal=3");
count=roiManager("count");
for (i=0; i<count; i++) {
        roiManager("select", i);
        run("Measure");
}
for (m=count; m<nResults; m++) {
```

```
	newparameter=getResult("Mean", m);
	setResult("KikumeGreen", m-count, newparameter);
}
IJ.deleteRows(count, nResults-1);
```

//loads outline masks and measures CD45_1 (channel 4) and CD45_2_calc (channel 5) expression

```
roiManager("reset");
roiManager("Open", "File path"+experiment+"\\Outlines_RoiSet_"+image+".zip");

Stack.setChannel(4)
run("Set Measurements...", "area mean redirect=None decimal=3");
count=roiManager("count");
for (i=0; i<count; i++) {
	roiManager("select", i);
	run("Measure");
}
for (m=count; m<nResults; m++) {
	newparameter=getResult("Mean", m);
	setResult("CD45_1", m-count, newparameter);
}

IJ.deleteRows(count, nResults-1);
Stack.setChannel(5)
run("Set Measurements...", "area mean redirect=None decimal=3");
count=roiManager("count");
for (i=0; i<count; i++) {
	roiManager("select", i);
	run("Measure");
}
for (m=count; m<nResults; m++) {
	newparameter=getResult("Mean", m);
	setResult("CD45_2_calc", m-count, newparameter);
}
IJ.deleteRows(count, nResults-1);
String.copyResults();
```

6.2.3 Macro for bacterial mKikume fluorescence measurement in MELC data

First run Macro 6.2.2 (Macro for fluorescence measurement of cell borders in MELC data) and close all image windows.

//loads cell masks and measures Staph mKikume expression of single masks

```
image=getString("enter image number", "Folder name")
subfolder=getString("deblurred?", "Folder name")
experiment=getString("enter experiment number", "Experiment number")

run("Clear Results");
roiManager("reset");
roiManager("Open", "File path"+experiment+"\\Cells_RoiSet_"+image+".zip");
count1=roiManager("count");
setBackgroundColor(0, 0, 0)

for (i=0; i<count1; i++) {
	roiManager("reset");
roiManager("Open", "File path"+experiment +"\\Cells_RoiSet_"+image+".zip");
	selectWindow("Composite");
	roiManager("Select", i);
	run("Duplicate...", " ");
	run("Clear Outside");
	rename("extract");
	run("Split Channels");
	selectWindow("C5-extract");
	close();
	selectWindow("C4-extract");
	close();
	selectWindow("C3-extract");
	close();
	selectWindow("C1-extract");
	resetMinAndMax();
	run("Duplicate...", " ");
	rename("C1-extract8bit");
	run("8-bit");
	selectWindow("C2-extract");
```

```
resetMinAndMax();
run("Duplicate...", " ");
rename("C2-extract8bit");
run("8-bit");
imageCalculator("Add create", "C1-extract8bit","C2-extract8bit");
rename("Combined8bit");
selectWindow("C1-extract8bit");
close();
selectWindow("C2-extract8bit");
close();
selectWindow("Combined8bit");
run("Smooth");
setAutoThreshold("Default");

run("Convert to Mask");
run("Invert");

roiManager("reset");
run("Analyze Particles...", "add");
count2=roiManager("count");

if (count2>1) {
        roiManager("Combine");
        roiManager("Add");
        roiManager("Select", count2);
        selectWindow("Combined8bit");
        close();
        selectWindow("C1-extract");
        roiManager("Select", count2);
        run("Set Measurements...", "area mean redirect=None decimal=3");
        run("Measure");
        selectWindow("C2-extract");
        roiManager("Select", count2);
        run("Measure");
}

if (count2<2) {
```

```
                roiManager("Select", count2-1);
                selectWindow("Combined8bit");
                close();
                selectWindow("C1-extract");
                roiManager("Select", count2-1);
                run("Set Measurements...", "area mean redirect=None decimal=3");
                run("Measure");
                selectWindow("C2-extract");
                roiManager("Select", count2-1);
                run("Measure");
        }

        selectWindow("C1-extract");
        close();
        selectWindow("C2-extract");
        close();
}

String.copyResults();
```

EHRENERKLÄRUNG

Ich versichere hiermit, dass ich die vorliegende Arbeit ohne unzulässige Hilfe Dritter und ohne Benutzung anderer als der angegebenen Hilfsmittel angefertigt habe; verwendete fremde und eigene Quellen sind als solche kenntlich gemacht.

Ich habe insbesondere nicht wissentlich:

- Ergebnisse erfunden oder widersprüchlich Ergebnisse verschwiegen,
- statistische Verfahren absichtlich missbraucht, um Daten in ungerechtfertigter Weise zu interpretieren,
- fremde Ergebnisse oder Veröffentlichungen plagiiert,
- fremde Forschungsergebnisse verzerrt wiedergegeben.

Mir ist bekannt, dass Verstöße gegen das Urheberrecht Unterlassungs- und Schadensersatzansprüche des Urhebers sowie eine strafrechtliche Ahndung durch die Strafverfolgungsbehörden begründen kann.

Ich erkläre mich damit einverstanden, dass die Arbeit ggf. mit Mitteln der elektronischen Datenverarbeitung auf Plagiate überprüft werden kann.

Die Arbeit wurde bisher weder im Inland noch im Ausland in gleicher oder ähnlicher Form als Dissertation eingereicht und ist als Ganzes auch noch nicht veröffentlicht.

Magdeburg, den_____ _____

(Elena A. Seiß)